DOE/NASA/0335-1
NASA CR-185109
GARRETT NO. 31-8071(1)

ADVANCED TURBINE TECHNOLOGY APPLICATIONS PROJECT (ATTAP)

1988 ANNUAL REPORT

Engineering Staff of
Garrett Auxiliary Power Division
A Unit of Allied-Signal Aerospace Company

April 1989

Prepared for
NATIONAL AERONAUTICS AND SPACE ADMINISTRATION
Lewis Research Center
Cleveland, Ohio 44135
Under Contract DEN3-335

for
U.S. DEPARTMENT OF ENERGY
Office of Transportation Systems
Heat Engine Propulsion Division
Washington, D.C. 20585

(NASA-CR-185109) ADVANCED TURBINE TECHNOLOGY APPLICATIONS PROJECT (ATTAP) Annual Report, 1988 (Allied-Signal Aerospace Co.) 249 p CSCL 10B G3/85

N90-14153

Unclas 0231740

DISCLAIMER

This report was prepared as an account of work sponsored by an agency of the United States Government. Neither the United Stated Government nor any agency thereof, nor any of their employees, makes any warranty, express or implied, or assumes any legal liability or responsibility for the accuracy, completeness, or usefulness of any information, apparatus, product or process disclosed, or represents that its use would not infringe privately owned rights. Reference herein to any specific commercial product, process, or service by trade name, trademark, manufacturer, or otherwise, does not necessarily constitute or imply its endorsement, recommendation, or favoring by the United States Government or any agency thereof. The views and opinions of authors expressed herein do not necessarily state or reflect those of the United States Government or any agency thereof.

Printed in the United States of America

Available from
National Technical Information Service
U.S. Department of Commerce
5285 Port Royal Road
Springfield, VA 22161

NTIS price codes[1]
Printed copy: All
Microfiche copy: A01

DOE/NASA/0335-1
NASA CR-185109
GARRETT NO. 31-8071(1)

ADVANCED TURBINE TECHNOLOGY APPLICATIONS PROJECT (ATTAP)

1988 ANNUAL REPORT

Engineering Staff of
Garrett Auxiliary Power Division
A Unit of Allied-Signal Aerospace Company

April 1989

Prepared for
National Aeronautics and Space Administration
Lewis Research Center
Cleveland, Ohio 44135
Under Contract DEN3-335

for
U.S. Department of Energy
Office of Transportation Systems
Heat Engine Propulsion Division
Washington, D.C. 20585

TABLE OF CONTENTS

TABLE OF CONTENTS (Contd)

LIST OF FIGURES

LIST OF FIGURES (Contd)

LIST OF FIGURES (Contd)

LIST OF FIGURES (Contd)

LIST OF FIGURES (Contd)

LIST OF FIGURES (Contd)

LIST OF FIGURES (Contd)

LIST OF FIGURES (Contd)

LIST OF FIGURES (Contd)

LIST OF TABLES

LIST OF TABLES (Contd)

LIST OF TABLES (Contd)

1.0 SUMMARY

This report describes progress and work performed by the Garrett Auxiliary Power Division, during the period August 1987 through December 1988, to develop and demonstrate the technology of structural ceramics for automotive engines and similar applications. This work was performed for the Department of Energy under NASA Contract DEN3-335, Advanced Turbine Technology Applications Project (ATTAP). This is the first in a series of technical summary reports to be published on an annual basis over the course of the five-year contract.

Project effort conducted under this contract is part of the DOE Gas Turbine Highway Vehicle System Program. This program is oriented to provide the United States automotive industry the high-risk, long-range technology necessary to produce gas turbine engines for automobiles with reduced fuel consumption and reduced environmental impact.

The ATTAP test bed engine is designed such that, when installed in a 3000 pound inertia weight automobile, it will provide:

- Low emissions
- 42 mpg fuel economy on diesel fuel
- Multifuel capability
- Competitive costs with current spark-ignition engines
- Noise and safety characteristics that meet federal standards.

1.1 Engine/Powertrain Design, Analysis, and Materials Assessment

A survey of the ceramics industry was performed in the early stages of the contract to identify those materials and suppliers with the potential for producing hardware to meet the goals of the ATTAP Reference Powertrain Design (RPD). The survey was used as a basis for selection of ceramic subcontractors to participate in ATTAP by developing and supplying ceramic components for evaluation in rigs and engines at GAPD. The selection of ATTAP subcontractors was based not only upon vendor material data, but also on confirming data generated by GAPD, plus a demonstrated capability on the part of the supplier to successfully fabricate components to complex shapes.

This RPD is essentially the same as that used in the previous AGT101 program. A Design Review (program Milestone No. 2) was conducted during the report period to update the RPD, and to incorporate improvements to the engine test bed design.

1.2 Ceramic Component Design

Activities in this area included a stress analysis of the ATTAP Flow Separator Housing, and stress analyses and life predictions of

critical ATTAP components, including the turbine rotor, turbine stators, and turbine shroud. These results were incorporated into the ATTAP Design Review, as formally presented to NASA in September 1988.

An effort to formulate and verify methods for ceramic life prediction, using a heated spin pit as a confirming test bed, was initiated with the design of a spin disk which will effectively subject a large volume of material to a high and nearly uniform level of biaxial stress. This design will be used later in the project in a heated spin pit, to verify predictions of life under high stress and temperature conditions.

A method to correct for surface effects upon component stresses is also presented in this section.

Work accomplished to date in the understanding of impact damage and development of methods to design for impact tolerance is described in detail. A program with the University of Dayton Research Institute (UDRI) was initiated to survey theoretical impact models, assess their applicability to structural ceramics, and test for the most significant parameters which affect impact damage.

A description of the topics presented in the ATTAP Design Review is also discussed. These topics include a modification to the ceramic turbine attachment coupling design, an update of the ATTAP Reference Powertrain Design, analyses of the temperatures and stresses in critical components, and a review of engine test bed critical interfaces. Information on reliability aspects of test bed operation were presented, as well, including a Failure Mode, Effects, and Criticality Analysis (FMECA), Preliminary Hazard Analysis (PHA), and Operating and Support Hazard Analysis (O&SHA).

1.3 Materials Characterization and Component Fabrication

Characterization of the subcontractor materials to expand the database on these materials and to provide additional input to the ceramic design function was begun with the collection of data on Norton/TRW NT154 hot isostatic pressed (HIPped) silicon nitride. Additionally, data on the materials used in engine components acquired through purchase was generated, to support their use in the test bed engine. Verification of thermal conductivity measurements was also conducted for one of the materials used in the ATTAP engine, and additional thermal conductivity testing was planned.

The implementation of NDE methods for ceramics was begun with the inspection of components prior to rig and engine test. Inspection results are retrievable, such that these can be referred to in the future, and the experience gained can be shared with ceramic subcontractors. Plans were also formulated for the development of NDE methods using seeded defect specimens as a control of the ability to find defects of given size and type.

Efforts of the three ATTAP subcontractors were kicked off. Norton/TRW Ceramics is working on development of the ATTAP rotor and stators, using their NT154 HIPped silicon nitride; Carborundum Co.* is developing processes to form their sintered alpha silicon carbide (SASC) into transition ducts, turbine backshrouds, and ceramic wave springs used in the ATTAP test bed engine, and Garrett Ceramic Components Division is developing the fabrication process for the ATTAP rotor using their GN-10 silicon nitride. Details of the activities of these subcontractors are given in the appendices to this report.

1.4 Component Rig Test

Rig testing is performed under ATTAP to assure the integrity of components to be built into test bed engines, to evaluate new designs, and to provide feedback into the development of NDE processes. A detailed series of pre-test operations and inspections is prescribed for each component to be tested. Specific test rigs include a combustor rig, a ceramic seals rig, and thermal proof rigs.

*A.K.A. Standard Oil Company

2.0 INTRODUCTION

This report is the first in a series of Annual Technical Summary Reports for the Advanced Turbine Technology Applications Project (ATTAP), authorized under NASA Contract DEN3-335 and sponsored by the DOE. This report has been prepared by Garrett Auxiliary Power Division (hereinafter referred to as GAPD), a unit of Allied-Signal Aerospace Company. The report includes information provided by Garrett Ceramic Components Division (hereinafter referred to as GCCD), Norton/TRW Ceramics Co., and the Carborundum Co., all subcontractors to GAPD on the ATTAP. The project is administered by Mr. Thomas Strom, Project Manager, NASA-Lewis Research Center, Cleveland, Ohio. This report presents plans and progress from August 1987 through December 1988.

Project effort conducted under this contract is part of the DOE Gas Turbine Highway Vehicle System Program. This program is oriented to provide the United States automotive industry the high-risk, long-range technology necessary to produce gas turbine engines for automobiles with reduced fuel consumption and reduced environmental impact.

The ATTAP test bed engine is designed such that, when installed in a 3000 pound inertia weight automobile, it will provide:

- Low emissions
- 42 mpg fuel economy on diesel fuel
- Multifuel capability
- Competitive costs with current spark-ignition engines
- Noise and safety characteristics that meet federal standards

It is nominally a 100-shp engine, capable of speeds to 100,000 rpm and operation at turbine inlet temperatures (TIT) to 2500F with a specific fuel consumption level of 0.3 pounds/hp-hr over much of the operating range.

The program is oriented toward developing the high-risk technology of ceramic structural component design and fabrication, such that industry can carry this technology forward to production in the 1990s. The ATTAP test bed engine, carried over from the previous AGT101 project, is used for verification testing of the durability of ceramic components, and their suitability for service at Reference Powertrain Design conditions.

The program schedule is depicted in Figure 1. The program continues technology work into Calendar Year 1992, culminating in the demonstration of ceramic engine operation for 300 hours under conditions simulating the Combined Federal Driving Cycle for automotive engines, and in the publication of a Ceramic Design Manual for use by industry as a guide to the use of fine ceramics in structural applications. In addition, a Reference Powertrain Design Cost

Analysis will be performed in late 1991, to provide industry with data on the costs of producing with structural ceramic materials.

This report reviews the effort conducted in the first 16 months of the project on development of ceramic technology, review and update of the Reference Powertrain Design, and improvements made to the test bed engine and test rigs. Appendices include reports of progress made by the major subcontractors to GAPD on the ATTAP: Carborundum, Norton/TRW Ceramics, and Garrett Ceramic Components Division.

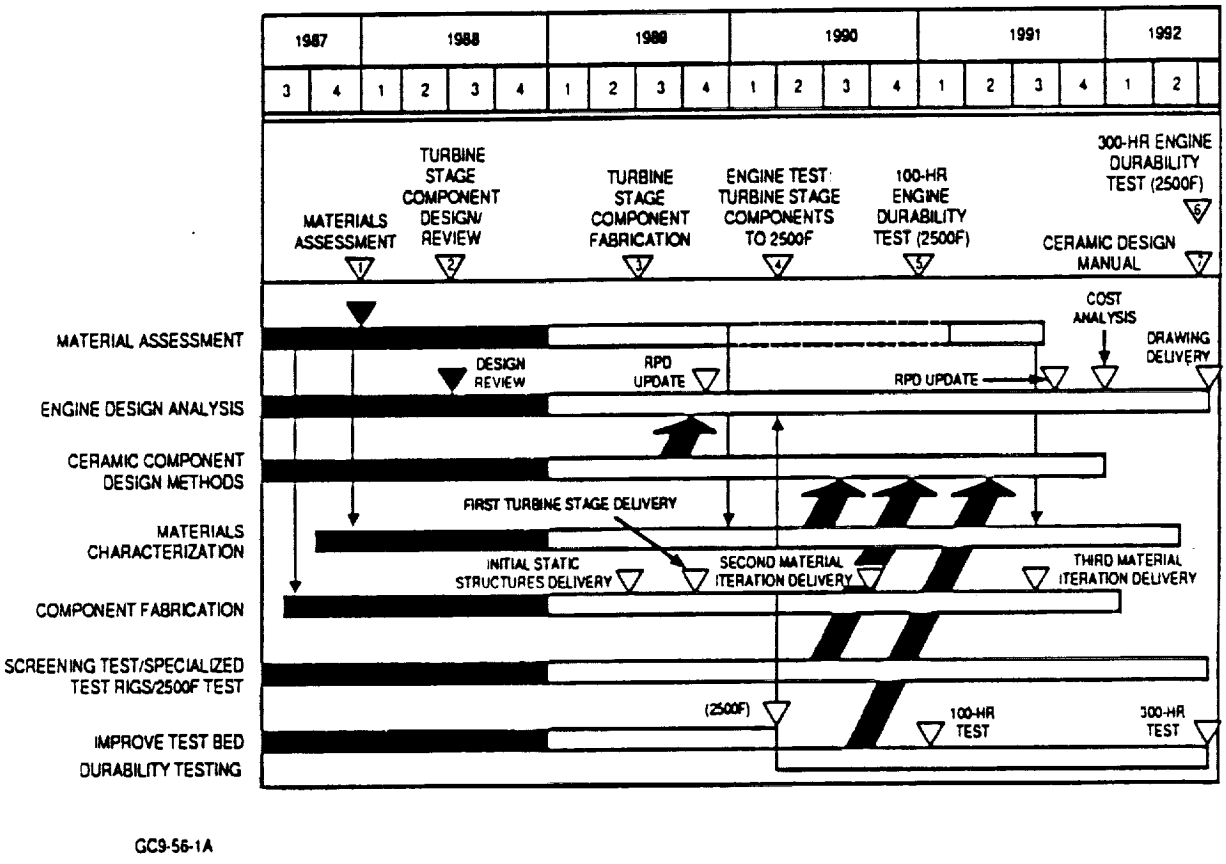

Figure 1. The GAPD Coordinated Plan for Conducting ATTAP Depicts Activities From Contract Award to Engine Durability Testing.

3.0 ENGINE POWERTRAIN DESIGN, ANALYSIS, AND MATERIALS ASSESSMENT

This section includes activities related to the assessment of the state-of-the-art in ceramic materials, design modifications to improve the engine test bed and to maintain it consistent with the state of development of ceramic components, and the periodic review of the Reference Powertrain Design.

3.1 Materials Assessment

Milestone 1 of the ATTAP program was to assess ceramic suppliers for material properties and shape fabrication capability. A letter was sent to over thirty ceramic and ceramic matrix composite suppliers in the United States. The letter described the ATTAP program, listed the minimum material property requirements and invited suppliers with materials exceeding the minimum material property goals and demonstrated shape capability to submit data and test specimens for consideration. Of the over thirty suppliers contacted for materials assessment to date, six materials were submitted for evaluation. Table 1 lists the ceramic suppliers that were contacted, suppliers that responded and suppliers that provided material for assessment. The materials were tested for fast fracture strength, stress rupture life and fracture toughness. The temperatures and stresses chosen for materials assessment were chosen depending on the material and potential use of the material according to the test matrices in Table 2.

Fast fracture and stress rupture tests are conducted in four-point flexure with outer spans of 1.50 inch, inner spans of 0.75 inch, and a crosshead speed of 0.02 inch/minute. The specimens have a cross section of 0.125 by 0.250 inch and the edges are chamfered 0.005-0.010 inch at 45 degrees. Chevron notch fracture toughness testing is performed in three-point bending with an outer span of 1.5 inch and a crosshead speed of 0.0005 inch/minute. The chevron notch specimens have a cross section dimension of 0.250 by 0.250 inch. The specimen and notch configuration is shown in Figure 2.

Data generated was compared with the data measured by the supplier to check for batch-to-batch consistency. Suppliers with state-of-the-art materials meeting or exceeding the ATTAP requirements were visited to survey their fabrication facilities and to examine hardware fabricated by the supplier.

Ceramic materials supplied by Norton/TRW and Standard Oil were assessed during the end of the AGT101 project in preparation for ATTAP. Norton/TRW's XL144H Silicon Nitride and Carborundom's Sintered Alpha Silicon Carbide (SASC-SA material) and TiB_2 toughened Silicon Carbide (SASC-ST material) were found to be acceptable for further evaluation during ATTAP.

TABLE 1. POTENTIAL CERAMIC SUPPLIERS FOR MATERIALS ASSESSMENT

Supplier	Received Response	Supplied Test Specimens
ACMC	X	
ALCOA Technical Center	X	X
Amercom		
Arco Chemical Co.		
Babcock & Wilcox		
Ceradyne, Inc.	X	
Ceramatec		
Ceramics Process Systems		
Cercom, Inc.		
Champion Livingston	X	
Coors Porcelain Co.		
Corning Class Works		
CVD, Incorporated	X	
Dow Chemical, U.S.A.		
Dupont Company	X	
Garrett Ceramic Components Division	X	X
General Electric		
GTE Laboratories, Inc.	X	X
Howmet Turbine Components Corp.		
Industrial Ceramic Technology, Inc.	X	
Kaiser Aerotech		
Laing Ceramics	X	
Lambertville Ceramic	X	
Midland	X	
Norton/TRW Ceramics	X	X
Refractory Composites, Inc		
Rockwell International		
Standard Oil	X	X
Superior Graphite	X	
Thermo Electron		
ESK-Wacker Chemicals	X	

TABLE 2. MATERIAL ASSESSMENT TEST MATRIX FOR ATTAP

Rotor - Si_3N_4	Fast Fracture	Stress Rupture (50 ksi)	Fracture Toughness
Room Temperature	5*	--	3
2000F	5	--	--
2200F	5	5	3
2300F	5	5	--

Static Component - Si_3N_4	Fast Fracture	Stress Rupture (30 ksi)	Fracture Toughness
Room Temperature	5	--	3
2200F	5	--	3
2400F	5	5	--
2500F	5	5	--

Static Component - SiC	Fast Fracture	Stress Rupture (30, 35 40 ksi)	Fracture Toughness
Room Temperature	5	--	3
2200F	5	--	3
2400F	5	--	--
2500F	5	3,4,3	--

*Numbers refer to test specimen quantities

Six materials have been submitted for assessment since the initiation of ATTAP. ALCOA provided two Sialon materials designated "alpha" and "beta" and a silicon carbide specimen called Beta SiC. GTE supplied PY6 silicon nitride; Norton/TRW sent NT154 hot isostatic pressed (HIPped) silicon nitride, and Garrett Ceramic Components Division GN-10 HIPped silicon nitride.

ALCOA Sialon

The flexure strengths of ALCOA alpha and beta Sialons are shown in Figure 3. The alpha Sialon has adequate strength to 2300F for the lower stressed, static components, but not for the turbine rotor. The decrease in strength of the beta Sialon at temperatures greater than 2000F makes it unsuitable for engine components.

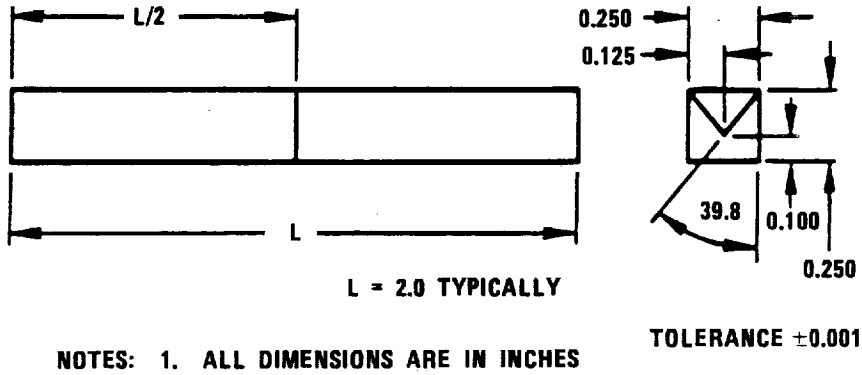

Figure 2. Configuration of Chevron Notch Specimens.

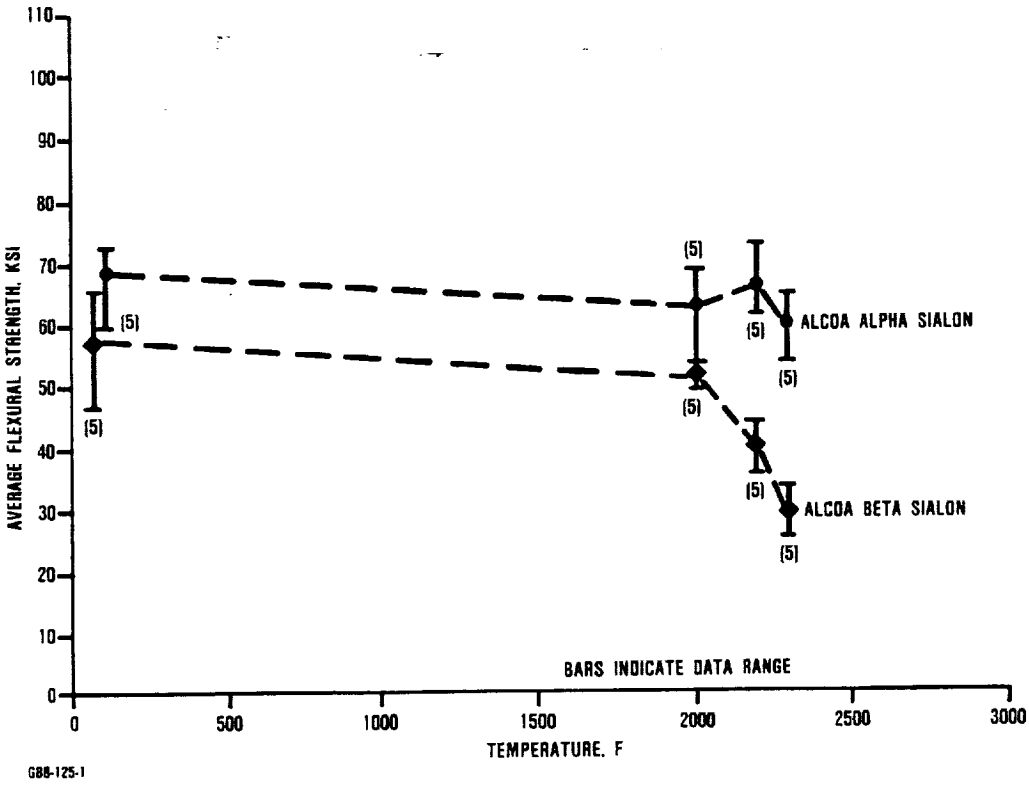

Figure 3. Fast Fracture Assessment, ALCOA Sialons.

ALCOA Beta Silicon Carbide

The strength of beta silicon carbide is shown as a function of temperature in Figure 4.

ALCOA beta silicon carbide was tested in flexural stress rupture at 2500F. The time to failure of the beta silicon carbide is plotted as a function of stress in Figure 5. At flexure stresses of 45 ksi, no failures occurred at exposure times up to 150 hours.

Chevron notch fracture toughness was also measured at room temperature and 2200F. The average fracture toughness of ALCOA Beta silicon carbide at room temperature is 2.95 ksi-in$^{\frac{1}{2}}$ and 3.93 ksi-in$^{\frac{1}{2}}$ at 2200F. The individual and averaged K_{IC} data is listed in Table 3.

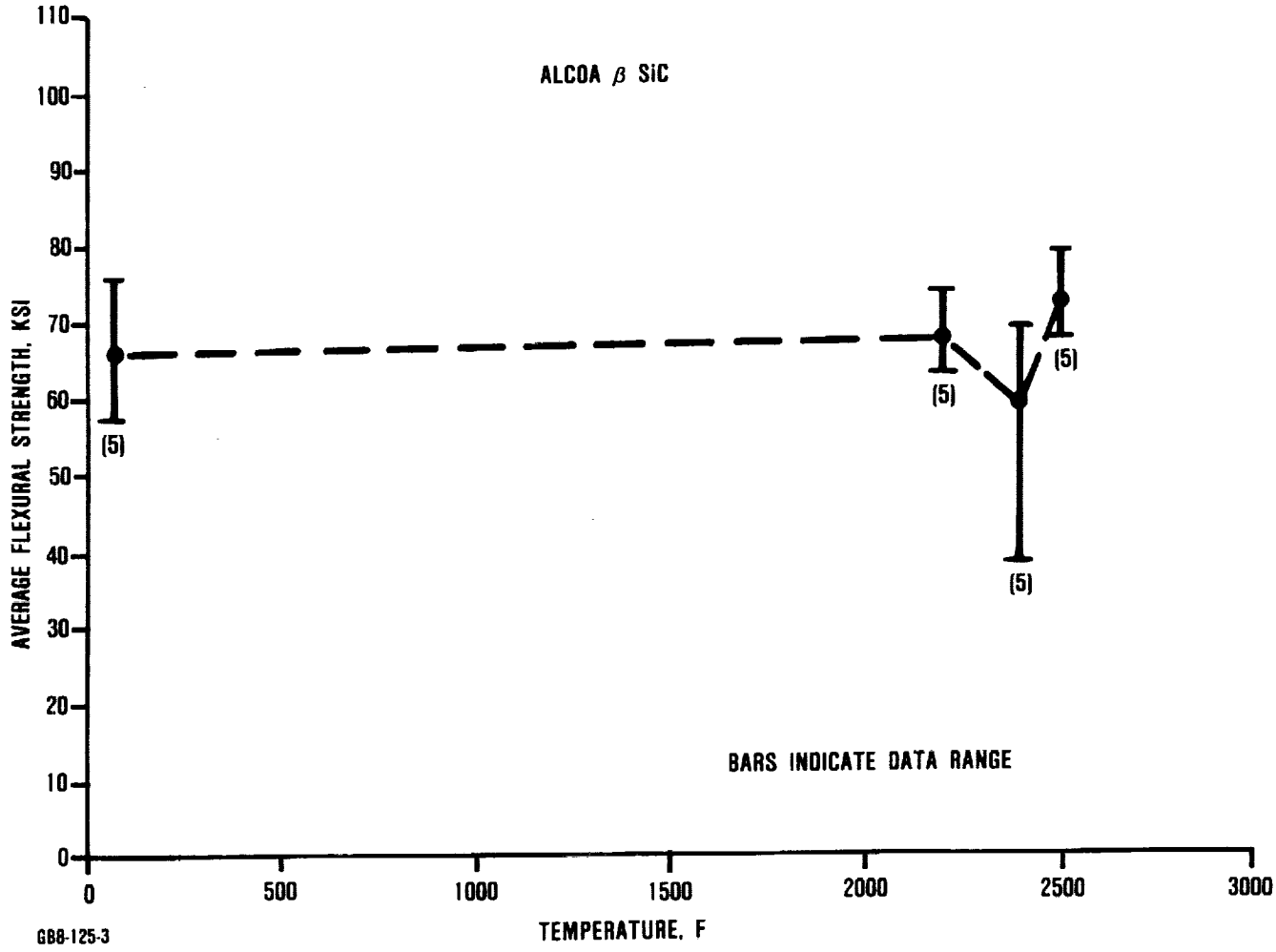

Figure 4. Fast Fracture Assessment, ALCOA Beta Silicon Carbide.

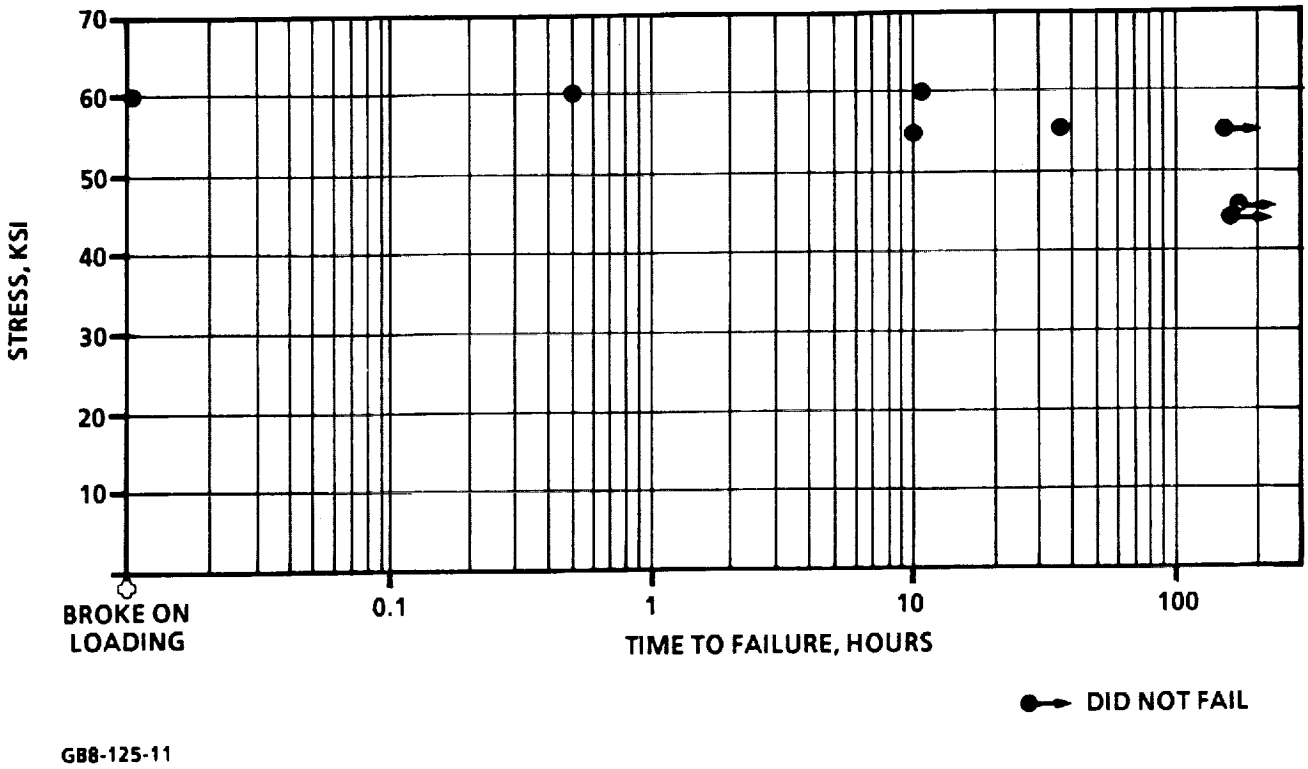

Figure 5. Stress Rupture Life of ALCOA Beta Silicon Carbide at 2500F (1370C).

TABLE 3. ALCOA BETA SILICON CARBIDE CHEVRON NOTCH FRACTURE TOUGHNESS

Temperature	Fracture Toughness, ksi-in$^{\frac{1}{2}}$	Average K_{IC} ksi-in$^{\frac{1}{2}}$
Room	2.78 3.23 2.84	2.95
2200F	3.40 3.56 4.80	3.92

GTE PY6

GTE PY6 injection molded and HIPped test specimens were evaluated for fact fracture strength from room temperature to 2500F. The data is shown in Figure 6. This batch of material assessed does not have an elevated temperature strength as high as is typical for GTE PY6. Because of this, no stress rupture testing was attempted. The 20 specimens intended for stress rupture testing were tested in fast fracture at room temperature.

GTE has recently installed a new state-of-the-art processing facility. The material tested was not processed in GTE's new facility. GTE intends to supply a second batch of PY6 for materials assessment from the new facility when completed.

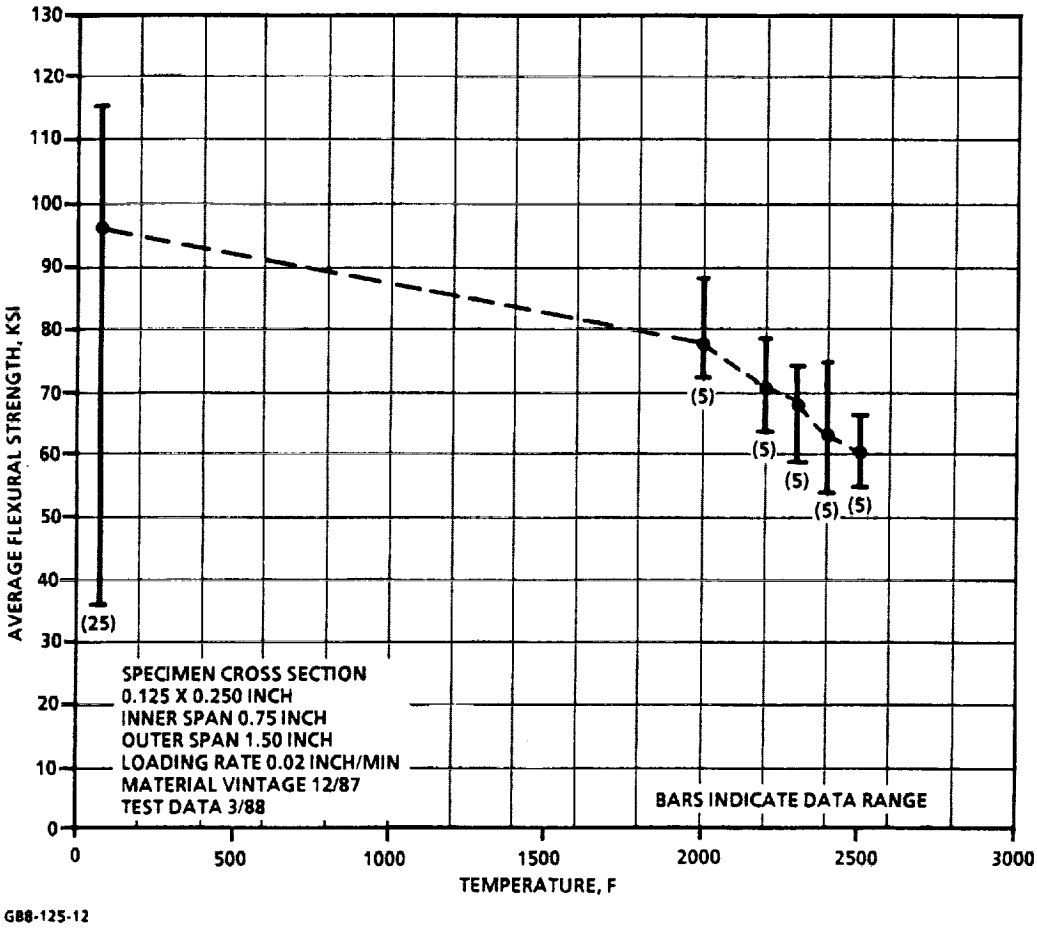

Figure 6. Fast Fracture Assessment GTE PY6.

GCCD GN-10

Garrett Ceramic Components Division (GCCD) GN-10 HIPped Si_3N_4 was assessed for fast and slow fracture and for fracture toughness. The fast fracture strength is plotted as a function of test temperature in Figure 7. The flexure strength is 120.4 ksi at room temperature and slowly decreased with increasing temperature to 77.3 ksi at 2500F (1371C). The stress rupture data are plotted in Figure 8. GN-10 far exceeds the stress rupture requirement of the ATTAP rotor of >100 hours at 2200F and 50 ksi. The chevron notch fracture toughness was measured and is tabulated in Table 4. At room temperature, the fracture toughness is 5.92 ksi-in$^{\frac{1}{2}}$ and at 2200F (1204C) the toughness is 5.27 ksi-in$^{\frac{1}{2}}$.

Norton/TRW NT154

Norton NT154 HIPped Si_3N_4 was assessed for fast fracture flexure strength. The flexure strength is plotted as a function of test temperature in Figure 9. The average room temperature flexure strength is very high (143.3 ksi). The strength decreased slowly with increasing temperature. At the peak rotor temperature of 2200F the strength is 108.4 ksi and at the peak stator temperature of 2500F the strength is still 88.0 ksi.

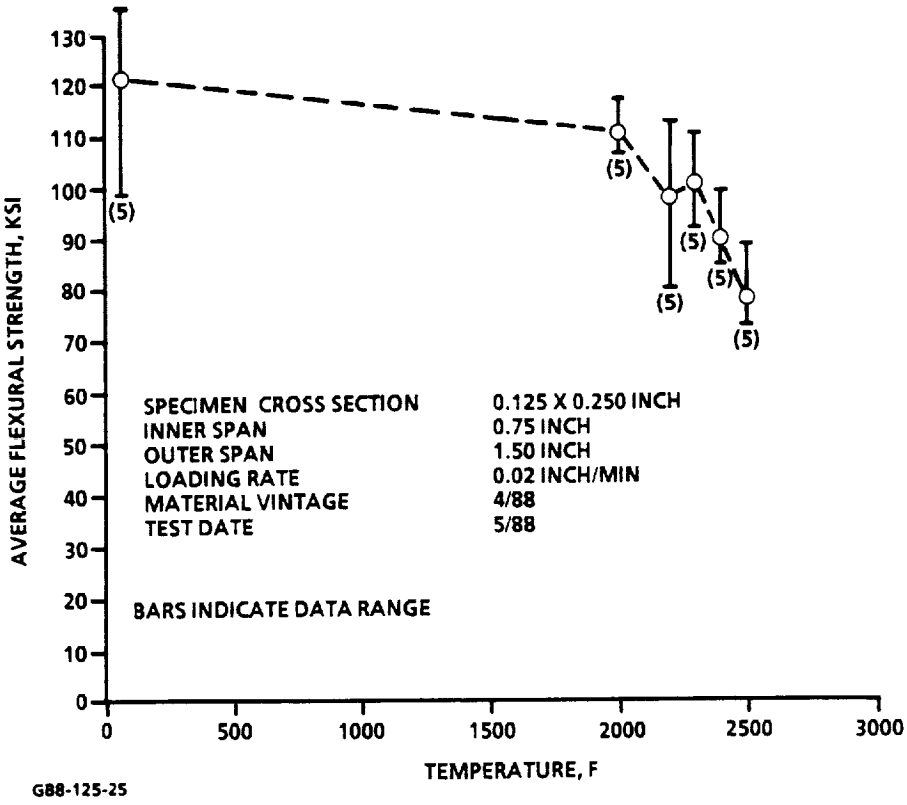

Figure 7. Fast Fracture Assessment of GCCD GN-10 Silicon Nitride.

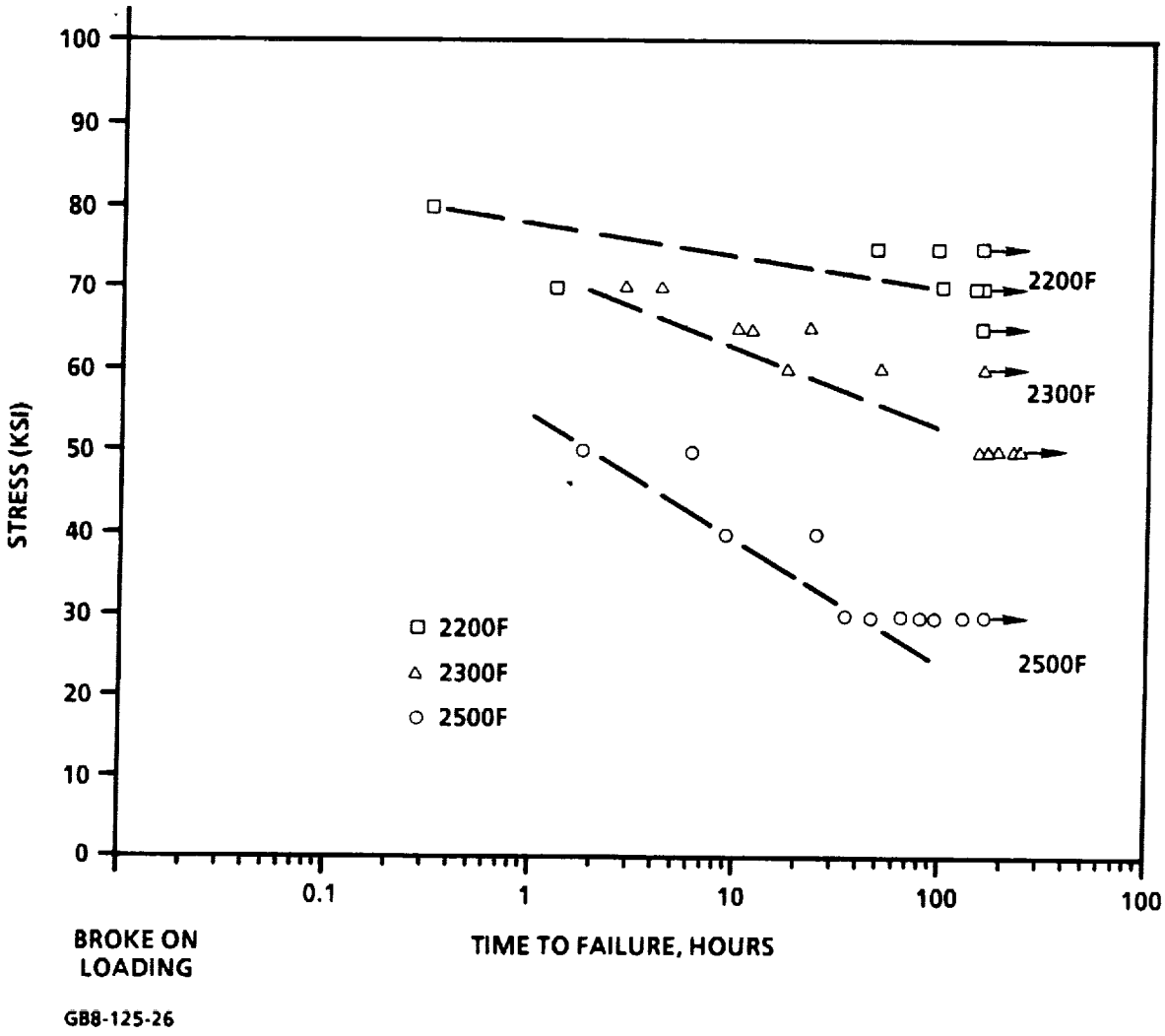

Figure 8. Stress Rupture Life of GCCD GN-10 Silicon Nitride.

Norton NT154, HIPped silicon nitride was assessed for stress rupture life at 2200, 2300, and 2500F. The times to failure are plotted as a function of stress in Figure 10. NT154 exceeds the stress rupture requirement for the ATTAP rotor.

An assessment of ceramic materials and supplier fabrication capabilities was given to key NASA materials personnel on January 27, 1988. This presentation completed Milestone 1 of ATTAP.

3.2 Reference Powertrain Design

A performance analysis on the Reference Powertrain Design (RPD) was generated and presented to NASA during the original AGT101 Design Review during the early stages of that program, and updated in the 1982 Go-Forward Plan. This analysis had not been updated since that time. An update was generated during ATTAP to re-establish the design assumptions used to support ceramic component development and test bed evaluations.

TABLE 4. GGCD GN-10 SILICON NITRIDE

Chevron Notch Fracture Toughness

Temperature	Fracture Toughness, ksi-$in^{\frac{1}{2}}$	Average K_{IC}, ksi-$in^{\frac{1}{2}}$
Room	6.79	
	6.01	
	5.75	
	5.91	
	5.79	
	6.11	
	5.94	5.92
	5.68	
	5.72	
	5.98	
	5.72	
	5.78	
	5.81	
2200F	4.74	
	5.13	
	5.45	
	4.93	
	5.06	
	5.13	5.27
	5.59	
	5.65	
	5.23	
	5.47	
	4.72	
	5.13	

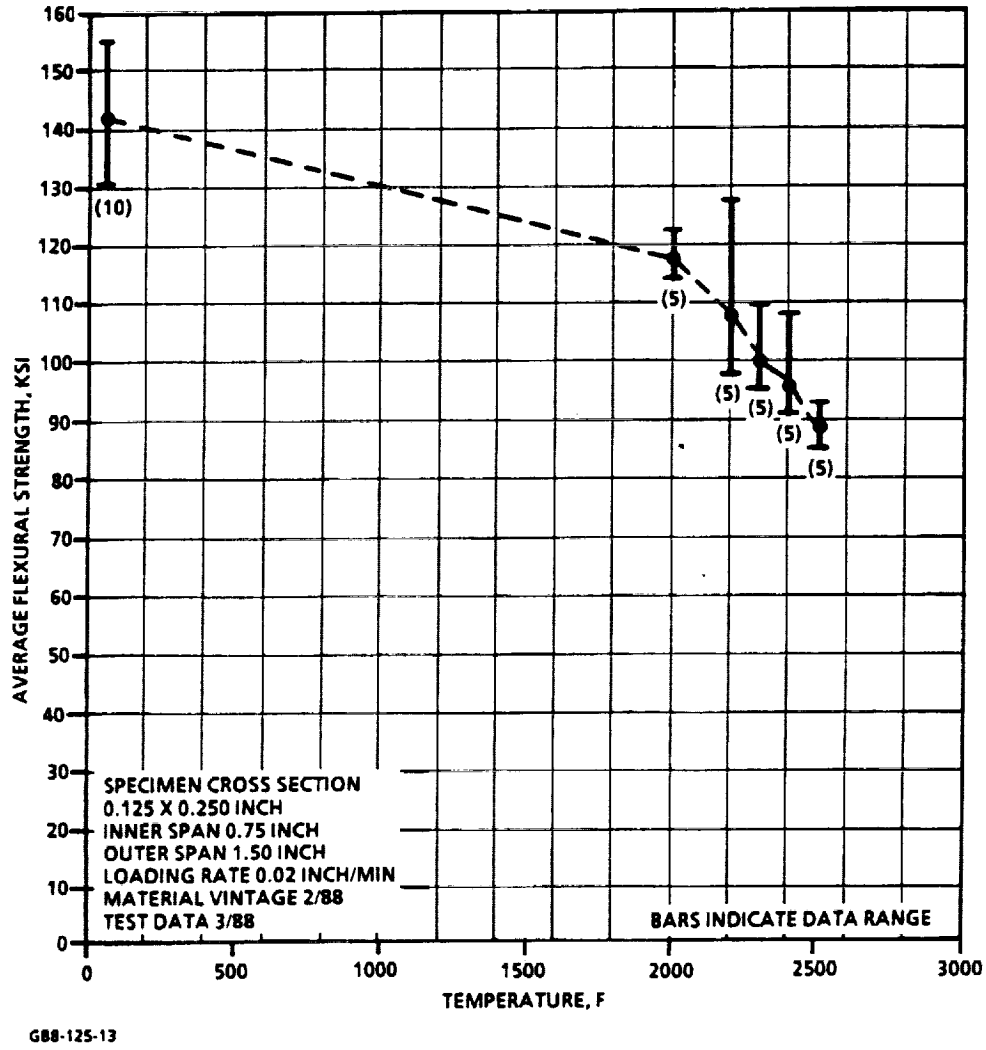

Figure 9. Fast Fracture Assessment of Norton NT154.

The ATTAP contract specifies that the RPD meet the following criteria:

- Low emissions
- 42 MPG fuel economy using DF-2 (over the Combined Federal Driving Cycle)
- Have multifuel capability
- Have competitive cost with current spark-ignition power plants
- Meet Federal standards for noise and safety.

The RPD analysis consists of an aerodynamic analysis of the engine system, an analysis which simulates the vehicular installation, and a mission analysis which operates the engine/vehicle

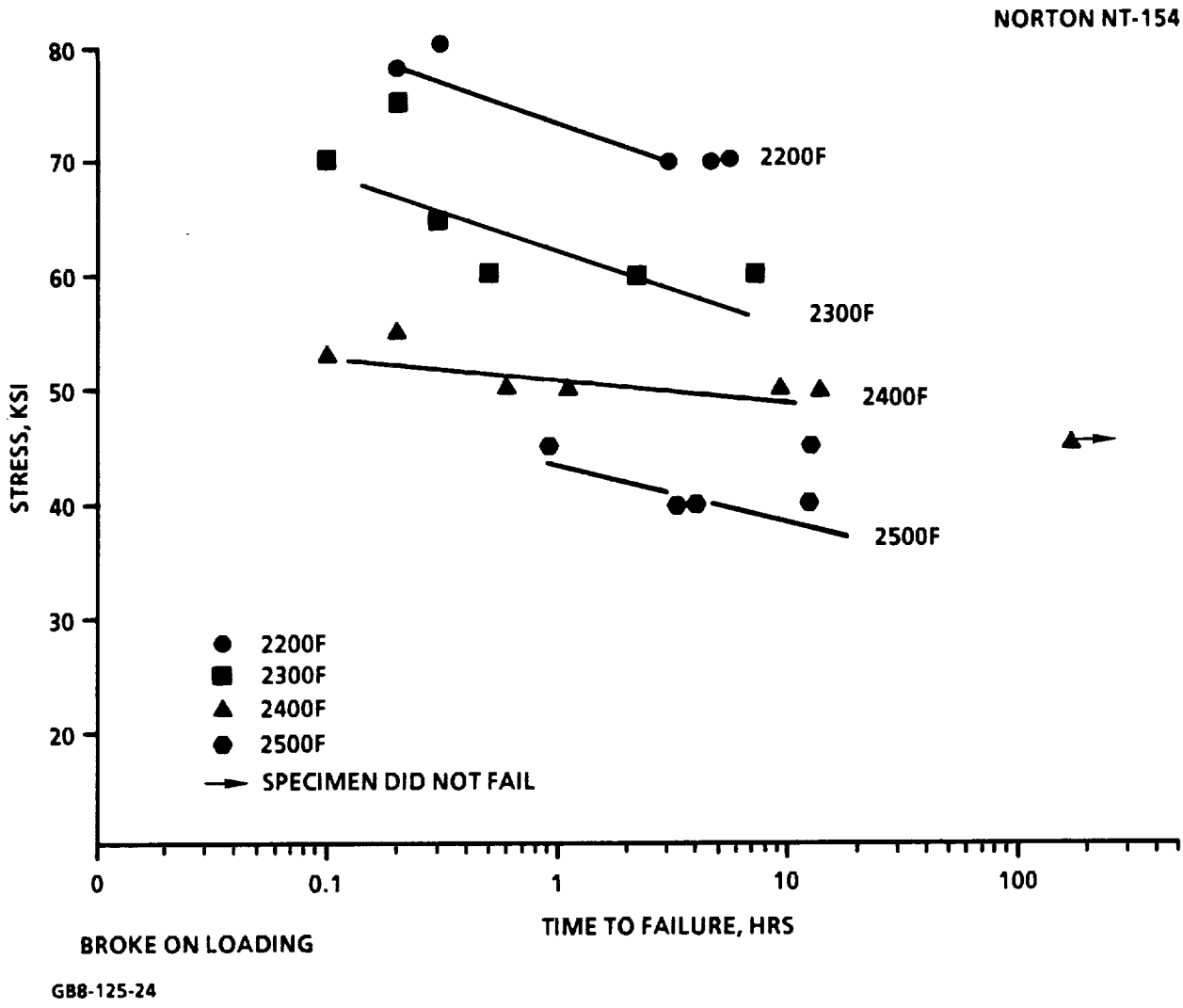

Figure 10. Stress Rupture Life of Norton/TRW NT154 Silicon Nitride.

system through the drivability tests and over the Combined Federal Driving Cycle.

The performance analysis used the engine cycle defined in the schematic in Figure 11. Included in the performance analysis are the aerodynamic component performance maps, flow path pressure losses, interpath gas and heat leakage, overboard gas and heat loss, and provisions for sacrificial cooling for the regenerator seals. The cycle is balanced for both gas flow and heat flow. The cycle specific fuel consumption (SFC) and output shaft power were calculated on a thermodynamic basis. Parasitic losses such as bearings and seals were provided in the vehicular mission analysis.

Component performance characteristics were utilized based on actual test data where appropriate. Compressor performance was based on AGT compressor rig testing, turbine performance was based

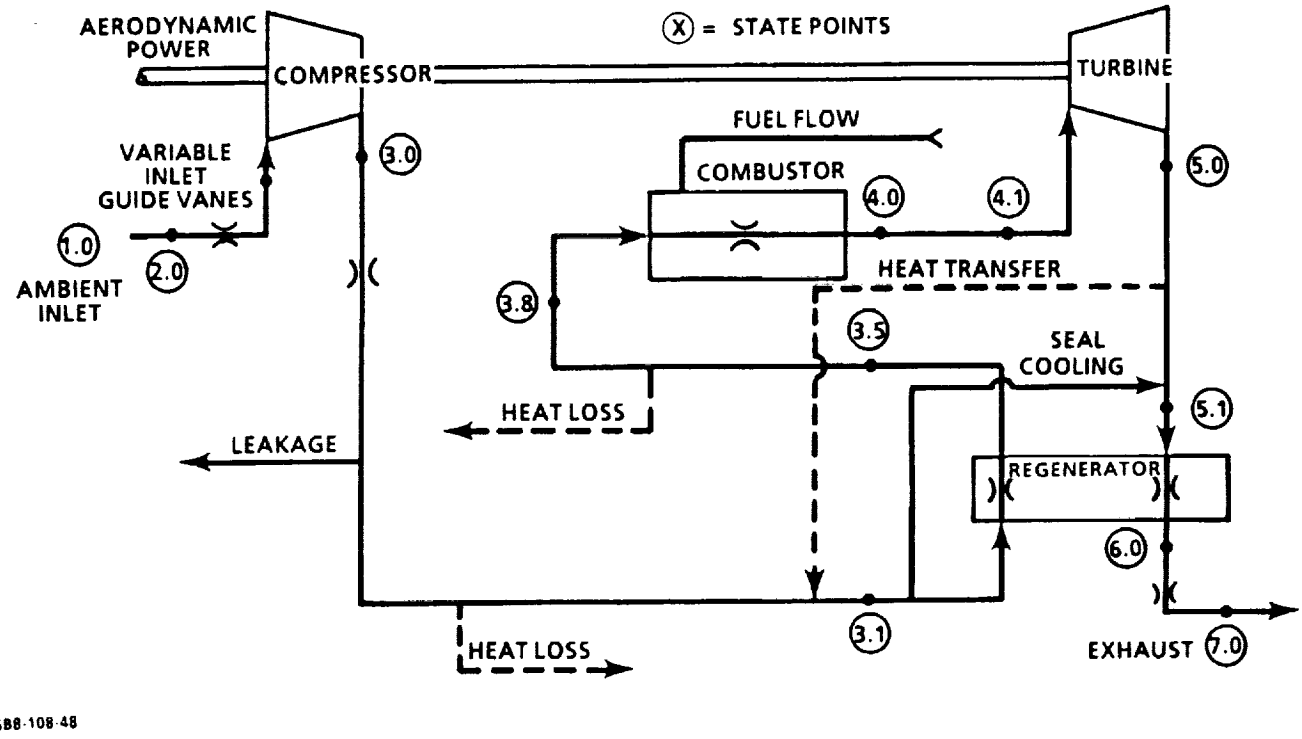

Figure 11. AGT101 Engine Cycle.

on AGT turbine rig testing, bearing, seals and rotor windage losses were confirmed during rotor dynamics rig testing, and regenerator core performance was predicted based on correlations generated from regenerator shuttle rig testing at Ford. The regenerator used in this analysis used a rectangular core matrix with 1200 cells/in^2, 0.0045-inch thick cell walls and uses magnesium aluminum silicate material.

The conditions assumed for the RPD analysis are listed below:

- Standard atmospheric conditions
- Maximum turbine inlet temperature, 2500F
- Maximum shaft speed at maximum power, 100,000 RPM
- Diesel fuel (DF-2) lower heating value of 18,360 Btu/lb
- Maximum regenerator rotational speed of 23.3 RPM

- o Allowable leakage
  - 3.2 percent combined regenerator seal leakage
  - 0.5 percent overboard leakage
  - 0.5 percent regenerator seal cooling flow
- o Compressor surge margin, 5 percent

The curve in Figure 12 shows how the minimum specific fuel consumption for the ATTAP RPD varies with the output shaft horsepower at sea level standard conditions. This curve was derived by analyzing the entire map of engine speeds and inlet guide vane positions using the maximum allowed operating temperatures. The charts in Figures 13 through 17 show the cycle state point conditions for sea level idle, highway cruise, flat-rated, maximum power, and high altitude flat-rated operating conditions.

The flat-rated condition is that which produces 100 aerodynamic horsepower. This power level was determined as the maximum power required in the RPD vehicle to achieve the acceleration and drivability goals. The RPD engine has the capability of producing this

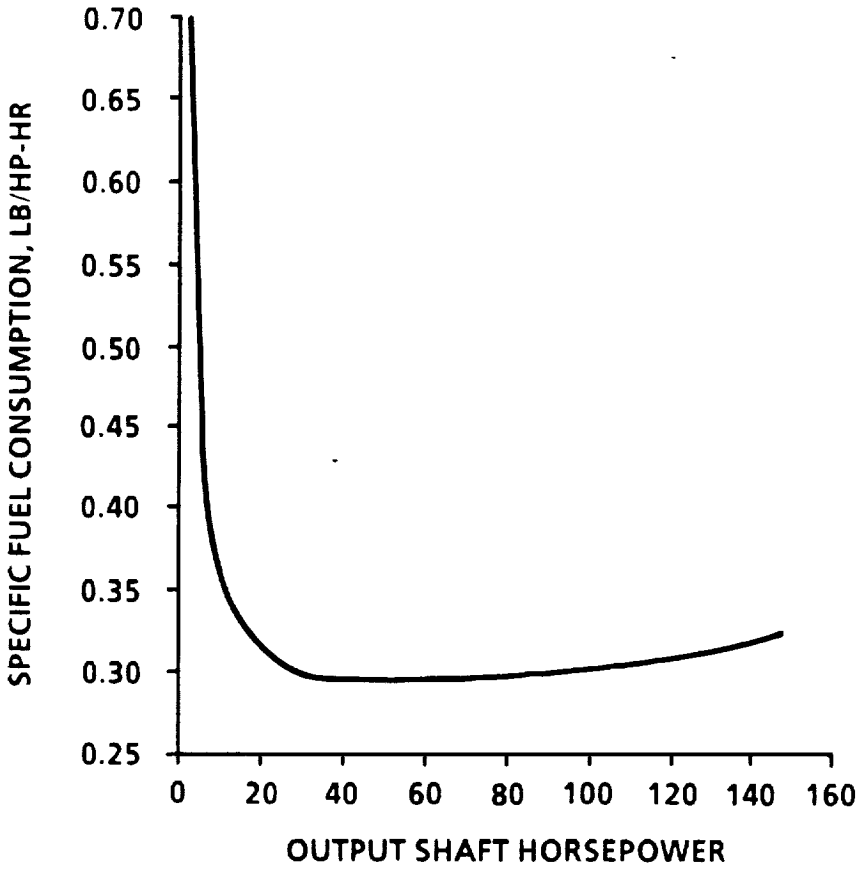

Figure 12. The AGT101 RPD Produces an Outstanding Fuel Economy.

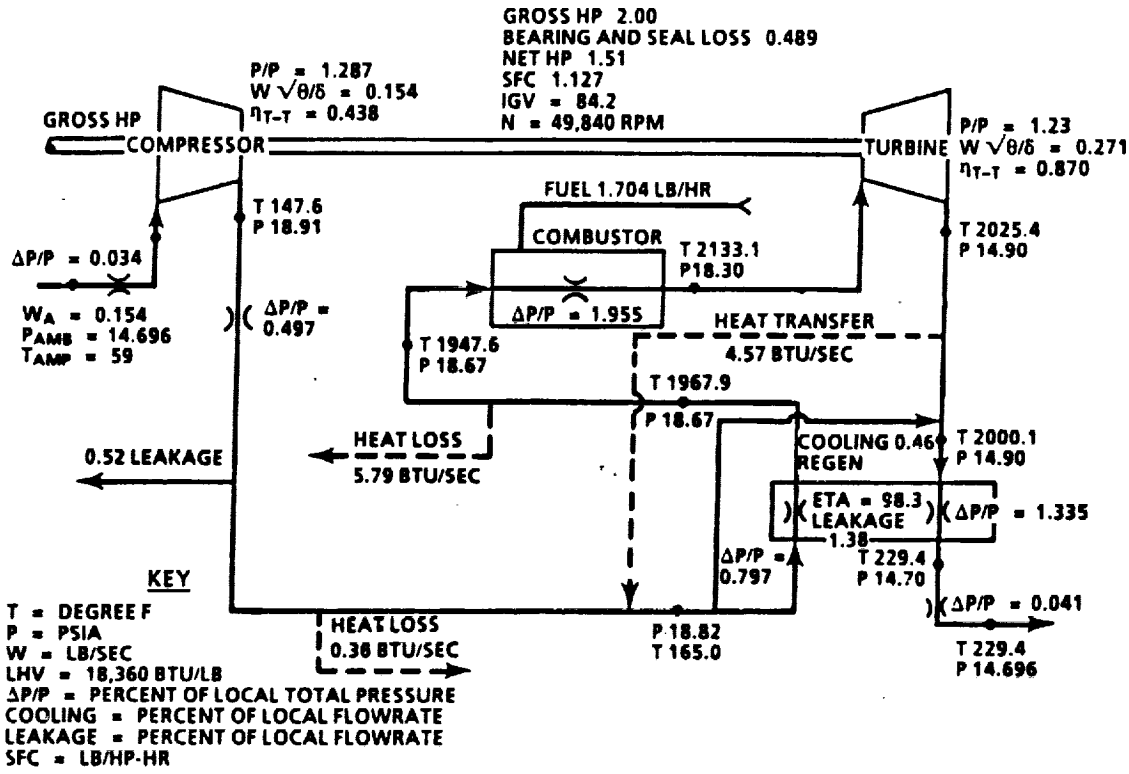

Figure 13. AGT101 Performance, Sea Level, Idle.

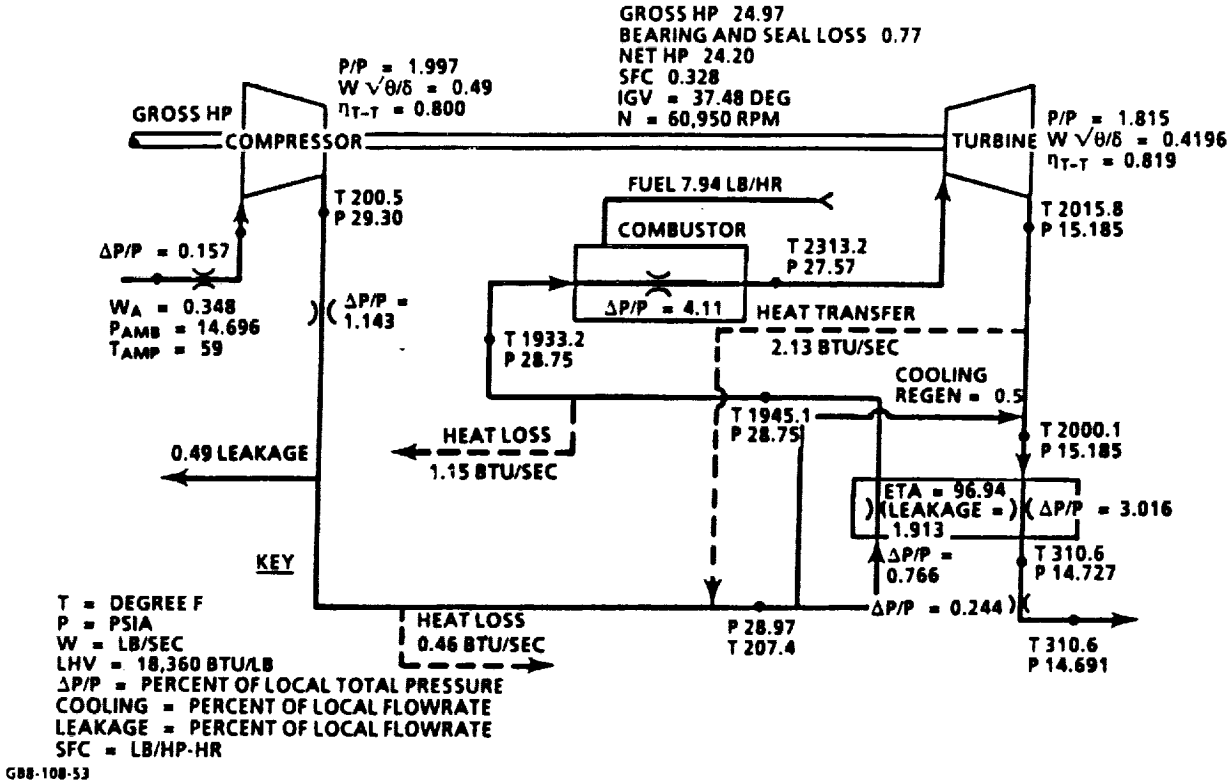

Figure 14. AGT101 Performance, Sea Level, Cruise (55 mph).

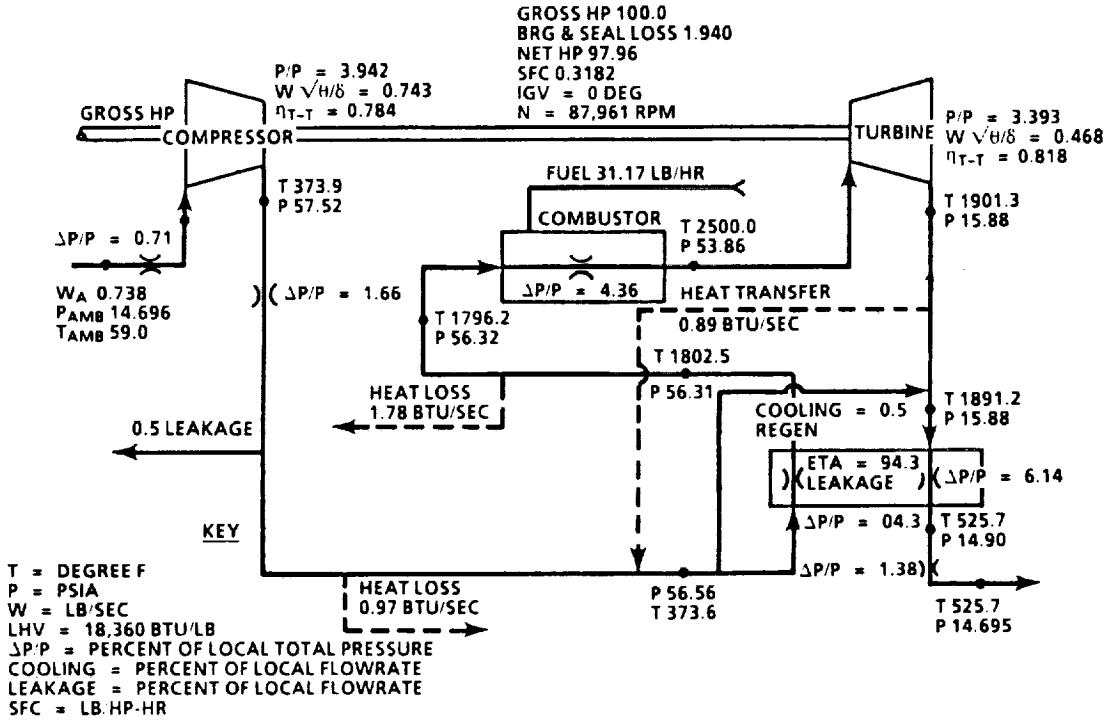

Figure 15. AGT101 Performance, Flat Rated, Sea Level.

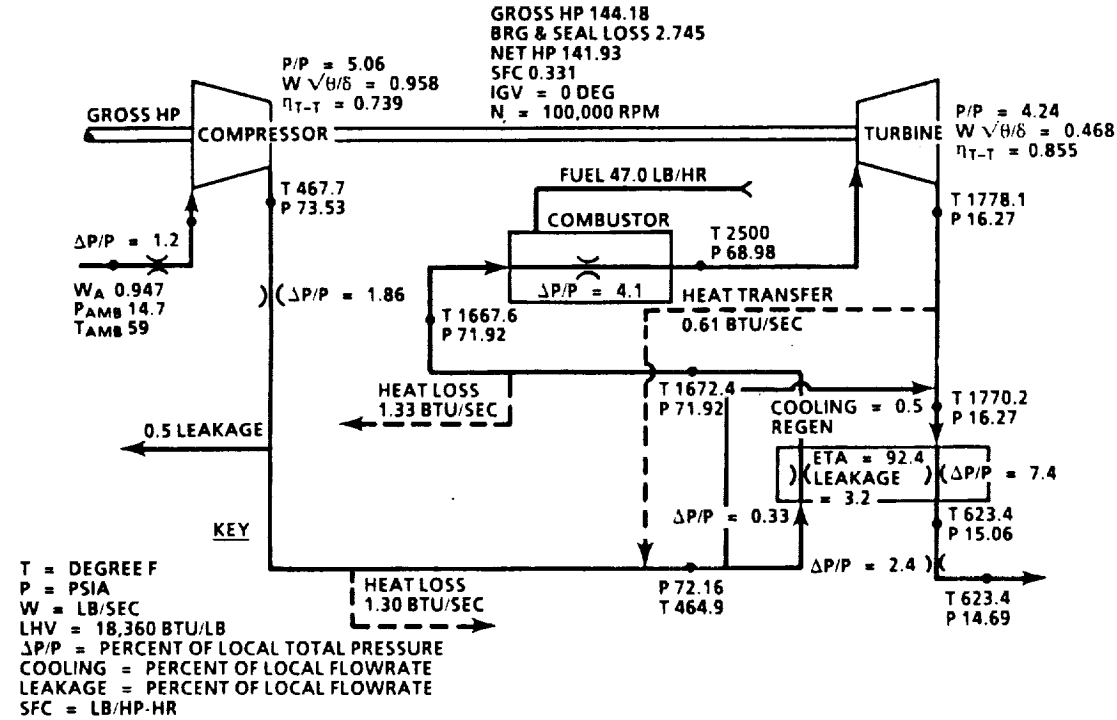

Figure 16. AGT101 Performance, Maximum Power, Sea Level.

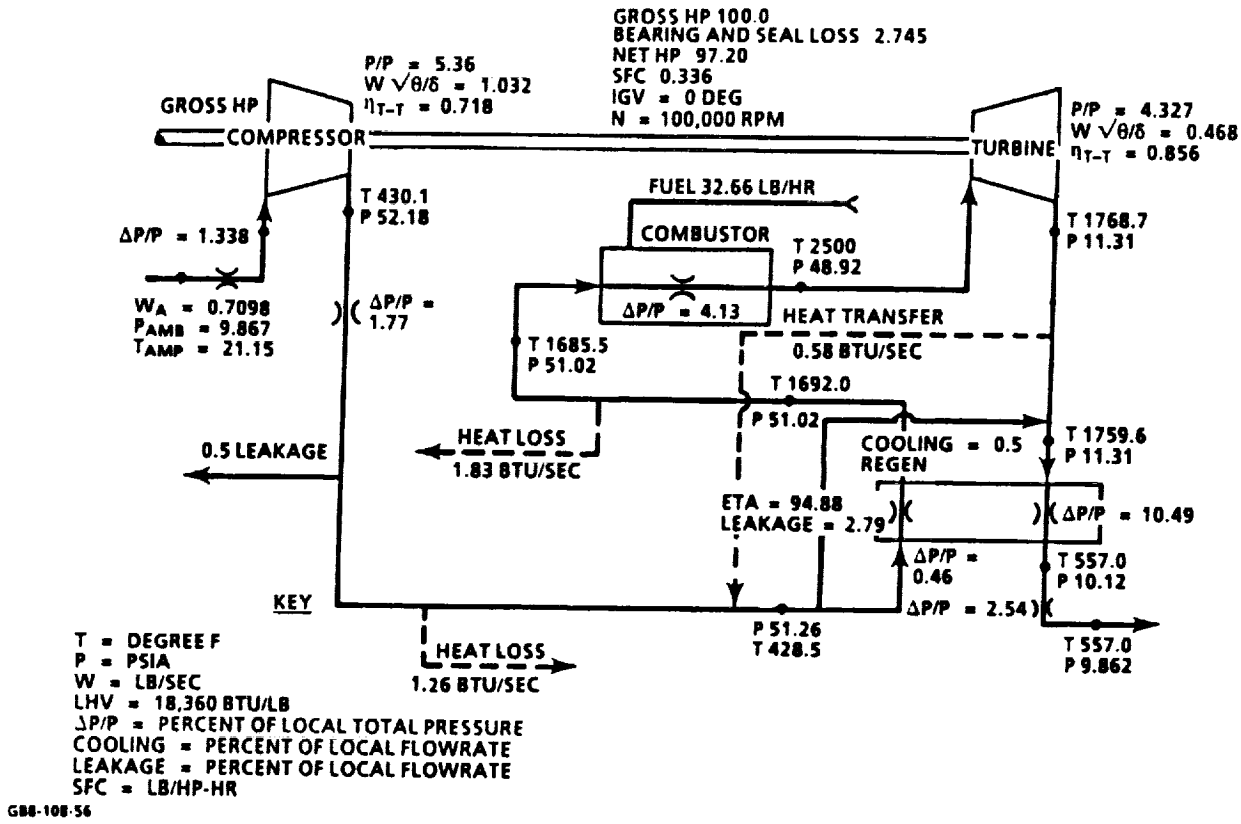

Figure 17. AGT101 Performance, Maximum Power, 10,615 Feet.

power level at altitudes up to 10,615 feet as shown in the curve in Figure 18.

With these most efficient operating conditions defined, the mission analysis determines how the engine operates in the vehicular installation. The schematic in Figure 19 defines the RPD vehicle with the power losses associated with the vehicle and accessories. Assumptions made during the analysis, based on the work performed during AGT101 are listed below:

- Vehicle gross weight, 3000 lb
- Vehicle frontal area, 21.7 sq ft
- Drag coefficient, 0.358
- Effective tire radius, 0.9806 ft
- Wheel and tire polar moment of inertia, 47.9 in-lb/sec^2
- Final drive ratio, 3.08
- Engine polar moment of inertia, 0.00724
- Ford 4-speed automatic overdrive transmission with variable stator torque converter

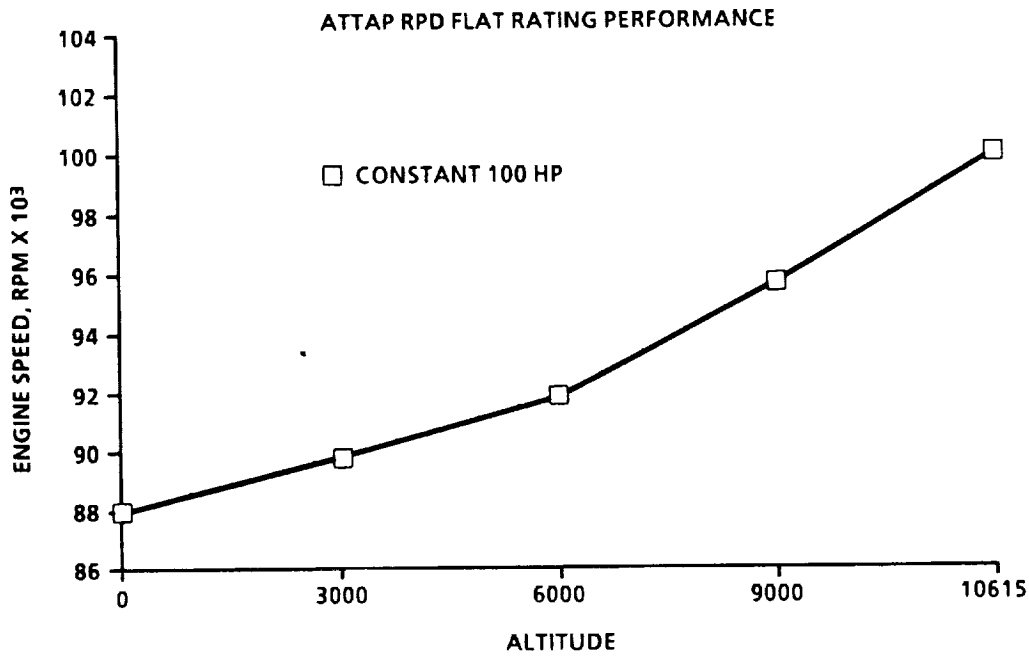

GB8-108-51

Figure 18. Flat Rating Provides Consistent Power Up to 10,000 Feet Altitude.

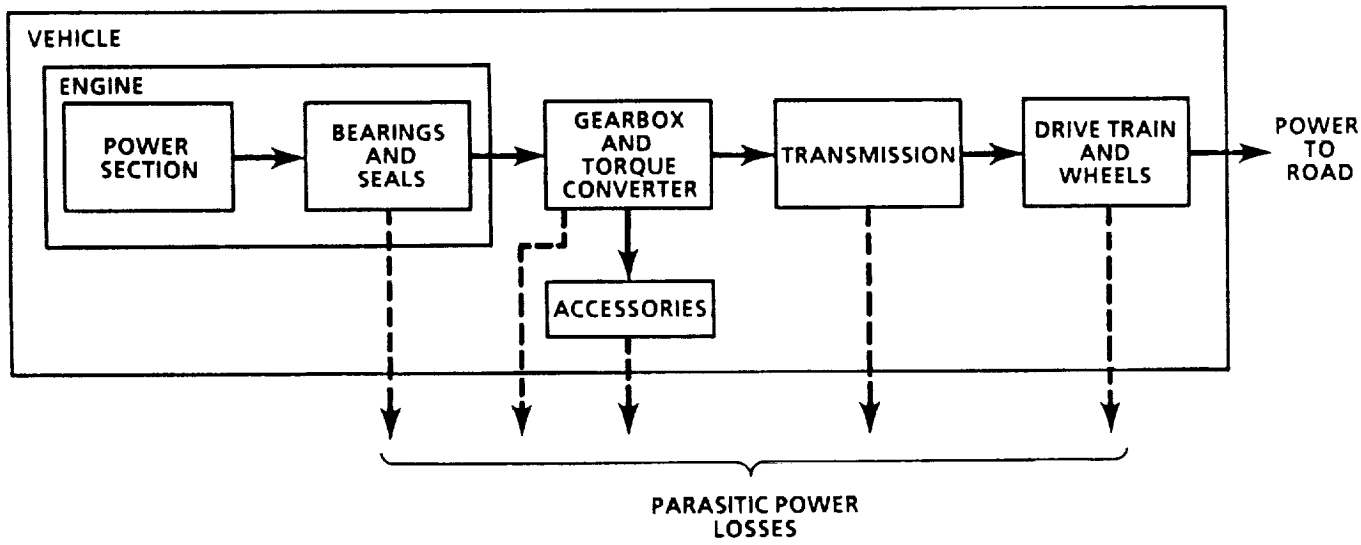

GB8-108-43

Figure 19. The RPD Simulates a Vehicular Installation.

The analysis was enhanced by using available test data where appropriate. Tires rolling resistance data was provided by Ford during the AGT, torque converter characteristics were provided from tests performed early in the AGT project. Power consumption of other accessories and auxiliaries are listed in Table 5 based on input from Ford.

Drivability requirements were supplied by Ford during AGT according to what they felt the consumer would accept.

- Engine start in 10 seconds
- Vehicle accelerates 8 feet in 2 seconds from a standing stop

TABLE 5. ACCESSORIES AND AUXILIARIES POWER ABSORBED

I	Auxiliary (hp Req.)	$\%N_E$	100	90	80	70	60	50
	Oil Pump (Engine Only)		0.25	0.21	0.18	0.14	0.10	0.07
	Fuel Pump		0.20	0.18	0.16	0.14	0.12	0.10
	Regenerator Drive		0.51	0.44	0.36	0.28	0.21	0.13
	Alternator (40A-1/2 Load)		0.80	0.77	0.74	0.70	0.65	0.60
	Oil Cooling Fan		0.15	0.12	0.10	0.07	0.05	0.04
	Total		1.91	1.72	1.54	1.33	1.13	0.94
II	Accessories (hp Req.)							
	Power Steering (Starter Ahead)		0.43	0.39	0.34	0.28	0.25	0.20
	A/C (Declutched)		0.25	0.23	0.20	0.18	0.15	0.13
	Total		0.68	0.62	0.54	0.46	0.40	0.33
	For Performance and Economy Projections							
	Total Accessories and Auxiliary (hp Req.)		2.59	2.34	2.08	1.80	1.53	1.27

During the AGT, a criteria for vehicle acceleration from a standing stop to 60 miles/hour in less than 16 seconds was considered. However, Ford had determined that "drivability" was more accurately characterized by low speed acceleration. It should be noted that the AGT RPD vehicle which meets the 8 foot in 2 second acceleration criterion also meets the originally proposed 16 second to 60 mph criterion.

These criteria were used in the mission analysis with the cycle performance data and the vehicle installation to establish the projected fuel economy of the RPD vehicle. The curves in Figure 20 show how drivability influences the fuel economy over the CFDC. Since a significant portion of the CFDC is spent with the vehicle at a standing stop, idling, the idle speed is an important parameter in the fuel consumed during the CFDC. Vehicle acceleration is also affected by the idle speed due to rotor inertia and the effect of low rotor speeds on thermodynamic cycle efficiency. This analysis shows that the RPD vehicle can achieve the 8 foot in 2 second drivability goal and the CFDC mileage goal of 42 miles per gallon with an engine idle speed of 49,840 RPM.

3.3 Reference Powertrain Design Cost Analysis

There was no activity in Reference Power Train Design Cost Analysis during the period of this report. RPD Cost Analysis activities are scheduled for the final year of the ATTAP.

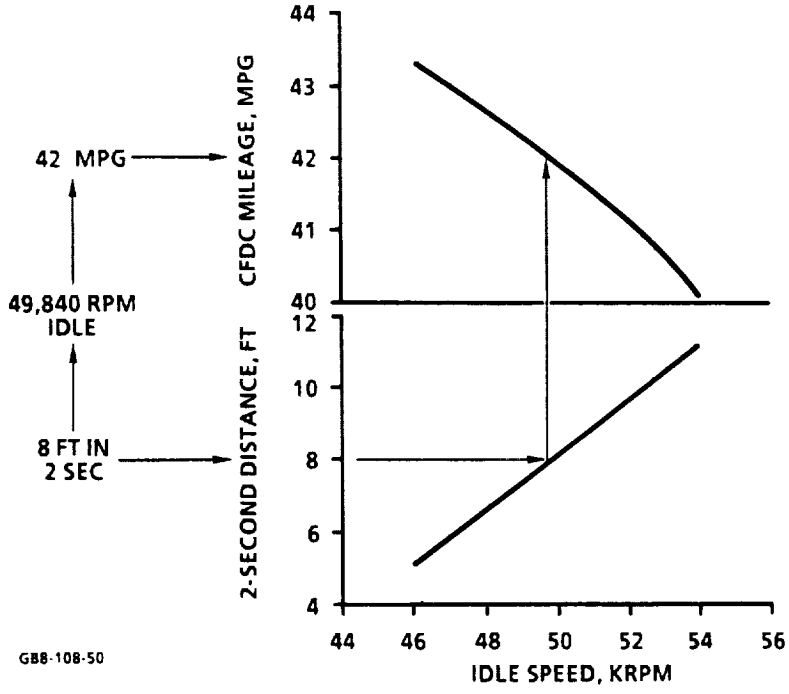

Figure 20. Mission Analysis Uses Drivability Criteria to Determine Fuel Economy.

3.4 Test Bed Engine Design

3.4.1 Turbine Coupling

The function of the turbine coupling, as shown in Figure 21, for the ATTAP RPD engine is to maintain alignment between the ceramic rotor and the titanium compressor. A redesign of this component, as shown in Figure 22, resulted in changing from a single piece design to a two piece design. The old design maintained the axial and radial alignment between these two components by means of an interference fit at the ceramic shaft interface and a Curvic® coupling at the interface with the compressor backface. The interference fit was obtained by heating the titanium coupling on installation to obtain a shrink fit. In this configuration, the interference induced distortion at the curvic teeth causing heavy "heel" contact at this interface. This localized contact caused teeth wear that resulted in poor rotor alignment, which could eventually lead to rotor dynamic problems. Also, the titanium material in the coupling usually degraded during the high temperature exposure required at installation.

The new coupling design reduced the axial distortion at the curvic surface as shown in Figure 23. The axial deformation at the curvic surface previously ranged from 0.6 to 1.8 mils on the old design, whereas the axial deformation on the new design ranged from 0.0 to 0.6 mils. In addition, the new coupling design increased the operating temperature capability of this assembly.

An additional analysis was performed on the turbine coupling with respect to the assembly procedure for installing the coupling onto the ceramic turbine shaft. This procedure raised questions regarding the effect of high temperature exposure on the properties of the titanium coupling. The analysis indicated that the peak temperature required to shrink the new design coupling onto the ceramic shaft would exceed 1000F. Exposure to this temperature would probably encourage oxygen absorption in the titanium and cause embrittlement. Therefore, a press fit was evaluated for the coupling installation. Preliminary analysis indicated that without geometrical modifications, the coupling stress could get as high as 84.0 ksi and the ceramic shaft stress as high as 42.9 ksi compression during installation. However, by slightly changing the geometry of the ceramic shaft and tapering the lead-in zone, as shown in Figure 24, the maximum coupling stress could be reduced to 72.7 ksi and the ceramic shaft stress could be reduced to 21.3 ksi compression. A tapered lead-in was therefore included in the new turbine coupling design.

ORIGINAL PAGE
BLACK AND WHITE PHOTOGRAPH

GB8-108-2

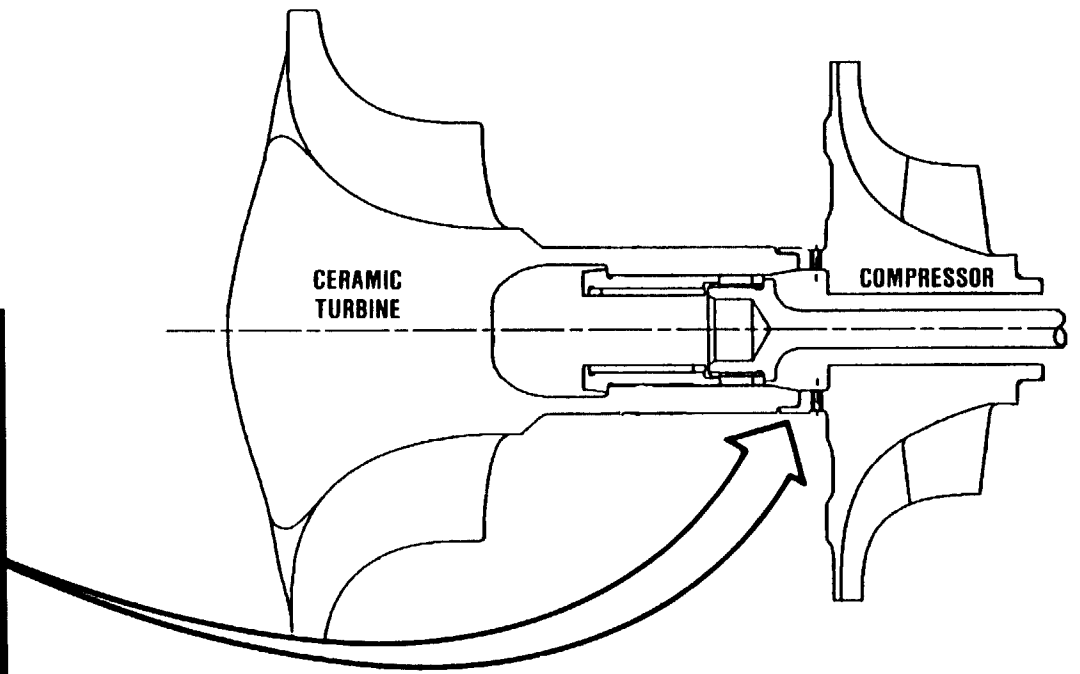

Figure 21. AGT101 Test Bed Engine Rotating Group.

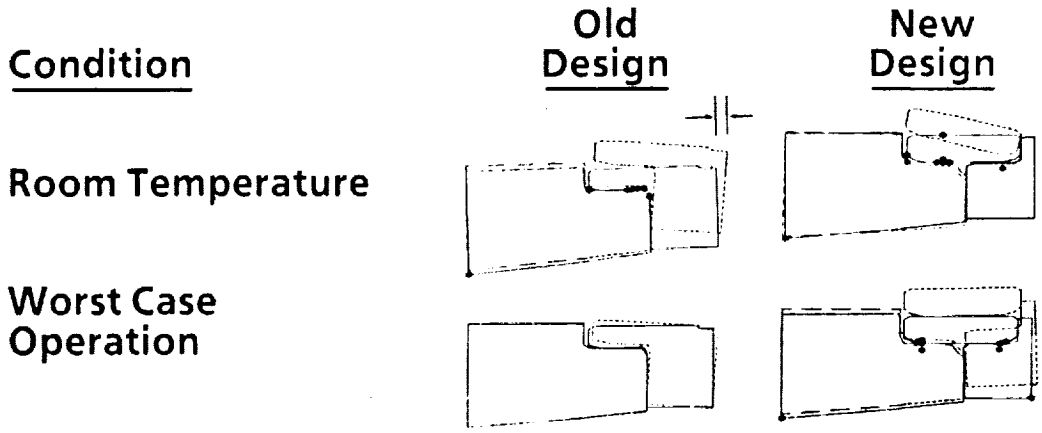

GBB-108-7

Figure 22. New Design Turbine Coupling Reduces Distortion.

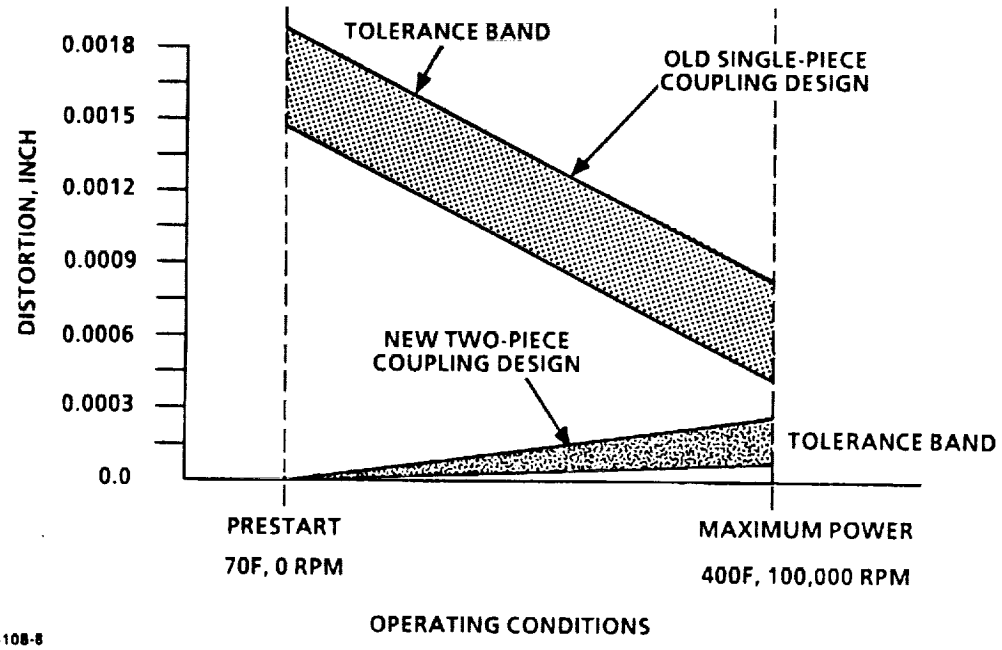

GBB-108-8

Figure 23. Curvic Coupling Axial Distoration Comparison.

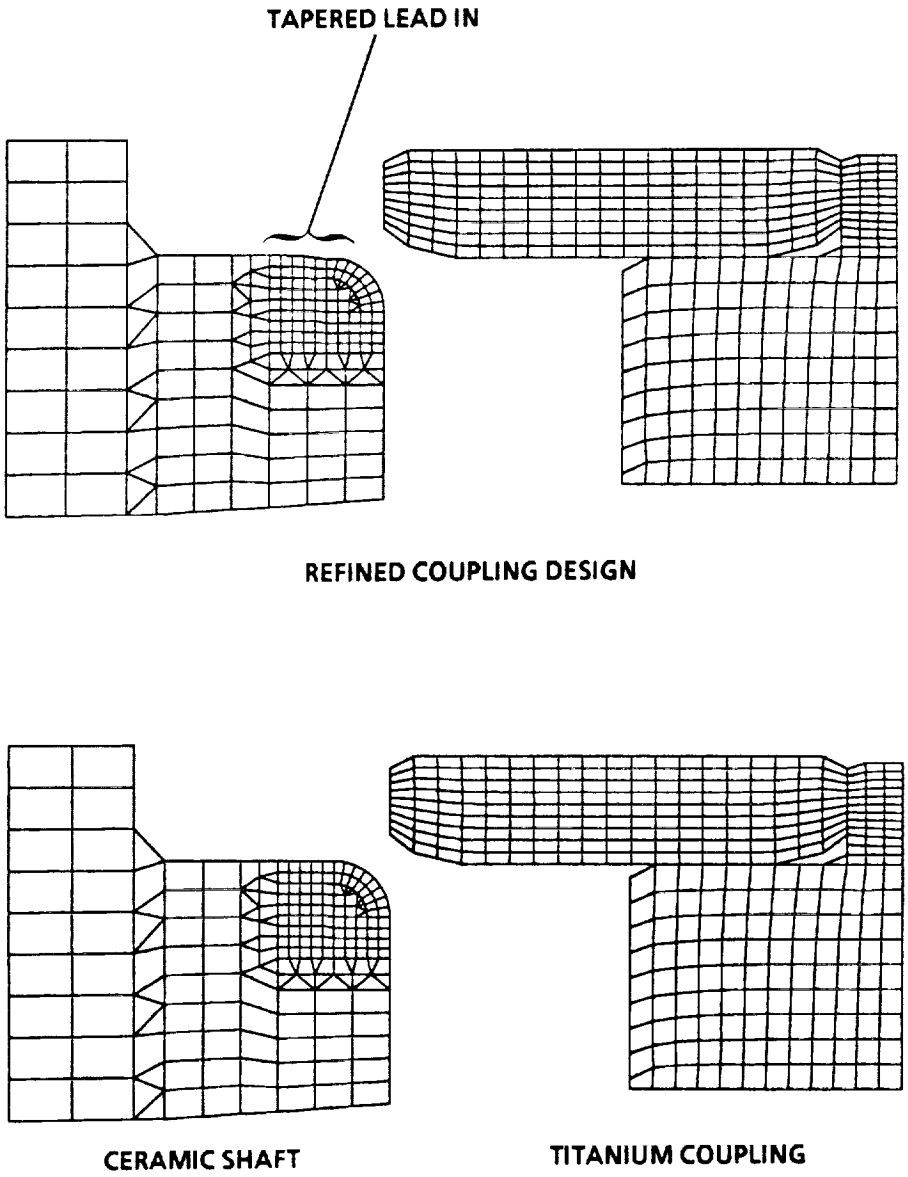

Figure 24. Stress Models for Turbine Coupling Analysis.

3.4.2 Ceramic Thermocouple Retainer

A resilient retainer was designed for a ceramic sheathed $T_{4.1}$ thermocouple. The design in Figure 25 uses an O-ring to retain the cold end of the ceramic sheathed thermocouple. The seal is caged between a "B" nut and the port fitting. The geometry of the port fitting is such that a positive stop is provided for the nut while controlling the compression on the seal. With ample clearance provided between the ceramic sheath and the adjacent engine structure, and a firm resilient support for the cold end of the thermocouple assembly, the hot end of the thermocouple/spacer assembly may translate while the cold end pivots in the resilient mount. Thus, excessive bending loads are avoided in the ceramic sheath.

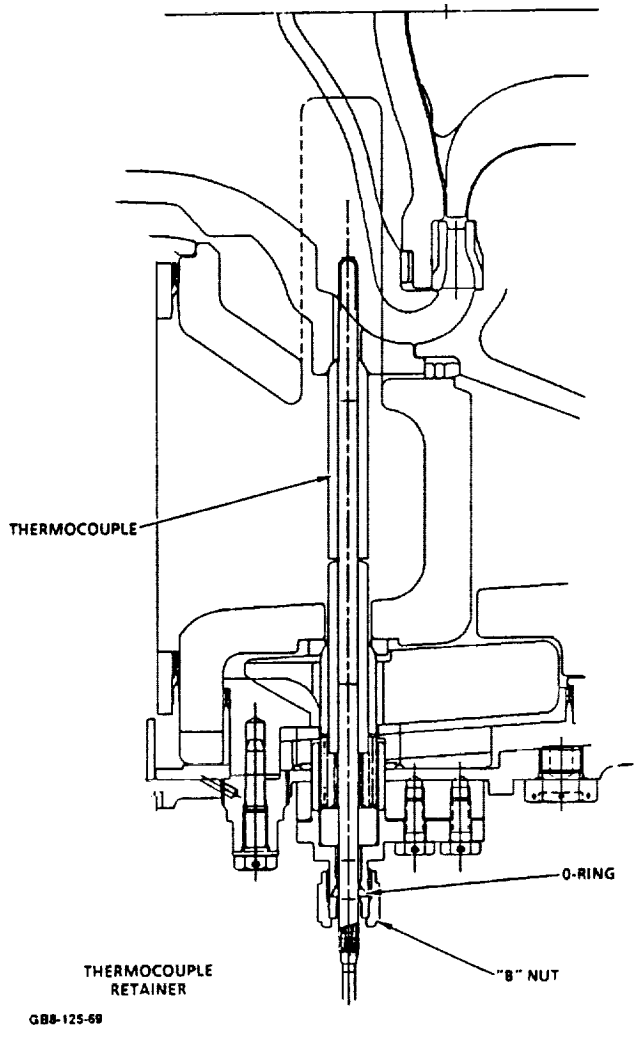

Figure 25. Ceramic Thermocouple Retainer Design.

3.4.3 Ring Support Housing Assembly

A redesign of this assembly has been made to increase the durability of the engine test bed. A problem with the previous design, described in Figure 26, has involved the loss of tension in the bolts which secure the ring support housing to the engine compressor housing during operation at turbine inlet temperatures of 2000F and higher. This occurs as the ring support housing in the metallic engine grows thermally into the compressor housing eliminating the diametrical clearance between the two parts. As a result, the radially oriented bolts which retain the housing are unloaded, and a gas leak forms under the bolt heads. When this occurs, a potential is created for the housing to shift or tilt relative to the compressor housing and the regenerator system. There have been no ceramic failures attributed to this condition.

A retaining system had to be designed which solved both of these concerns. The configuration shown in Figure 27 is a modification of the current engine configuration that provides a set of sealed shoulder bolts acting as radial pins to restrain the axial movement of the ring support housing under all conditions. Since these bolts are threaded to and sealed at the compressor housing the leak is eliminated. This feature was incorporated into the engine assembly design.

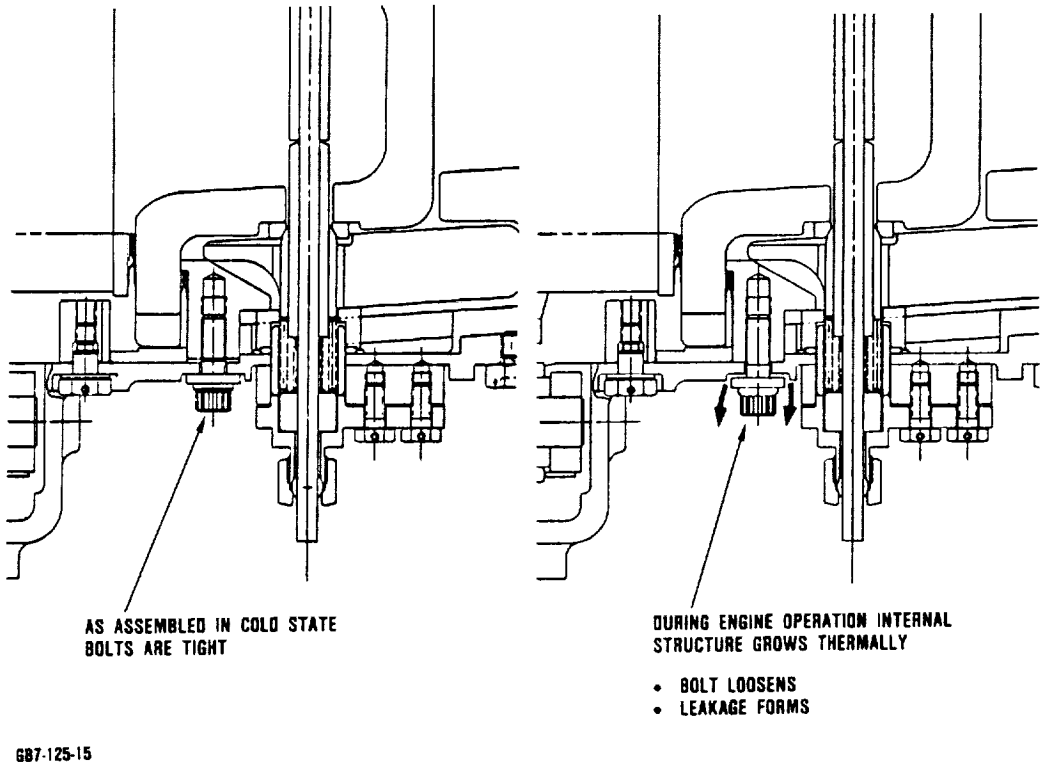

Figure 26. Ring Support Housing Bolts Loosened During Engine Operation.

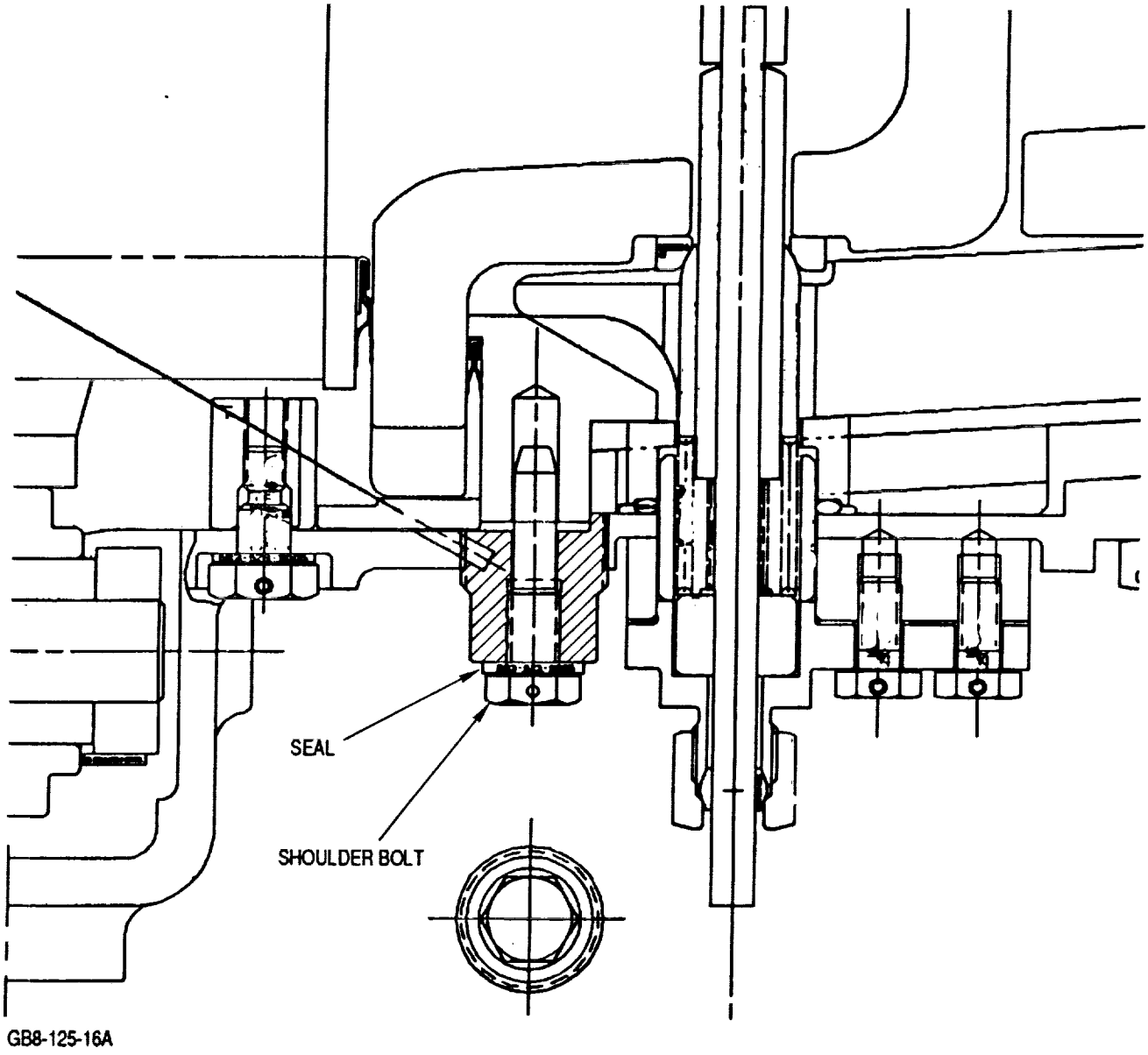

Figure 27. Improved Ring Support Housing Configuration Features Shoulder Bolts Threaded To Compressor Housing.

3.4.4 External Foil Bearing Cooling Air

The need for external foil bearing cooling air was reviewed and it was decided to discontinue its use. The foil bearing external cooling air consisted of cool, pressurized air supplied from the laboratory facility. The cooling air was ducted into the engine through the compressor gas flow path, along the turbine discharge

gas flow path to the foil bearing housing. This air cooled the foil bearing carrier, thereby controlling the changes in the foil bearing sway space due to thermal influences from within the engine. Studies performed during the AGT101 program indicated that external cooling air actually had a minimal impact on the foil bearing sway space. This characteristic is described in Figure 28. The absence of external cooling air will result in a decrease of only 0.5 mil over the range of engine speed conditions. The external cooling air feature was not deleted at that time because there was no evidence that it harmed the engine.

In another review, the effect of this cooling air on the turbine shaft was considered to be slightly detrimental due to the steep thermal gradient imposed on the shaft near where the cooling air exits the foil bearing housing and sprays the shaft surface.

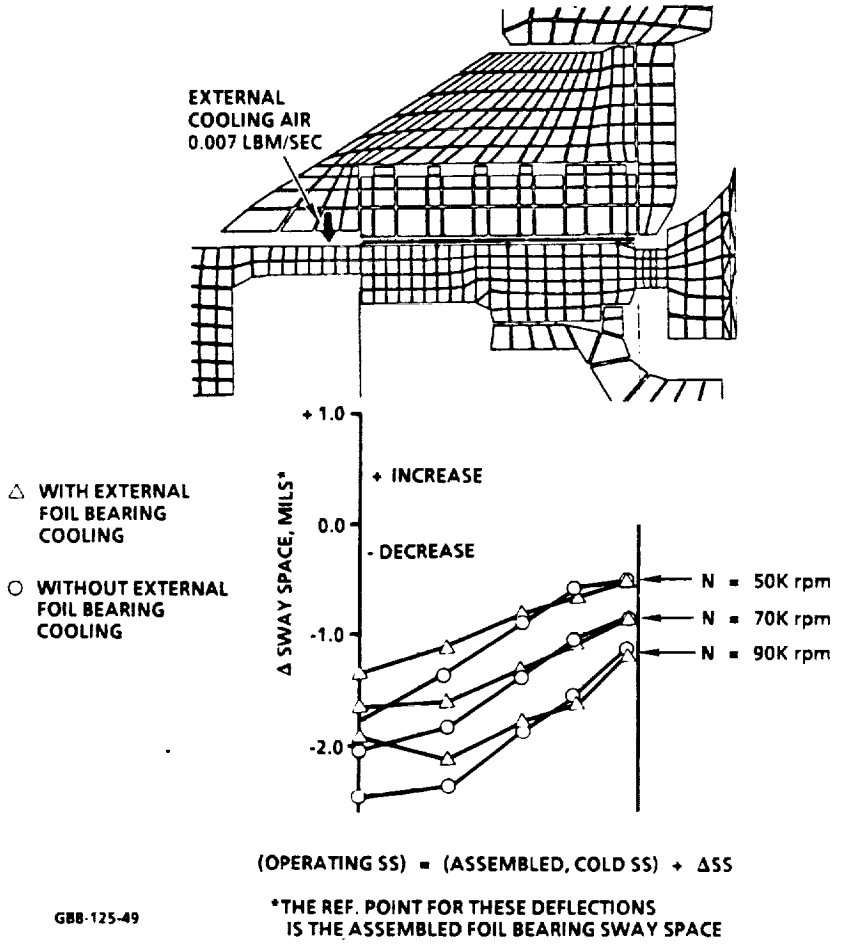

Figure 28. Foil Bearing Sway Space Change for Different Steady-State Operating Points.

The use of this cooling air and transfer tubes presented a potential leak path for the compressor discharge air to the turbine discharge flow path. A significant leak at the cooling air tube could impose an additional thermal stress field on the turbine inner diffuser and increase the risk of fracture in that component.

The external foil bearing cooling air tubes and transfer tubes also make the engine assembly more complex. The transfer tubes must be shimmed to ensure a proper seal, and the cooling tubes interfere with the preformed insulation, requiring additional insulation fitting. In engine operation, the external cooling air is an additional air line which must be set and monitored.

Based on preceding description, the decision was made to delete the cooling air tubes from the metallic engine assembly and plug the holes in the compressor backshroud and housing.

3.4.5 Flow Path Insulation

Improvements were made to improve the flow path insulation used in the ATTAP engine testbed at the turbine discharge zone. The previous material was not stable at engine operating conditions, causing cracks to occur and setting up the potential to generate debris within the engine.

Four alternate insulation materials were evaluated for dimensional stability following 100 hours of exposure to 2000F conditions. Only one insulation, PROCAL HT-280, exhibited less than 1 percent change in dimension and weight loss. The other three candidates all showed 4 to 30 percent shrinkage and 5 to 10 percent weight loss following the 100 hours exposure to 2000F condition. This data on weight loss and dimensional stability is shown in Figures 29 and 30, respectively.

As a result of this study a material change to PROCAL HT-280 was incorporated into the engine testbed design for the insulation in four locations.

3.4.6 Combustor Cap

A thermal model of the existing combustor section of the engine was completed. This model included all the components inboard of the exhaust housing/combustor cap from the fuel nozzle to the transition duct. Steady-state cycle points have been analyzed.

3.4.7 Combustor

Work relative to the combustor during this report period was confined to rig improvements as discussed in Section 6.2.5.

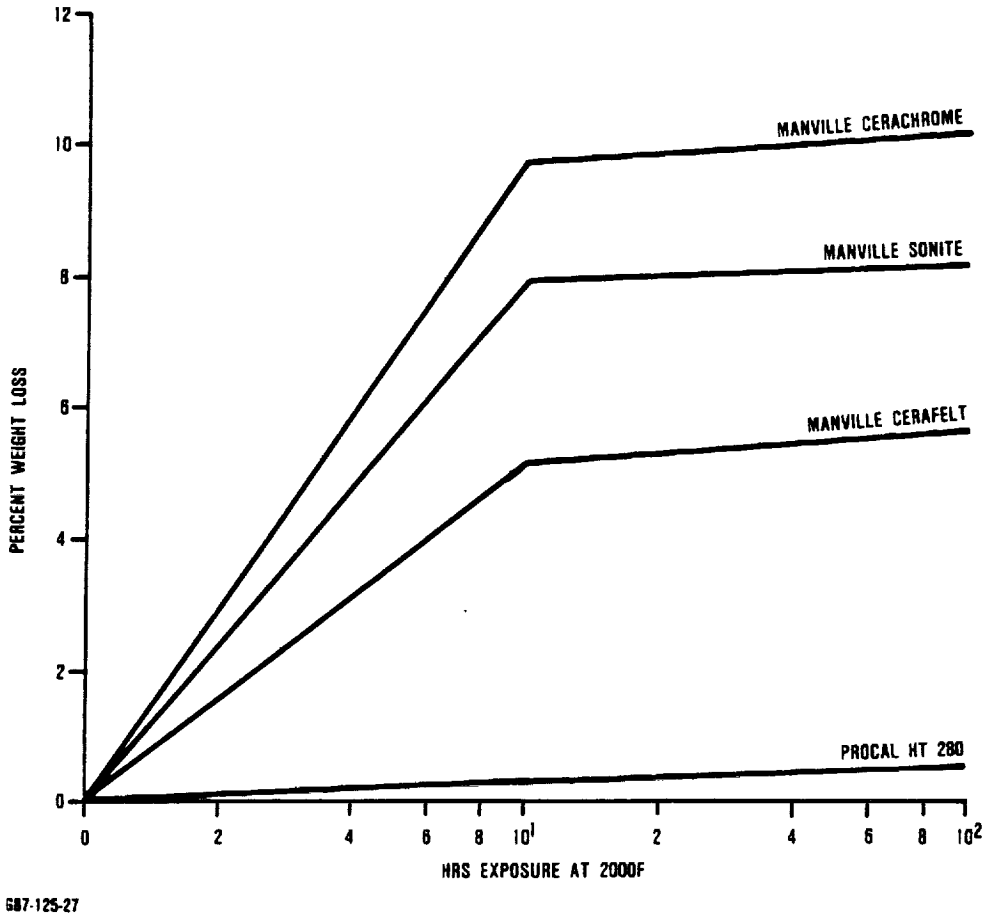

Figure 29. Insulation Weight Loss Comparison.

3.4.8 Turbine Inlet Particle Separator

As a result of the turbine rotor failure by foreign object damage (FOD) during testing under AGT, concern was raised regarding the susceptibility of the rotor and stators to this type of risk. Development of a Turbine Inlet Particle Separator (TIPS) was initiated in the previous AGT program to address this concern. Because carbon generated by the combustor is a likely source of the FOD, the designs considered have concentrated in the area downstream of the combustor and upstream of the turbine stators.

During the reporting period, design/development of the ramp/splitter TIPS configuration shown in Figure 31 continued. Particle separation testing during the previous reporting period revealed that the poor performance of the configuration was a result of turbulence inside the trap. Flow visualization testing using lamp black was employed to determine the flow patterns inside the trap. Figure 32 shows the swirl pattern inside the ramp/splitter configuration and Figure 33 is a cross section of the geometry modifications made to decrease turbulence. This improved configuration retained all particles which were separated and shifted

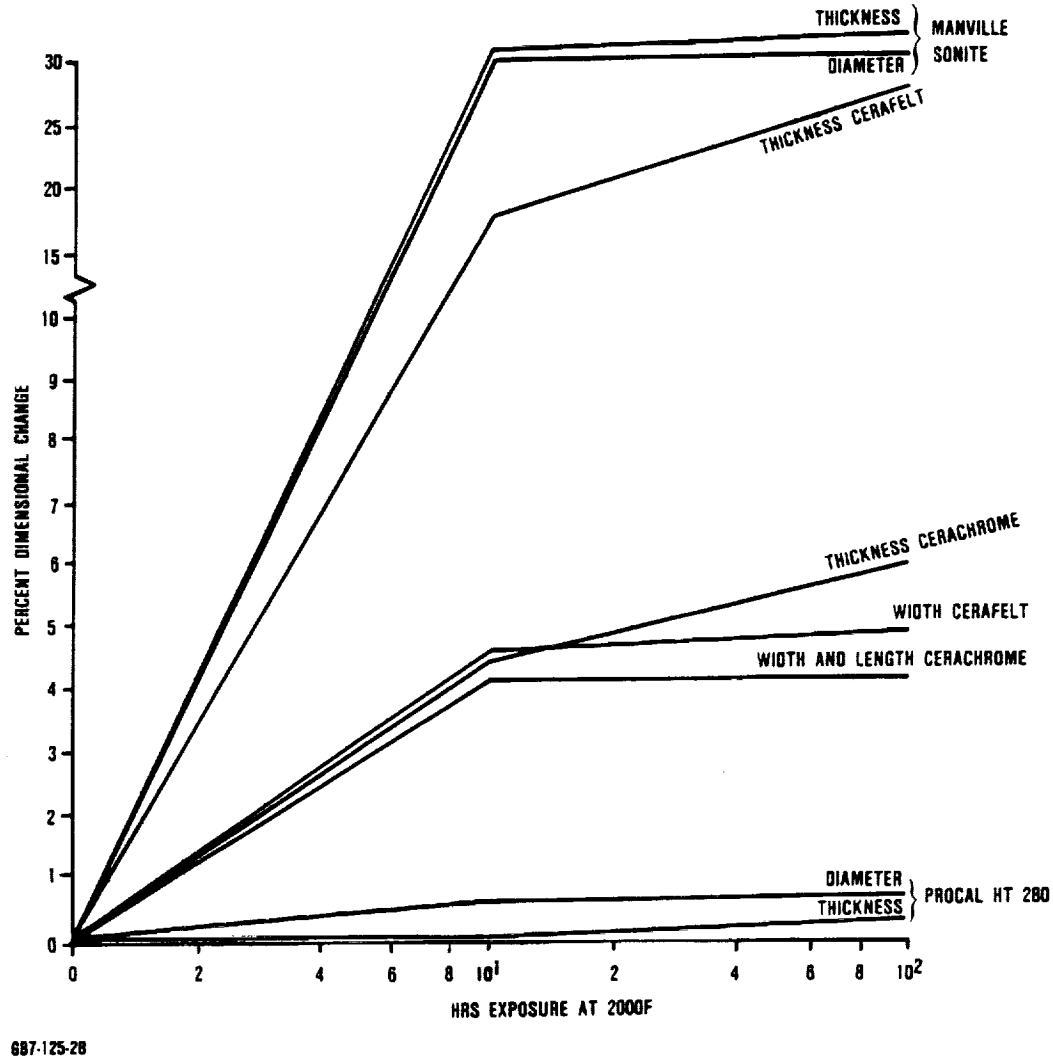

Figure 30. Insulation Dimensional (Stability Comparison).

emphasis from retention to separation performance. To improve separation performance, Taguchi methods were employed, which indicated the critical factors in the ramp/splitter geometry. At the end of the period, the configuration shown in Figure 33 demonstrated separation efficiencies between 80 and 90 percent in several tests at flow conditions between idle and maximum power.

During the reporting period, the analysis group began a search to identify a viscous flow code which could be used to model potential particle separator geometries. The search identified the fluid dynamics analysis package (FIDAP), a three dimensional, viscous flow code which will be used to predict flow patterns and determine pressure drop for TIPS configurations. After learning to use the code, the aerodynamics/installations group began modeling the ramp/splitter configuration.

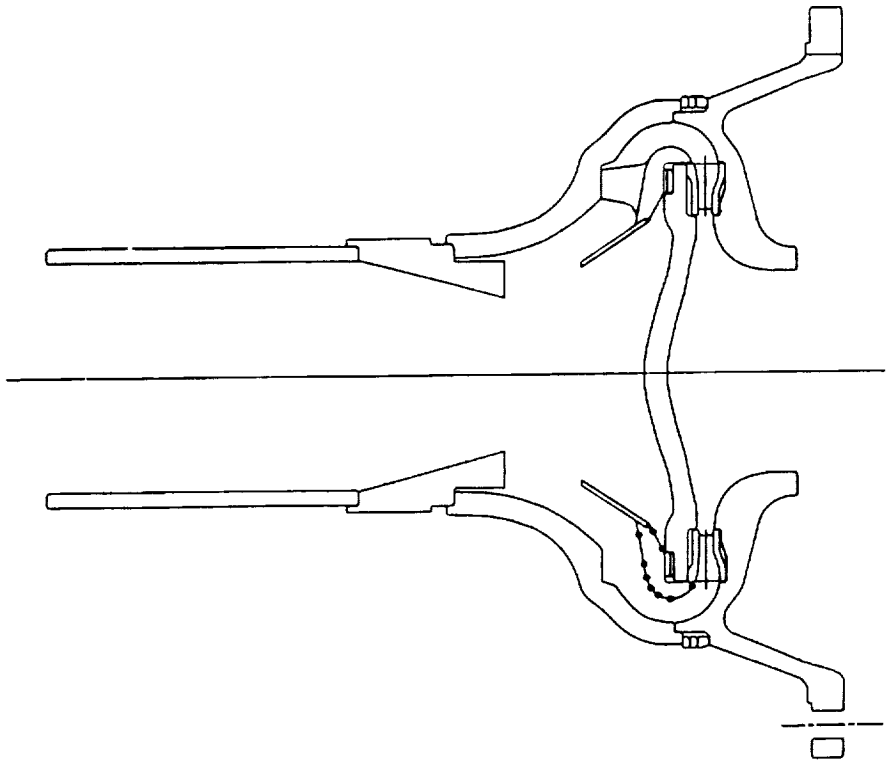

Figure 31. Ramp/Splitter TIPS Configuration.

3.4.9 Regenerator Seal

Seal Analysis

Preliminary results from an elastic stress analysis of the seal crossarm indicate the mechanical forces caused by high pressure difference across the substrate, and friction forces from the core loading were enough to cause a lateral deformation for the crossarm.

Figures 34 and 35 indicate the distorted shape and stress distribution in the crossarm shoe as a result of the core friction and pressure loading. The distorted shape predicted by the model is similar to that noted from the August 1987 test. However, this analysis did not predict the distorted oval shape of the shoe inner periphery that also occurred in the test. An additional radial force on the crossarm was necessary to cause this distortion. This force could have come from the restriction in thermal growth causing friction at the crossarm/C-shoe interface. The curve in Figure 36 shows the crossarm inner-peripheral stress as a function of radial load. Note that at the 2000F operating temperature, creep may be a significant factor in the yielding of the crossarm at loads above 50 lbs.

Figure 32. Lamp Black Illustrates Flow Patterns in the Particle Trap.

Preliminary results from the seal C-shoe analyses indicate the external mechanical forces alone might not have been great enough to cause the distortion of the C-shoe. However, deformation could have resulted from the restriction of thermal growth through a pinching effect with the crossarm or by the pins in the alignment ring.

Materials Study - Regenerator Seal Shoe/Coating

Further review of alternate metallic material candidates was conducted for the hot-side regenerator seal shoe substrate. The original material used for this component was Inconel 601 (IN601), and was found to have insufficient strength at the 2000F operating temperature of the hot-side seal. A preliminary review indicated

ORIGINAL PAGE
BLACK AND WHITE PHOTOGRAPH

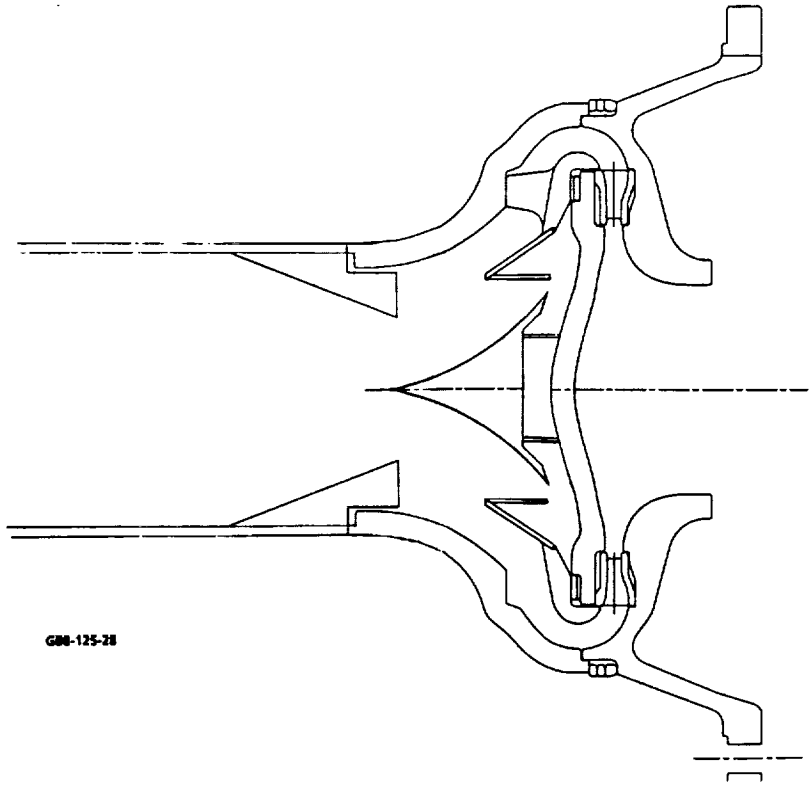

Figure 33. Evolved Version of the Ramp/Splitter TIPS.

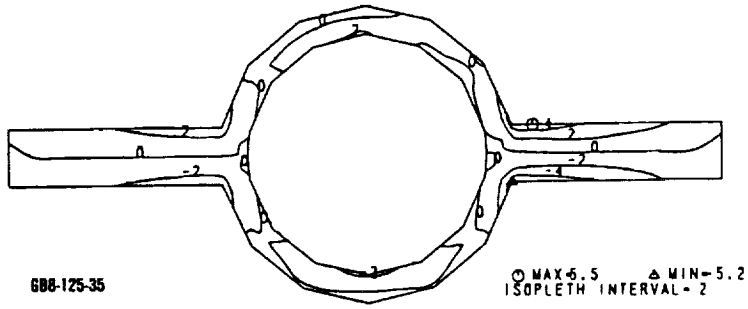

Figure 34. Regenerator Seal Crossarm Pressure and Force Analysis.

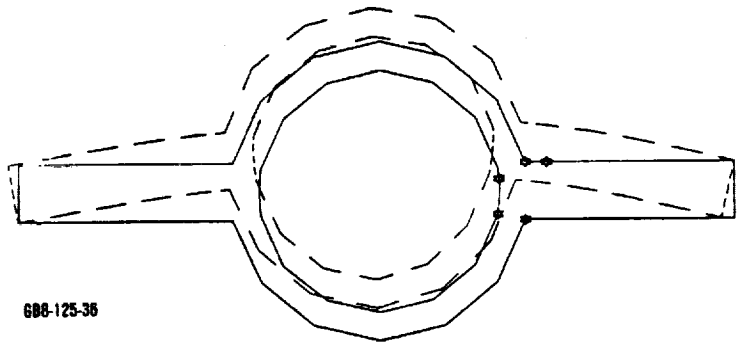

Figure 35. Regenerator Seal Crossarm Distortion.

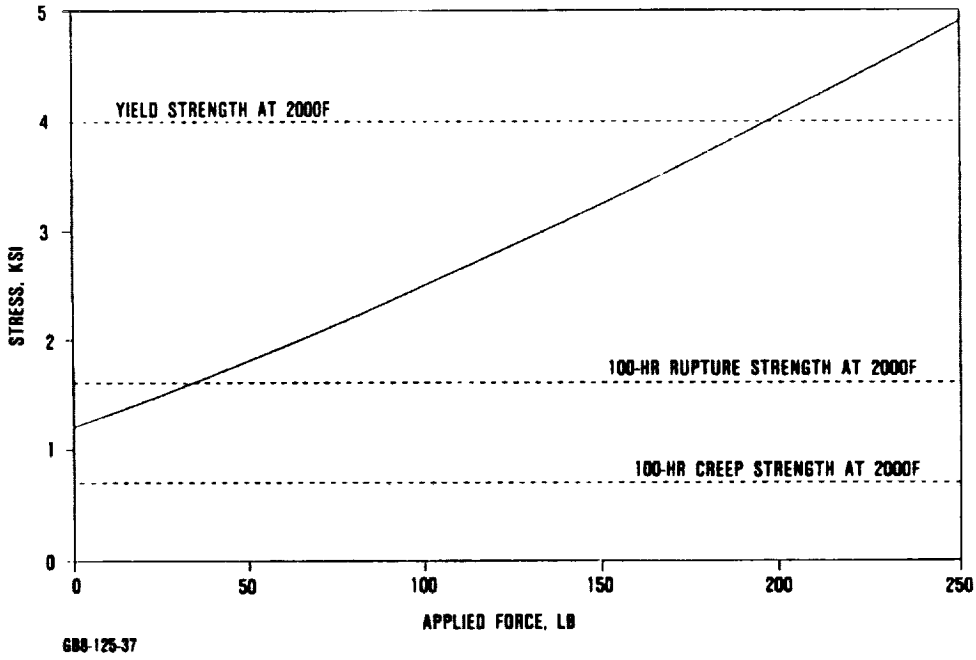

Figure 36. Radial Force to Initiate Oval Distortion.

that Haynes Alloy 230 (HA230) might be an acceptable alternate material because the specification literature indicated a two to three fold increase in 2000F yield strength over IN601. Inco MA956, an oxide dispersion strengthened iron base alloy was also selected as a candidate due to its superior stress rupture properties at 2000F.

The high temperature yield stress rupture strengths of the candidate materials are compared in Table 6.

ORIGINAL PAGE
BLACK AND WHITE PHOTOGRAPH

TABLE 6. PROPERTIES OF SHOE CANDIDATE MATERIALS

Material	Yield Strength, ksi (2000F)	Rupture Strength, ksi (100 hrs at 2000F)
IN601	4.0	1.6
HA230	10.0	2.3 (1900F)
MA956	12.3	8.3

To evaluate compatibility of the candidate substrate materials, specimens were procured consisting of substrate coated with the I-00/I-112 seal coating systems. These specimens were then heat treated at 2000F in air for 1 hour and then examined.

Ten specimens of each material combination were tested. The three specimens in Figure 37 were typical of the results. The IN601 and MA956 specimens both showed coating spallation and the MA956 also showed severe corrosion. The HA230 specimens showed the best compatibility with the coating system of the three candidates. There was only minor substrate oxidation and limited coating disbonding (not enough for coating spallation).

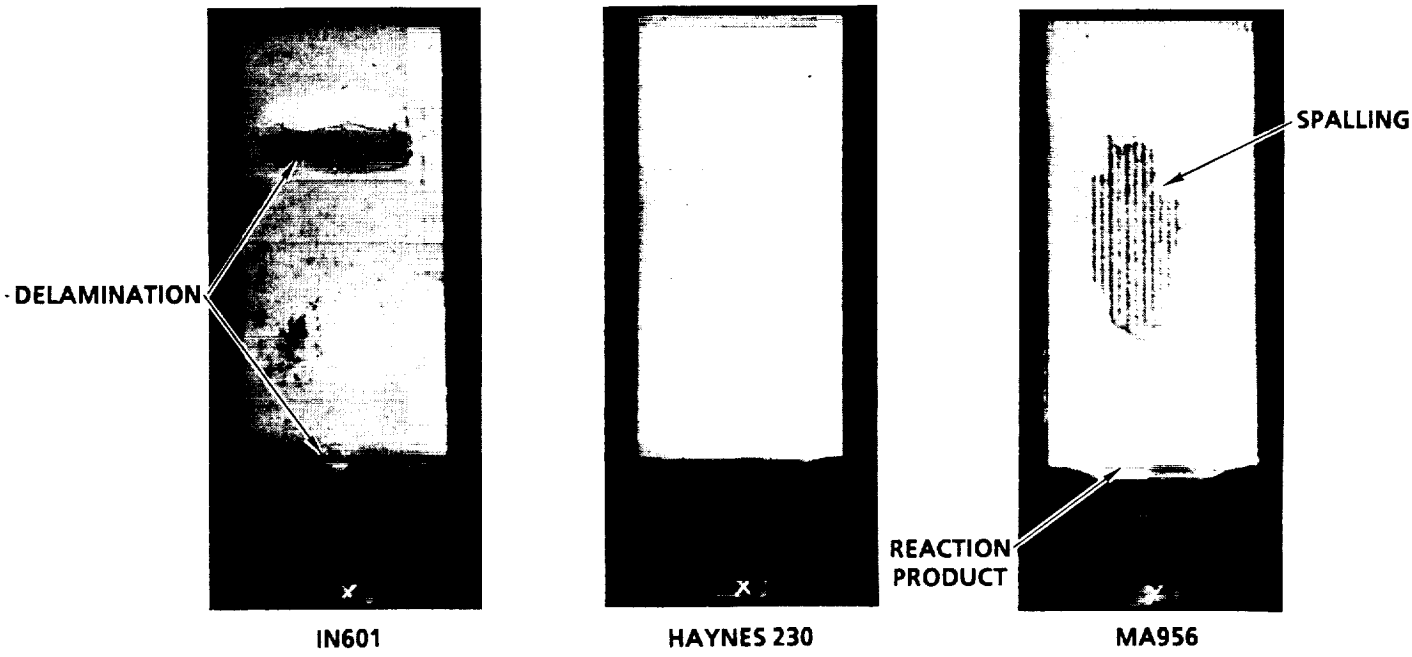

Figure 37. Static Air Heat Treatment at 2000F for One Hour Performed to Screen Seal Configurations.

Seal Redesign

A contributing factor in failure of the regenerator seals in the August 1987 test was mechanical binding between the seal shoe components. This binding is described in Figure 38. To eliminate this binding the hot seal shoe was redesigned.

The new design eliminated binding between seal components through a redesigned end clip. The modification insures that the seal cross-arm can expand without restriction.

In other seal development activities, the regenerator system technology generated by Ford during the AGT Project was transferred to Garrett for continued development. This included a complete set for drawings for the AGT101 regenerator system, the hot regenerator rig, the static seal rig, regenerator seal hardware and tooling, and the regenerator core ring gear attachment apparatus.

The Ford regenerator seal drawings were converted to GAPD standards and formats to augment further development. This work involved generating 37 additional new drawings for the AGT configuration regenerator seals.

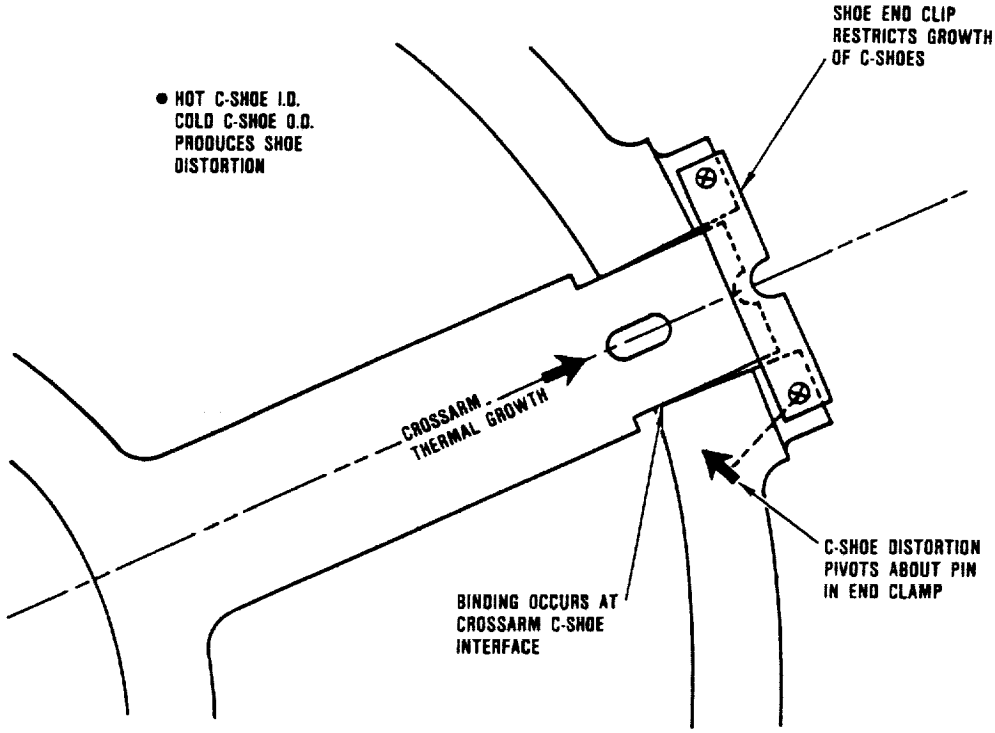

GB7-125-21

Figure 38. Distortion of the C - Shoes Caused Binding at the Crossarm Interface.

4.0 CERAMIC COMPONENT DESIGN

Ceramic Design in the ATTAP consists of two major elements: analysis and methods development. Also treated in this section is the Design Review, a review of the state of the ATTAP engine test bed design during the first contract year.

4.1 Ceramic Design

4.1.1 Ceramic Design Methods

4.1.1.1 Life Prediction Methods

Development of ceramic life prediction methods in ATTAP addresses several failure modes, including fast fracture, slow crack growth, impact, contact, and thermoelastic considerations. During this first reporting period, the majority of effort in life prediction methods development was concentrated in the areas of impact methods and preparation for hot spin testing in support of time dependent methods development.

Spin Disk Design

The hot spin testing activity will consist of spinning ceramic disks of special design at high temperature and stress levels, such that failure is predicted within a reasonable time. Failure of the disks in a time frame which agrees with the life, as predicted by the method employed, will support the applicability of that method. In preparation for this spin activity, a spin disk was designed which simulates the size and stresses of the ATTAP turbine rotor at a lower cost. The spin disk has an integral shaft and blades, as shown in Figure 39.

The spin disk was designed to verify fast fracture and time dependent component design methods, and for testing at room and elevated temperatures in a spin pit. The specific design objectives included:

- The spin disk should have a greater volume exposed to stress than the AGT101 rotor.
- The maximum internal stress in the spin disk should be greater than the surface stress.
- The spin disk should have a simple geometry to reduce cost.
- The spin disk diameter must be no greater than the rotor diameter to allow both to be tested in the same spin pit.

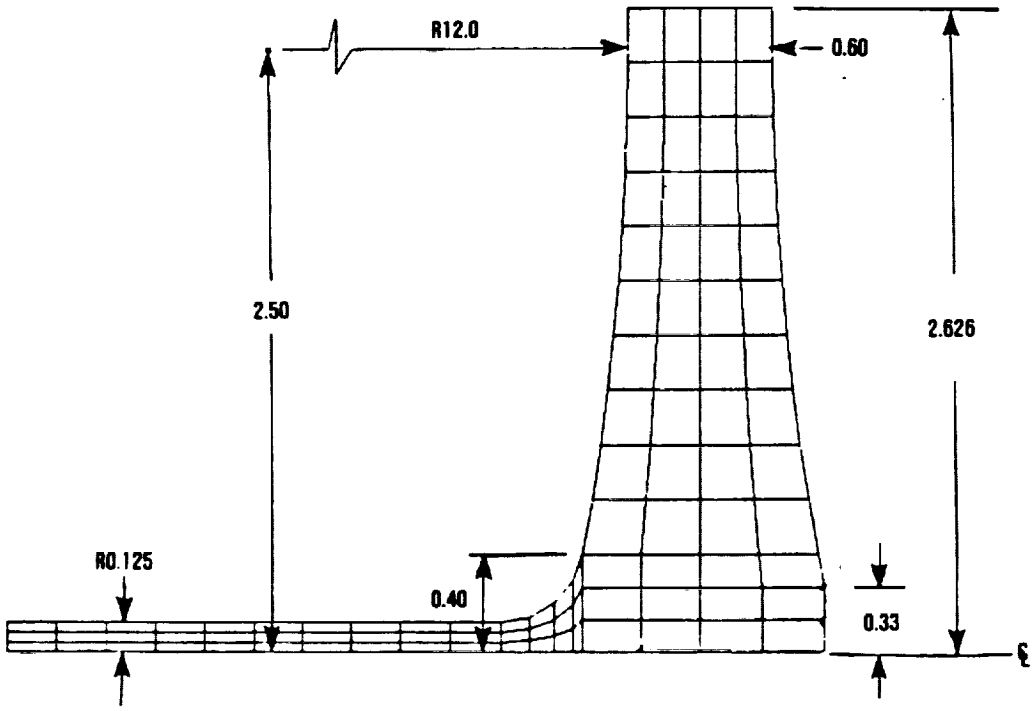

Figure 39. Spin Disk Geometry for Ceramic Life Prediction Methods Verification.

- The spin disk should have higher stresses than the rotor at the same rotational speed to reduce demands on the spin-pit motor.

The spin-disk has higher internal stress than surface stress as shown in Figure 40. Also, the maximum stress in the spin disk of 74.5 ksi, at 100 krpm, is significantly larger than the 43.6 ksi in the AGT101 rotor at the same speed. This ensures that speeds required to fail the spin disk can be achieved in the spin pit. The spin disk also has more stress volume than the rotor as shown in Figure 41. The spin disk meets all design objectives.

Surface Stress Correction

A method for calculating accurate surface stresses from conventional finite element solutions was developed. Accurate component surface stresses are required for predicting ceramic component failure probability. This method of calculating surface stresses does not require highly refined finite element models or an additional surface stress model.

The surface stress correction method was developed from the concepts of conjugate approximations. The conjugate approximation was modified to force the conjugate stress to exactly predict

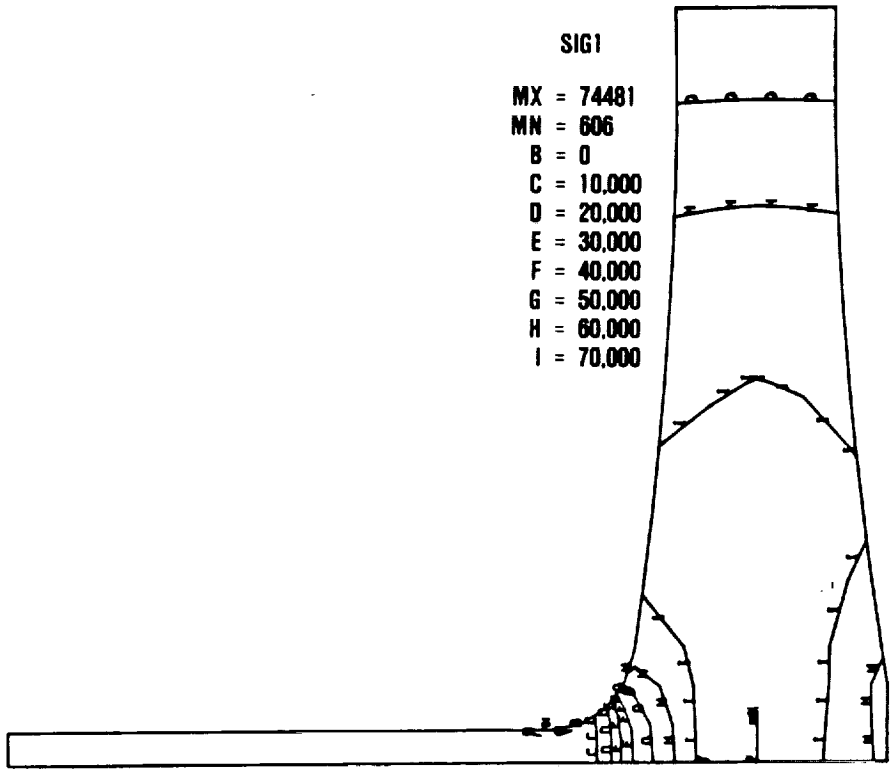

GB9-85-11

Figure 40. Spin Disk Principal Stress Plots for 100,000 rpm.

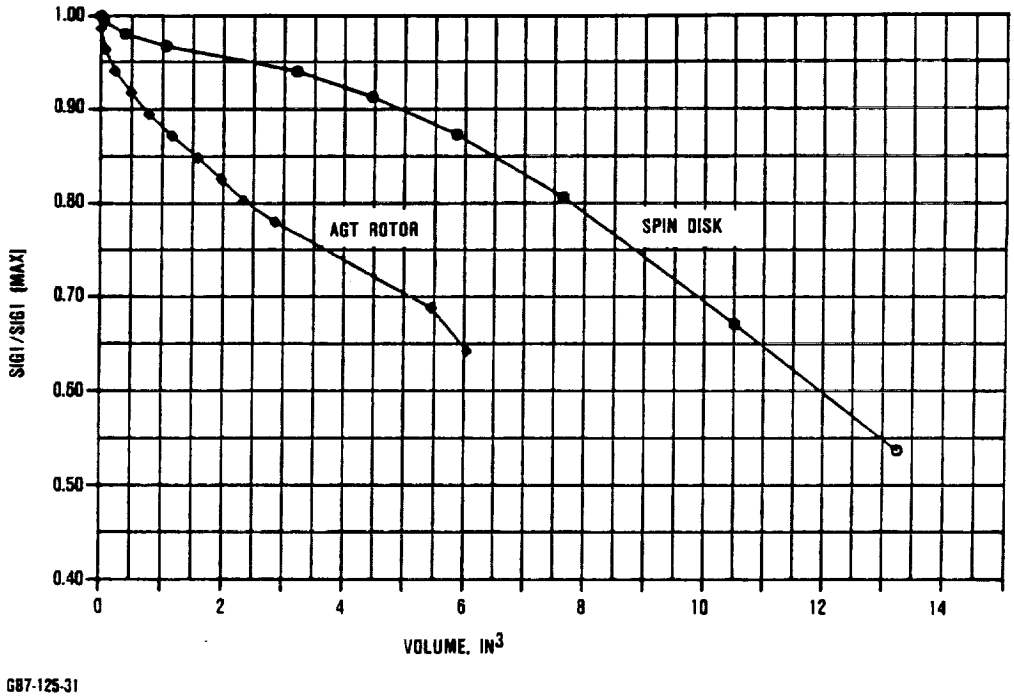

GB7-125-31

Figure 41. The Spin Disk Has Considerably More Stressed Volume than the AGT Rotor.

stresses which are known at the outset. Typically, these known values are on component surfaces (such as stress free boundaries). The resulting constraint equations

$$[C]\ \{\sigma\} = \{P\}$$

are used to modify the original system giving

$$\begin{bmatrix} G & C^T \\ C & 0 \end{bmatrix} \begin{Bmatrix} \sigma \\ \hline L \end{Bmatrix} = \begin{Bmatrix} R \\ \hline P \end{Bmatrix}$$

where

$$\{R\} = \int_{\text{all elements}} N^T\ D\ \bar{\sigma}\ dv$$

$$[G] = \int_{\text{all elements}} N^Y\ D\ \bar{\sigma}\ dv$$

L = Lagrange multipliers

$\bar{\sigma}$ = conventional stresses

D = material matrix (E,G,ν)

$\{\sigma\}$ = nodal values of conjugate stresses

This stress enhancement technique is applied to the ANSYS finite element code. It is applied to ANSYS solution files and does not require modifications to the ANSYS code.

The surface stress correction method has been tested with a rectangular beam model loaded in torsion. ANSYS FEM stresses calculated with and without the surface stress correction were compared to the exact stresses obtained from elasticity theory. The surface stress correction methods reduced the maximum error in shear stress from 47.6 ksi to 5.5 ksi, as shown in Figure 42.

The conjugate stress approach of calculating surface stresses appears to provide a significant improvement over conventional FEM calculated stresses. Additional test case will be performed to evaluate the improvements in component stress and failure probability that can be obtained with this method.

4.1.1.2 Impact Design Methods

Methods to predict impact damage are essential for the application of ceramics in turbine engines. Turbine blades and stators are

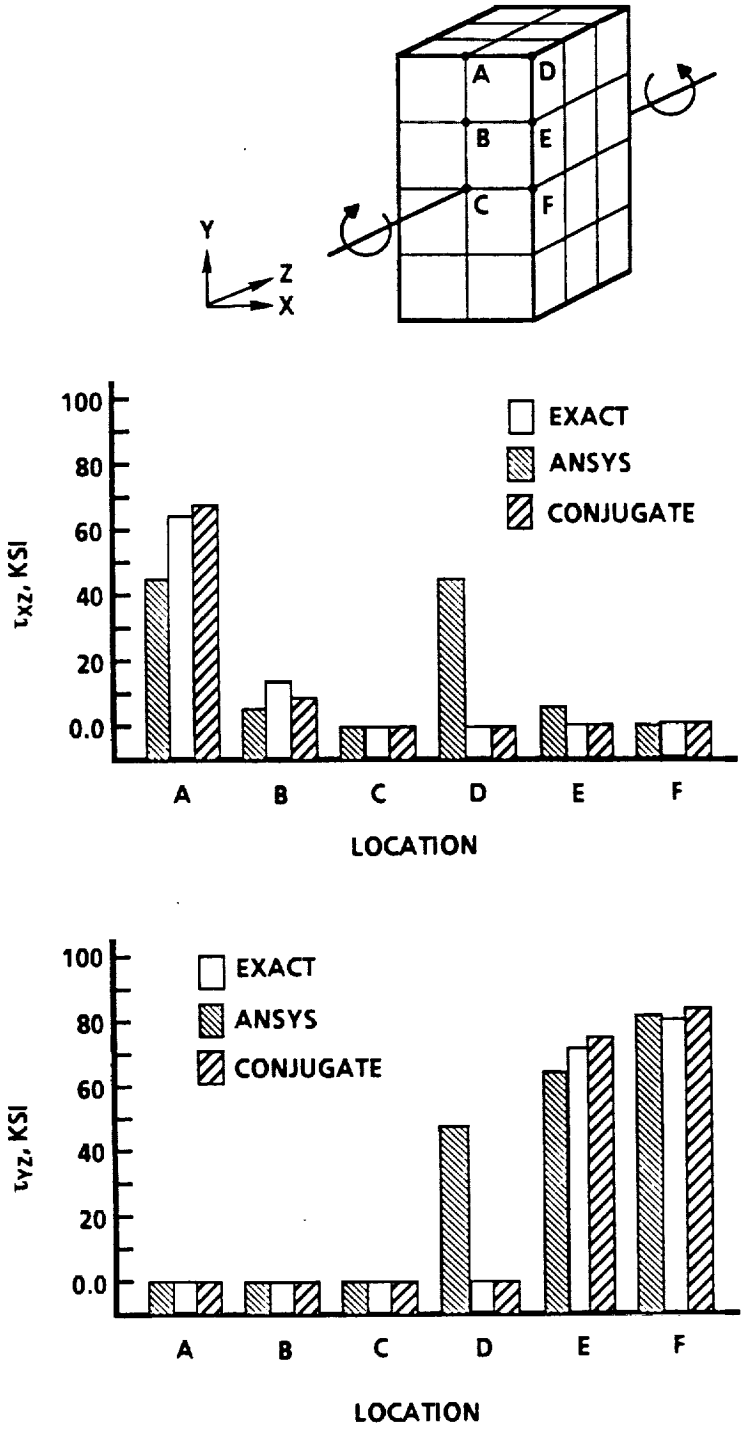

GB8-125-50

Figure 42. Comparison of Shear Stresses Predicted With ANSYS and Corrected With the Conjugate Stress Method, for a Bar in Torsion Test Case.

the most impact susceptible turbine engine components. These components may be impacted by a variety of particle materials at velocities above 2000 ft/sec. Methods that can predict the impact conditions that will reduce the strength or life of a stator or turbine blade are being developed in this program.

Initial Impact Testing on Ceramics at GAPD

An initial impact testing study was performed to identify the predominant modes of impact damage in a Si_3N_4 and to provide guidelines for subsequent impact testing in the ATTAP program. This study was partially conducted under the ATTAP program.

Experimental Procedure - The targets were 2 x 2 x 2-inch cubes and 0.250 x 0.500 x 2.0-inch test bars. The target material was a sintered silicon nitride fabricated by cold isostatic pressing. The surface of the targets was finish ground with a 320-grit diamond grinding wheel. The projectiles used were Norton NC-132 hot pressed silicon nitride spheres, 52100 and 440CVM steel spheres, and POCO graphite cylinders. The spherical projectiles were commercially available 0.125- and 0.0625-inch diameter ball bearings. The graphite cylinders were machined from 0.125-inch diameter rods. Cylinders instead of spheres were used because at the time of this study satisfactory graphite spheres could not be obtained.

The targets were impacted at room temperature at the University of Dayton Research Institute (UDRI). Figure 43 shows the three target configurations selected to assess different impact response. The geometry and dimensions of the cube were selected to eliminate structural bending stresses and back reflection of the impact shock wave. The test bars impacted in a fixed support configuration were designed to simulate turbine stators and the test bars impacted under a tensile load simulated the effect of background stress as in the turbine rotor.

Figure 44 shows the test bars used for the impact tests. Aluminum tabs were attached to the ends of the bars with epoxy resin so that the bars could be gripped without damaging the ceramic. The test bars were loaded to 10 ksi in tension via a dead-weight loading arrangement. Strain gages were attached to the test bars to estimate the amount of bending, which was found to be approximately 10 percent.

A schematic of the impact equipment is presented in Figure 45. Lexan sabots were used to support the projectiles, which enabled different size projectiles to be propelled in the same gun barrel. Compressed helium gas was used to propel the projectiles up to 1000 ft/sec while chemical powder charges were used for higher velocities up to 3700 ft/sec. The projectile velocity was measured using electronically coupled laser lights.

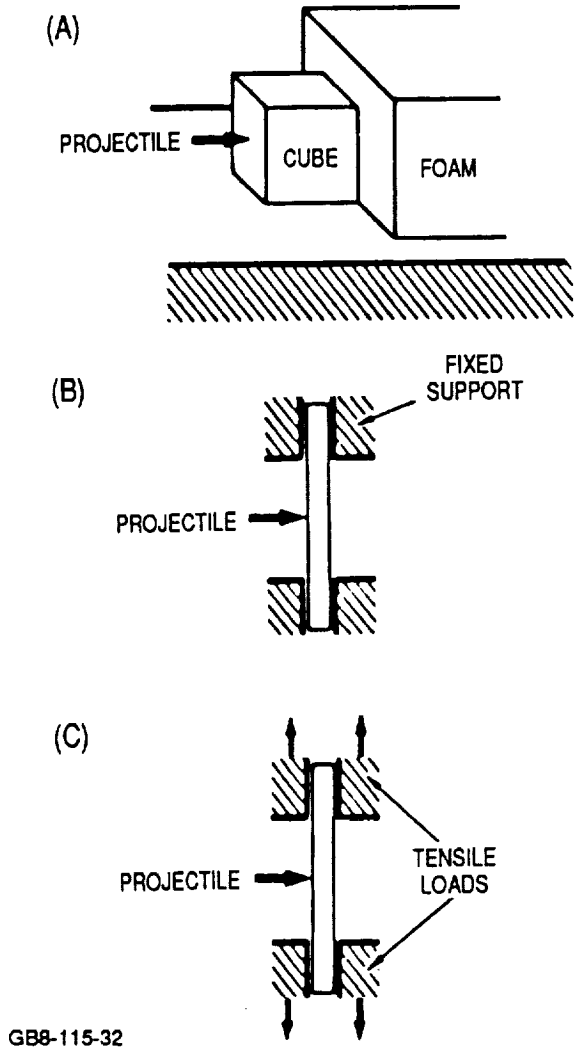

Figure 43. Target Configurations Used to Evaluate Impact Response.

This impact study was performed in two parts: 1) the critical velocity of projectiles which just caused cracking on the target surface was estimated and 2) the strength degradation due to projectile impact was evaluated. In the first part, the critical velocity was determined by impacting the cubes with projectiles at a range of velocities. Impact damage was then determined with a 40X stereo microscope and scanning electron microscopy (SEM).

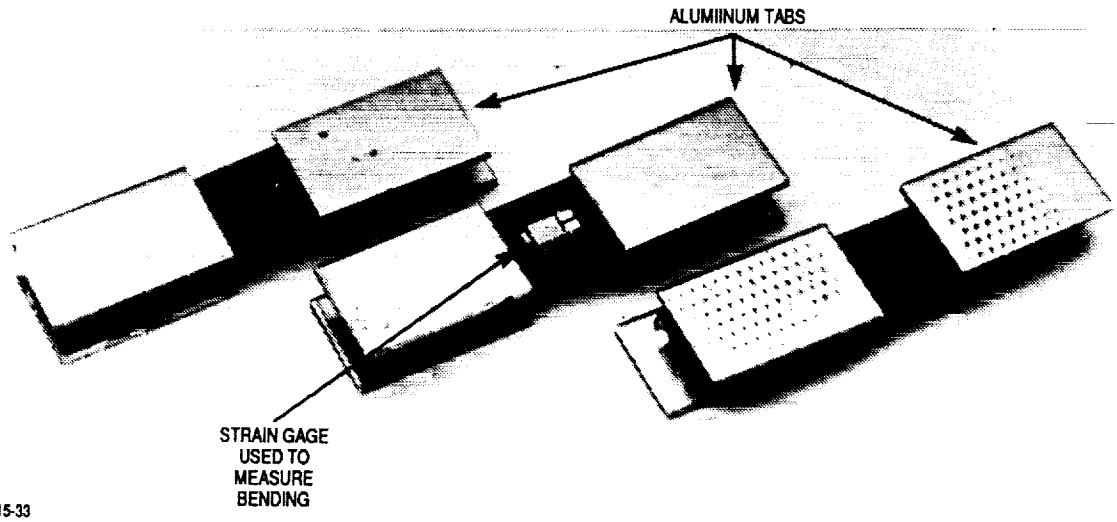

Figure 44. Test Bars With Aluminum Tabs Were Used To Evaluate Impact Damage Under Different Stressed Conditions.

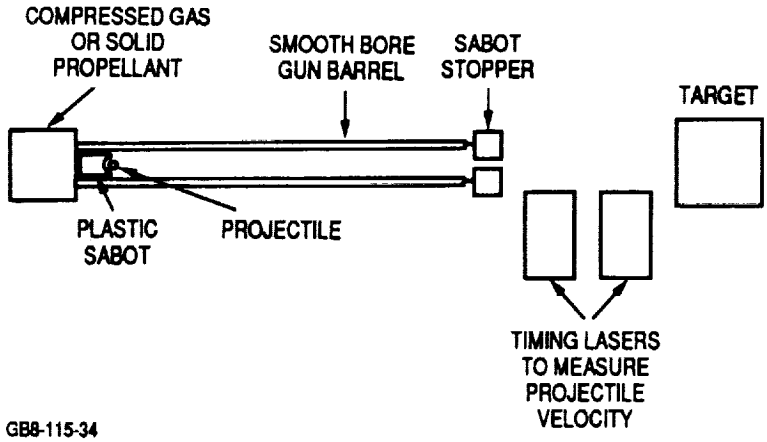

Figure 45. Schematic of the Impact Equipment At University of Dayton Research Institute (UDRI).

ORIGINAL PAGE
BLACK AND WHITE PHOTOGRAPH

ORIGINAL PAGE
BLACK AND WHITE PHOTOGRAPH

In the second part, the critical velocity at which the surface cracks caused strength degradation was estimated. Three sides of the cubes were impacted with one projectile per face. Test bars were then machined from the cubes with the impact location in the middle of the test bars, shown in Figure 46. For the fixed support and tensile loaded test bars, the aluminum tabs were removed after impact through heating in an air furnace up to 900F. These test bars were later broken in four-point bending. Detailed fractographic analysis was performed to determine whether failure originated from the impact site. Twenty 0.250 x 0.500 x 2.0-inch as-received test bars bend tested at the same time had an average flexure strength of 126 ksi.

Critical Velocity By Visual Inspection - The critical velocities for the cube specimens based on visual inspection are shown in Table 7 and plotted in Figure 47. The data showed that the ceramic projectiles were the most damaging. The critical velocity of the ceramic projectiles are four to five times lower than the steel projectiles of comparable size. This is probably due to the higher elastic modulus and compressive strength of the ceramic projectiles, which result in higher tensile stress below the point of contact. The critical velocity was 183 ft/sec for the larger ceramic projectiles and 335 ft/sec for the smaller ones.

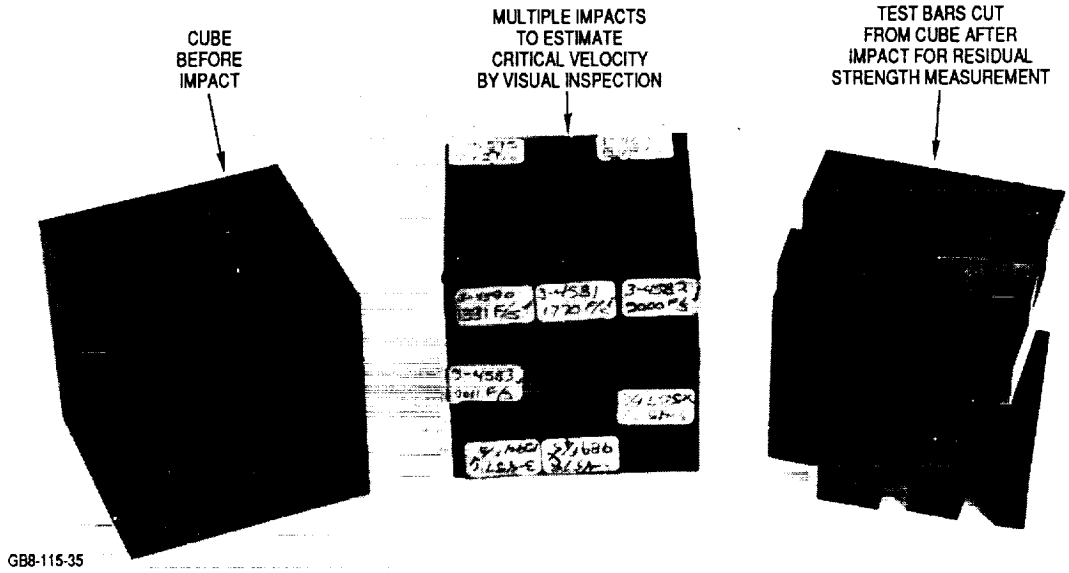

Figure 46. Silicon Nitride Cubes Were Used for Targets for Impact Damage Evaluation.

TABLE 7. CRITICAL VELOCITIES (V_c) OF SILICON NITRIDE TARGET ESTIMATED BY VISUAL INSPECTION.

Projectile Diameter, in	Ceramic, NC-132		Steel, 440CVM		Steel, 52100		Graphite	
	V_c***	Wt***	V_c	Wt	V_c**	Wt***	V_c	Wt
0.125	183	0.0543	920	0.1271	1048	0.1311	1096+	0.0047
0.0625	335	0.0068	1316	0.0159	1512	0.0164		

+Graphite projectile disintegrated above 1096 ft/sec. No damage to target up to 2100 ft/sec.

*The ceramic and steel projectile are precision-ground ball bearings. The graphite projectiles are 0.125 x 0.090-inch cylinders.

**V_c = Estimated critical velocity of the projectile in feet per second, which will cause cracking of the target material.

***Wt = Average weight of projectile in grams.

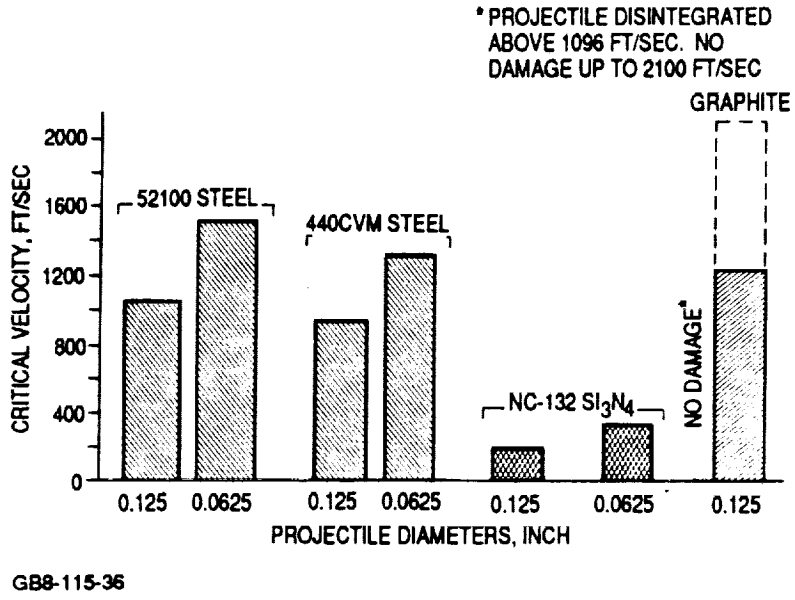

Figure 47. Critical Velocities for Silicon Nitride Target Were Estimated by Visual Inspection.

ORIGINAL PAGE
BLACK AND WHITE PHOTOGRAPH

The typical damage caused by ceramic and steel projectiles on some of the target surfaces is shown in Figures 48 through 50. The type of cracks caused by these projectiles are similar. The damage typically consisted of circumferential cracks around the center of impact. The number of circumferential cracks increased with increasing projectile velocities. At higher projectile velocities, radial and lateral cracks begin to appear, as shown in the SEM micrographs in Figure 49.

The ceramic projectiles also left indents on the target surface while the steel projectiles, being much softer than the target material, did not leave any such indents on the target.

Comparing the two steel projectile materials, the critical velocity of the 440CVM steel is consistently lower than the 52100 steel. This probably occurs because the 440CVM steel is softer than the 52100 steel and plastically deformed on the target surface. The extent of deformation of the 440CVM steel after impact can be seen in the SEM micrographs in Figure 51. The 440CVM projectiles were selected for the strength degradation evaluations based on this result because it is the more damaging of the steel projectiles.

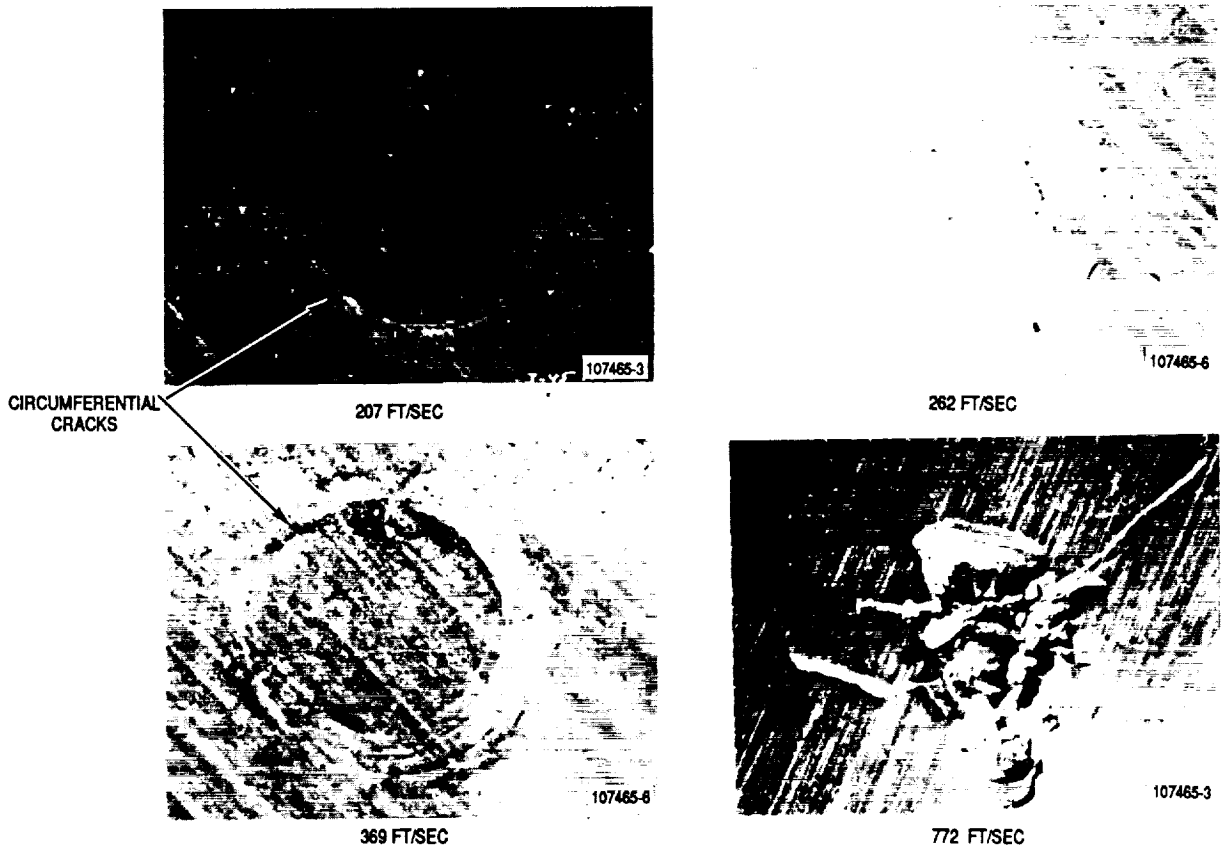

Figure 48. Photographs Illustrate Typical Damage By Ceramic Projectiles.

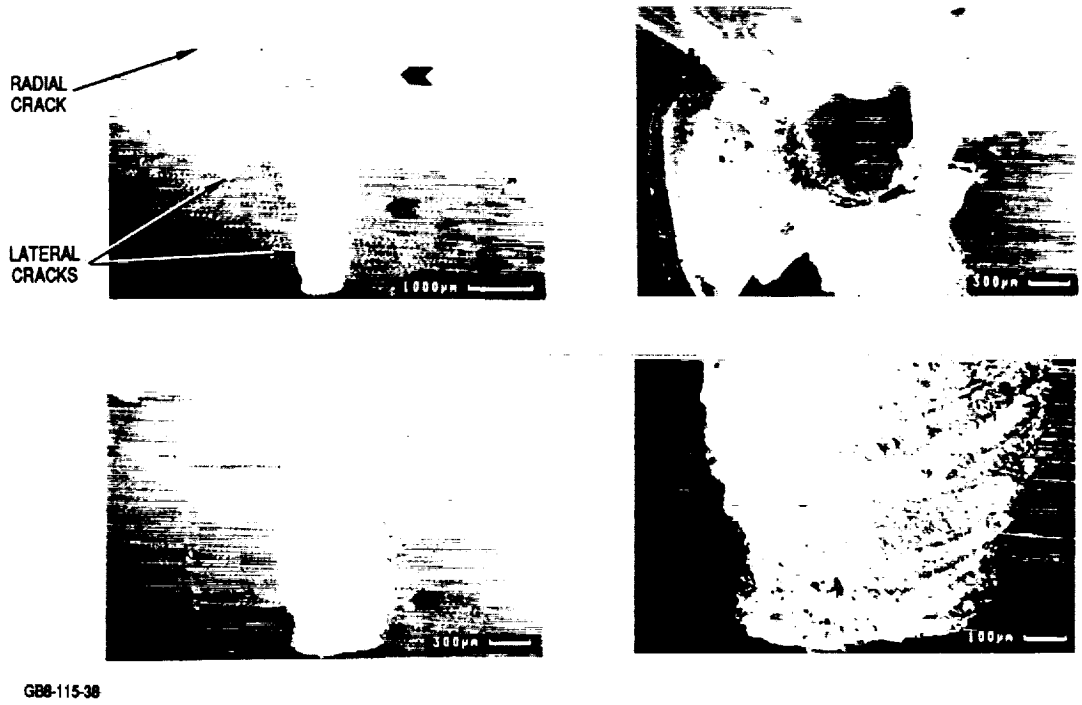

Figure 49. SEM Micrographs Of A Damaged Site Showing Radial and Lateral Cracks (Si_3N_4 Spheres, 0.125 in Dia, 772 ft/sec).

The graphite projectiles did not cause any damage to the target up to 2100 ft/sec in this experiment. The projectiles fragmented when launched above 1096 ft/sec. The smaller graphite fragments were then less damaging than a single large projectile. The evidence of disintegration were the multiple impact marks on the target surface, shown in Figure 52, and the multiple traces on the oscilloscope when the fragments interrupted the timing laser beams.

Residual Strength After Impact - The residual strength results for test bars machined from the cubes are shown in Figures 53 and 54. Results for test bars impacted by the silicon nitride projectiles are shown in Figure 55 and those impacted by the steel projectiles are shown in Figure 56. Bars that fractured from the impact locations are represented by the darkened symbols. Detailed fractography was performed on the broken test bars to identify the fracture origins and to determine whether the fracture originated from the impact site. Fractures that did not originate from the impact site indicate that

ORIGINAL PAGE
BLACK AND WHITE PHOTOGRAPH

ORIGINAL PAGE
BLACK AND WHITE PHOTOGRAPH

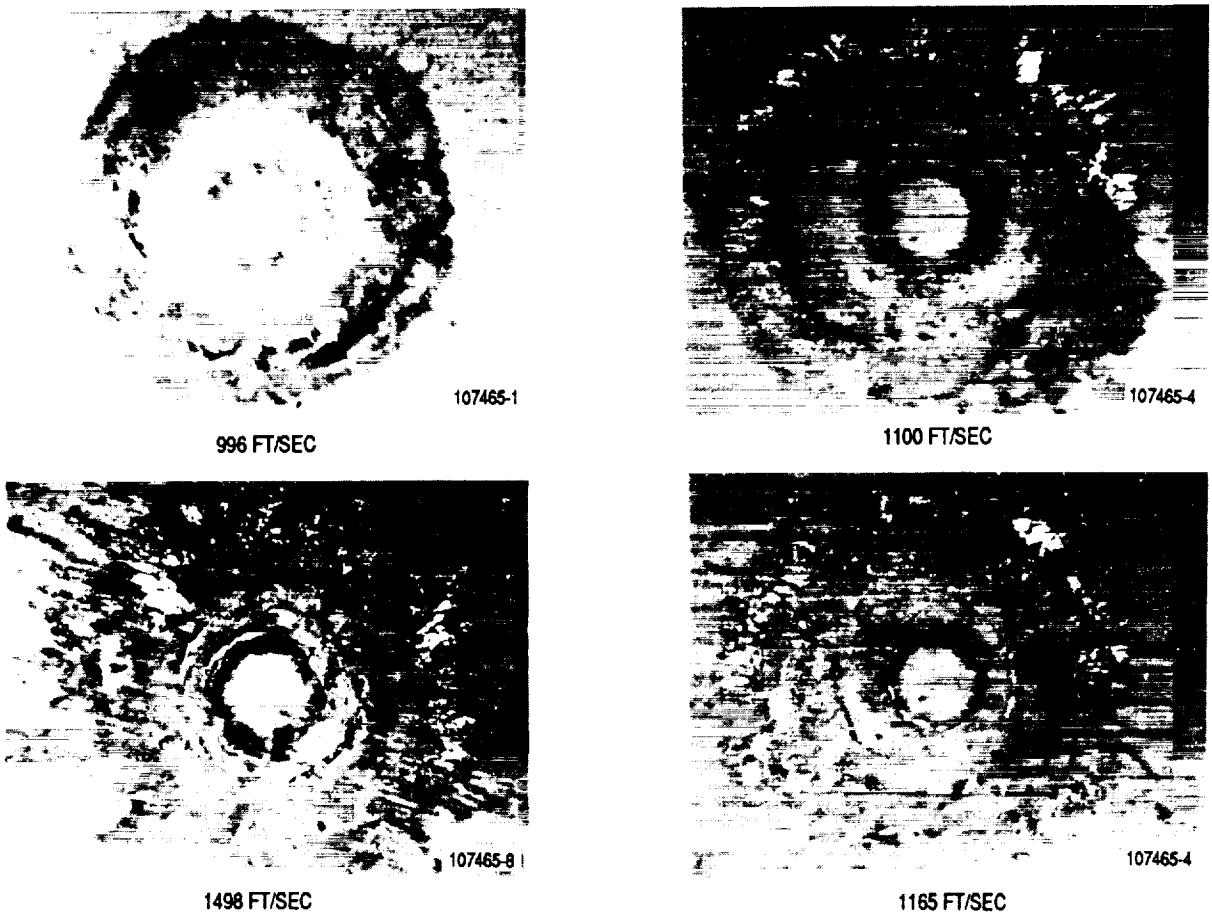

Figure 50. Typical Damage By Steel Projectiles.

the projectiles did not cause flaws that are more severe than existing ones. Typical impact damage fractures originated from the tip of the Hertzian cone cracks about 0.003 to 0.005-inch below the tensile surface.

The critical velocity estimated from the residual strength agreed well with that determined by visual inspection method despite the large scatter in strength data. As seen in Figures 53 and 54, excellent agreement was found for the larger projectiles (0.125 inch) impacts and the critical velocities were about 10-percent lower for the smaller (0.0625 inch) projectile impacts. The reason for the lower critical velocity determined by visual inspection may be that when the cracks detected were small and comparable in size to existing material defects, they were not large enough to cause preferential failure.

(A)

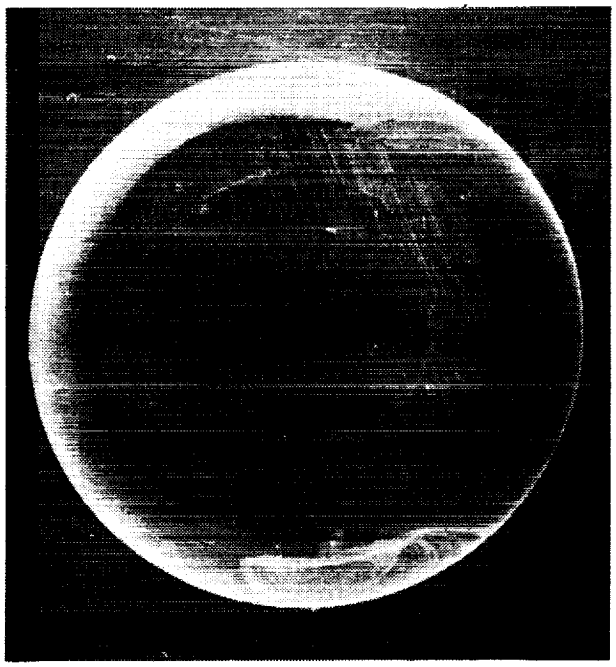

923 FT/SEC

(B)

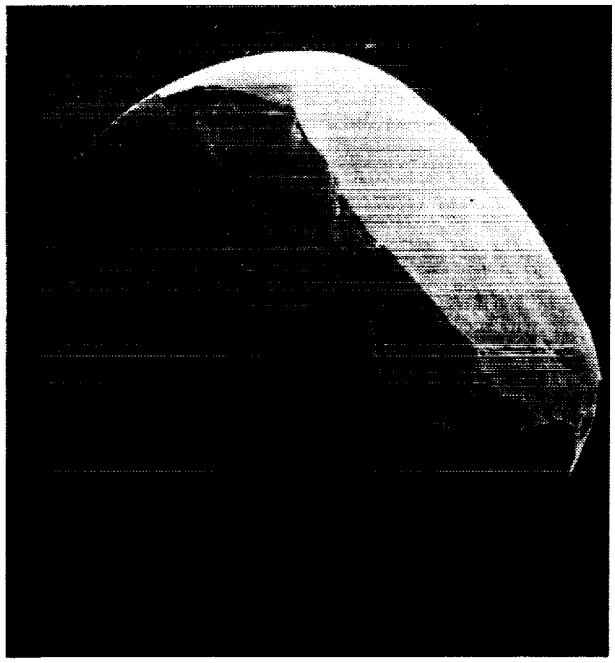

1160 FT/SEC

GB8 115-40

Figure 51. SEM Micrographs Illustrate Deformation Of 440CVM Steel Projectiles After Impact.

ORIGINAL PAGE
BLACK AND WHITE PHOTOGRAPH

ORIGINAL PAGE
BLACK AND WHITE PHOTOGRAPH

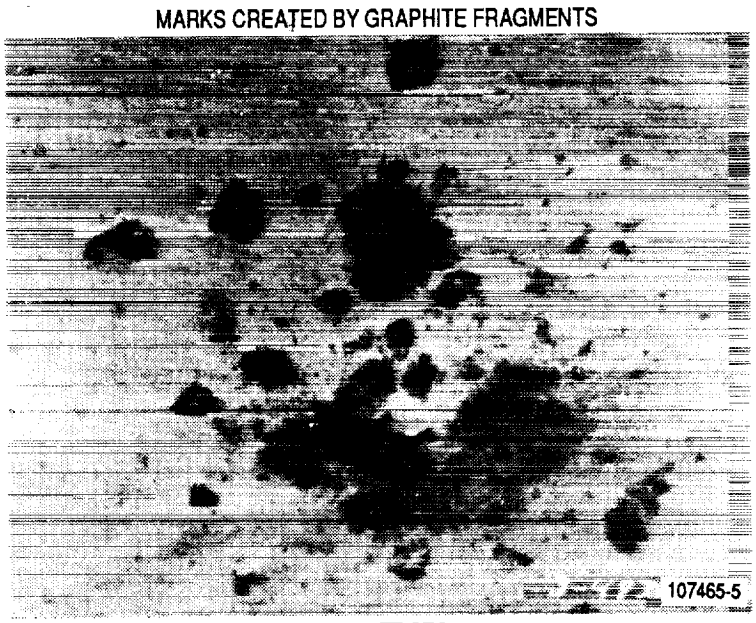

Figure 52. Photograph Illustrates Disintegration of the Graphite Projectile.

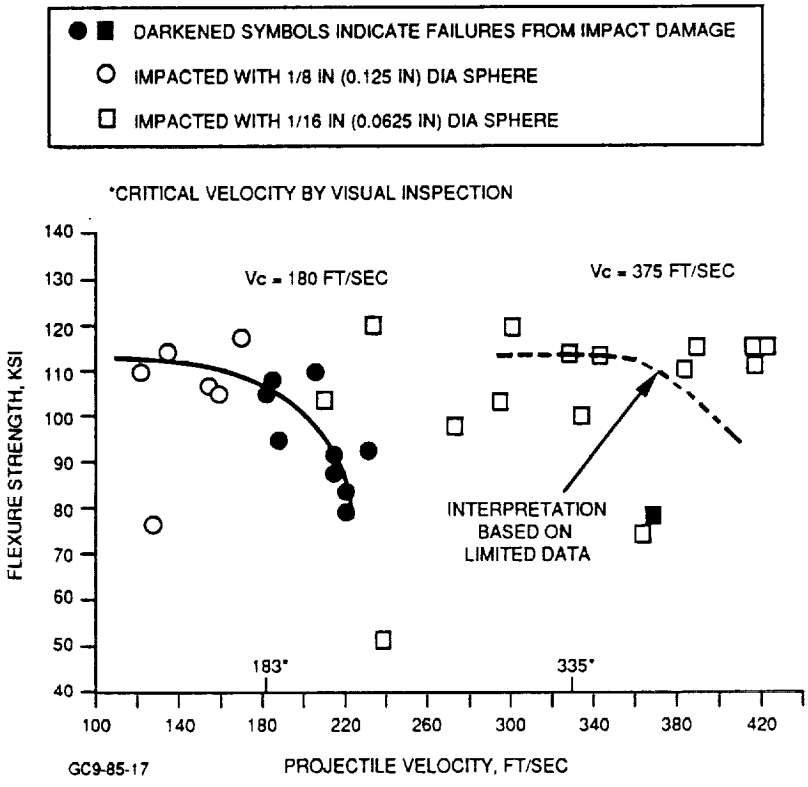

Figure 53. Residual Strength of Test Bars Cut From Cubes Impacted by Si_3N_4 Spheres.

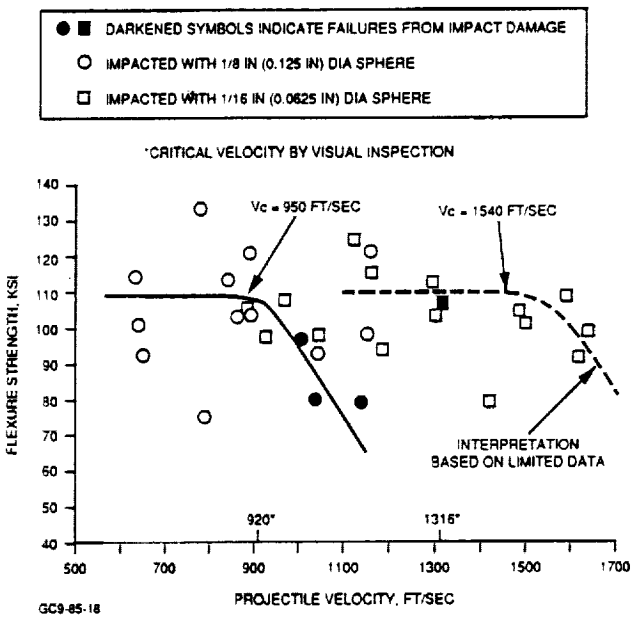

Figure 54. Residual Strength of Test Bars Cut From Cubes Impacted By Steel Spheres.

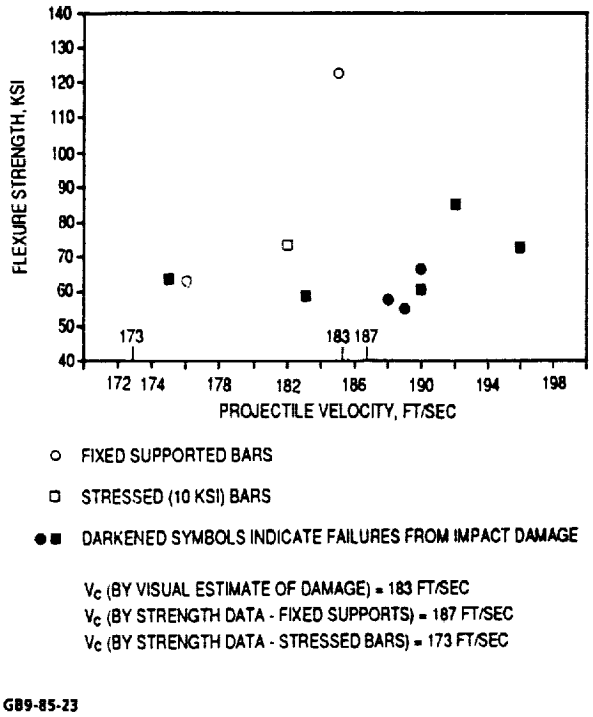

Figure 55. Residual Strength of Test Bars Impacted By 0.125-Inch Diameter Si_3N_4 Spheres At Fixed Support and Stressed Configurations.

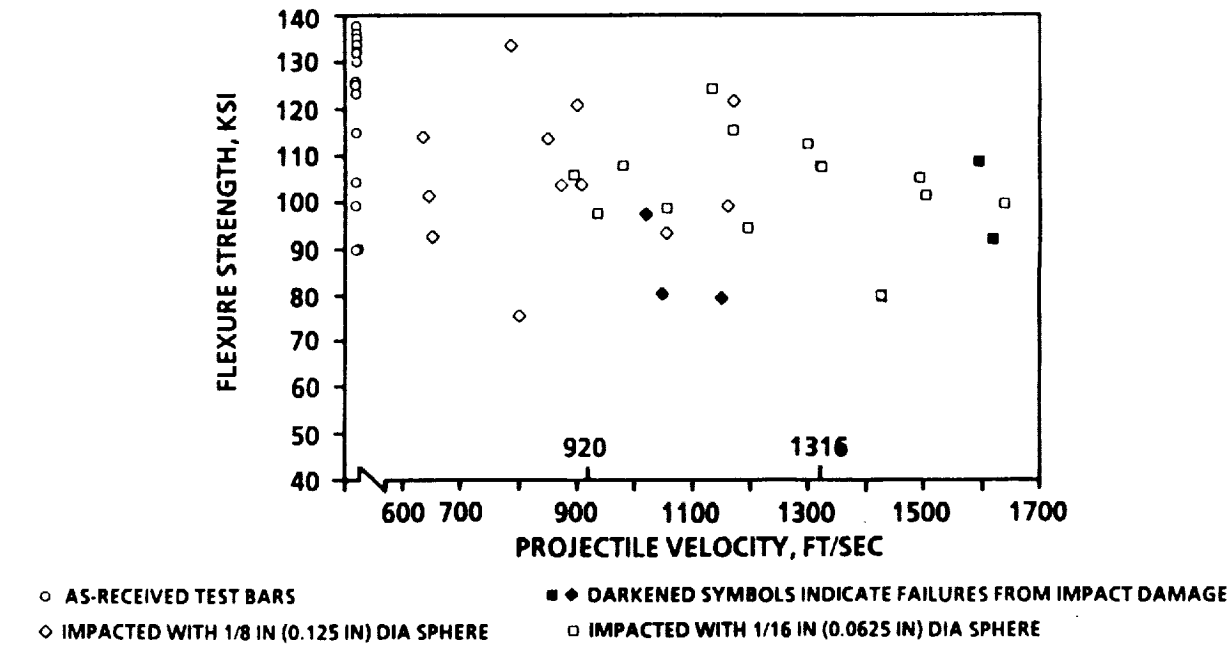

Figure 56. Impact Damage of Silicon Nitride Cubes by Steel Spheres.

Test bars impacted above the critical velocity tend to fail from the impact site and the strength decreases with increasing impact velocity. For the smaller diameter projectiles, the strength degradation was either small or insignificant, probably due to the small size of the cracks created.

The residual strength of the test bars impacted in the fixed support and tensile loaded configurations by 0.125-inch diameter ceramic projectiles is shown in Figure 57. The critical velocity of the test bars under stress appears to be lower.

The residual strength data of the test bars showed large scatter and the scatter is greater for test bars impacted in the fixed support and tensile stressed configurations. Recognition should be given that measuring the strength degradation to assess the impact damage cracks is an indirect method. The cracks formed during impact may affect the flexure strength

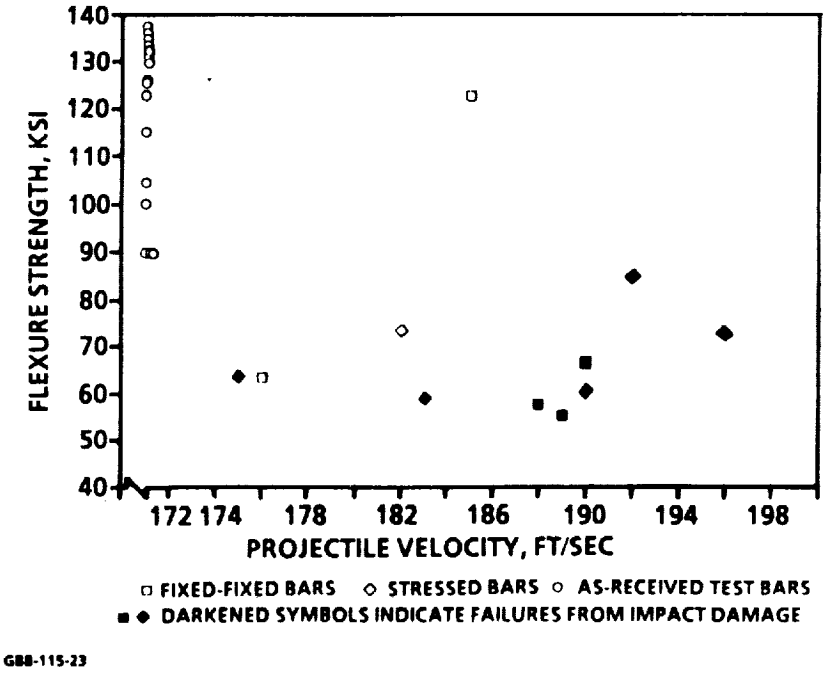

Figure 57. Impact Damage of Fixed and Stressed Test Bars by 0.125 in Diameter Si_3N_4 Spheres.

differently depending on their size, shape, orientation, and location on the test bars. In addition, other strength influencing factors due to the experimental setup, may increase the data scatter for test bars impacted under fixed support and tensile stressed configurations.

Conclusions - The study showed that the critical velocity or threshold damage velocity for silicon nitride is within the AGT101 engine conditions for projectile velocity and size. It is possible for ceramic or steel particles in the gas path to damage the silicon nitride components. The ceramic projectiles are more damaging than steel and graphite projectiles. The critical velocity of impact damage by ceramic projectiles is 4 to 5 times lower than steel. The actual critical velocity of the graphite projectiles was not determined in this study due to projectiles breaking up into less damaging fragments during launching. However, the velocity is estimated to be higher than 1096 ft/sec.

Visual inspection for damage at impacted sites appeared to be a convenient method for estimating the critical velocity and to assess the impact resistance of a ceramic. However, the

critical velocity determined by this method may be lower than the critical velocity determined by the residual strength method for impacts with small (0.0625 inch) projectiles. The small impact damage flaws detected visually were not always the weakest flaws and did not always cause strength degradation.

The three methods used to identify critical impact velocity produced different results. Visual inspection before flexure testing identified cracks at the lowest velocities of the three methods. Residual flexure strength was not affected until higher input velocities, indicating that small impact cracks are less severe to inherent material.

Impact Damage Models for Ceramic Engine Components

The objective of this program is to develop mechanistic impact models that are capable of predicting impact damage of ceramic components over the wide range of turbine engine impact conditions.

This program will include analysis and testing required to develop a model for ceramic stator and turbine blade impact damage prediction. This program is divided into three phases:

- **Phase I** - Screening impact models and variables: identify candidate models through a literature survey and establish hierarchy of variables through impact testing;
- **Phase II** - Impact model development: characterize the effects of significant impact variables on impact behavior of a ceramic through testing; develop an impact damage prediction model and implement it into the EPIC finite element stress code;
- **Phase III** - Impact model verification: predict stator impact damage using the model and verify the prediction with stator impact test results.

More detailed tasks contained in the three phases are illustrated in a flow chart shown in Figure 58.

Specimens for Phase I testing have been prepared for impact testing and candidate impact models have been identified.

Phase I, Literature Study on Impact Modeling - An extensive literature search has been completed at GAPD. The purpose of the search was to collect information on:

- modes of ceramic impact damage
- candidate ceramic impact damage models

The findings from this review have been summarized and examined, and will be included as an introductory section to

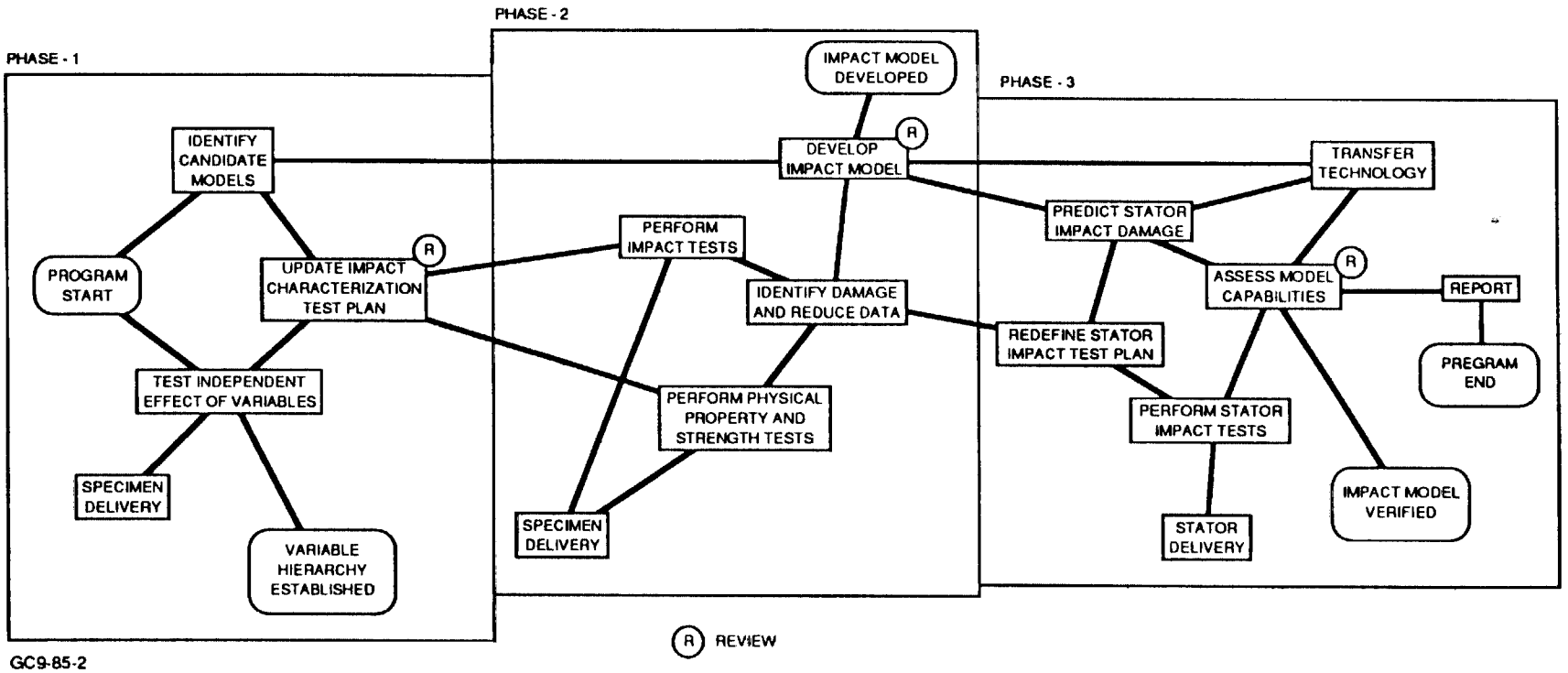

Figure 58. Impact Damage Models for Ceramic Engine Components.

impact design in the ATTAP ceramic design manual. The detailed test plan in Phase II has been worked on based on the results from this study.

In gas turbine engine applications, the impact damage that will degrade ceramic component integrity can be categorized into two modes:

- o elastic
- o elastic/plastic

The characteristic damage patterns associated with the three impact modes are schematically illustrated in Figure 59. In the elastic mode, there is no permanent indention at the impact site and shallow annulus surface cracks can be seen around the impact center. These small cracks are less detrimental to strength than radial cracks. In the elastic/plastic mode, there is a permanent indentation left at the impact center. The stress field around the indentation is drastically altered because of this indention. The maximum tensile stress is along tangential directions, and causes radial cracks emanating from the center of impact. The circumferential cracks formed earlier in an impact process will propagate inward and develop into cone cracks. The propagation of radial and cone cracks can penetrate deep into the material thus cause final separation or severely reduce strength.

Six candidate mechanistic impact damage models in literature have been carefully reviewed. These models are:

TCK — L.M. Taylor, E. Chen, and J.S. Kuszmaul, "Microcrack-Induced Damage Accumulation in Brittle Rock under Dynamic Loading", Computer Methods in Applied Mechanics and Engineering, Vol. 55, 1986, pp.301-320.

LKE — B.M. Liaw, A.S. Kobayashi, and A.F. Emery, "Theoretical Model of Impact Damage in Structural Ceramics", Journal of the American Ceramic Society, Vol. 67, No. 8, pp. 544-548.

CSS — D.R. Curran, D.A. Shockey, and L. Seaman, "Dynamic Fracture Criteria for a Polycarbonate", Journal of Applied Physics, Vol. 44, No. 9, 1973, pp. 4025-4038.

SCSRP — D.A. Shockey, D.R. Curran, L. Seaman, J.T. Rosenberg, and C.F. Peterson, "Fragmentation of Rock under Dynamic Loads", International Journal of Rock Mechanical Science and Geomechanics Abstract, Vol. 11, 1974, pp. 303-317.

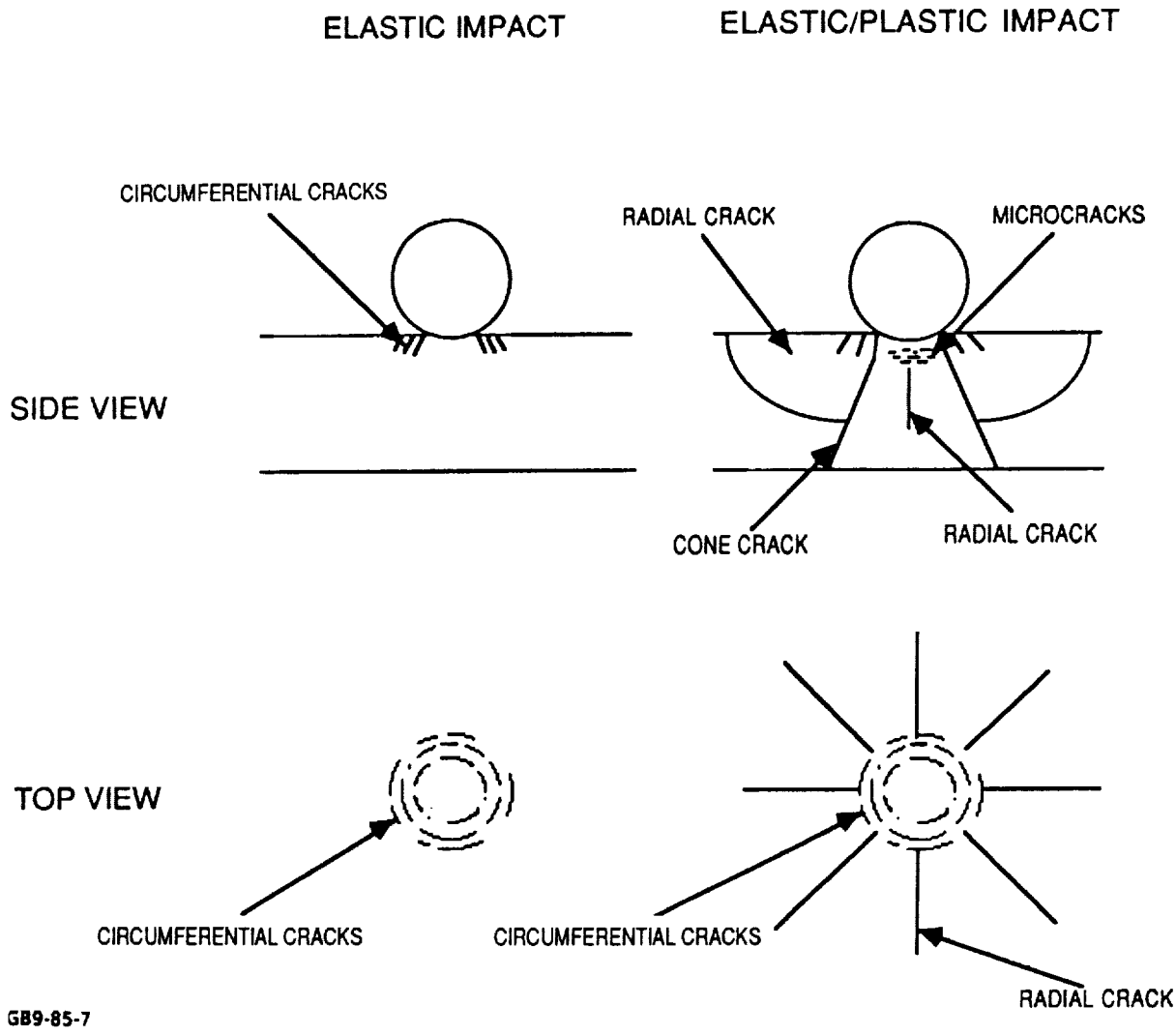

Figure 59. Different Damage Patterns in Two Different Impact Models in Ceramics.

CS L.S. Costin and C.M. Stone, "Implementation of a Finite Element Damage Model for Rock", Constitutive Laws for Engineering Materials Theory and Applications, C. S. Desai et al Editors, Elserier Publishing Co., 1987, pp. 829-841.

Margolin L.G. Margolin, "Microphysical Models for Inelastic Material Response", International Journal of Engineering Science, Vol. 22, No. 8-10, 1984, pp. 1171-1179.

Although the majority of these models were developed for applications involving rocks and oil shale, they have some applicability to structural ceramics.

A common approach shared by a number of impact models is depicted in the flow chart in Figure 60. It can be seen that there are two major aspects in this approach: dynamics of element nodes and material routine. Basic physical principles

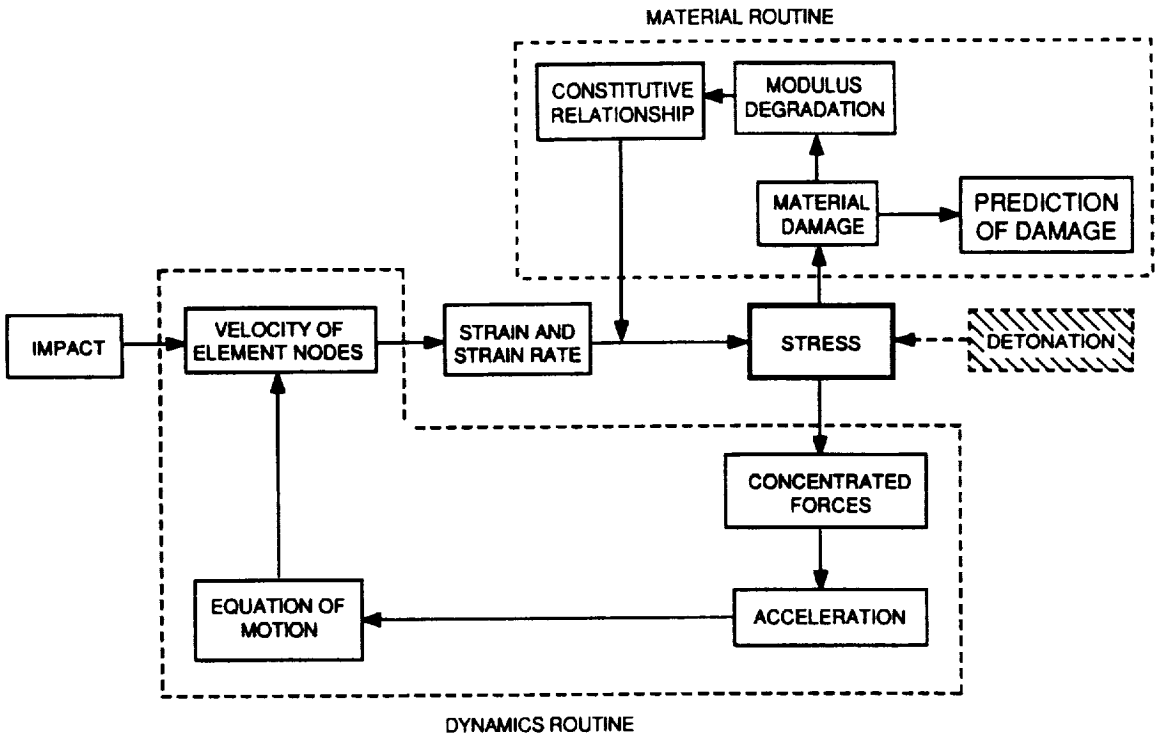

Figure 60. A Typical Scheme Used in Impact Damage Prediction Models.

such as conservation of momentum and Newton's Second Law are used to determine the velocity of every node. Strain and strain rates can be calculated based on nodal velocities. Stress distribution in the material can be obtained using a selected constitutive relationship. At any given instant the stress field in the material will determine the extent of material damage using a selected material damage criterion. This material damage is believed to be in the form of microcracks. The development of these microcracks will cause stress relaxation and material softening due to the deformation associated with the formation and opening of these cracks. At the macroscopic level, this process is demonstrated by the inelastic stress-strain behavior. This behavior is accounted for by the degradation of elastic moduli of the material. The change of elastic moduli will in turn affect the stress field in the next time interval. Figure 61 illustrates all the elements contained in a material routine. The six models reviewed differ from each other mainly on the contents in these elements. A comparison of these models is given in Table 8.

Currently two of the six models, TCK and Margolin, have been implemented into finite element computer codes at UDRI to be used in conjunction with EPIC-2 and EPIC-3 impact codes.

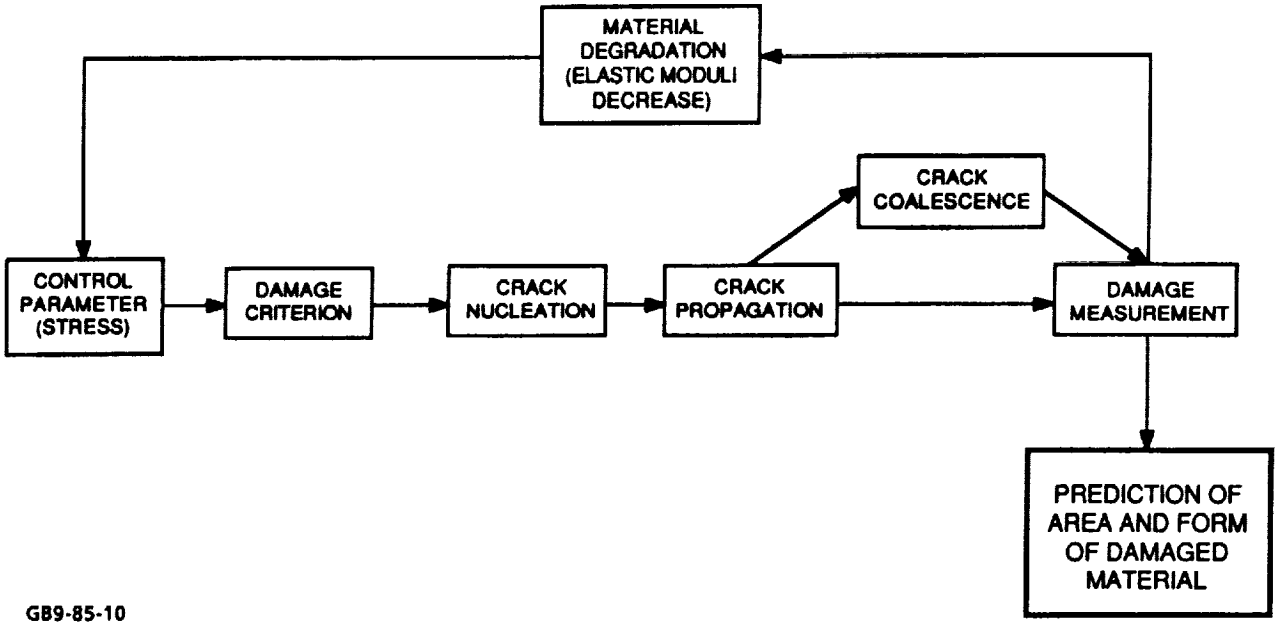

Figure 61. Elements in a Typical Material Routine in Impact Damage Models.

TABLE 8. COMPARISON OF EXISTING IMPACT DAMAGE MODELS

MODEL	DAMAGE CRITERION	CRACK NUCLEATION	CRACK PROPAGATION	MATERIAL DEGRADATION	CONSTITUTIVE RELATIONSHIP	DAMAGE PARAMETER	DAMAGE PREDICTION
TDK	material starts cracking under dilatational stress of any magnitude	$N=k(P/3K)^m$ N: number of cracks P: dilatational stress K: bulk modulus k,m: material const.	inversely proportional to strain rate	elastic moduli decrease while crack density increases	linear elastic under tension; elastic/perfectly plastic under compression	crack volume fraction	damaged area where damage parameter is equal to a prescribed value
LKE	$\sigma_1>\sigma_{uts}$ $\tau_{max}>\tau^*$ τ^*: shear strength	crack nucleates when the damage criterion is met	once a crack is nucleated it extends to full element	a cracked element cannot carry any tensile load across the crack	linear elastic	none	cracks with sizes and orientations
CSS	$\sigma > \sigma_{no}$ $\sigma > \sigma_{go}$	crack nucleation rate: $\dot{N}=\dot{N}_0 \exp\left[\frac{(\sigma-\sigma_{no})}{\sigma_1}\right]$	crack propagation rate: $\dot{R}=\left[\frac{(\sigma-\sigma_{go})}{4\eta}\right]R$	elastic moduli decrease with crack volume increase	linear elastic isotropic	crack volume	size distribution of cracks at different locations
SCSRP	cracks larger than the critical size c^* will grow $C^*=\pi K_{IC}^2/4\sigma^2$	preexisting flaw size distribution was determined experimentally	constant crack propagation rate: 1/3 of longitudinal wave speed	elastic moduli decrease with crack volume increase	linear elastic isotropic	crack volume	size distribution of fragmentation at different locations
CS	$K_I \le K_{IC}$	random discribution of preexisting microcracks	prescribed crack extension	stiffness reduces along a direction parallel to the crack growth direction	linear elastic	accumulation of crack extension under tensile stress	failed area with sudden drop of stiffness
Margolin	generalized Griffith criterion	preexisting flaw distribution determined experimentally	constant crack progation speed: a fraction of shear wave speed	effective stiffness reduces while cracks propagate	linear elastic	Υ: crack numbers time cube of crack size for all cracks	damaged area with γ equal to a prescribed value

The EPIC computer codes needed in ceramic impact damage model development have been installed at GAPD. The EPIC codes were developed specifically for impact and detonation applications. They were developed at Honeywell for the U.S. Air Force Armament Laboratory, Eglin Air Force Base, Florida, under contract F08635-83-C-0506. We have requested and received EPIC-2 and EPIC-3 codes from the U.S. Air Force Armament Laboratory. These two codes have been tested on VAX785 and CYBER 990 computer systems at GAPD. Plots from a test run of an impact example are shown in Figure 62. Both programs are operational and are ready to be used for the impact model development in Phase II.

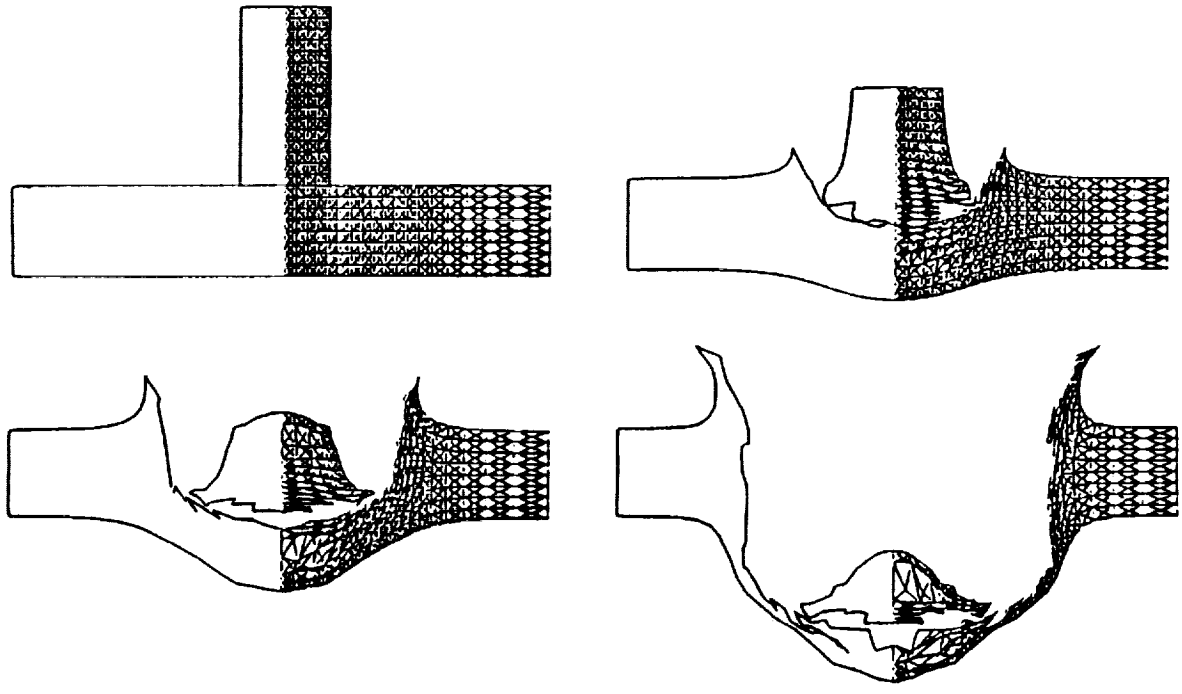

GB9-85-15

Figure 62. Results From a Metallic Impact Test Problem Using EPIC-2.

The models previously described only deal with impact damage caused by shock waves. Another impact damage which might occur on engine blades and stators is the structural failure caused by the dynamic response of a component. This type of failure will be studied using a conventional finite element code. The dynamic load imparted by projectiles will be obtained through an analysis using EPIC code. This load is needed for the dynamic analysis of the component. The failure will be predicted using an in-house computer program WESTAC developed to predict fast fracture failure for ceramics. This mode of impact damage may be more applicable to blade damage produced by carbon projectiles.

Phase I, Impact Variable Screening Testing - Based on results and experience gained from the initial impact testing, additional testing was performed in Phase I at the University of Dayton Research Institute (UDRI).

Impact tests will be performed in the first phase of this program to evaluate impact variables not considered in the initial impact program. The variables being evaluated and the number of tests and test conditions being run are given in Table 9.

TABLE 9. IMPACT TESTS PLANNED FOR PHASE I

Impact Variable	Test Conditions	Number of Tests
Baseline	90 Degree Impact Angle, Room Temperature	20
Impact Angle	45 Degrees	4
Projectile Geometry	Cone or Cylinder	4
Target Thickness	0.030 inch	4
Target Temperature	2400F	6
Target Geometry	Impact Radius	4
Target Surface Condition	Polished	4
Target Material	SiC	4

The objective of these tests is to eliminate the insignificant variable before starting the comprehensive testing and analyses planned for Phase II.

Specimens for Phase I have been fabricated and sent to UDRI. The room temperature test specimens are shown in Figure 63. GAPD has recommended the fixture shown in Figure 64 for room temperature testing. Elevated temperature targets are 2-inch cubes. UDRI has developed a furnace for these tests.

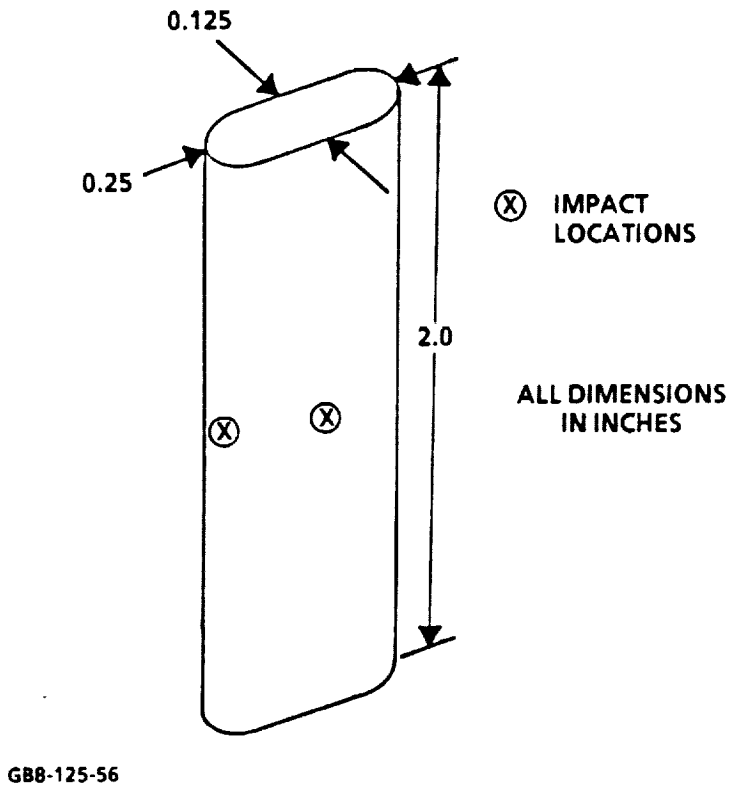

Figure 63. Phase 1 Room Temperature Test Specimen Configuration.

4.1.2 Ceramic Design Analysis

Flow Separator Housing

Thermal and mechanical stress analyses were performed on the flow separator housing. This effort was initiated to update the thermoelastic stress analysis based upon engine test derived heat transfer coefficients. These results will be used to determine the stress rupture life of this component. This work also supported the development of the integral hot side regenerator seal, which requires the regenerator face of the flow separator housing to be as flat as possible to minimize seal leakage.

The 3-D finite element model for the LAS flow separator housing without struts was completed. The model consisted of 8111 elements and 11,640 nodes. A stress analysis was done at the 2500F flat rated condition for pressure loading only. Peak principal stresses were found in the radii of the crossarm casting cavities at the backside of the component. A plot of the maximum principal stresses is shown in Figure 65.

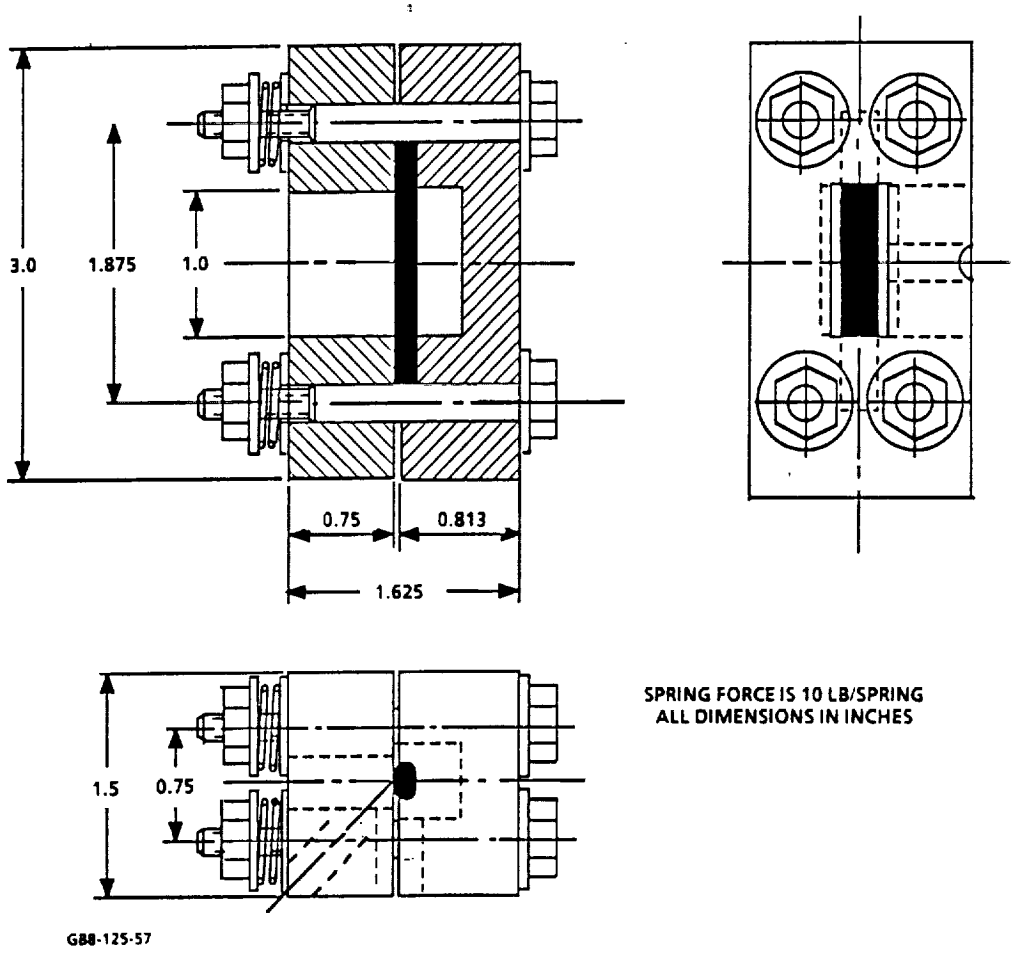

Figure 64. Impact Test Fixture (Room Temperature).

The empirical evaluation of the heat transfer coefficients on the flow separator housing has also been completed. The heat transfer coefficients were evaluated based on transient thermocouple response data of a metallic flow separator housing at a reduced engine combustor temperature operation. Iterative changes were made on the boundary conditions (heat transfer coefficients) of the thermal analysis until analytical results duplicated test results.

Life Prediction

In conjunction with the Design Review failure probabilities were calculated for the ATTAP rotor, turbine shroud, and stators with NT154 material properties. Weibull-based risk integration methods were used in these calculations. Results show each of these turbine section components has low failure probability.

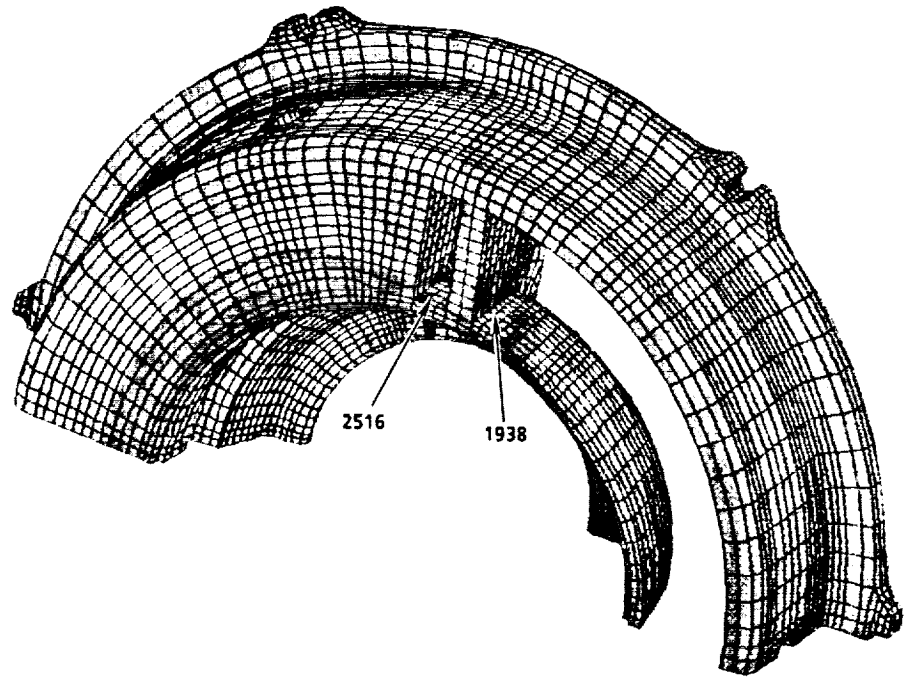

MAXIMUM PRINCIPAL STRESSES (PSI)
2500F FLAT RATED PRESSURE LOADING

MX = 2516
MN = -270

-76.9	1323
123	1523
323	1723
523	1923
723	2123
923	2323
1123	2516

GB8-125-74

Figure 65. Pressure Stress for the LAS Flow Separator Housing.

The risk of failure for the rotor, shroud, and stator were calculated from the finite element stress and temperature results given in the Design Review (Section 4.2). The probability of surface and volume survival was calculated for each element:

$$CPS_V = \prod_{i=1}^{n} e^{-V_i \left(\frac{\sigma i}{\sigma_{oV}}\right)^{M_V}}$$

$$CPS_A = \prod_{i=1}^{n} e^{-A_i \left(\frac{\sigma i}{\sigma_{oV}}\right)^{M_A}}$$

The total component survival probability is the product of the surface and volume survival probabilities:

$$CPS_{total} = CPS_v \times CPS_A$$

The Batdorf, normal stress, multiaxial fracture criteria was used to calculate the effects of multiaxial stresses and failure risk. The Batdorf criteria predicts failure probability increases as the stress ratio, σ_2/σ_1, approaches unity (1). This is shown in Figure 66.

A slow crack growth model was combined with the fast fracture methods to calculate the risk of delayed failure. The slow-crack-growth power-law shown in Figure 67 was integrated with respect to time to derive the time to failure equation also shown. This equation was combined with the Weibull fracture criteria to obtain the time dependent failure probability function in Figure 67. This function becomes the fast fracture criteria at time equals zero.

Fast fracture parameters, slow crack growth parameters and fracture toughness were determined from the NT154 data provided in Section 5.1. Weibull strength plots are shown in Figure 68. The NT154 properties used for these analyses are given in Tables 10 and 11. Only two internal failures were observed at 70F, which is insufficient for reliable calculation of internal properties. Therefore, the 75F internal Weibull parameters used for component risk analyses were scaled from the 2200F properties, and are included in Table 10.

The failure probabilities for the rotor, stator, and turbine shroud are summarized in Table 12. The shroud and stator have very low risks of failing during a normal lightoff cycle. The turbine was calculated to have a fast fracture failure probability of 0.019 percent at 100 krpm with 2500F TIT, and 1.8 percent failure probability after 1000 hours at these conditions.

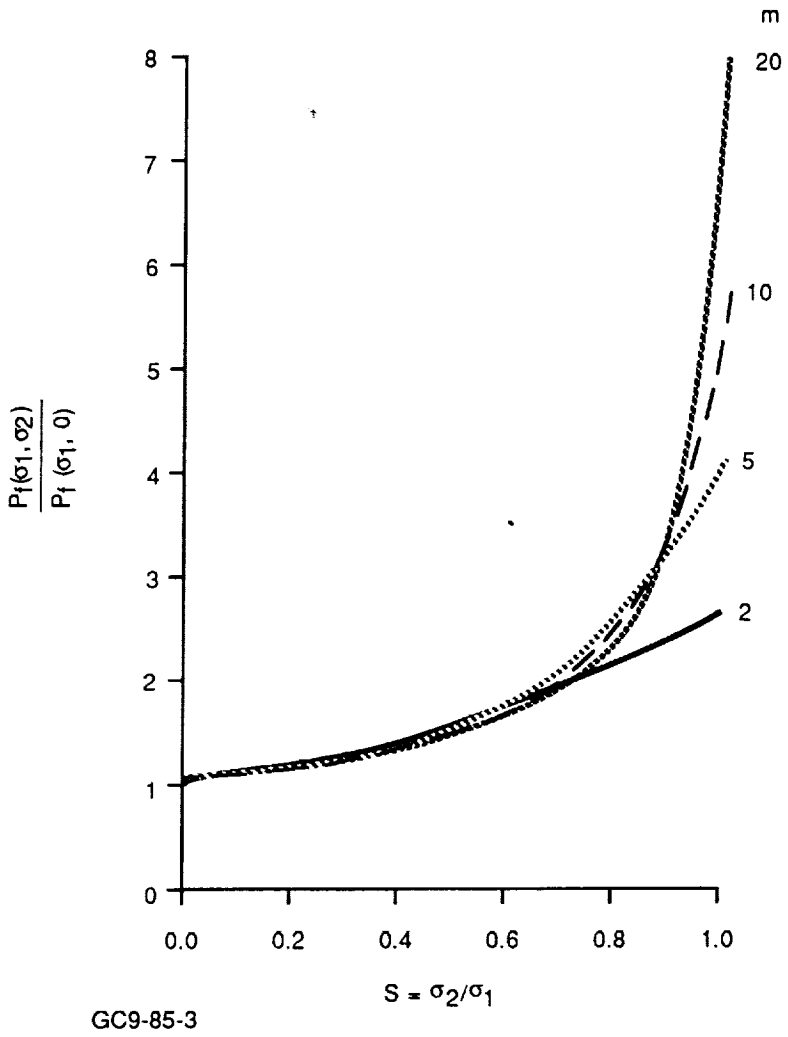

Figure 66. Batdorf Normal Stress Integration Predicts Higher Failure Risk With Increasing Biaxial Stress, and Weibull Modulus, m.

The turbine shroud failure risk was assessed over the first five minutes of the lightoff cycle. The maximum failure risk of each element in the shroud FEM model does not occur at the same time in the cycle. Therefore, the total shroud failure risk is the combined failure risk of each element in the shroud model at its maximum risk time. The combined failure probability, PF, was calculated according to:

$$PF = 1 - (RA \times RV)$$

$$RA = \prod_{i=1}^{n} RA_{i,m}$$

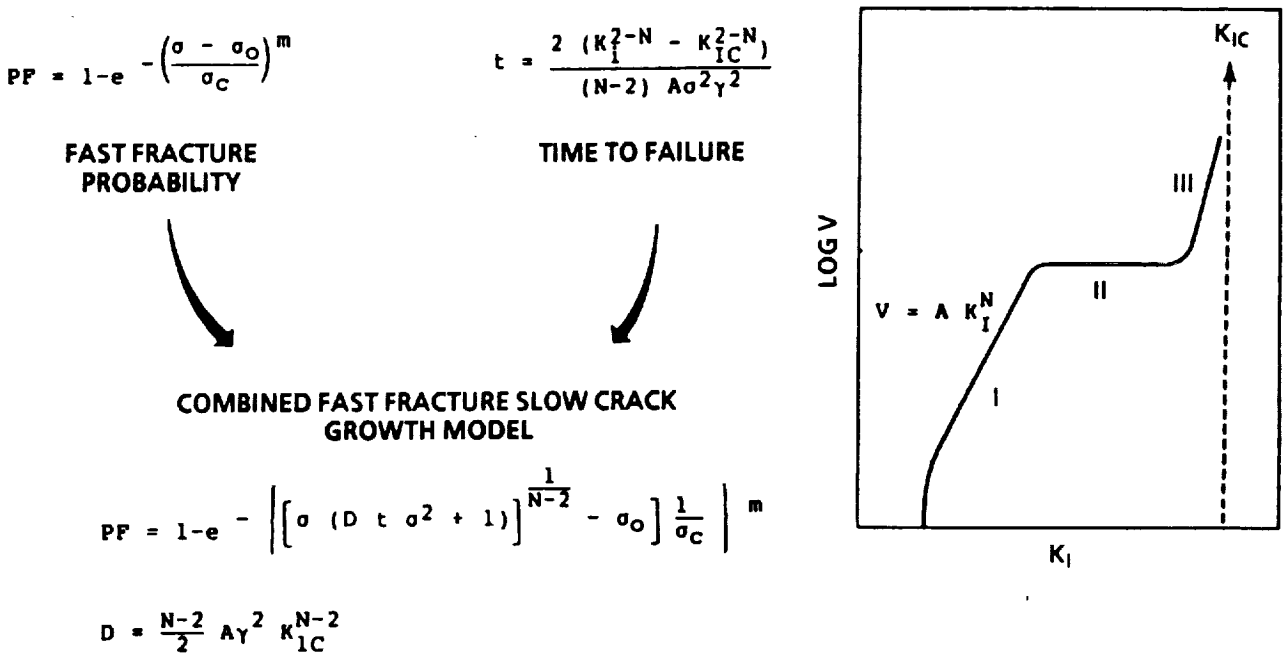

Figure 67. The Weibull Fast-Fracture and Slow-Crack-Growth Function Were Combined Into a Single Risk Function.

$$RV = \prod_{i=1}^{n} RV_{i,m}$$

i = element number
m = time with lowest area reliability
n = time with lowest volume reliability

Results from the shroud failure prediction are shown in Figure 69. This figure includes stress at the maximum stress location superimposed on a bar chart of the number of maximum stress elements that occur at 10-second intervals during the liftoff cycle. Many elements have their maximum risk at the first 10-second interval. However these elements have low failure risks and the overall

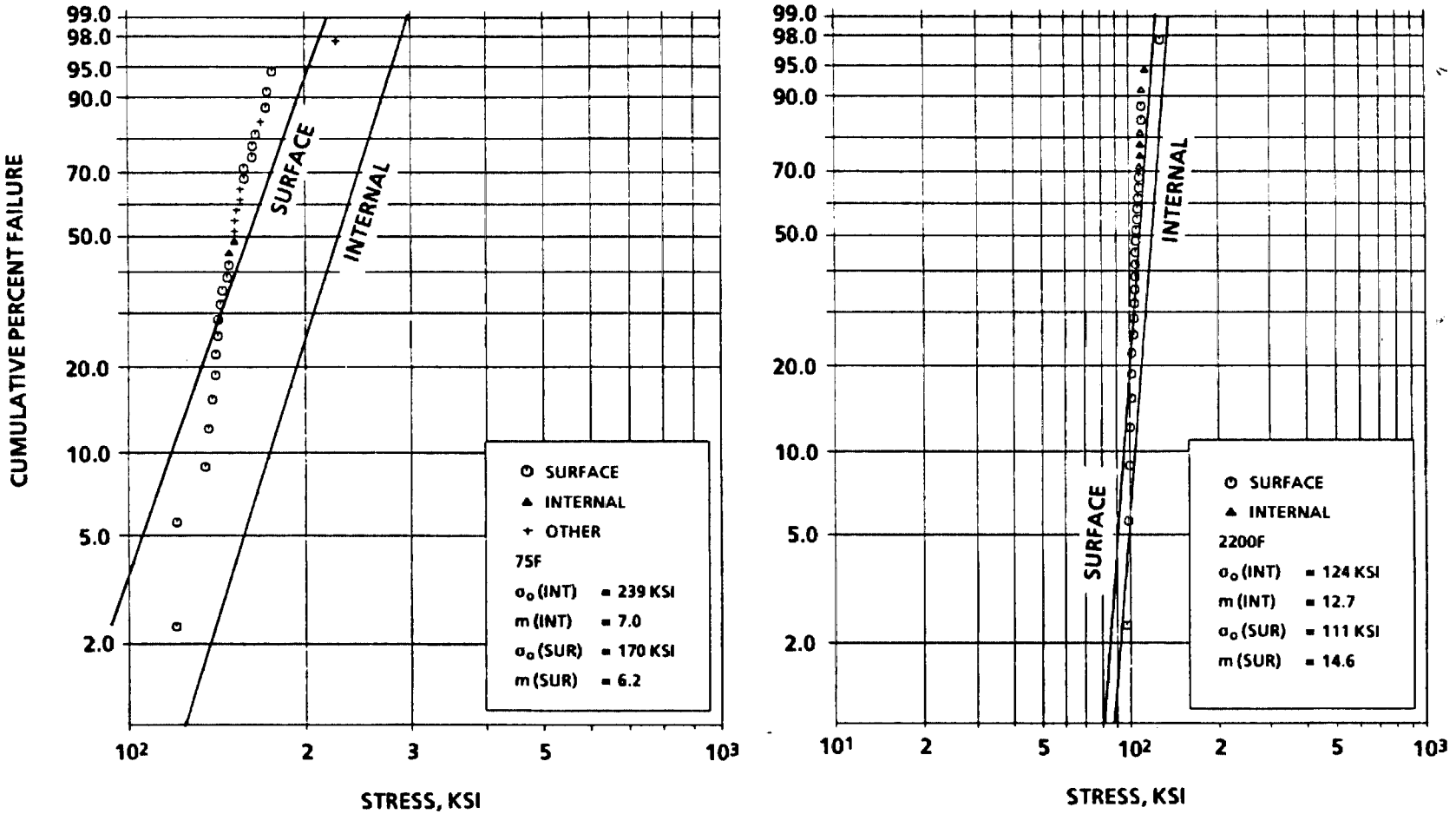

GB9-85-20

Figure 68. NT154 Weibull Surface and Interval Strength Distributions Determined From Flexure Bar Tests Run at 75 F and 2200F.

TABLE 10. NT154 WEIBULL STRENGTH PARAMETERS WERE USED TO CALCULATE COMPONENT FAILURE PROBABILITIES.

	σ_o ksi	M	Number of Failures	Specimen Size
T = 75F				
Surface	170.4	6.2	21	0.188 in^2
Internal	238.8	7.0	2	0.00146 in^3
Internal*	190.	5.4		0.00183 in^3
Total	162.0	6.8	30	
T = 2200F				
Surface	111.4	14.6	24	0.188 in^2
Internal	123.8	12.7	6	0.000855 in^3
Total	109.5	14.2	30	

*parameters used for component analyses

TABLE 11. SLOW CRACK GROWTH PARAMETERS AND FRACTURE TOUGHNESS VALUES USED TO CALCULATE COMPONENT FAILURE PROBABILITIES.

Slow Crack Growth		
Parameter- A	3.5×10^{-23}	3.5×10^{-23}
Parameter - n	2.8	33.6
Fracture Toughness		
K_{IC}	5.9	5.3

TABLE 12. TURBINE SHROUD, STATOR AND ROTOR FAILURE PROBABILITIES BASED ON NT154 PROPERTIES.

Component	Condition Analyzed	Time, (Hrs)	Failure Probability (absolute)
Turbine Shroud	Normal Lightoff	0.0	0.000020
Stator	Normal Lightoff	0.0	0.000001
Turbine Rotor	Partial Power (70 krpm, 2200F TIT)	0.0	0.000001
		100,000	0.000005
	Maximum Power (100 krpm, 2500F TIT)	0.0	0.00019
		100	0.0067
		1,000	0.018

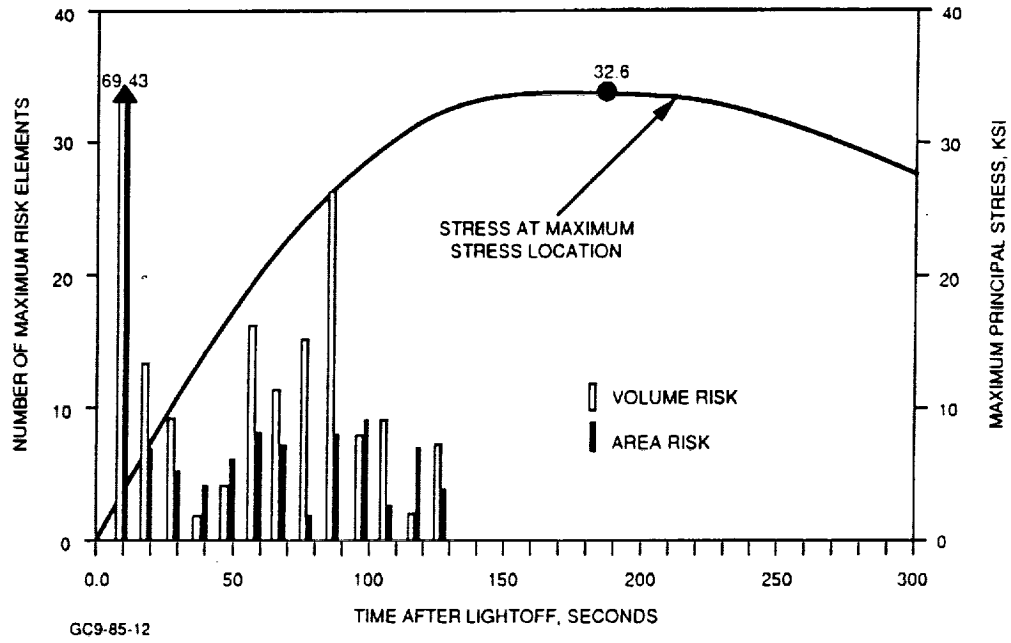

Figure 69. This Bar Chart Shows the Number of Elements in the NT154 Turbine Shroud Model That Reach Their Maximum Failure Risk at Each 10-Second Interval in the Lightoff Cycle. Failure Risk Does Not Coincide With Maximum Stress.

failure risk is very low at that time. The maximum risk at any single time is 0.00186 percent, at 90 seconds. The combined failure risk over the entire cycle is 0.00222 percent. A failure probability of 0.00120 percent would be predicted if failure probability was evaluated only at the maximum stress time of 180 seconds.

The failure risk of the stator at its maximum stress time in a normal lightoff cycle is less than 0.0001 percent. Because this failure risk is negligible failure risk was not evaluated over the entire stator lightoff cycle.

Rotor failure probabilities were calculated for two operating conditions, 70 krpm with 2200F TIT, and 100 krpm with 2500F TIT. The rotor failure probabilities at operating conditions of 100 krpm with 2500F TIT are plotted in Figure 70. This plot includes failure risks calculated for rotors made from NT154 and the previous best AGT101 Si_3N_4 material. These failure risk are acceptable since the AGT101 engine would rarely, if ever, operate at these severe conditions.

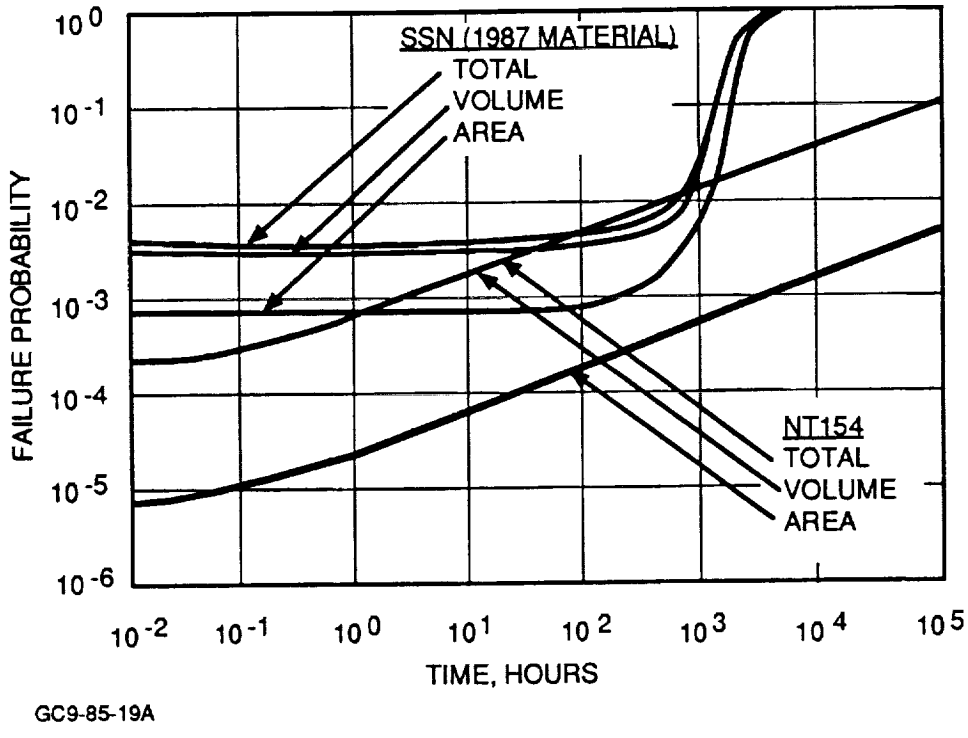

Figure 70. Rotor Failure Predictions for Operation at 100 krpm and 2500F TIT.

These analyses indicate that NT154 is a good material for the ATTAP turbine section components. These calculations are preliminary and will be upgraded as improved life prediction methods and more complete design data become available.

4.2 Design Review

A meeting was held with NASA/DOE at the NASA-Lewis Research Center in Dayton, Ohio to review the current state of the ATTAP engine Test Bed Design. This fulfilled the second ATTAP contract milestone for the Turbine Stage Design Review. Included in this Design Review were discussions and transmittals on the following subjects:

- o Reference Powertrain Design
- o Ceramic Component Thermal/Stress Analysis
- o Ceramic Component Life Prediction
- o Failure Modes, Effects, and Criticality Analysis
- o Hazards Analysis
- o Test Bed Critical Interfaces and Dimensions

Turbine Coupling Redesign

A redesign of the turbine coupling was also presented at the design review. Documentation of this subject can be found in Section 3.4 (Test Bed Engine Design).

4.2.1 Reference Powertrain Design

Refer to Section 3.2.

4.2.2 Ceramic Component Thermal/Stress Analysis

As part of the design review the stress analyses of three ceramic components were updated for a "state of the art" ceramic material. Norton/TRW NT154 was chosen for this study. Life predictions based upon these stress analyses were also presented as part of the Design Review. Details of these life predictions are given in Section 4.1.2 Ceramic Design Analysis.

The ATTAP RPD engine ceramic hot section consists of 75 static structural and support system components, and a ceramic radial inflow turbine rotor, as shown in Figure 71. The three components selected for this material update study are the turbine rotor, the stator, and the shroud. These components were selected because their requirements were typical for all ceramic applications in turbine engines.

The turbine rotor experiences a predominately mechanical high stress field over a long duration of operational time induced by the centrifugal loading. The primary failure mode is stress rupture.

ORIGINAL PAGE
BLACK AND WHITE PHOTOGRAPH

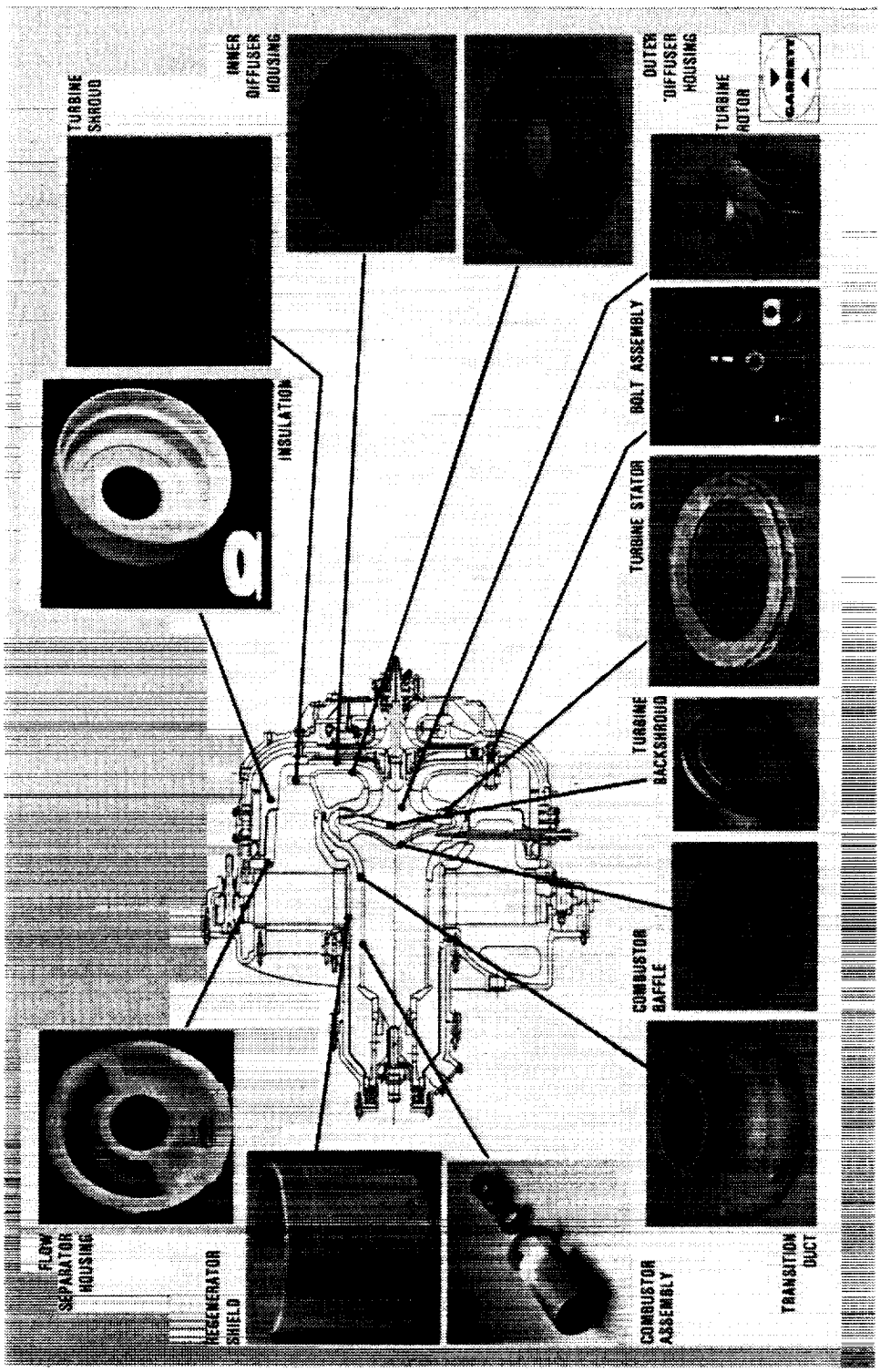

Figure 71. AGT101 Ceramic Components.

The turbine stator runs hotter and operates close to the turbine inlet temperature. High core flow velocities produce high heat transfer coefficients, which coupled with the required nonuniform vane profile, creates high thermal stresses at the vane trailing edge during engine lightoffs.

The turbine shroud is also exposed to high thermal stresses but at a lower operating temperature and over a much larger volume than those of the turbine stator. The turbine shroud must survive the thermal transient stresses that are induced as the local thermal boundary conditions change along the meridional flow path. These nonuniform boundary conditions result in high thermal gradients and polyaxial stresses within the shroud, predominately during light-off conditions. The greatest influence on the thermal gradients is the variation in heat transfer coefficients.

Maximum principal tensile stresses and temperatures for these three components fabricated out of NT154 are shown in Table 13 at three engine operating conditions (two steady-state conditions and one transient light-off condition). The temperatures at the peak principal tensile stress locations are shown as well as the principal tensile stresses at the peak temperature locations. The transient lightoff results are based on the normal engine light-off cycle to 65 krpm cruise as shown in Figure 72.

TABLE 13. CRITICAL CERAMIC COMPONENTS STRESS SUMMARY

	MATERIAL	ENGINE LIGHTOFF		STEADY STATE MAXIMUM POWER				STEADY STATE IDLE			
		PEAK STRESS	TEMP	PEAK STRESS	TEMP	PEAK TEMP	STRESS	PEAK STRESS	TEMP	PEAK TEMP	STRESS
ROTOR	NT154	28.0	1000	41.6	2009	2159	<5.0	23.7*	1278*	2043*	<5.0*
SHROUD	NT154	32.6	1155	<5.0	2400	2450	<3.0	<5.0	2050	2100	<3.0
STATOR	NT154	14.0	1125	<5.0	2475	2475	<5.0	<3.0	2125	2125	<3.0

* PARTIAL POWER CYCLE POINT (70,000 RPM, 2200 DEG F)

ALL STRESSES ARE MAXIMUM PRINCIPAL STRESSES (KSI)
ALL TEMPERATURES ARE IN DEGREES F

GB8-108-70

C-2

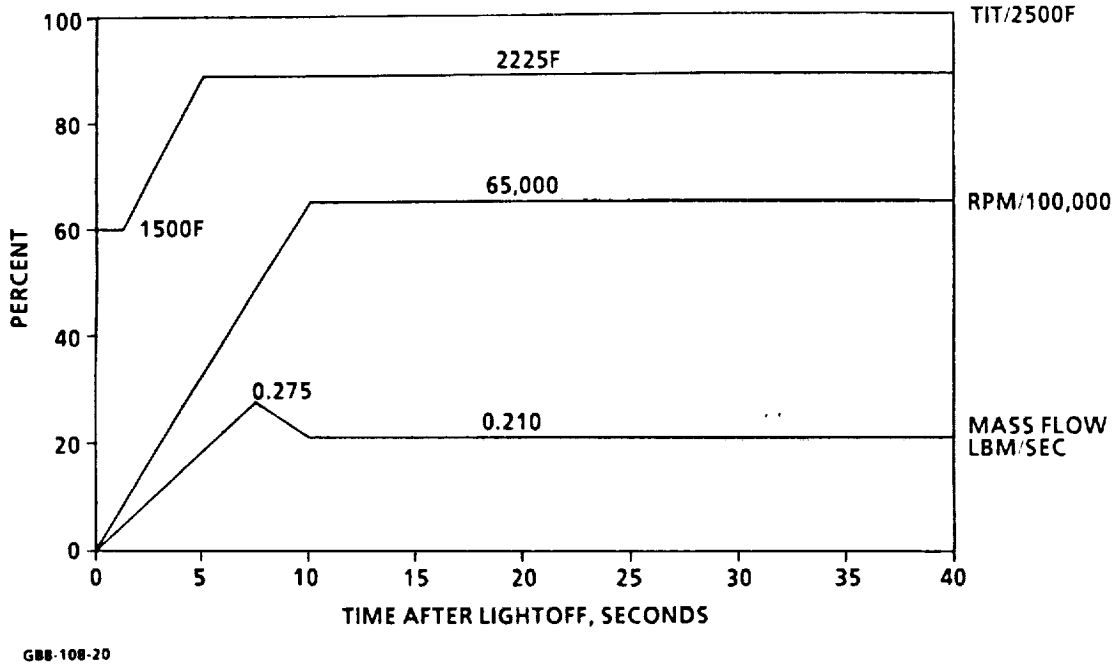

Figure 72. Normal Engine Lightoff Cycle.

Figure 73 shows the transient stress response for the NT154 turbine shroud for the normal engine lightoff. The maximum principal tensile stress (32.6 ksi) occurs 180 seconds after light-off in the shroud seal area (location A2). The temperature distribution at this critical time on the turbine shroud is shown in Figure 74. The temperatures vary from 1700F plus at the shroud inner bore to less than 1200F at the shroud flange outer edge. This temperature gradient creates a bending stress in the shroud seal area as shown in Figure 75.

The transient stress response for the NT154 turbine stator is shown in Figure 76. Because of the high heat transfer coefficients on the stators, the maximum principal tensile stress peaks at 22 seconds after lightoff. The temperature distribution at 22 seconds after lightoff is shown in Figure 77. The temperatures varies from 1125F at the mid-vane trailing edge to 595F at the platform outer forward contact surface. The maximum principal tensile stress (14.0 ksi) occurs at the mid-vane trailing edge as shown in Figure 78.

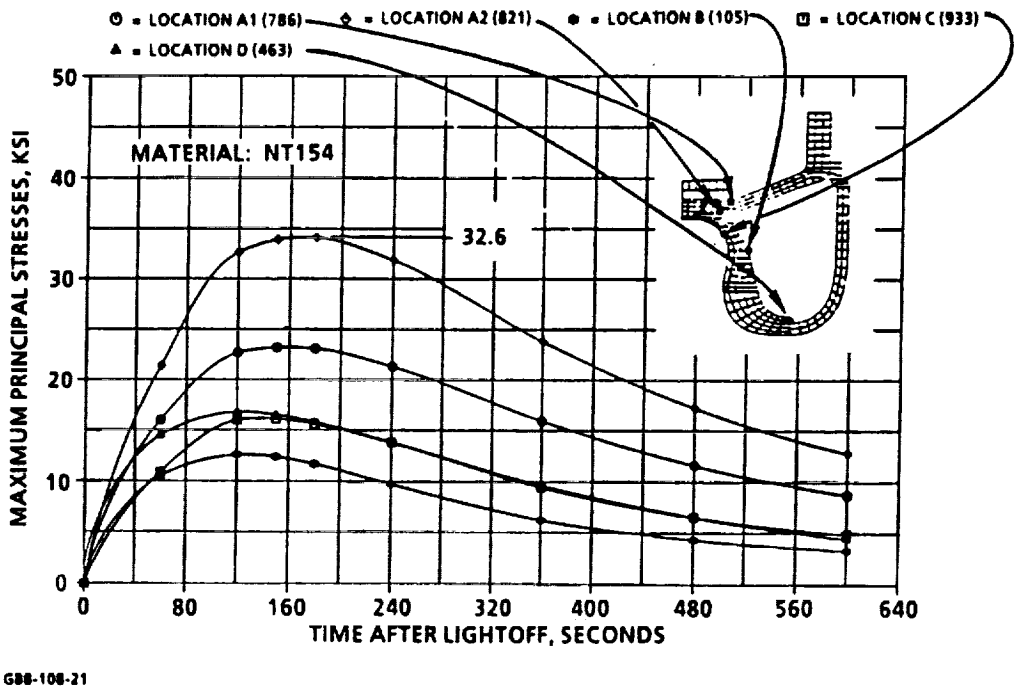

Figure 73. Turbine Shroud Maximum Principal Thermal Stress Response During a Normal Engine Lightoff.

The peak tensile stresses on the turbine rotor at two steady state conditions have been analyzed, the maximum power (100 krpm) condition and a partial power cruise (70 krpm) condition. The temperatures and maximum principal stresses for the maximum power condition are shown in Figures 79 and 80, respectively. The peak tensile stress (41.6 ksi) occurs in the blade saddle region while a lower tensile stress (30.6 ksi) occurs at the hub centerline. The temperatures and maximum principal stresses for the partial power condition are shown in Figures 81 and 82, respectively. At this condition the stresses are lower than they are for the maximum power condition. The peak tensile stress (23.7 ksi) occurs at the blade fillet radius. The peak tensile stress at the hub centerline is 16.4 ksi.

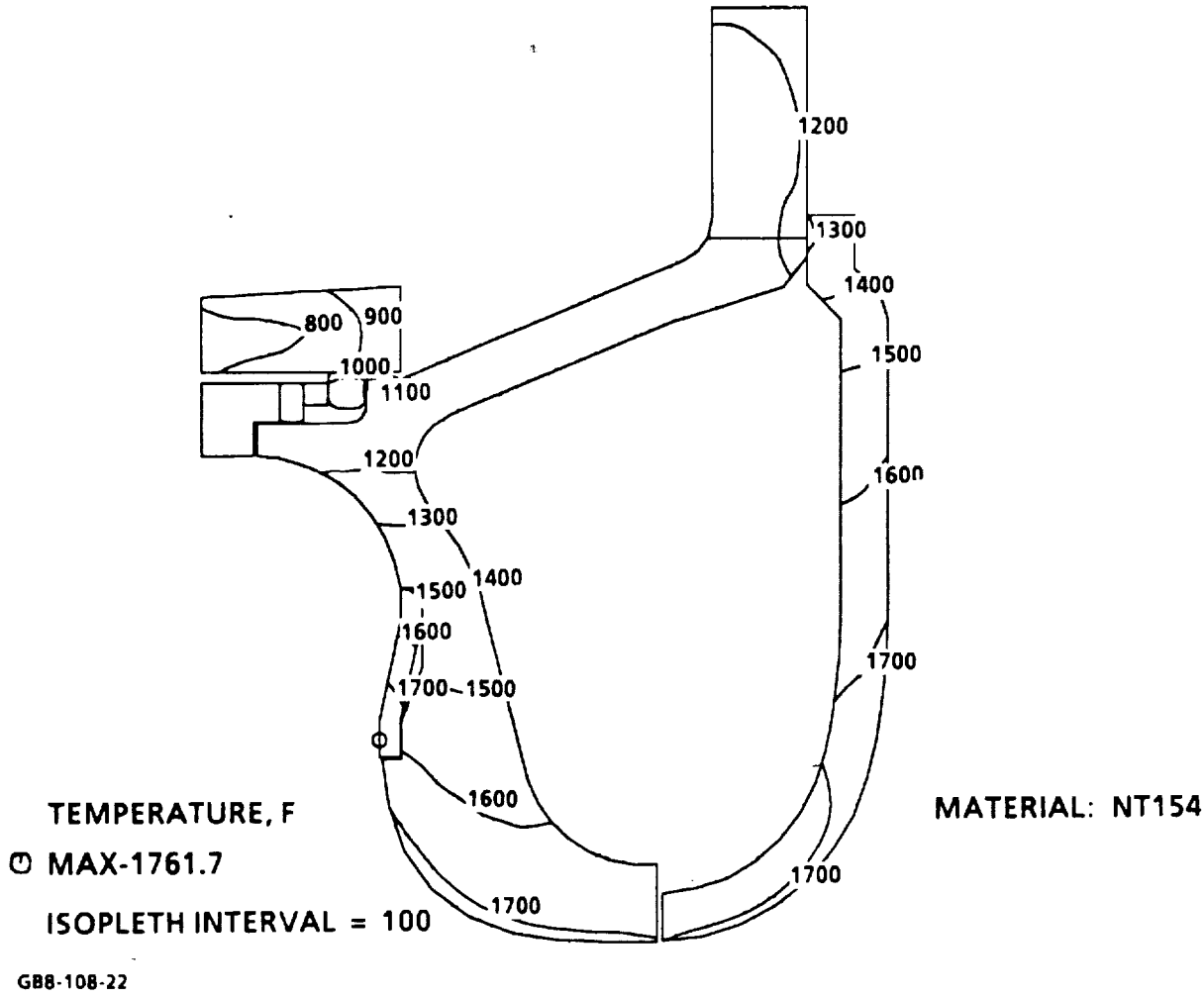

Figure 74. Turbine Shroud Temperature Distribution 180 Seconds After a Normal Engine Lightoff.

4.2.3 Test Bed Critical Interfaces and Dimensions

A summary of critical interfaces and dimensions were compiled and transmitted to NASA/DOE at the Design Review. This package included a summary of test bed build dimensions, an axial tolerance analysis of 91 component stacks, and a summary of 47 radial fits within the engine test bed.

4.2.4 Failure Mode, Effects, and Criticality Analysis (FMECA)

The FMECA was prepared in compliance with paragraph C2, Exhibit B, contract DEN3-335, for ATTAP. GAPD Report Number 31-7554 documents the FMECA for the ATTAP test bed engine, as delineated on engineering drawing number PA3610131 and related drawings and specifications as of August 1988.

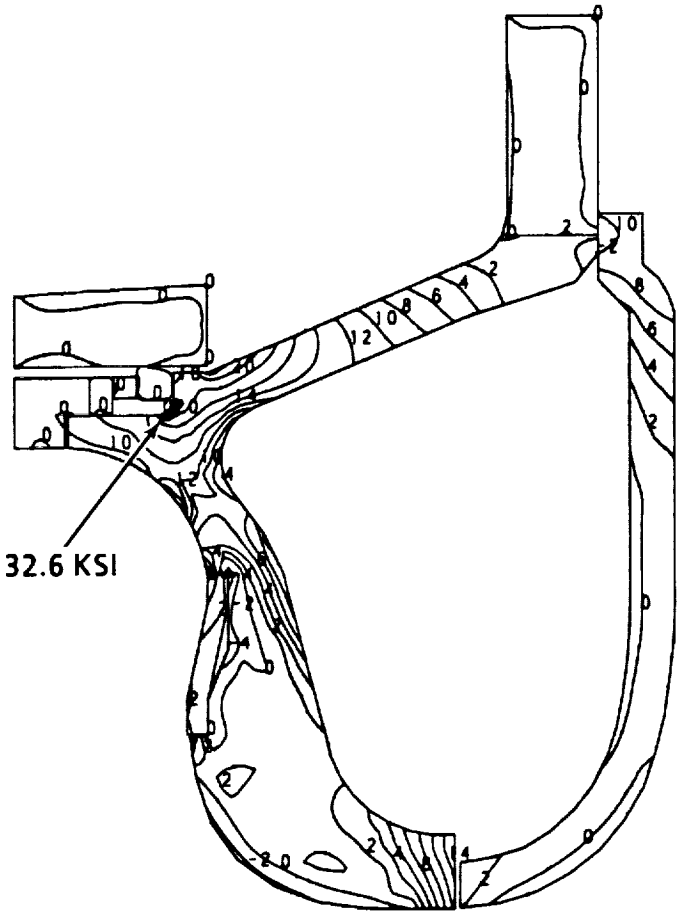

Figure 75. Turbine Shroud Maximum Principal Thermal Stresses 180 Seconds After a Normal Engine Lightoff.

Purpose

The purpose of this analysis was to systematically identify, evaluate, and document potential failure modes, and effects, and to classify each potential failure according to its severity and probability of occurrence. This analysis may supplement and support other engineering tasks such as safety, maintainability, logistics and trade studies during the ATTAP or future development programs as applicable.

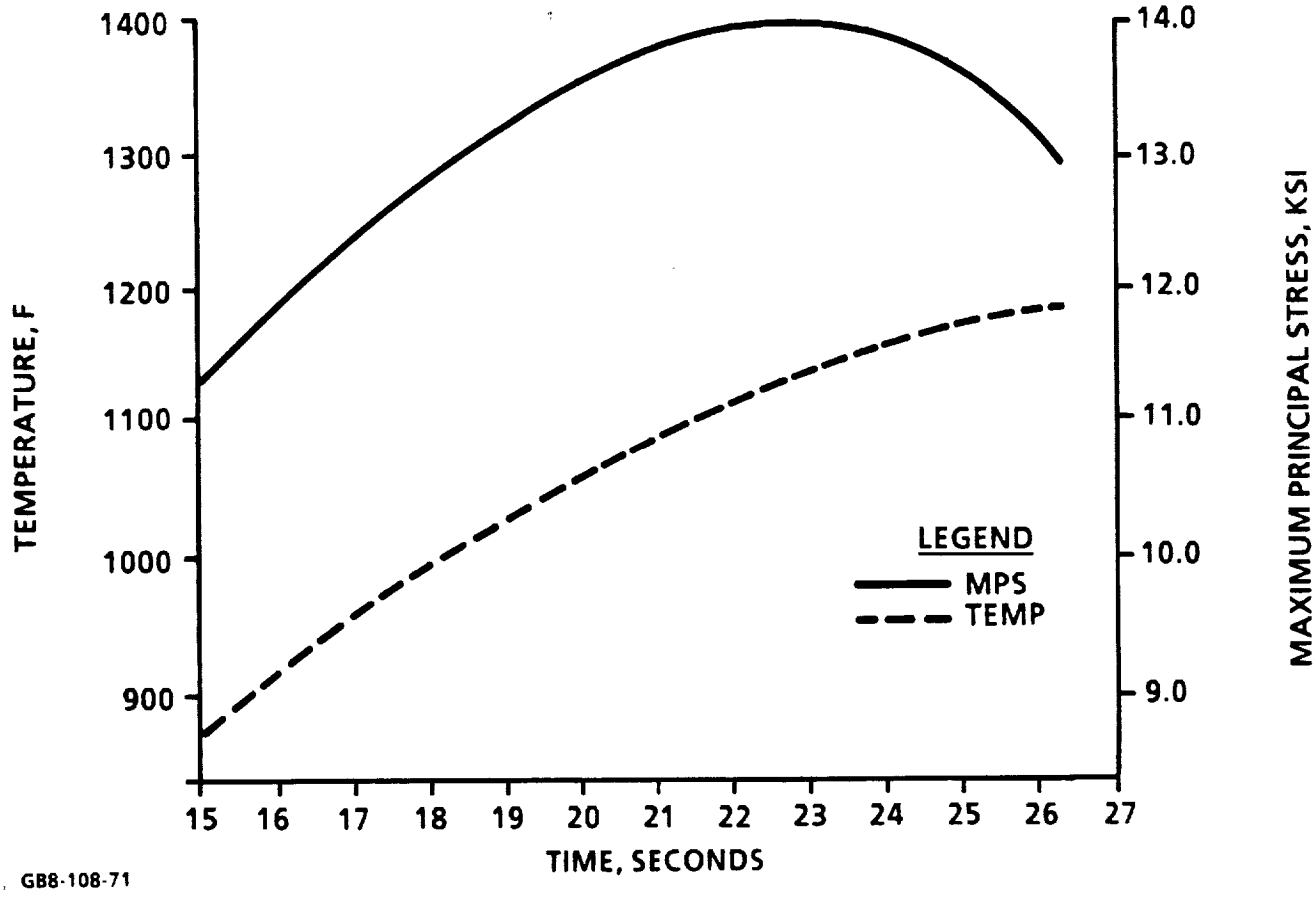

Figure 76. Turbine Stator Maximum Principal Stress and Temperature at Mid-Vane Trailing Edge During a Normal Engine Lightoff.

Scope

The FMECA includes potential failure modes, failure effects (local, next higher level/secondary, and end) and criticality (impact on readiness, system safety, and demand for maintenance). The analysis was limited to major components and did not necessarily include nuts, bolts, washers, shims, spacers, gaskets, screws, lock-wires, packings, sleeves, etc. The data to generate this FMECA report was stored in an IBM Personal Computer, using Database III Plus, to facilitate data entry, modification, storing, and output-ting.

General Analysis Procedure

A review of contributing information available on the engine assembly was conducted to facilitate system definition. Then, the engine assembly was broken down into major functional systems and components, and numerically coded for identification and tracking. The AGT101 engine assembly, considered as indenture level 1, was broken down into level 2 sections and seven level 3 subsystems as

ORIGINAL PAGE IS
OF POOR QUALITY

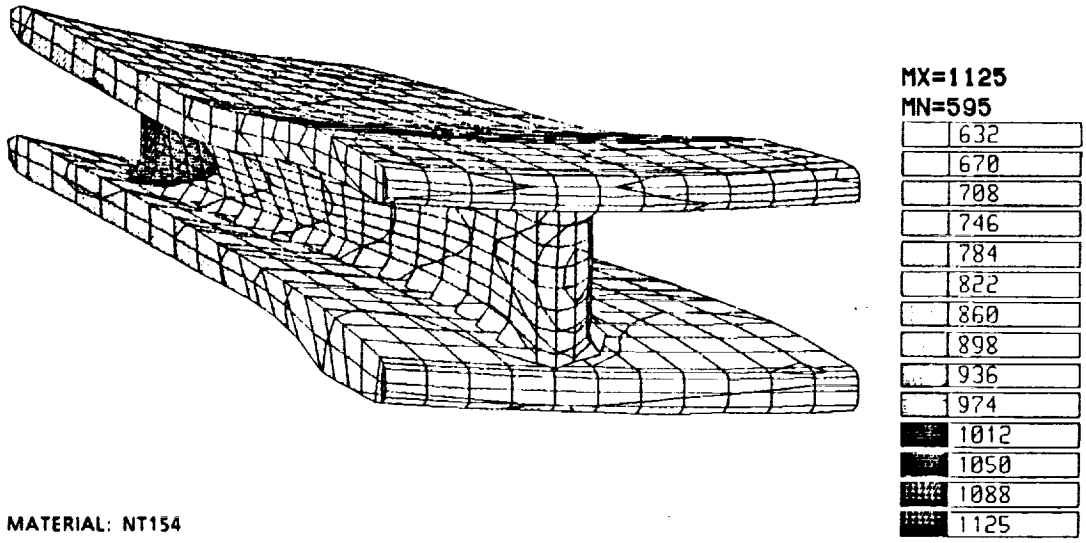

Figure 77. Turbine Stator Temperature Distribution at 22 Seconds After a Normal Engine Lightoff.

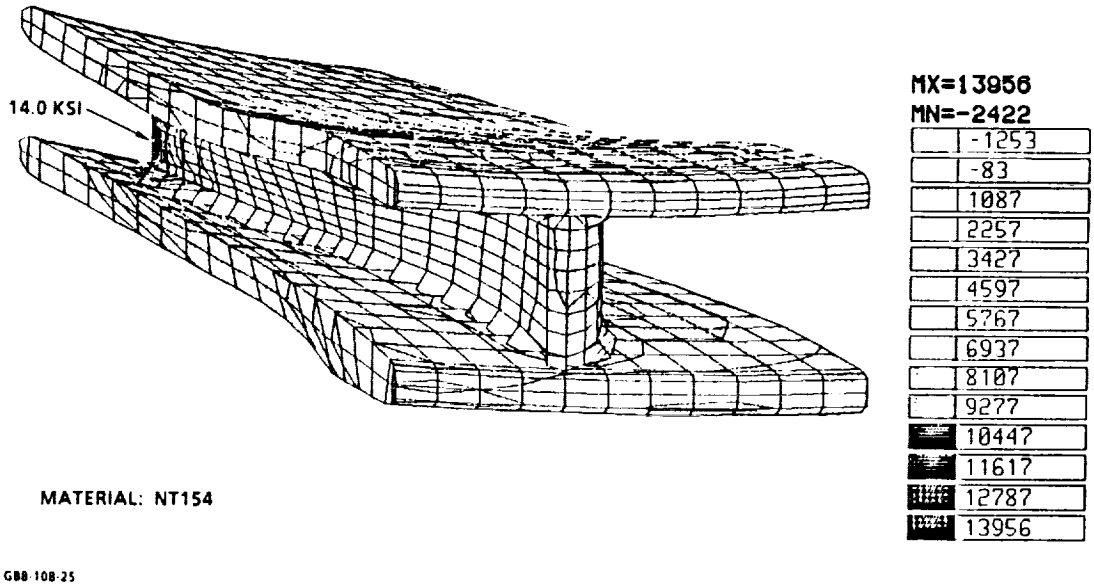

Figure 78. Turbine Stator Maximum Principal Transient Thermal Stresses at 22 Seconds After a Normal Engine Lightoff.

ORIGINAL PAGE IS
OF POOR QUALITY

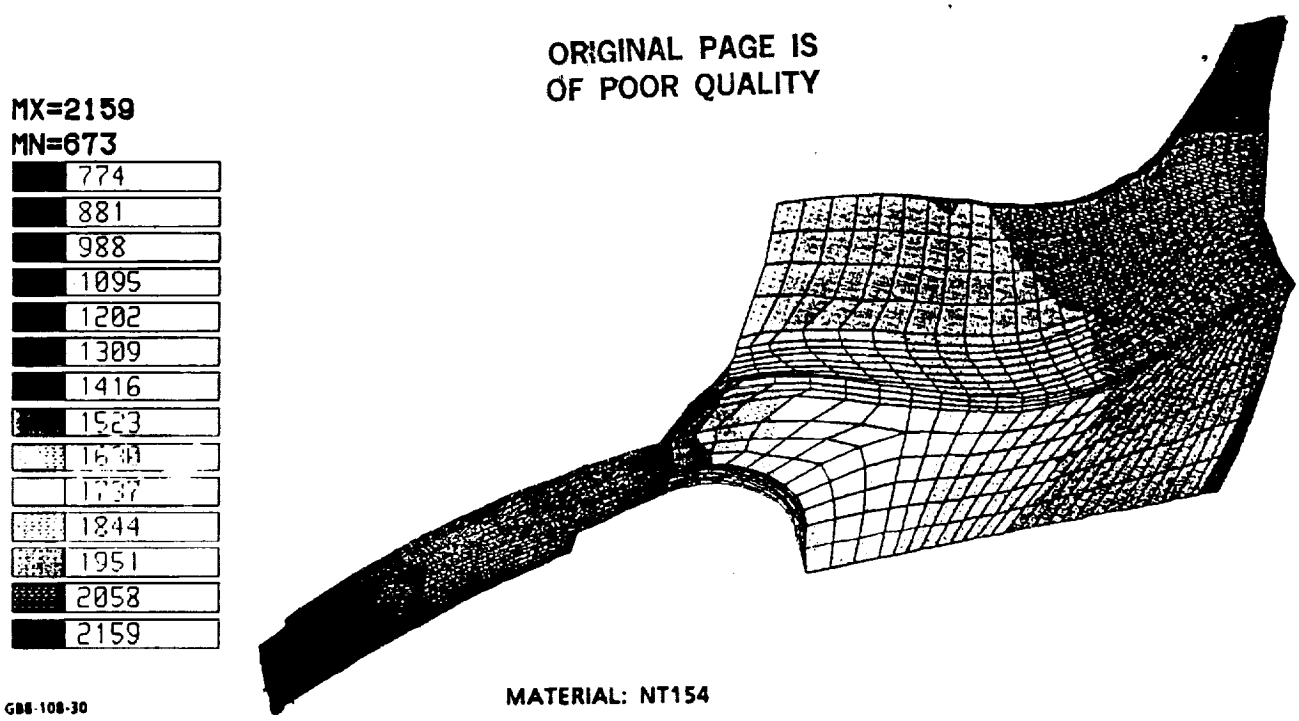

Figure 79. Rotor Steady-State Temperature Distribution At Maximum Power Condition (100 KRPM, 2500F).

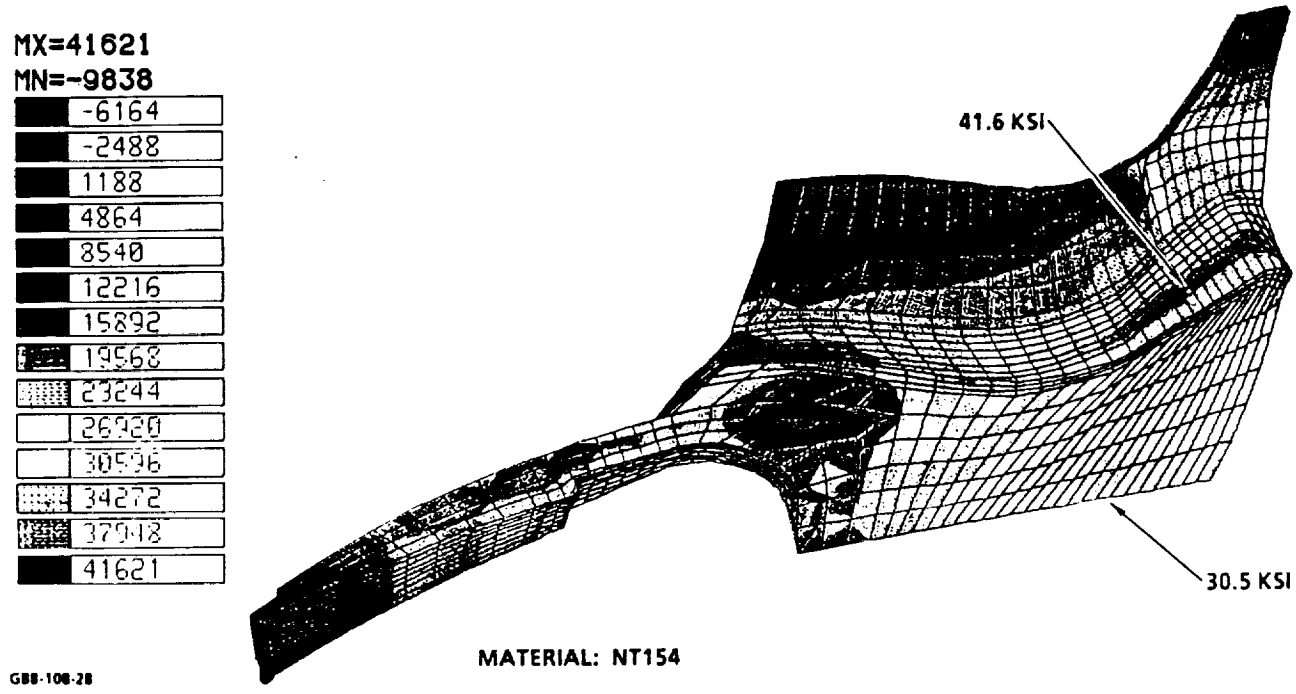

Figure 80. Rotor Steady-State Maximum Principal Stresses At Maximum Power Condition.

ORIGINAL PAGE IS
OF POOR QUALITY

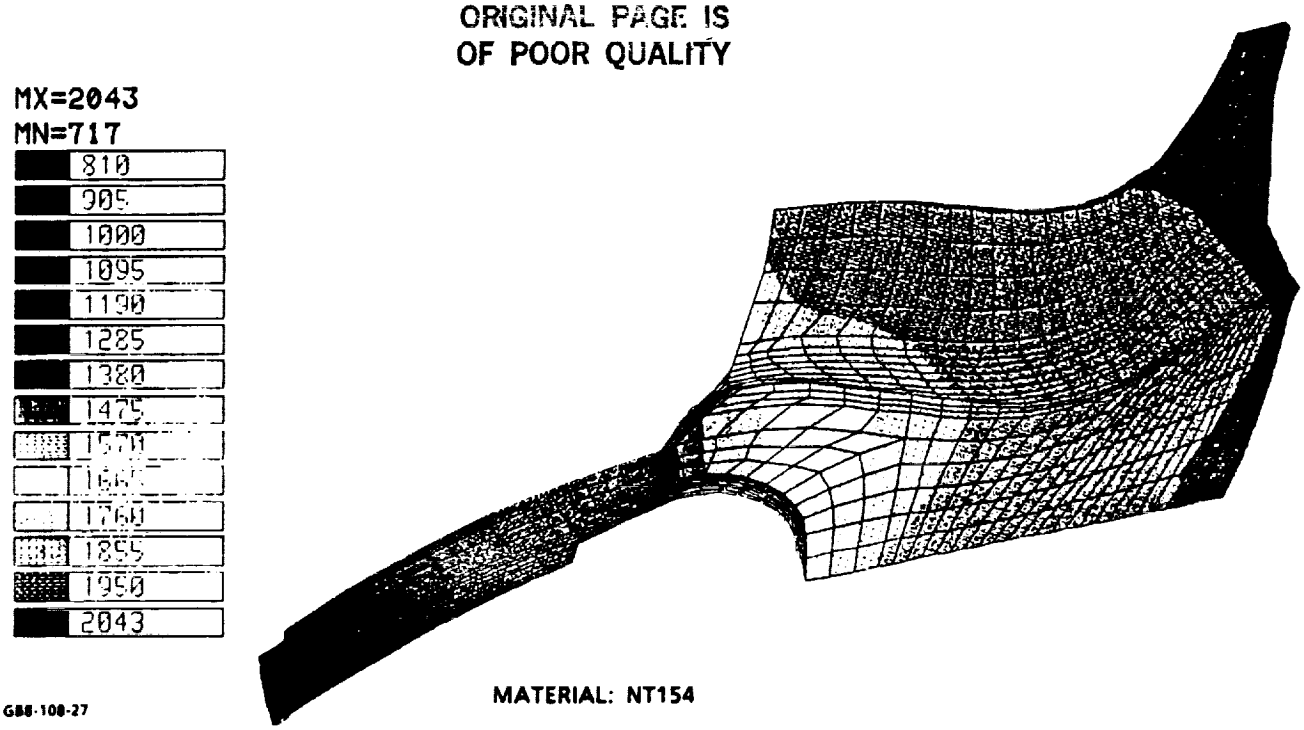

Figure 81. Rotor Steady-State Temperature Distribution At Partial Power Condition.

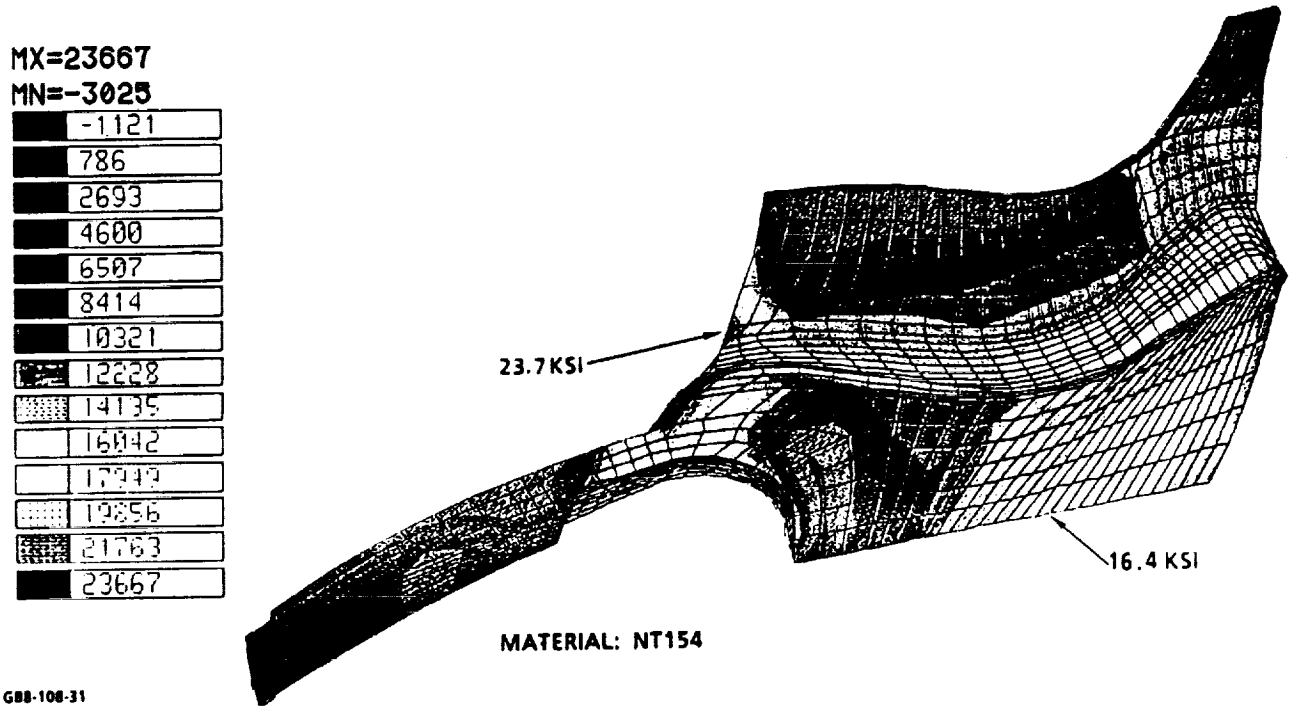

Figure 82. Rotor Steady-State Maximum Principal Stresses At Partial Power Condition.

depicted in Figure 83. The subsystems were further broken down into level 4 components. As an example, only the compressor subsystem breakdown is shown here. In the case of the ECU, level 4 indicated the input/output functional circuitries rather than the component breakdown.

The FMECA utilizing the computerized worksheets was performed and severity classifications and probability levels were assigned in accordance with assumptions and ground rules discussed in FMECA Report 31-7554. A sample FMECA sheet is shown in Figure 84. The definitions of severity classifications and probability levels are presented in Tables 14 and 15, respectively. For more details and ground rules refer to FMECA report.

Results and Discussion

The FMECA evaluated 206 potential failure modes. Overall distribution of the failure modes, as related to both engine subsystems and severity, is tabulated in Table 16. Figure 85 is a criticality matrix showing the severity classification and probability level for each of these modes. One hundred thirty-eight of these failure modes were identified as Probability Level D or E type failures and therefore not likely to occur during the ATTAP. These failures relate to the test bed controls, accessories, and metallic engine components. Of the remaining failure modes, 7 were identified as having minor severity categories (2 in B and 5 in C levels).

The A Probability failure modes, concerning the hot side regenerator seal, the ceramic bolt (3 used), the combustor inner spring, and the wave spring are currently being addressed in ATTAP. New designs will be introduced in the next iteration of the Test Bed which will improve the failure probabiliy level to at least a B for the regenerator seal and to a C for the springs and the bolt. Long term development of the regenerator seal will provide the seal with a failure probability level of C or better.

Many of the failure modes for the engines ceramic components were rated with a probability level of B and C due to the lack of data on durability of ceramic components. These levels were assigned subjectively based on the confidence in the methods used to design and analyze these components. As ceramic design methods improve and life prediction methods are verified during ATTAP, these components may be redesigned or reevaluated to improve the failure probability level.

ATTAP has an objective for demonstrating the potential for 3500 hours of engine durability over a simulated automotive duty cycle. This means that the failure modes with probability levels of A and B will have to be addressed during the ATTAP test bed development

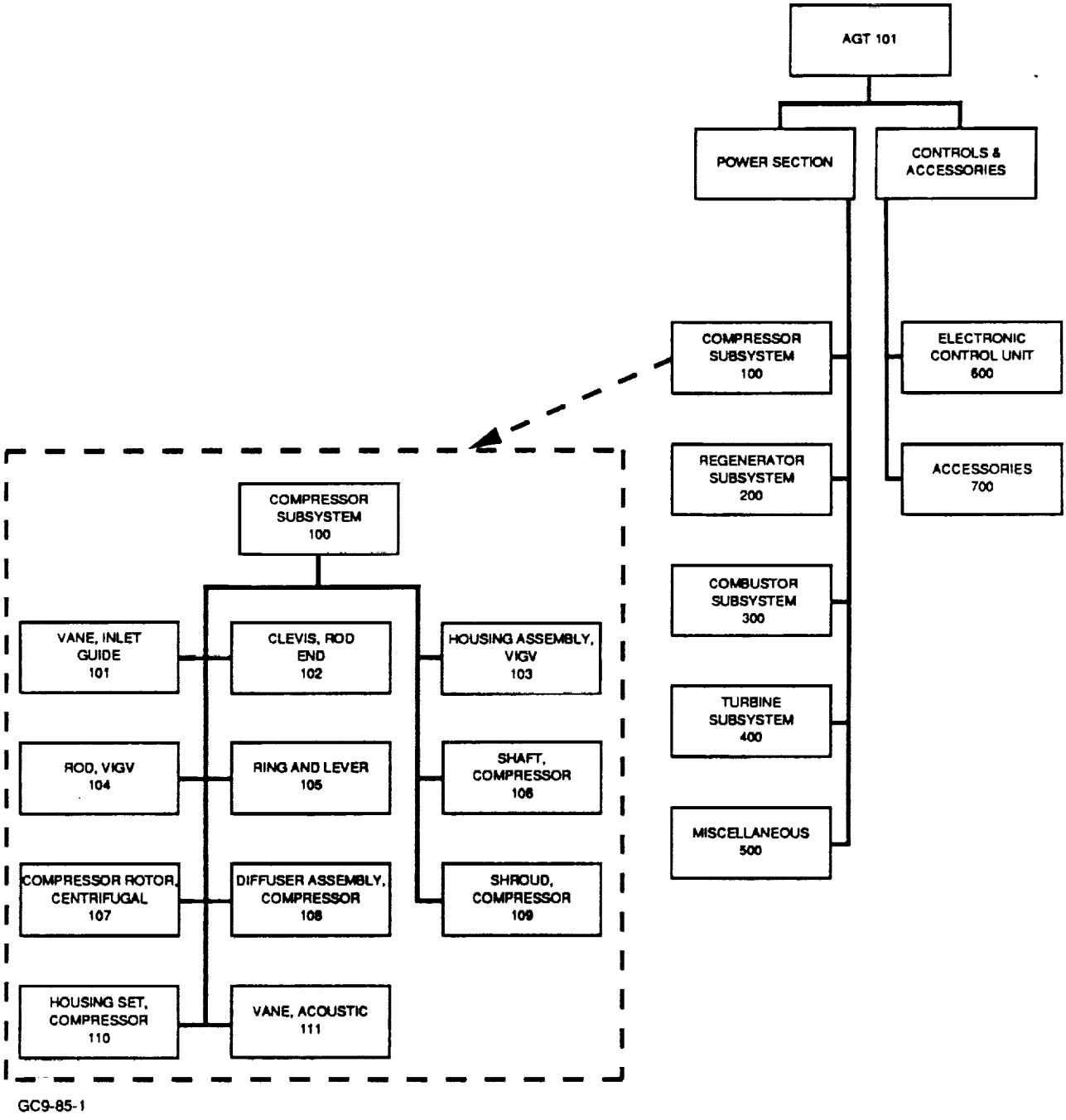

Figure 83. AGT101 Engine Assembly Breakdown Diagram.

FAILURE MODE, EFFECTS, AND CRITICALITY ANALYSIS FOR ADVANCED TURBINE TECHNOLOGY APPLICATION PROJECT

IDENT. NO.: 203	PART NO.: PA3609655-1	PREPARED BY: Reza Eskandari /	Page
COMPONENT: Housing, Flow Separator (LAS)		DATE: 9/22/88	17

COMPONENT FUNCTION: Provides flow path split between high and low pressure portions of the engine to accommodate the regenerator waste heat recover

FAILURE MODE(S) & CAUSE(S)	PHASE *	FAILURE EFFECTS a) LOCAL b) HIGHER LEVEL / SECONDARY c) END	FAILURE DETECTION METHOD	CRITICALITY SEVER **	CRITICALITY PROB ***	REMARKS
203a) Partially broken or cracked - thermal stress - vibration - high mech. stress overload - corrosion / erosion - FOD - contact stress - internal material flaws - surface machining flaws - deflection - improper installation/ handling - stress concentration at thermocouple holes	A	a) The air leaving high pressure side of regenerator may bypass combustor and turbine. b) Damage to downstream components due to fragment release. c) Depending on the amount of damage, the output power will be reduced or engine shutdown may occur.	Reduction in engine output output power or shutdown may occur.	III	B	The initial cracked or broken surface will result in local stress concentration. Due to brittle nature of ceramic and pressure/ temperature differences imposed on regenerator, this failure mode will quickly propogate and result in fractured housing. See next failure mode.
203b) Fracture into pieces - thermal stress - vibration - high mech. stress overload - corrosion / erosion - contact stress - internal material flaws - surface machining flaws - deflection - improper installation/ handling - stress concentration at thermocouple holes - FOD	A	a) Total loss of function b) Possible severe damage to adjacent components c) Engine shutdown will occur	Loss of engine function	II	B	Although the separator is exposed to low pressure hot flow and high pressure cold flow simultaneously, the low coefficient of thermal expansion for the separator reduces deflection due to thermal expansion.

* PHASE
S - START
O - OPERATION
A - ALL

** FAILURE MODE SEVERITY CLASSIFICATIONS
I - CATASTROPHIC
II - CRITICAL
III - MAJOR
IV - MINOR

*** FAILURE MODE PROBABILITY LEVELS
A - FREQUENT
B - PROBABLE
C - OCCASIONAL
D - REMOTE
E - EXTREMELY UNLIKELY

Figure 84. Sample FMECA Sheet.

TABLE 14. DEFINITION OF SEVERITY CLASSIFICATIONS

Catastrophic	I	A failure mode which may cause major uncontained engine damage or major damage to the test facility.
Critical	II	A failure mode which may cause extensive damage within the originating engine subsystem and extensive damage to other engine subsystems.
Major	III	A failure mode which may cause extensive damage within the originating subsystem, limited damage to components within other subsystems, or result in engine shutdown.
Minor	IV	A failure mode which may cause only minor damage in the originating subsystem and no damage to other engine subsystems. Engine operation may be affected, resulting in operating envelope limitations or performance degradation.

TABLE 15. DEFINITION OF PROBABILITY LEVELS

Probability Level	Description
A	The failure mode is expected to occur within 100 hours of engine operation
B	The failure mode is expected to occur at between 100 and 1000 hours of operation
C	The failure mode is expected to occur at between 1000 and 10,000 hours of operation
D	The failure mode is expected to occur at between 10,000 and 100,000 hours of operation
E	The failure mode is expected to occur after 100,000 hours of operation

TABLE 16. DISTRIBUTION OF 206 FAILURE MODES BY SEVERITY AND ENGINE SUBSYSTEMS

ID	Subsystem	Cat I	Cat II	Cat III	Cat IV	Total
100	Compressor	0	2	13	4	19
200	Regenerator	0	2	20	3	25
300	Combustor	0	8	13	2	23
400	Turbine	0	15	7	1	23
500	Misc. Power Section	0	8	15	8	31
600	ECU	0	2	39	28	69
700	Accessories	0	0	4	12	16
	Total	0	37	111	58	206

effort. These improvements will be assessed during the limited durability testing performed during ATTAP such as the 100 hour test at maximum design conditions and during a 300 hour cyclic endurance test.

It should be noted that there were no failure modes in Category I, that is, no modes involving uncontained rotating component failure which might disable the test facility. This is primarily due to the positive containment provided by the test bed engine housing and to the low energy available in the failure of the ceramic turbine rotor. The housing was designed to contain the high energy available in the hub separation of the compressor impeller.

Conclusions and Recommendations

It is very important to recognize that the ATTAP engine test bed is used to evaluate ceramic components which are in a high risk state of design. The limited test experience gathered during the AGT101 project was the sole source for establishing the failure modes and criticality for these ceramic components. The methods used to design and predict the life of these components are not verified and therefore suspect. Without additional durability data, it is difficult to establish all of the potential failure modes and failure probabilities associated with ceramic components.

The power section ceramic components are the dominant contributors to failures having higher criticality effects. This arrives from the very nature of the ceramic materials, being brittle and lacking resilence when exposed to stress concentrations from interfacial contact or impact by foreign particles.

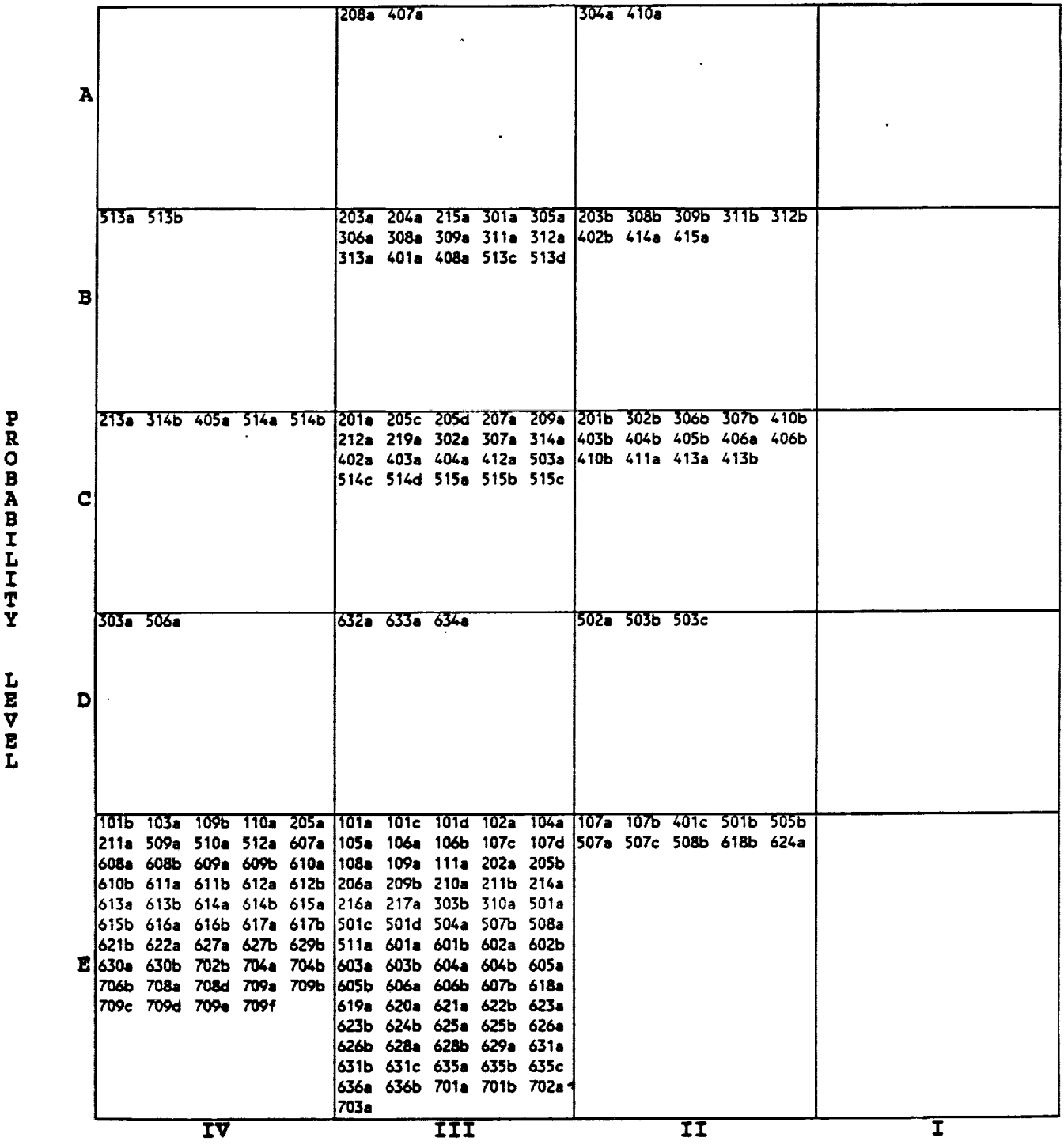

Figure 85. Criticality Matrix.

It is recommended that current and future engine development with ceramic components generate a data base and determine the mechanisms in which failures occur, with life prediction related information. Programs should be initiated to determine design modifications that may reduce the failure effect severity, and increase their life in engine applications.

It is further recommended that the FMECA be periodically updated to evaluate modifications to the present design. With respect to future engine applications (i.e., automotive, etc.), it is highly recommended to perform thorough FMECAs for specific applications and interfaces with other machinery and operators.

4.2.5 Preliminary Hazard Analysis (PHA)

The PHA was performed in accordance with paragraph B, Exhibit B, Statement of Work, Contract No. DEN3-335. The PHA was accomplished in accordance with Task 202 of MIL-STD-882B.

Purpose

The purpose of the PHA was to identify safety critical areas, evaluate hazards, and identify safety design criteria. The purpose of the PHA was not to affect control of all risks but to fully recognize the hazardous states with all of the accompanying system implications.

Scope

The analysis addresses the AGT101 gas turbine engine and its interfaces as the engine is to be tested in a test cell environment. The data to generate this PHA report was stored in an IBM Personal Computer for processing in the same manner as the FMECA data.

General Analysis Procedure

The analysis was based on a review of the historical experience of the AGT101, safety requirements, and the current design of the engine. The analysis included a determination of the potential hazards, including energy sources and provisions for hazard control. Where the hazard control exists, it was so identifed; otherwise, the hazard control was identified as a recommendation.

The PHA was documented by completing the appropriate worksheets (sample shown in Figure 86). A separate worksheet was developed for each hazard.

The hazard "description" provides a description of a condition. The hazard "cause" was a listing of the more significant causes which can lead to the condition (hazard) described.

PRELIMINARY HAZARD ANALYSIS FOR ADVANCED TURBINE TECHNOLOGY APPLICATION PROJECT

PHA IDENT. NO.: 12	PREPARED BY: JAMES HOGSTAD	DATE: 8/27/88	PAGE 12
COMPONENT: AGT101 Engine Combustor	REVISED BY:	DATE:	

HAZARD DESCRIPTION / CAUSE	PHASE *	HAZARD EFFECTS a) ON ENGINE b) ON PERSONNEL c) OTHER	HAZARD CONTROLS ** a) DESIGN b) SAFETY / WARNING SYSTEM c) PROCEDURES / TRAINING	HAZARD RISK INDEX SEVERxPROB *** ****	REMARKS
Hazard High combustor temperature Cause(s) Fuel/air mixture ratio approaches stoichiometric mixture ratio.	1	(a) Major damage to ceramic stator and ceramic rotor (b) No effect on personnel	(b) Automatic shutdown shall be provided with high combustor temperature (high T4.1 turbine inlet temperature) [E]	IIxE	The theroretical maximum burn temperature of JP-4 and DF-2 fuels are above the maximum temperature limits for the ceramic stator and ceramic turbine rotor. See Appendix VIII for Acronyms & Abbreviations

* PHASE
1 - OPERATING
2 - MAINTENANCE

** HAZARD CONTROLS
[E] - EXIST
[R] - RECOMMENDED

*** HAZARD SEVERITY CLASSIFICATIONS
I - CATASTROPHIC
II - CRITICAL
III - MARGINAL
IV - NEGLIGIBLE

**** HAZARD PROBABILITY LEVELS
A - FREQUENT
B - PROBABLE
C - OCCASIONAL
D - REMOTE
E - IMPROBABLE

Figure 86. Sample PHA Sheet.

Hazard controls included both existing (E) and recommended action to control the hazard and were further subdivided into: design, safety/warning systems, and procedures/training. The "design" hazard control category is design in the broadest sense and includes safety design features built in, drawing requirements such as proof tests, and the design of engine interfaces. The hazard control subdivision "safety/warning systems" includes systems internal and external to the engine. The hazard control subdivision "procedures/training" encompasses both general and specific procedures and training that control the hazard being analyzed. The hazard risk index was determined based on the hazard probability and hazard severity, given the existing and recommended hazard controls.

The definitions of hazard probability and hazard severity (different from FMECA) are given in Tables 17 and 18, respectively.

Results and Discussion

The analysis identified and analyzed 36 hazards. The analysis included determining the hazard, hazard cause and effect, hazard severity and probability of occurrence, and required hazard controls.

Thirty-two (32) of the 36 hazards were judged to be "low risk" based on hazard severity and probability of occurrence as depicted in Figure 87. No hazard was determined to be "high risk". Four (4) hazards were determined to be "moderate risk". These are:

- Foreign object damage
- Coking
- Ceramic rotor failure
- Ceramic structural failure

It should be noted that these four hazards are inherent to ceramic gas turbine development, thus, these hazards are continually addressed as a part of the ongoing ATTAP development program.

Based on the analysis, 96 percent (101 out of 105) of the hazard controls exist. The recommended hazard controls are:

- Regenerator Shaft Guard
- Output Shaft Guard
- Round edges and corners
- Change air purge solenoid from "NC" normally closed to "NO" normally open

TABLE 17. DEFINITION OF HAZARD PROBABILITY*

Description	Level	Specific Individual Item
Frequent	A	Likely to occur frequently
Probable	B	Will occur several times in life of an item
Occasional	C	Likely to occur sometime in life of an item
Remote	D	Unlikely but possible to occur in life of an item
Improbable	E	So unlikely, it can be assumed occurrence may not be experienced

TABLE 18. DEFINITION OF HAZARD SEVERITY*

Description	Category	Mishap Definition
Catastrophic	I	Death or system loss
Critical	II	Severe injury, severe occupational illness, or major system damage
Marginal	III	Minor injury, minor occupational illness, or minor system damage
Negligible	IV	Less than minor injury, occupational illness, or system damage

*The resulting combination of the hazard probability and hazard severity is a Hazard Risk Index per MIL-STD-882B.

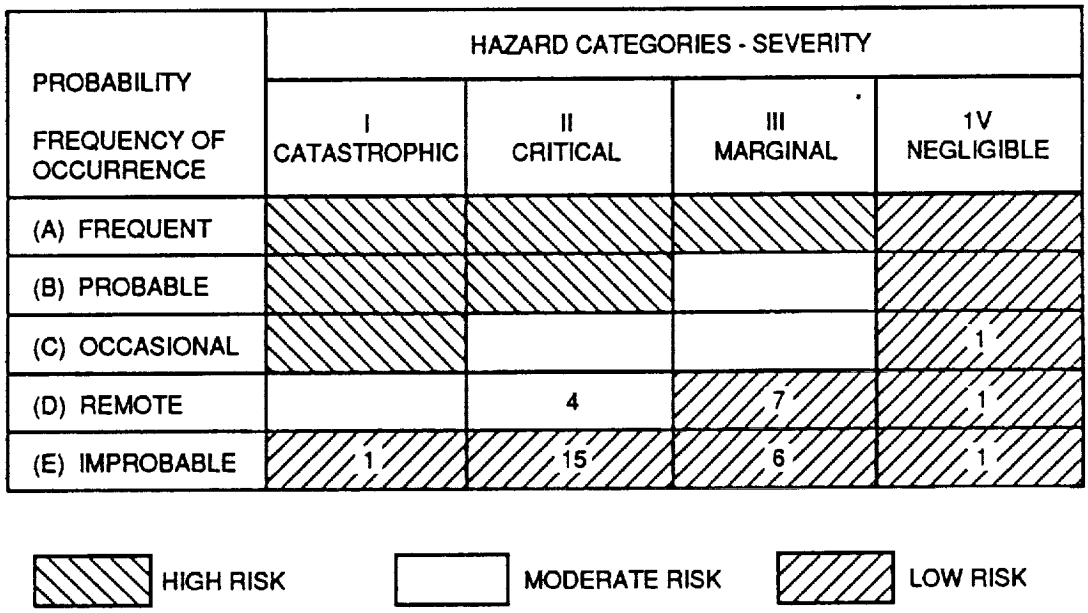

Figure 87. Risk Summary.

4.2.6 Operating and Support Hazard Analysis (O&SHA)

The O&SHA was performed in accordance with Paragraph B, Exhibit B, Statement of work, Contract DEN3-335. The O&SHA was accomplished in accordance with Task 205 of MIL-STD-882B.

Purpose

The purpose of this task was to perform and document O&SHA to identify hazards and recommend actions to control the hazards.

Scope

The analysis addresses the AGT101 gas turbine engine test activity hazards as the engine is to be tested in a test cell environment. The data to generate the O&SHA report was stored in an IBM Personal Computer for processing in the same manner as the FMECA data.

General Analysis Procedure

The analysis was based on a review of the historical experience of the AGT101, safety requirements, and the current design of the engine. The analysis included a determination of the potential hazards, including energy sources and provisions for hazard control. Where the hazard control exists, it was so identified; otherwise, the hazard control was identified as a recommendation.

The engine test activity which was considered for O&SHA includes the following phases:

- Engine Installation
- Test Cell Checkout
- Pre-Test Operations
- Test Operations
- Posttest Operations
- Engine Maintenance
- Engine Removal
- Engine Rebuild

The tasks associated with each of these phases are shown in Figure 88.

The O&SHA was documented by completing the appropriate worksheets (sample shown in Figure 89). A separate worksheet was developed for each hazard.

The hazard "description" provides a description of a condition. The hazard "cause" was a listing of the more significant causes which can lead to the condition (hazard) described.

Hazard controls included both existing (E) and recommended action to control the hazard and were further subdivided into: design, safety/warning systems, and procedures/training. The "design" hazard control category is design in the broadest sense and includes safety design features built in, drawing requirements such as proof tests, and the design of engine interfaces. The hazard control subdivision "safety/warning systems" includes systems internal and external to the engine. The hazard control subdivision "procedures/training" encompasses both general and specific proce-

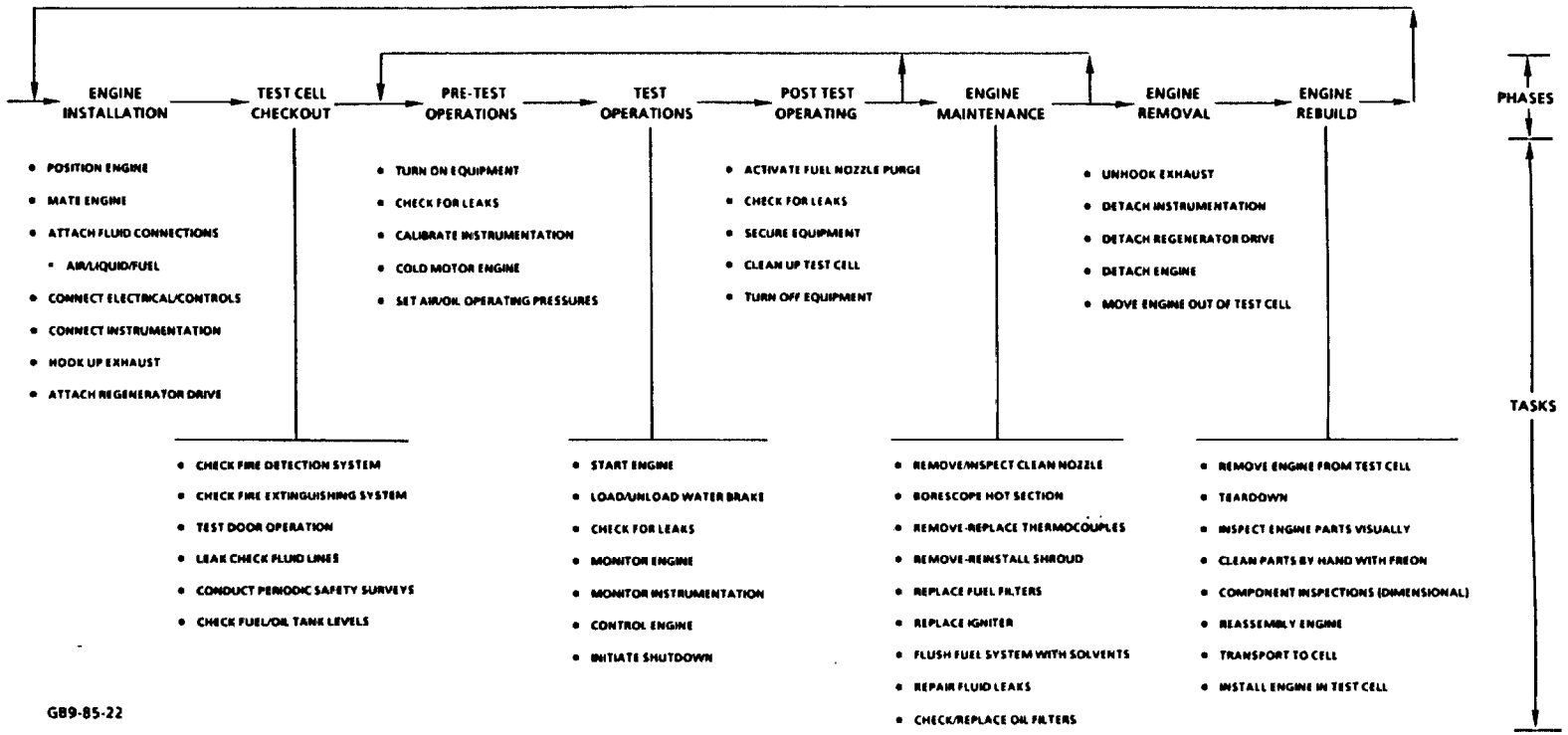

Figure 88. Engine Test Activities.

O&SHA IDENT. NO.: 17	PREPARED BY: JAMES HOGSTAD	DATE: 8/27/88	PAGE 17
COMPONENT: AGT101 Engine	REVISED BY:	DATE:	

HAZARD DESCRIPTION / CAUSE	PHASE *	HAZARD EFFECTS a) ON ENGINE b) ON PERSONNEL c) OTHER	HAZARD CONTROLS ** a) DESIGN b) SAFETY / WARNING SYSTEM c) PROCEDURES / TRAINING	HAZARD RISK INDEX SEVERxPROB *** ****	REMARKS
Hazard Fuel/oil fire Cause(s) Fuel leakage in combination with ignition source Hydraulic oil fluid leakage in combination with ignition source	3.4 5	(a) Major engine damage (b) Severe injury to personnel (c) Damage to adjacent equipment and test cell	(a) Emergency shutdown shall be provided per GAPD S&H Manual, Section 2.3 II (11) [E] Electrical euqipment shall be approved for use in Class I, Division I, Group D as defined by NFPA 70 [E] (b) Five prevention and protection shall be in accordance with NFPA 10 [E] (c) Personnel operating engine test facilities shall be qualified on specific equipment (GAPD S&H Manual, Section 2.3 II (18)) [E] All exposed fluid and electrical liner and corrections shall be plugged or capped when not in use. (GAPD S&H Manual, Section 2.3 II (12)) [E]	IIxE	Autoignition temperature of JP-4 is 850F Autoignition temperature of DF-2 is 495F Flash point of JP-4 is -40F Flash point of DF-2 is 104F Flash point of ATF is 320F Per GAPD policy, no one is allowed in test cells with running engines. Exceptions require written management approval See Appendix IX for Acronyms and Abbreviations.

* PHASE		** HAZARD CONTROLS	*** HAZARD SEVERITY CLASSIFICATIONS		**** HAZARD PROBABILITY LEVELS	
1 - ENGINE INSTALLATION	5 - POST TEST	[E] - EXIST	I - CATASTROPHIC	III - MARGINAL	A - FREQUENT	C - OCCASIONAL
2 - TEST CELL CHECKOUT	6 - ENGINE MAINTENANCE	[R] - RECOMMENDED	II - CRITICAL	IV - NEGLIGIBLE	B - PROBABLE	D - REMOTE
3 - PRE-TEST	7 - ENGINE REMOVAL					E - IMPROBABLE
4 - TEST	8 - ENGINE REBUILD					

Figure 89. Sample O&SHA Sheet.

ORIGINAL PAGE IS
OF POOR QUALITY

dures and training that control the hazard being analyzed. The hazard risk index was determined based on the hazard probability and hazard severity, given the existing and recommended hazard controls.

The definitions of hazard probability and severity (different from FMECA) were previously given in Tables 17 and 18, respectively.

Results and Discussion

The analysis identified and analyzed 59 hazards. The analysis included determining the hazard, hazard cause and effect, hazard severity and probability of occurrence, and required hazard controls.

Fifty-five (55) of the 59 hazards were judged to be "low risk" based on hazard severity and probability of occurrence as depicted in Figure 90. No hazard was determined to be "high risk". Four (4) hazards were determined to be of "moderate risk". These are:

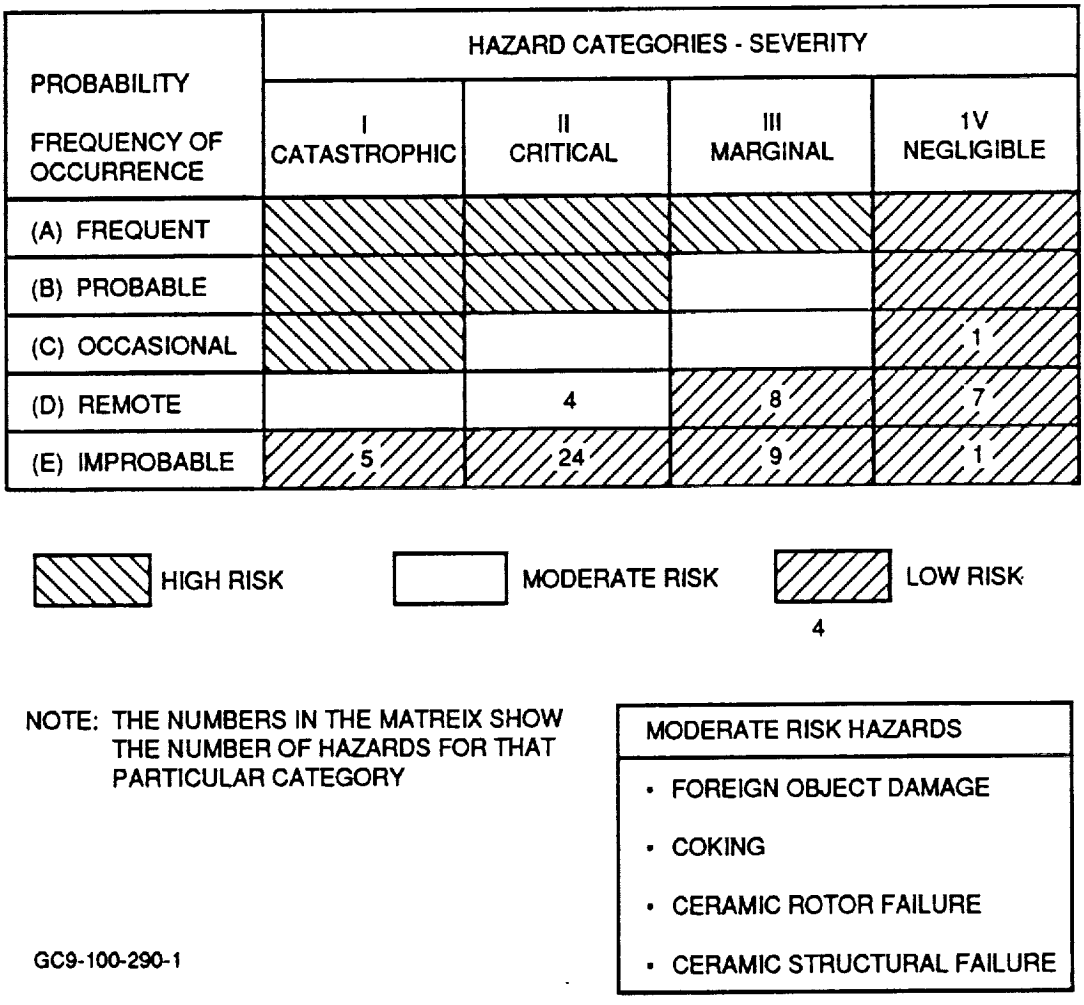

Figure 90. Risk Summary.

- Foreign object damage
- Coking
- Ceramic rotor failure
- Ceramic structural failure

Note that these four hazards are inherent to ceramic gas turbine development, thus, these hazards are continually addressed as a part of the ongoing ATTAP development program.

Based on the analysis, 97 percent (164 out of 169) of the hazard controls exist. The recommended hazard controls are:

- Regenerator Shaft Guard
- Output Shaft Guard
- Round edges and corners
- Change air purge solenoid from "NC" normally closed to "NO" normally open

5.0 MATERIALS CHARACTERIZATION/CERAMIC COMPONENT FABRICATION

This section treats the materials effort which supports design, component fabrication and component test activities. During this report period, this effort concentrated primarily on the characterization of Norton/TRW's NT154, Corning Glass Works' Lithium Aluminum Silicate (LAS), and Kyocera's SN251. Additional work was done in the area of NDE development and inspection of components in preparation for rig and engine testing, and confirming vendor data on the thermal conductivity of SN251.

Ceramic component fabrication relates primarily to the work done by the three ATTAP subcontractors, Norton/TRW Ceramics, Carborundum, and Garrett Ceramic Components Division. This work is treated in detail in the appendices to this report.

5.1 Materials Characterization

Suppliers which had materials which performed well in the materials assessment and mature net shape forming capability were chosen to become major subcontractors to Garrett's ATTAP program. These materials as well as materials being used for components under parts buy are characterized to more fully evaluate the fast fracture, stress rupture, and fracture toughness properties. The materials characterization test matrix is shown in Table 19. Following is a summary of the materials characterized during 1988.

Norton/TRW NT154

Norton/TRW slip cast NT154, HIPped silicon nitride was obtained to perform the more extensive materials characterization test matrix. Prior to any testing, all specimens were heat treated at 1800F/50 hours to minimize the effect of machining. The fast fracture tests resulted in a strength value of 158 ksi at room temperatures and slowly decreased in value with increasing temperature to 84 ksi at 2500F (1370C), as shown in Table 20 and Figure 91.

Fracture toughness was measured using chevron notch fracture toughness specimens. Five tests were conducted at room temperature, 1800F, 2200F, and 2500F. The average fracture toughness values measured are listed in Table 21. The measured toughness was 6.24 ksi-$in^{1/2}$, at room temperature, 5.60 ksi-$in^{1/2}$ at 1800F, and 4.66 ksi-$in^{1/2}$ at 2200F. Stable crack growth could not be achieved at 2500F, so data is not available. The flexural stress rupture life of Norton/TRW NT154 was measured at 2300, 2400 and 2500F. The data is presented in Figure 92.

TABLE 19. MATERIALS CHARACTERIZATION ENCOMPASSES A COMPREHENSIVE TEST MATRIX

Test Condition, C (F)	Number of Specimens Tested			
	Fast Fracture Tests[1]	Stress Rupture Tests[1]	Fracture Toughness Tests[2]	Tensile Rupture Tests
RT (Large Specimen)	30	--	--	--
RT	30	--	5	--
760 (1400)	10	--	--	--
982 (1800)	10	--	5	--
1093 (2000)	10	--	--	--
1204 (2200)	30	12	5	9*
1260 (2300)	10	12	--	9*
1316 (2400)	10	12	--	9*
1371 (2500)	10	--	5	9*

1 Four-Point Flexure
2 Chevron Notch
*9 Specimens at three temperatures.
Test temperatures will depend on material and intended use.

TABLE 20. NORTON/TRW NT154 FAST FRACTURE CHARACTERIZATION

Test Temperature, F	Average MOR, ksi	Specimen Quantity
Room Temperature	158.2	20
Room Temperature (Large Volume)	145.2	30
1400	138.8	9
1800	125.1	10
2000	120.3	5
2200	106.2	25
2300	104.2	5
2400	94.6	5
2500	84.0	5

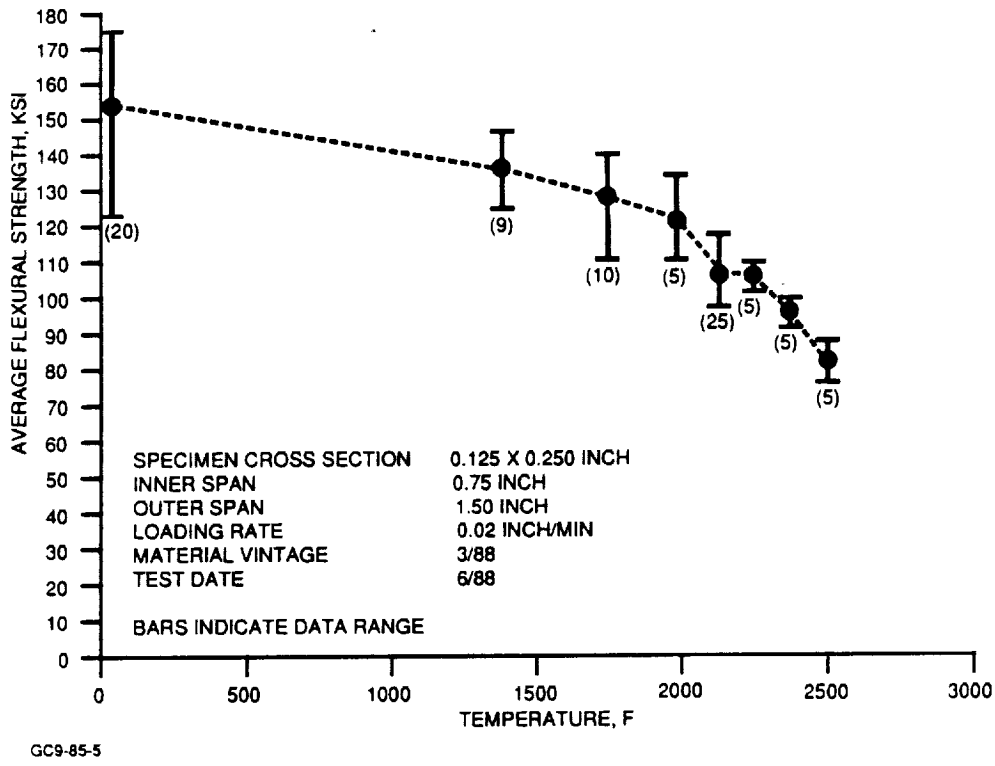

Figure 91. Fast Fracture Characterization of Slip Cast Norton/TRW NT154.

TABLE 21. NORTON/TRW NT154 MATERIALS CHARACTERIZATION CHEVRON NOTCH FRACTURE TOUGHNESS

Temperature, F	Specimen Quantity	Average Fracture Toughness, ksi - $in^{\frac{1}{2}}$
Room	5	6.24
1800F	5	5.60
2200F	5	4.66
2500F	5	Stable crack growth not achieved

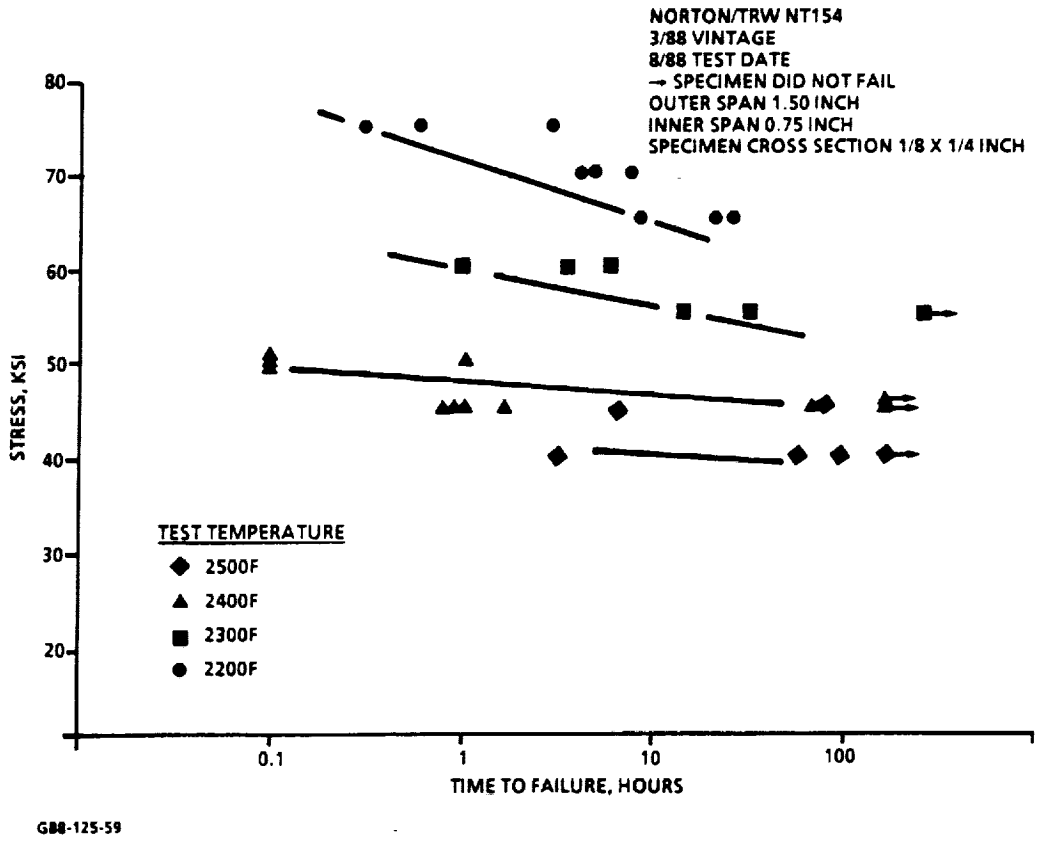

Figure 92. Flexural Stress Rupture Characterization of Norton/TRW NT154.

Corning LAS

Test specimens of Corning LAS cut from flow separator housing S/N 78 were evaluated for fast fracture strength and fracture toughness. (Stress rupture testing was in progress at the end of the report period.)

The data is summarized in Table 22. The average fast fracture strength remains relatively constant from room temperature to 2000F at 12 ksi (Figure 93). The flexure strength of machined specimens is essentially the same as specimens machined such that the surface in tension during test is as-cast. The room temperatue fracture toughness as measured by the chevron notch method is 1.33 ksi-in$^{\frac{1}{2}}$.

TABLE 22. MATERIALS CHARACTERIZATION FAST FRACTURE TEST RESULTS ON CORNING LAS MATERIAL

Test Temperature	Average MOR (ksi)	Specimen Quantity	Fracture Origin, Percent		Predominant Origin
			Surface	Internal	
RT	12.9	30			
RT (as cast)	13.2	10			
1400	11.5	10			
1800	12.8	10			
2000	12.6	30			

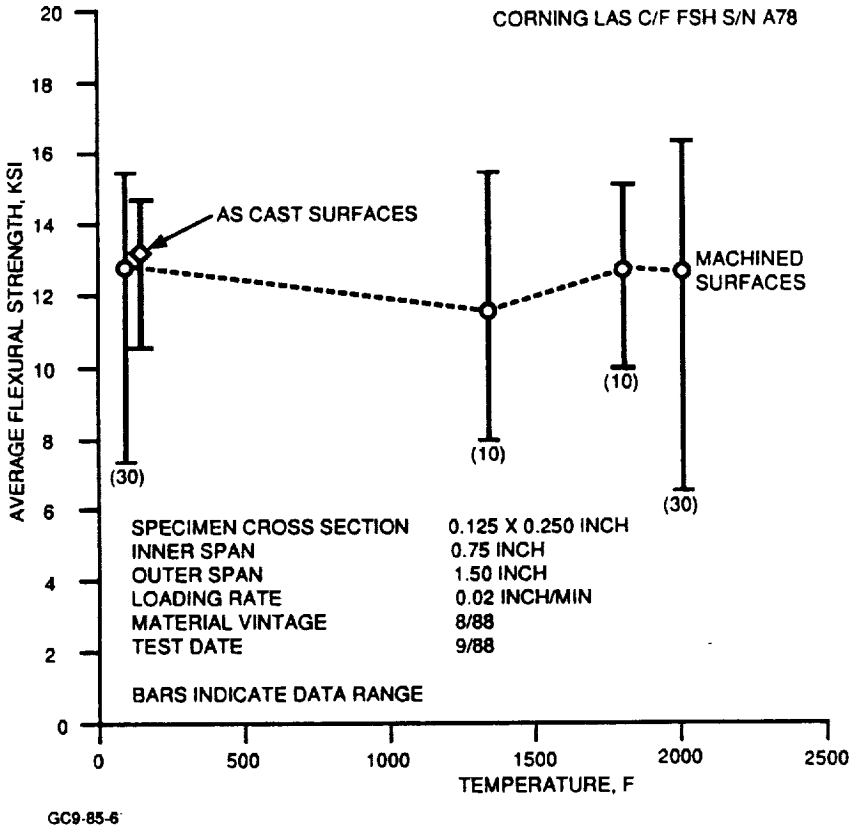

Figure 93. Fast Fracture Characterization of Corning LAS.

Kyocera SN251

Kyocera SN251 was characterized for fast fracture flexure strength, fracture toughness and stress rupture from room temperature to 2500F. Material from two sources was evaluated. Specimens were machined from the hubs of ATTAP rotors and from a billet co-processed with ATTAP turbine shroud Serial Number 307. The fast fracture data is shown in Figure 94. The average room temperature strength is 88.7 and 98.5 ksi for the rotors and billet, respectively. The strength gradually decreases with increasing temperature and at 2500F the average strength still remains at 65 and 67.2 ksi for the rotors and billet. Although the strength of SN251 is not as high as other silicon nitrides available today, the material shows consistency with little data scatter.

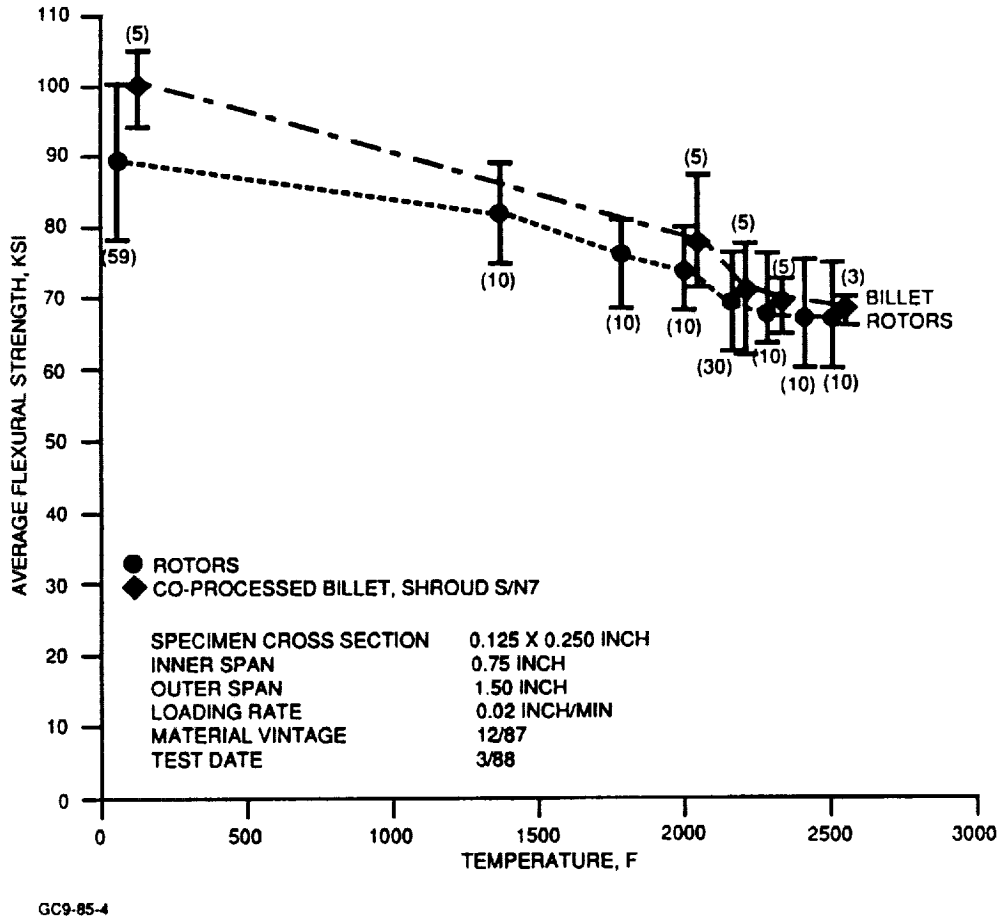

Figure 94. Fast Fracture Characterization of Kyocera SN251.

The fracture toughness of SN251 is also extremely high for a silicon nitride. The fracture toughness data ranges from 6.38 to 7.16 ksi-in$^{\frac{1}{2}}$ over the temperature range of room temperature to 2500F as shown in Table 23. The high toughness appears to be due to the material grain structure. Figure 95 shows the fracture origin and fracture surface of a fast fracture specimen. Many randomly oriented needle shaped grains 50 - 150 microns in length are distributed throughout the microstructure.

TABLE 23. KYOCERA SN251 CHEVRON NOTCH FRACTURE TOUGHNESS

Temperature, F	Average Fracture Toughness, ksi-in$^{\frac{1}{2}}$			
	From Rotor	Quantity	From Billet	Quantity
R.T.	7.16	5	7.15	2
1800	6.70	5	--	0
2200	6.28	5	6.60	2
2500	7.04	5	--	0

The flexural stress rupture life of Kyocera SN251 was measured at 2300, 2400 and 2500F. The data is presented in Figure 96.

Thermal Conductivity Testing

Thermal conductivity was measured at Purdue University facilities on Kyocera SN251 to confirm the vendor's data. Results are given in Figures 97 and 98. The first figure compares the preliminary data from Purdue with vendor data on the same material, and with vendor data on a different material. The second graph shows the complete range of data generated at Purdue.

A second confirming measurement was made at Energy Materials Testing Laboratory (EMTL).

Data on specific heat, as measured over the entire temperature range by the Differential Scanning Calorimetry (DSC) method at EMTL, shows disagreement with the Purdue data (also measured by DSC, but extrapolated between 600 and 1390C) and so this effort will be continued by investigating an alternative method of measuring specific heat (drop-ice calorimetry), still at EMTL.

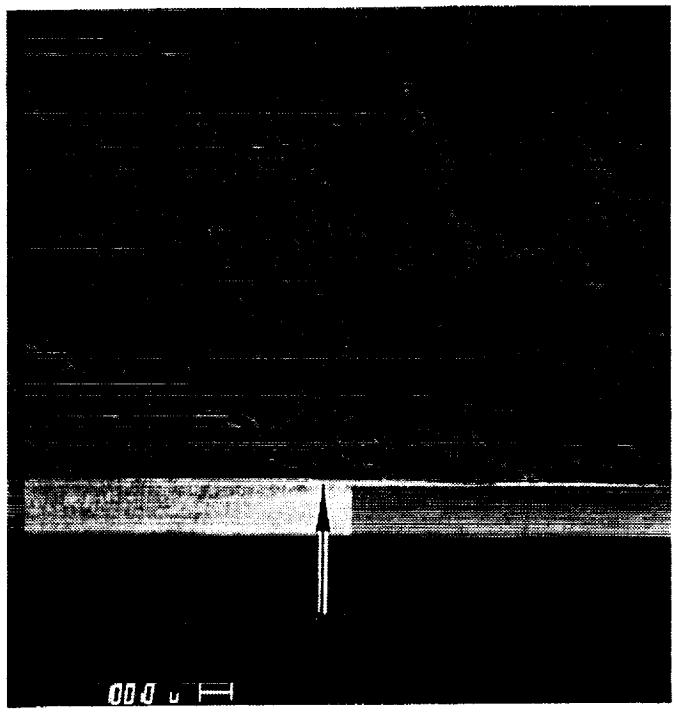

40X

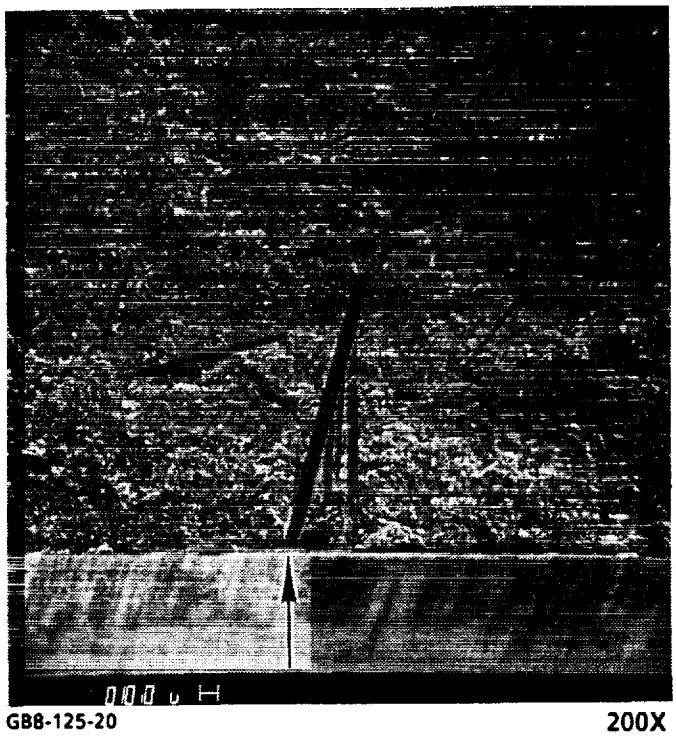

GB8-125-20

200X

Figure 95. Kyocera SN251 Fracture Origins - Many Needle Shaped Grains Are Visible on the Fracture Surface.

ORIGINAL PAGE
BLACK AND WHITE PHOTOGRAPH

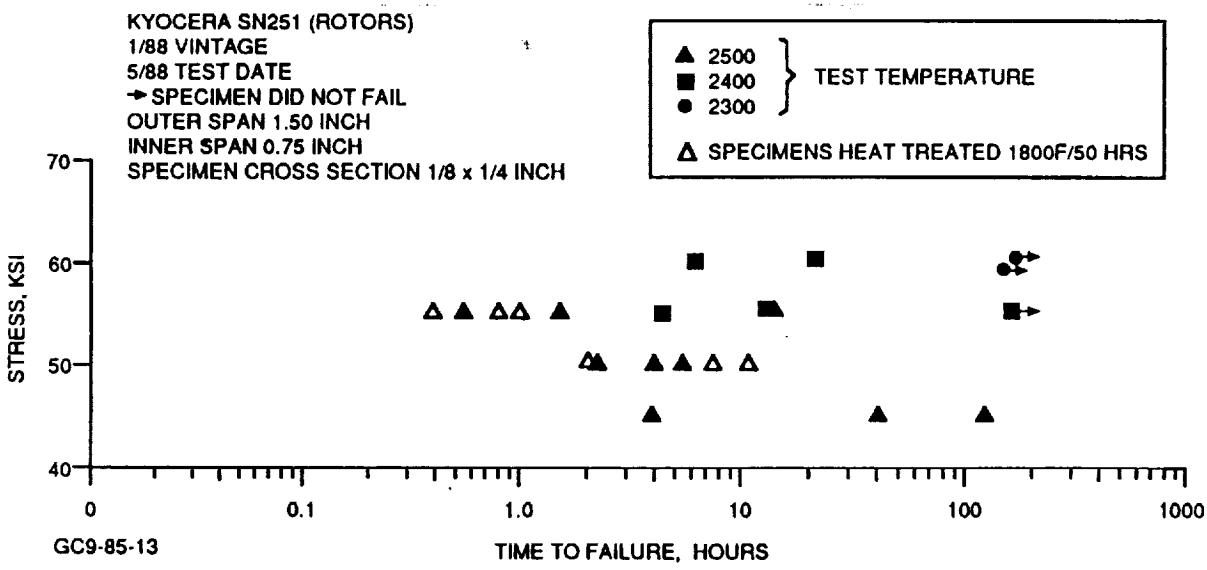

Figure 96. Flexural Stress Rupture Characterization of Kyocera SN251.

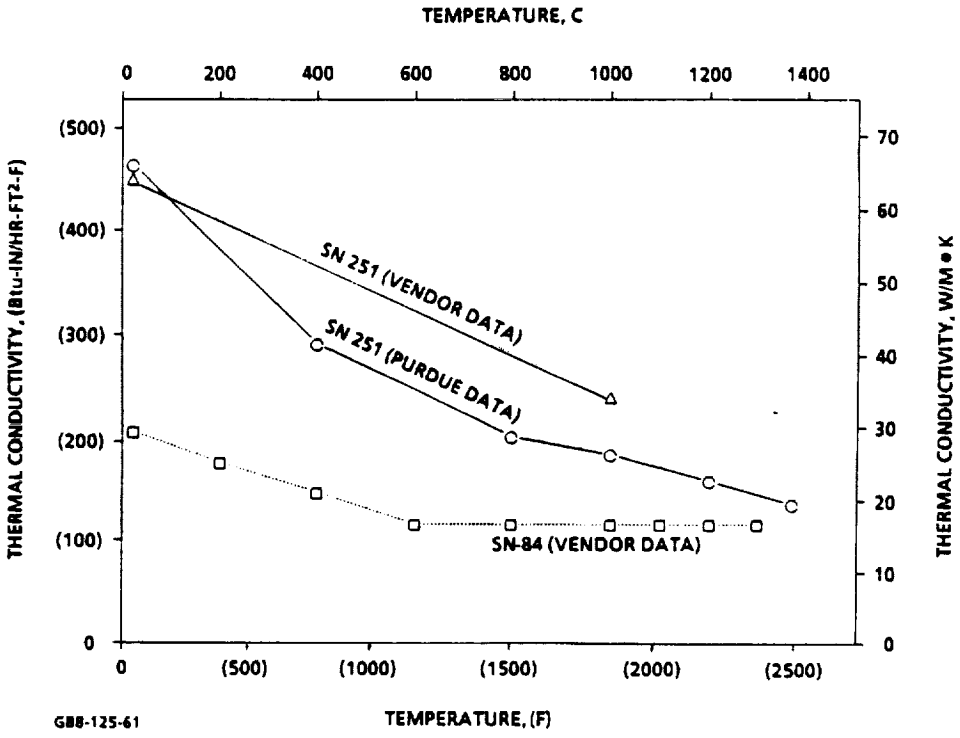

Figure 97. Thermal Conductivity of SN251 and SN84.

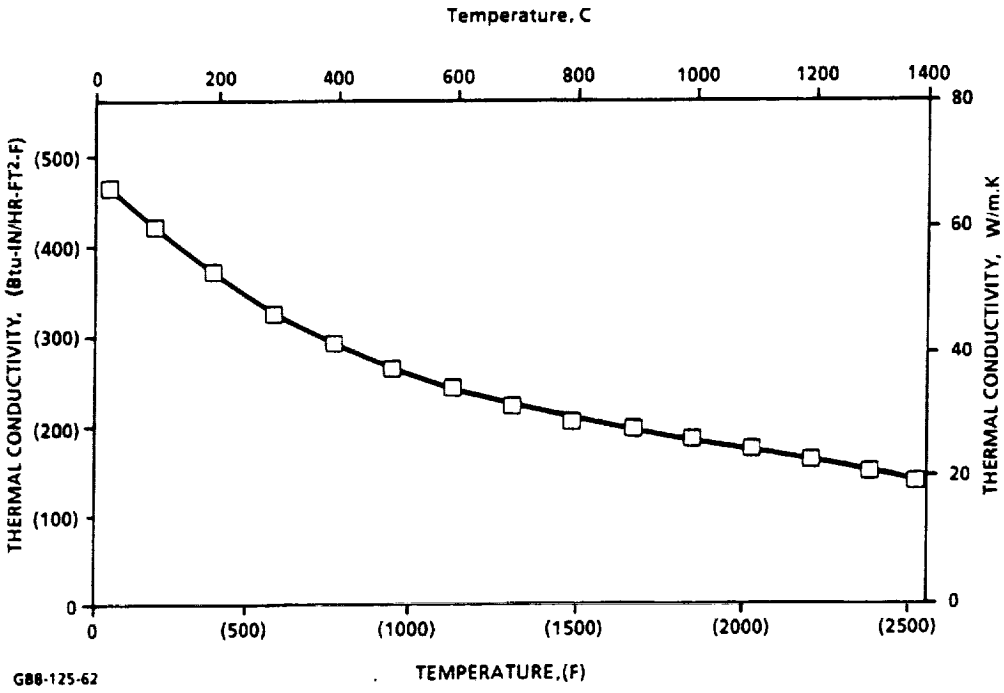

Figure 98. Purdue Thermal Conductivity Measurements of Kyocera SN251.

5.1.1 Materials Characterization - NDE

The ATTAP Nondestructive Evaluation (NDE) effort is an integral part of the materials characterization effort. Ceramic materials present some unique NDE challenges as the materials are extremely sensitive to small anomalies (10-200 microns). These anomalies may be due to material property differences such as density or grain size variation, or from discrete flaws such as voids, inclusions, and cracks. In order to produce engine quality hardware, components with detrimental material conditions must be eliminated. NDE is one way to identify and eliminate these conditions. The goals of this effort are:

- o to assess the ability of NDE as a materials characterization tool,
- o to assess the detectability limits for discrete flaw types found in ceramic materials and components,
- o to determine appropriate inspection techniques for ceramic materials and components, and
- o to write NDE process specifications for ceramic materials

During the first year of ATTAP, an overall plan to achieve these goals has been developed and documented in the work plan. The plan includes both the NDE performed by the ceramic material suppliers and the NDE performed by GAPD on finished materials and components. In order to assess detectability limits, careful correlation of NDE data from complementary techniques with destructive data is required. To facilitate this correlation, data tracking methods have been established. Fixtures have been designed and built to hold test specimens and reduce the amount of specimen handling.

Coordination meetings were held with the major ceramic subcontractors to discuss the NDE requirements and begin designing seeded defect specimens. The first seeded defect specimens will address discrete defects (voids and inclusions) and will be evaluated with multiple NDE techniques in the green and dense conditions. Two different design approaches were established for seeded defect specimens, and specimen fabrication was begun by the ceramic suppliers. Further detail on this work at subcontractors Norton/TRW and GCCD are discussed in the appendices to this report. Forming defects (internal cracks, fold lines, agglomerations, etc.) have also been identified as an area of concern for NDE detectability. These defects are not easy to produce in controlled specimens with known location and dimensions so each ceramic supplier is investigating ways to generate these types of defects for the NDE studies.

A review of applicable NDE techniques for ceramic materials was conducted and multiple NDE techniques have been identified for application during ATTAP. Some of these techniques will be investigated by the ceramic suppliers for green component evaluation while others will be investigated by GAPD for final component NDE. NDE technique repeatibility will be examined by comparing data from supplier and GAPD common NDE methods. Table 24 summarizes the methods identified to date for use in ATTAP.

Component inspections were initiated on hardware transferred from the AGT101 Program to support rig test requirements.* Strict cleaning procedures were established for components prior to NDE as surface contamination can mask indications or cause excessive evaluation time due to background problems.** Surface finish of

*These inspections are discussed further under "Ceramic Component and Specimen Preparation".

**These surface conditions include residual wax from the machining operation, oxide buildup on the surface from heat treating and/or rig testing. Where possible, these conditions will be removed prior to the NDE or the NDE will be performed prior to the operation that induces the condition.

TABLE 24. NDE METHODS FOR ATTAP PROGRAM

Method	Application			NDE Method Type		Applied By	
	Green Specimen/ Component	Final Specimen/ Component	Component Test/ Process Monitor	Surface	Internal	Ceramic Supplier	GAPD
Acoustic Emission			X				X
Acoustic Microscopy	X	X		X	X		X
Computed Tomography	X	X			X	X	X
Film Radiography, Conv	X	X			X		
Film Radiography, µfocus	X	X			X		
Fluorescent Penetrant	X	X		X		X	X
Magnetic Resonance Imaging	X				X	X	
Real-Time Radiography	X	X	X		X	X	X
Ultrasonics, Conventionally	X	X				X	X
Ultrasonics, High Frequency	X	X			X		X
Ultrasonic, Velocity/Atten	X	X	X		X	X	X

components has been identified as a potential limiting factor in detectability for both fluorescent penetrant inspection and more sensitive surface techniques as acoustic microscopy.

5.2 Ceramic Component Fabrication

The Carborundum Company

In January of 1988, Gary Boyd (GAPD Project Engineering) and Laura Lindberg (GAPD Materials Engineering) visited Carborundum for preliminary discussions on the ATTAP work plan for this subcontractor. This was a preparatory meeting to a visit in February 1988 by Reza Eskandari (GAPD Reliability), Laura Lindberg, Janet Minter (GAPD Materials Engineering), and Bob Morey (GAPD Project Engineering). Purpose of the February trip was to assist personnel of Carborundum (CBO) in defining the input of their work plan for ATTAP, and to gain a better insight into the fabrication processes of the components under development with this subcontractor An overview of the NDE methods available at CBO was presented as well.

A visit from CBO personnel to Phoenix was made in late September 1988, to discuss progress to that date. Mr. Harry Lawler, newly named as CBO's Project Manager to replace Monika TenEyck, was introduced to GAPD personnel at this meeting. Some of the issues that were raised centered around the evaluation and selection of a compound to be used for injection molding of transition ducts, collection of data from test bars, status of ram pressing experiments and specimens for NDE evaluation.

During the course of the discussions, GAPD made the following requests:

- CBO was asked to rethink their decision to use SX-05 compound over the SX-09 formulation in pursuing the injection molding of transition ducts, as not all parameters involved in the comparison study were held constant.

- No further injection molding runs of transition ducts (which must be done outside due to in-house capacity limitations) should be attempted until additional progress is made with the simpler ring shape (as a learning tool).

- Increased emphasis needs to be put on the formulation of designed experimental matrices and the communication of their purpose with GAPD.

In December of 1988, Dave Carruthers (GAPD Materials Engineering) and Bob Morey of GAPD visited CBO at Niagara Falls to discuss the progress made to date and to redirect certain efforts. Specifically, the development work for the injection molded transition duct will now include a subscale transition duct shape, to be molded on the 250-ton Reed injection molder which is part of CBO's in-house

equipment. Effort on a ring shape will be dropped in favor of this subscale transition duct. CBO has the assignment to analyze various geometries in order to address as many of the significant injection molding parameters as possible, so as to effectively duplicate or simulate the injection molding of a fullscale transition duct.

In addition, the wave spring effort was cut from three part numbers to one part number, because it was determined that it is not necessary to use SASC material in two of the three engine locations employing wave springs. Work on the two proposed wave spring forming methods, sheet extrusion/stamping and dry pressing, will continue until the superior method for forming the remaining part is identified.

The meetings with the subcontractors provide an opportunity to communicate more closely than is possible by telephone or coordination memo. Communications links will be kept more active by the scheduling of telephone calls on a regular basis.

Additional detail of technical progress by the Carborundum Company is reported in Appendix A.

Norton/TRW

In December of 1988, a trip was made to Northboro, MA by Bob Morey, to gain familiarity with the personnel and facilities of Norton/TRW Ceramics, and to review the progress that had been made to-date on fabrication techniques for the rotor and stator.

Technical progress by Norton/TRW is reported in Appendix B.

Garrett Ceramic Components Division

In April of 1988, Laura Lindberg and Bob Morey traveled to Torrance California to review the status of Garrett Ceramic Components Division's (GCCD) silicon nitride material, designated GN-10. The data which GCC presented at that time indicated that the GN-10 material was a suitable candidate to be used for component development work under ATTAP. Confirming data was obtained at GCC and at GAPD, and a subcontract was let in the summer of 1988 for GCCD to develop the fabrication techniques for the ATTAP turbine rotor.

A meeting was held in May at Phoenix to discuss GCCD's proposed work plan for the ATTAP project. At that time there was further opportunity for the personnel of GAPD and GCCD to become acquainted with one another.

A further meeting was held in Phoenix in September 1988. GCCD discussed their recent accomplishments under the ATTAP program, and their latest draft of the Work Plan was reviewed. GCCD had accomplished a significant amount of work in the relatively short time that they were actively involved in the ATTAP. They claimed to be

behind their anticipated schedule, and had recently hired two people to better maintain schedule.

Another meeting was held in Phoenix in December. GCCD updated their progress on the ATTAP rotor development, as they had done not long before for NASA.

Detailed technical progress by Garrett Ceramic Components Division is reported in Appendix C.

5.3 Ceramic Component and Specimen Preparation

Component Inspections and Preparations

Ceramic components and specimens are prepared for rig and engine testing in a number of ways. These include, for test specimens, non-destructive evaluations to generate a record of the flaws which the specimens may contain prior to subjecting the specimens to destructive testing. In this way, information about the effectiveness of the NDE methods as well as about the flaw population of the subject material can be gained.

In the case of components, preparation includes laser marking for positive identification, visual inspection, NDE, final machining, dimensional inspection, mechanical proof testing, and thermal proof testing. These preparation steps are detailed for each component on a tracking sheet, a sample of which is shown as Figure 99. Tracking sheets normally follow the individual components as they pass through each stage of the preparation, and upon completion are returned to the responsible Project Engineer and kept on file as a confirming record of the components which have been prepared for further rig and engine tests.

At the conclusion of the AGT101 project, a number of ceramic components had been received which had not undergone the required preparation. These components were removed from the storeroom and the various inspections and proof tests necessary to qualify them for engine testing were begun. In addition, new hardware listed in Table 25 ordered under the ATTAP, was received during the course of 1988, and this hardware was slated for the required preparation activities as well.

The following paragraphs give samples of the types of preparation the components receive. The operations described are chosen largely as a result of experience gained on the AGT101 program.

THIS SHEET MUST STAY WITH PART!!

ATTAP CERAMIC COMPONENT TRACKING SHEET

PART NAME: TURBINE ROTOR PART NO: PA3612439-1 SERIAL:

SOURCE: MATERIAL: DENSITY:

OPERATION	DATE	INITIALS
Received		
PC Database record established		
Visual inspection		
Laser marking of S/N		
FPI (and clean)		
Visual inspection (damage?)		
Blade ring*		
Machining of shaft features		
FPI (and clean)		
Ultrasonic inspection		
Real-time X-Ray		
Visual inspection (damage?)		
Dimens'l inspect'n (jrnl OD=)		
Contour insp'n - Hub & Shroud Lines		
Visual inspection (damage?)		
Zeiss blade contours*		
Visual inspection (damage?)		
Curvic & collet installation		
Curvic inspection		
Balance		
Cold spin proof test		
To stores/Rig /Engine (CIRCLE)		

Additional comments:

* Required only if prior data not available for this mat'l & process.

GB8-125-9

Figure 99. Sample Part/Component Tracking Sheet, P/N 3612439-1.

TABLE 25. ATTAP HARDWARE RECEIPTS THROUGH 1988

Part Number	Description	Quantity	Material
PA3610213-2	Transition Duct (I.M.)	2	SASC
PA3612439-1	Rotor	2	SN84
PA3609655-1	Flow Separator	2	LAS
PA3611753-1	Wave Spring, Regenerator Shield	10	SN84
PA3612920-1	Support, Pilot Combustor	3	SN84
PA3612922-1	Combustor Swirler	3	SN251
PA3611660-7	Combustor Dome	3	SN84
PA3611434-3	Insulation, Compr. Backshroud	6	HT-280
PA3611435-2	Insulation, Ring Support	6	HT-280
PA3610670-2	Turbine Shroud	3	SN251
PA3611744-3	Wave Spring, Baffle	3	SN251
PA3611747-3	Seal Ring, Flow Separator	10	SN251
PA3612084-4	Insulation, Combustor	6	HT-280
PA3612921-1	Pilot Combustor	3	SN251
PA3612923-4	Insulation, Combustor Spring	6	HT-280
PA3612425-1	Wave Spring, Baffle	5	SASC

Transition ducts are radiographed (x-rayed) at CBO and the results delivered with the part to GAPD. Density is checked at GAPD, and fluorescent penetrant inspection (FPI) is normally performed both prior to and after thermal proof testing. X-ray inspection at GAPD confirms results obtained at CBO, and this part's geometry also makes it a candidate for ultrasonic test methods, although this has not yet been done on a regular basis. Dimensional inspections (including contours) are performed, and in many cases touch-up machining is performed (usually restricted to hand finish or dressing of critical radii) as a result of visual inspections under magnification. Parts made of sintered alpha silicon carbide (SASC) are heat-treated at 1204C (2200F) for 8 hours following any machining done at GAPD; in fact this oxidation heat treat is normally applied as a matter of routine. Thermal screen proof testing consists of flowing heated, vitiated air through an assembly consisting of a transition duct and combustor baffle. The screening or proof cycle is described fully in Section 6.2.2, Thermal Proof Testing.

Rotors are normally received with the blade edges machined to the correct contour for mating with the shroudline, and with the backface correctly machined, but with extra stock on the journal and shaft internal features (the rotor is a hollow-shaft design). Shroudline contours are checked and hub contours are routinely inspected. Final machining of the shaft O.D. and internal features is performed at GAPD by diamond grinding. Visual inspections under magnification are performed, and in addition such NDE methods as real-time x-ray, FPI (before and after in-house machining, and after cold spin proof testing), and ultrasonic testing (UT) are applied. Laser marking is on the cone area adjacent to the journal. Markings are made in triplicate, since this is an area of material removal during the balance operation. For the current silicon nitride rotors, no heat treat is applied. If no prior data exists for the material in question, blade ring data (to confirm blade-to-blade consistency and to characterize the stiffness of the blades) may be taken. Zeiss (ultra-light contact inspection) contour data on the blades will be taken, but again only in the case where no prior data is available for the material and supplier in question. Attachment hardware (curvic coupling and internal collet) is installed prior to balance and proof testing, which consists of a cold spin to 115 krpm (15 percent overspeed). Prior to operation in an engine environment, ceramic rotors are operated to full speed, 1600F TIT in an engine with metallic structures, as a final proof test. This particular test is done just prior to installation in the ceramic engine, and so is performed only for those rotors which have been selected for use in the ceramic engine.

Flow separators are sent to GAPD in the as-cast state for x-ray examination, after which those castings which show no excessively large voids or other obvious problems are returned to Corning for grinding to final shape. Once ground (so that a seal can be effected on the face toward the regenerator), they are pressure checked to 65 psig (on the high pressure (HP) side) at Corning prior to shipment to GAPD. Failure of the proof test by pressurizing in this way is the responsibility of the supplier, Corning. Also any flaws uncovered during the machining operations are grounds for rejection by GAPD. A discussion of potential modifications to this procedure is found under Ceramic Engine Component Fabrication. No laser marking is done on the LAS material of the Flow Separators; the porous material absorbs the ink of a marker easily for positive identification.

Wave springs are inspected for dimensional accuracy as well as being visually checked for surface flaws that could potentially induce fracture. When present, these are hand finished out. They also undergo FPI, and each wave spring is subjected to a proof test to verify that it can be deflected a minimum amount and to ascertain at the same time its spring constant. In the case of SASC wave springs, the maximum load applied does not induce more than 40 ksi in the part. Wave springs of SASC which have relatively high design stress are not normally laser marked, although others are marked in an area of little or no stress.

Combustor hardware (includes combustor liner, combustor dome, combustor swirler, pilot combustor, and pilot combustor support) receives visual inspections and FPI and x-ray, just as do most other components. Laser marking is done, as usual restricting this to an area of low stress. Dimensional inspection is followed by touch-up machining where indicated. In certain instances hardware will be purchased without all of the final machining done, as GAPD is capable of performing this machining, and deliveries can often be shortened. The thermal proof test for combustor hardware is done in a combustor rig, which is also used for combustor development work. This rig is capable of simulating the worst engine thermal condition on the parts - start to full temperature with a cold regenerator core (ambient combustor inlet).

Seal rings are subject to visual inspection and dimensional verification, as well as FPI for surface flaws. Laser marking is normally done on the flat face of the ring, except in the case where a ring is of LAS material (these have been made in-house at GAPD from cylindrical stock). SSN is the other material option.

Insulation is not normally put through a proof testing or NDE checks. It is dimensionally inspected to assure that it will fit with the surrounding hardware. The currently favored material, a fibrous alumina product called HT-280 by the supplier FOSECO, has not yet been run in an engine. It is believed capable of withstanding the erosion effects of the gas flow without surface treatment, and so none is planned. Further testing in 1989 will indicate whether a surface treatment to rigidize the flowpath surfaces is required.

Turbine shrouds receive laser marking and dimensional inspections at GAPD, as well as x-ray and FPI. The geometry of the part may lend itself to inspection by ultrasonics, but this is not yet performed on a regular basis. Machining of the shroud contour and stator pocket area is normally done at GAPD, as well as any required touch-up machining or hand finish. For certain of the SSN materials used for this component, oxidation heat treat prior to rig or engine operation is recommended. Thermal proof testing is done in a fashion similar to that for the transition duct. A more detailed description of the test procedure and thermal cycle is given in Section 6.2.3, Turbine Shroud/Stator Thermal Proof Rig.

Because of manpower constraints in the early phase of the ATTAP, not all of this preparation activity for the hardware listed was completed prior to the end of 1988.

Machining Capability Improved

During 1988, the prototype machine shop at GAPD received a new surface grinder. The machine is equipped with the COMMEC system, an electrical discharge system to keep the interface between the workpiece and the grinding medium free of debris. Trials employing only

the creep-feed capability of the machine were made, and the one-half inch wide wheel was able to remove hot-pressed silicon nitride material to a depth of 0.150 inch at a rate of 2 inches/minute of travel. This already represents a substantial improvement over the methods previously employed, and further improvements are anticipated when the COMMEC feature is made operational. This machine will be invaluable in the slicing operations required for making test bars from billets or components.

Part Data Tracking

Discussions were held regarding necessary modifications to the existing Total Information and Evaluation Retrieval System (TIERS), so that this sophisticated computerized database could accommodate the research part numbers (PA prefix) used in the AGT and the ATTAP program. For production hardware, this system allows efficient tracking of the inspection and machining operations performed on hardware. It was later learned that the TIERS system could not be modified to accommodate the research parts, and so a system whereby the progress of each component is kept on paper records was established. Forms to assist in the tracking of ceramic hardware as it proceeds through the various operations required for qualification as an engine test article were constructed. Examples are given in Figures 100 and 101.

This tracking system was initiated with the submission of ten seal rings and three wave springs in August 1988. These parts underwent various marking, inspection, and NDE operations, according to the tracking sheet samples shown in Figures 100 and 101. This trial preparation cycle using the new forms was completed in September with data recording of the ten seal rings (PA3611747-3).

Special Instance - Rotor Flaws

Machining of the internal features of one rotor was begun in January 1988. Progress in machining this rotor was slowed by the difficulty of keeping clean the abrasive wheel used to grind the internal feature. Grit blast cleaning was eventually used with good effect. Difficulty was also experienced because this rotor was the first to be machined with the modified shaft bore (the depth of the internal hollow was decreased to reduce stress). The abrasive wheel had to be reconfigured to accommodate the shape change, and a new supply of this custom grinding wheel was ordered.

THIS SHEET MUST STAY WITH PART !!

ATTAP CERAMIC COMPONENT TRACKING SHEET

PART NAME: TURBINE SHROUD PART NO: PA3610670-2 SERIAL:

SOURCE: MATERIAL: DENSITY:

OPERATION	DATE	INITIALS
Received		
PC Database record established		
Visual inspection		
Laser marking of S/N		
Visual inspection (damage?)		
Radiography		
Ultrasonic testing		
Machining of flowpath contours		
Visual inspection (damage?)		
FPI (and clean)		
Dimensional inspection		
Visual inspection (damage?)		
Contour inspection		
Visual inspection (damage?)		
Mechanical proof test		
Thermal proof test		
Visual inspection (damage?)		
To stores/Rig /Engine (CIRCLE)		
Use spaces below for additional operations as required.		

Additional comments:

GE88-125-10

Figure 100. Component Tracking Sheet.

THIS SHEET MUST STAY WITH PART!!

ATTAP CERAMIC COMPONENT TRACKING SHEET

PART NAME: SEAL RING PART NO: PA3611747-3 SERIAL: 8110

SOURCE: KYOCERA MATERIAL: SN251 DENSITY: 3.41

OPERATION	DATE	INITIALS/STAMP
Received	5 Apr 88	RM
PC Database record established	2 Jun 88	RM
Visual inspection (L.Lindberg) x3037	3 Aug 88	L²
Laser marking of S/N (Norm Baker)	4/8/88	NB
Dimensional inspection (Dev shop insp)	8.14-88	[illegible]
Visual inspection (damage?) (Lindberg) x3037	17/8/88	L²
Heat treat (SiC only)	not req'd	
FPI (and clean) (Janet Minter) x3037	8/19/88	jm
Radiography (Janet Minter)	8/28/88	Ran for J.M.
Ultrasonic testing (Janet Minter) x3037	Not req'd	J.M.
Density measurement (Ho Fang) x3120	9/22/88	HF
Use following for additional operations as required.		

Additional comments:

GB8-125-64

Figure 101. ATTAP Ceramic Component Tracking Sheet.

During machining of the rotor, a flaw was discovered near the curvic coupling end of the ceramic shaft. It follows the inside surface all the way around, just inside the hollow, as shown in Figure 102. A portion of the flaw traverses the flat surface which supports the titanium curvic coupling. It was at first suspected that the flaw was introduced during injection molding of the blade ring portion of the rotor, which includes the journal. Two other rotors, as well as the scrap ends of shafts of two rotors previously cut for test bars, display similar defects. The supplier was contacted, and agreed to replace the rotors.

FPI was used to detect the flaws in the pieces, and in fact once the location of the suspected defects was known, visual inspection was sufficient to confirm the existence of the flaw in the other rotors on that order. Unfortunately no NDE had been done on this rotor prior to machining, as it was scheduled in order to take advantage of a slack period in the machine shop.

The supplier assures that the parts were visually inspected and radiographed prior to shipment, and so apparently these flaws went undetected until machining revealed their existence. Further communications with the supplier revealed that they were satisfied the flaws were introduced during cold spin proof testing, which they performed after their NDE inspections. The culprit was a spin arbor design which introduced significant stress in the small radius at the end of the journal. The supplier has since modified the spin tooling.

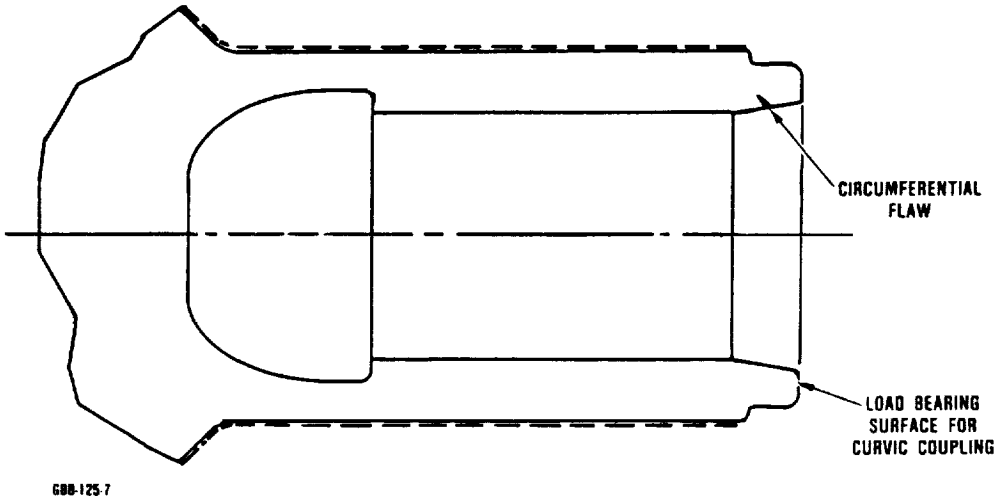

Figure 102. Flaw Revealed in Curvic Load Bearing Surface of Hollow Shaft Rotor.

5.4 Ceramic Engine Component Fabrication

Because not all of the ceramic components in the ATTAP test bed engine are under development by the ATTAP subcontractors, ceramic hardware purchases from other sources are provided for. In many cases the initial ATTAP test activity could be supported by existing ceramic hardware transferred from the AGT101 program. Receipts of hardware originally ordered on AGT and of additional ATTAP purchases are tabulated below.

ATTAP Ceramic Hardware Receipts Through December 1988

AGT "leftovers"

Subcontractor Orders

5	PA3612425-1	Wave Spring, Baffle
5	PA3612423-1	Wave Spring, Seals
10	PA3612424-1	Wave Spring, Reg. Shield

Ordinary Purchase Orders

2	PA3609655-1	Flow Separator
1	PA3610670-2	Turbine Shroud
3	PA3612439-1	Rotor

First-Year ATTAP Orders and Receipts

3	PA3611744-1	Wave Spring, Baffle
3	PA3610670-2	Turbine Shroud
10	PA3611747-3	Seal Ring, Flow Separator
3	PA3612921-1	Pilot Combustor
3	PA3612922-1	Swirl Vane
3	PA3612920-1	Support, Pilot Combustor
3	PA3610660-7	Support, Combustor Liner
10	PA3611753-1	Wave Spring, Regen. Shield
6	PA3612923-4	Insulator, Fuel Nozzle
6	PA3612084-4	Insulator, Combustor Cap
6	PA3611434-3	Insulator, Compressor Backshroud
6	PA3611435-2	Insulator, Ring Support
4	PA3613543-1	Core, Regenerator
2	PA3613542-1	Core, Regenerator
4	PA3613980-1	Combustor Spacer Sleeve
3	PAP255627	Insulator, Rig

Quotations were received for test specimens, spin disks, and spin rotors for the hot spin pit effort. These quotes are being discussed to verify that the vendors can supply these items with enough consistency to meet the test objective of verifying design methods. The potential for synergism between ATTAP and the ORNL Life Prediction Program was studied, with the result that the ATTAP and ORNL programs will each fund a portion of the spin disks necessary for this design methods work. The ATTAP budget provides for the purchase of spin disks and specimens in 1989.

At the end of the reporting period, a review of the ceramic hardware on hand was being conducted to determine appropriate order quantities for existing and new part numbers. Pilot combustors, pilot combustor supports, and combustor swirlers will not be placed on reorder until such time on Turbine Inlet Partical Separator work identifies the correct geometry.

6.0 COMPONENT RIG TEST

6.1 Component Rig Design

6.1.1 Hot Spin Pit Design and Fabrication

The parametric studies that were made of various materials and component configurations led to a design which is simple and inexpensive to install, yet should still provide reliable operation to the anticipated test speeds up to 140,000 rpm. Review of the chosen design for the pit "hot box" by an outside supplier, specializing in vacuum furnaces, resulted in a few minor changes in the design. Detail and assembly drawings of the ATTAP hot spin pit were completed and released enabling hardware to be ordered. The configuration of the hot spin pit is given in Figure 103.

Designs of the rotating spin disk (subelement), the spin rotor (modified shaft feature), the arbor, and the spindle design have all been finalized. The rotating spin disk and the spin rotor designs were submitted for quotes along with the test specimens necessary to the methods development activity. Figures 104 and 105 show the configurations for the rotor/arbor/spindle assemblies for both the subelement spin disk and the fully bladed spin rotors.

A silicon nitride shaft which meets the geometry requirements of the spin disk shaft, was successfully ground in the prototype machine shop. A billet of Columbium is available for machining into an arbor. A proof-of-design test was formulated to evaluate the gripping capability of the metallic arbor to the ceramic rotor shaft.

The special high speed motor, required for the testing to verify design methods, was received, but has not yet been installed to verify its operation. A test plan needs to be formulated to kick off this testing.

Hot Spin Pit Testing has been coordinated with the ORNL Life Prediction program to realize the greatest benefit for both programs. The design and testing of the hot spin pit will continue as an ATTAP activity.

Further work on the heated spin pit has been delayed pending the outcome of an investigation to determine whether or not dissociation of silicon nitride at elevated temperatures and very low pressures (as anticipated for the hot spin pit testing) will prevent the testing from yielding correct conclusions.

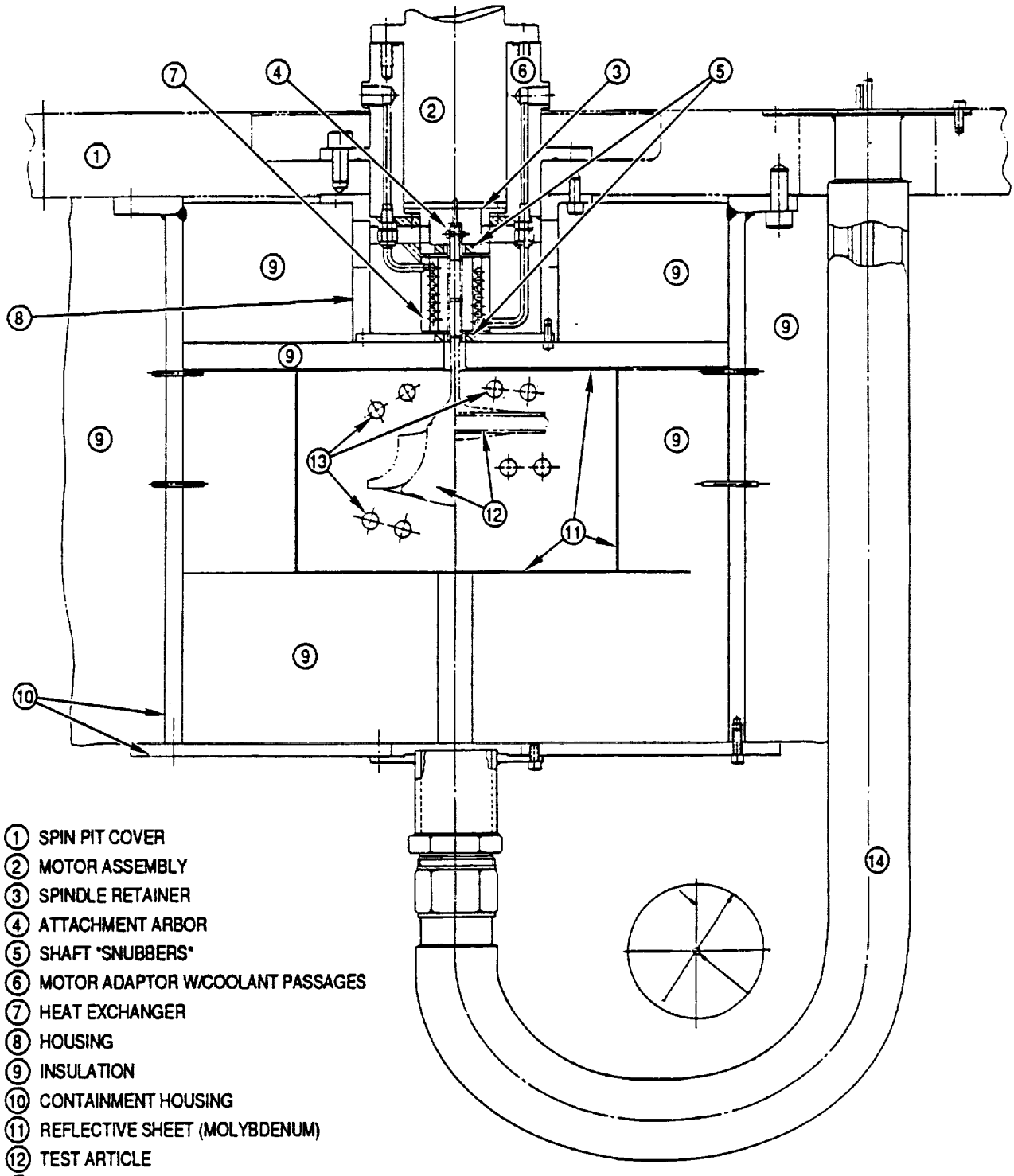

Figure 103. Hot Spin Pit Test Rig.

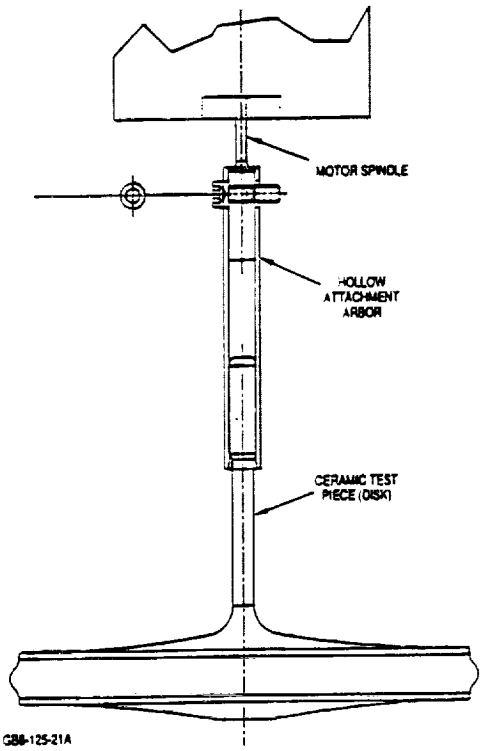

Figure 104. Spin Disk Assembly.

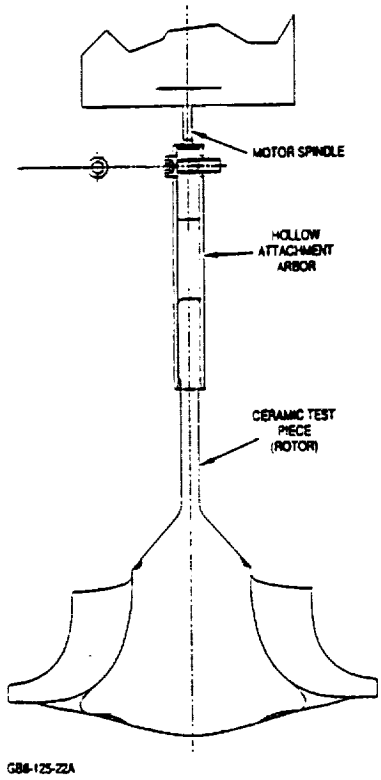

Figure 105. Spin Rotor Assembly.

6.2 Component Rig Testing

6.2.1 Regenerator Rig Test

A regenerator rig test was performed at the end of the AGT project which represented the state of regenerator seal development at the beginning of the ATTAP. Build 13 of the hot regenerator rig was tested at Ford during August 1987. The regenerator rig was operated with 2000F regenerator inlet temperature for 17 hours. The test was terminated after regenerator leakage became excessive. On teardown, significant regenerator system distress was noted. Most significant was the distortion of the hot side seal components and delamination of the seal coatings.

The causes of the seal distress were attributed to:

- Loss of substrate strength due to excessive temperature
- Insufficient seal shoe section modulus due to serrations cut on both sides of the seal shoe for improved coating adherence
- Distortion of the seal outer periphery shoe such that binding occurs at the outer periphery shoe/crossarm interface at operating temperatures

No further regenerator rig work has been done on ATTAP, pending the results of materials investigations and redesign activities discussed in Section 3.4 Test Bed Engine Design.

6.2.2 Transition Duct/Baffle Thermal Screening Rig

At the beginning of the year, a test plan was submitted to NASA for approval. After the plan was accepted, hardware was selected for thermal screening. At first, eight transition ducts and thirteen baffles, transferred over from the AGT program, were scheduled for testing. However, after deliberation, it was determined that only hardware with material properties suitable for use in an engine would be screened. This narrowed the field to three baffles and two transition ducts. Final machining, along with dimensional, visual, and other nondestructive inspections were made on the hardware before being considered ready for testing.

Before testing could begin, repairs had to be made on the test rig. A special geometry insulation piece had to be made. This insulation, procal HT-280, made by Foseco, is required to withstand temperatures in the vicinity of 1800F and still remain structurally sound, since the ceramic hardware is supported by it. When the insulation arrived, it was installed in the rig, thus concluding the repairs.

In a test, a transition duct and a baffle are screened together, stacked as they are in an actual engine to provide as much authenticity as possible. Each set of hardware goes through at least two thermal cycles, reaching a temperature of 1800F with an airflow rate of 22.6 pounds/minute. This cycle can be seen in Figure 106.

After the thermal screening was complete, the hardware was submitted for nondestructive evaluation. This includes visual and fluorescent penetrant inspections (FPI). The visual inspections did not reveal any posttest damage. The FPI has not been completed at this time. If no damage is determined with this test, the hardware will be considered acceptable for use in an engine.

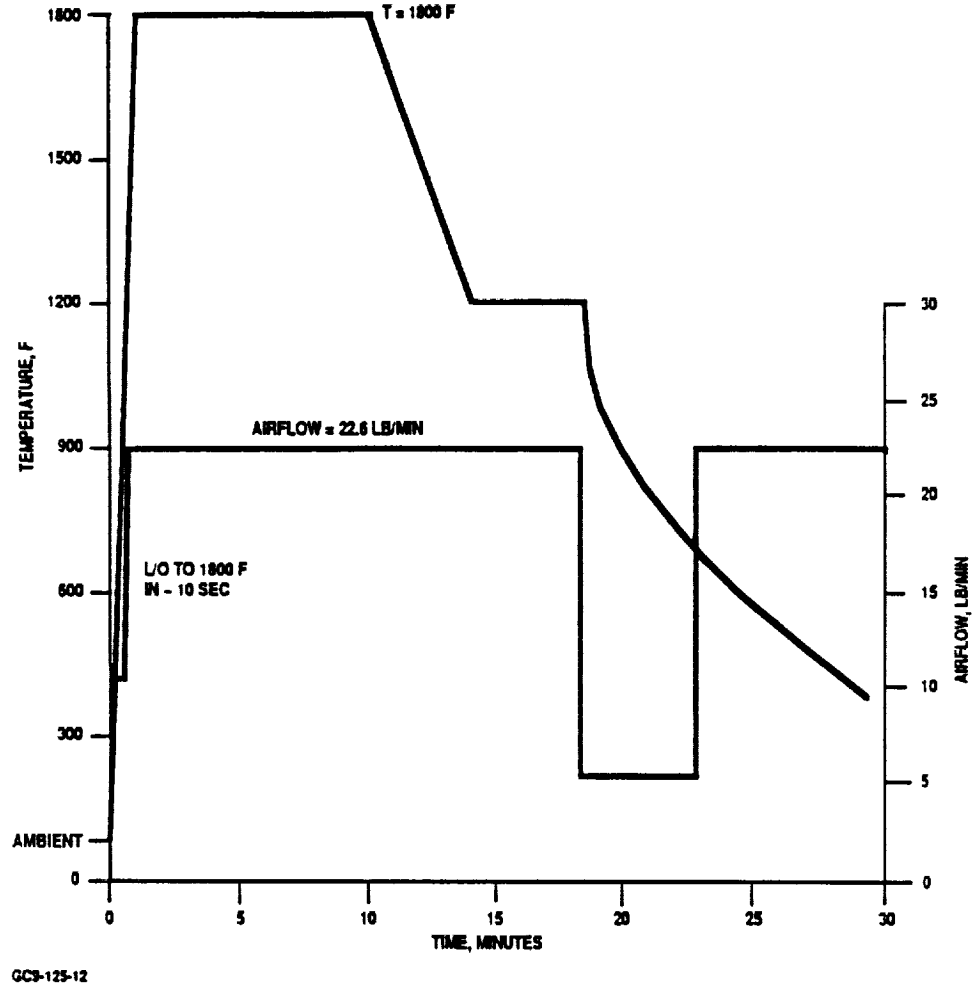

Figure 106. Transition Duct/Combustor Baffle Thermal Screening Cycle.

A new design is being considered for the supporting structure in the rig. Instead of using insulation to support the baffle and transition duct, ceramic hardware will be machined to provide a more stable platform along with providing a more engine-like flowpath.

6.2.3 Turbine Shroud/Stator Thermal Proof Rig

After a test plan was approved by NASA, modifications to provide a stable support for the turbine shroud in the Turbine Shroud/Stator Thermal Proof Rig were considered. The current rig does not provide a support that is completely rigid. The turbine shroud rests directly on the insulation on the bottom of the rig. Depressions in the insulation keep the shroud in place, as shown in Figure 107. If the insulation were to collapse, the stack of parts resting on the shroud, which have pressure applied to them axially,

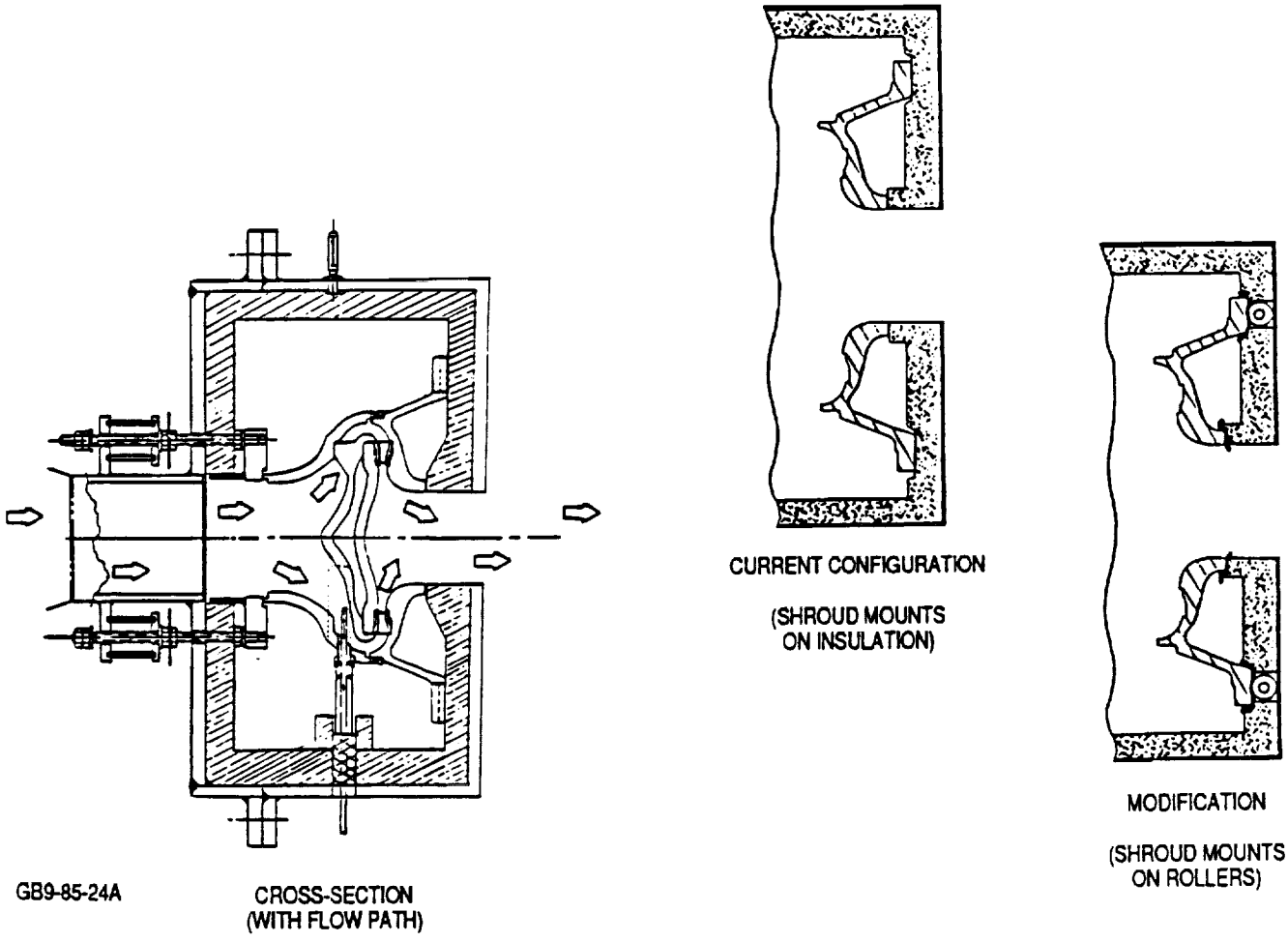

Figure 107. Turbine Shroud/Stator Thermal Proof Rig.

could unload. If this happened, the parts would risk damage due to impact and chattering.

A modification to the rig would use a silicon nitride support under each foot of the turbine shroud. The supports would be approximately 1 inch long and 1 inch in diameter. By lying on their sides on the rig metal, they theoretically provide a line contact with the feet of the shroud. In case a line contact is not achieved, a compliant layer, Nextel cloth, would be placed between the feet of the turbine shroud and the supports to prevent a point contact.

The previous insulation can be adapted to meet this design. In the new configuration, the shroud will never rest directly on the insulation, as shown in Figure 107. A wool-like ceramic insulation will be placed around the areas of the shroud that were previously in contact with the insulation in the old test rig. The new wool-like insulation is compressed against the old insulation when a load is applied to the turbine shroud, thus providing a seal. This prevents hot gases from blowing between the insulation and the turbine shroud. The recirculation of these gases on the backside of the turbine shroud would create a non-engine condition.

Currently, five turbine shrouds and six stator sets are being prepared for testing. This includes machining, dimensional inspections, and various forms of NDE.

6.2.4 Ceramic Seals Rig

In mid-October 1988, the testing rig for the flow separator housing piston ring seals was assembled. During the pressure check prior to the actual seals testing, a failure occurred in the turbine shroud. Steps taken to ensure this type failure will not reoccur include accurately tracking the part histories for all parts in the rig, along with mechanical screening of the ceramic hardware before being placed in the rig. A portion of the rig, a plug which fits into the center of the turbine shroud, has also been redesigned. The new plug uses Ultra High Molecular Weight Polyethylene (UHMW) instead of stainless steel, and distributes the pressure load over a larger surface area.

This rig failure provided an excellent opportunity to develop a failure report form, which is required by contract. Using input from the Material Development, Mechanical Component and Design, Reliability, and Project groups, the Component Failure Reporting and Correction System (CFRACS) was devised. Hopefully, through this database being placed in a computer, and by also keeping hardcopy files, this system will not only provide information as to what parts have failed or broken, but it will also be able to help determine whether or not a pattern is developing. A sample of the form used is shown in Figure 108.

COMPONENT FAILURE REPORTING AND CORRECTION SYSTEM 0017

FAILURE TYPE (P)RIMARY OR (S)ECONDARY [ ]

EUF # 38-3129-4034[31]
MWO # 3409-246405-___-_____
PROJECT ENG'R_____EXT.____

	MO	DA	YR
EVENT OCCURRED			
REPORT FINALIZED			

(STATUS OPEN)
(STATUS CLOSED - REQUIRES PROJECT SIGNATURE)_____

TEST DESCRIPTION

RIG/ENGINE	
BUILD NO.	
TEST CYCLE	
TEST HOURS	
NUMBER L/O'S	

COMPONENT INFORMATION

NAME	
SERIAL NO.	
PART NO.	
MATERIAL	
VENDOR	

PREVIOUS TEST HISTORY

NO. MECH RIG	
NO. THERMAL RIG	
TOTAL ELEV TEMP HRS	
TOTAL L/O CYCLES	

PRIMARY FAILURE MODE

MECHANICAL LOAD	
IMPACT	
CONTACT	
THERMOELASTIC	
UNKNOWN	
OTHER	

FAILURE ORIGIN (DESCRIPTION - 20 CHARACTERS MAX)

CAUSE OF FAILURE - (S)URE, (L)IKELY, OR (P)OSSIBLE

COMPONENT DESIGN		MATERIAL	
ENGINE DESIGN		ASSEMBLY	
TEST PROCEDURE/EQPT		OTHER	

CONTIGUOUS SECONDARY FAILURE(S)_____

PROJECT SUMMARY_____

_____ENGINEER_____

MAT'L ENG'R'G RESULTS_____

_____ENGINEER_____

MCD RESULTS_____

_____ENGINEER_____

TASKS ASSIGNED TO COMPLETE TROUBLE ANALYSIS	RESPONSIBLE	DUE

(REFER TO ATTACHMENTS FOR REPLY AND ADDITIONAL DETAIL, I.E. PHOTOS, DATA, RELATED DOC'TS)

CONCLUSIONS_____

CORRECTIVE ACTION_____

RELIABILITY CONFIRM DATA ENTRY OF ALL BOXED INFO (CLOSED REPORT) BY CHECKING HERE - [ ]

Figure 108. Sample CFRACS Form Establishes Database.

6.2.5 Combustor Rig

Design of a new emissions/pressure/temperature rake, initiated under the previous AGT program, continued. A heat transfer analysis was performed to determine the required air and water cooling flows. The rake layout design and its installation in the exhaust duct is shown in Figure 109.

A new rig cart was designed and fabricated during the reporting period. The rig features quick-disconnect hook-ups for ease of installation and removal. At the end of the period, the rig was installed on the cart. New instrumentation was installed in the rig and connected to panels on the cart.

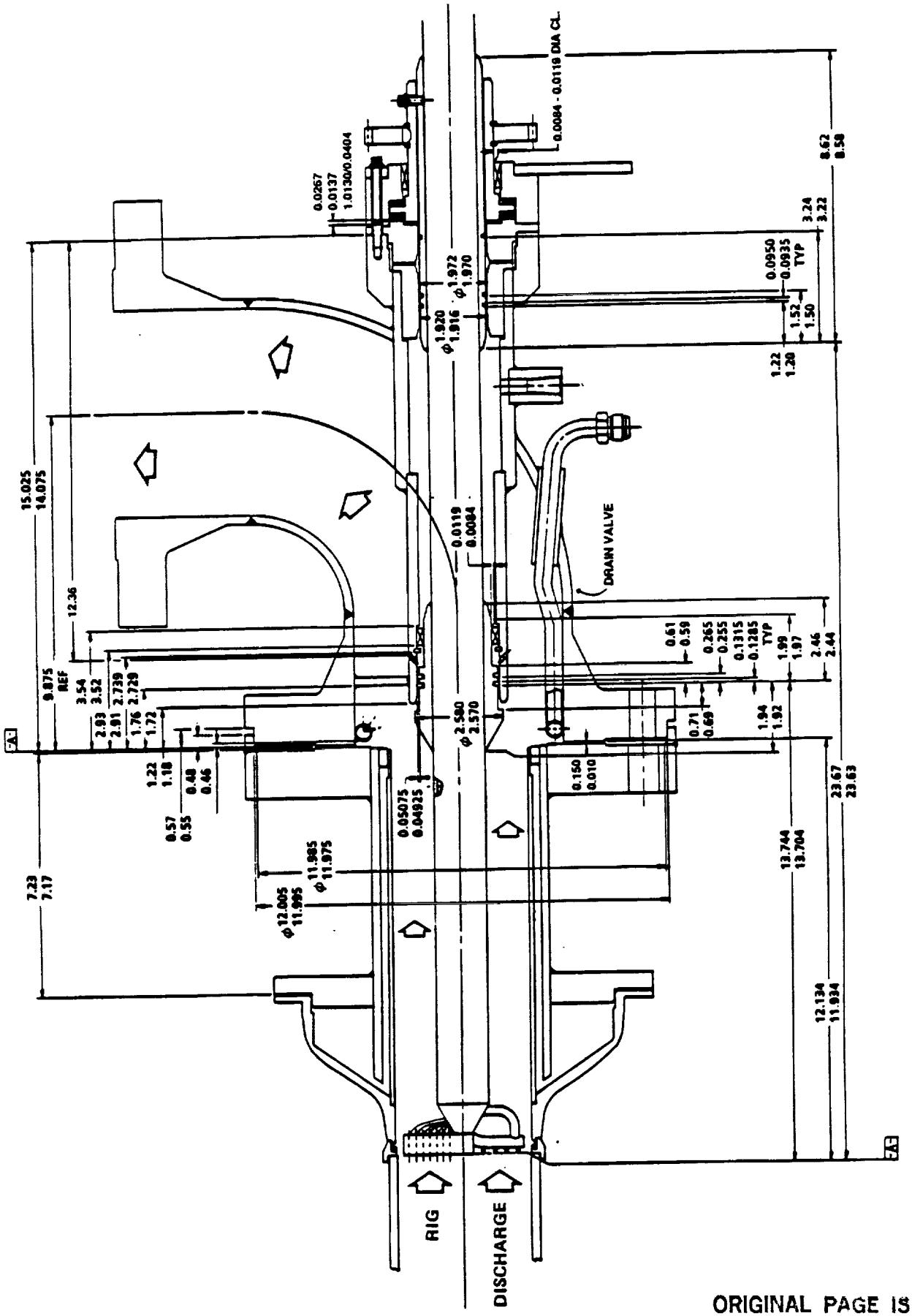

Figure 109. Emissions/Pressure/Temperature Rake Design.

ORIGINAL PAGE IS
OF POOR QUALITY

7.0 PERFORMANCE AND DURABILITY TESTING

There was no engine performance or durability test activity in this reporting period.

8.0 PROJECT MANAGEMENT AND REPORTING

The primary reportable activity in this area relates to presentations at Coordination and Society Meetings. Foremost among these is the Automotive Technology Development Contractors Coordination Meeting, held annually in the Detroit area. GAPD's Mr. Gary Boyd presented an overview of the ATTAP and of the progress made to date, and Mr. Ho Fang made a presentation on GAPD's approach to impact testing for design methods development.

APPENDIX A

ANNUAL TECHNICAL PROGRESS REPORT
NORTON/TRW CERAMICS

(39 pages)

ADVANCED TURBINE TECHNOLOGY APPLICATIONS PROJECT
COMPONENT DEVELOPMENT PROGRAM

Annual Technical Progress Report
for the period
February 1, 1988 to December 31, 1988
under
GAPD Purchase Order Nos. P1776307,
dated February 18, 1988,
and
P1772578, P1772588, P1772598, and P1772608
dated July 7, 1988.

Submitted by
NORTON/TRW CERAMICS
Goddard Road
Northboro, MA 01532-1545

Bryan J. McEntire
Program Manager

Report Date: January 26, 1989

Prepared for
NASA-LEWIS RESEARCH CENTER
Cleveland, OH 44135

Submitted to
Garrett Auxiliary Power Division
ALLIED SIGNAL AEROSPACE COMPANY
Phoenix, AZ 85034

EXECUTIVE SUMMARY

This report presents a summary of Norton/TRW Ceramic's (NTC) work in support of the Advanced Turbine Technology Applications Project (ATTAP) for the 1988 program year. As a participant in ATTAP, NTC is responsible for the development of ceramic fabrication processes for the rotor and stator components of the AGT101 gas-turbine engine. Activities towards these objectives have centered on completion of seven tasks: (1) Design and Cost Analysis; (2) Forming Methods; (3) Process Engineering; (4) NDE; (5) Quality Assurance; (6) Deliverables; and (7) Project Management. For each task, all first-year program milestones were achieved.

NTC supplied and subsequently qualified a Si_3N_4 material at GAPD for use in the ATTAP. Designated NT154, the material is a Y_2O_3-doped Si_3N_4 prepared by HIP densification. Excellent physical and mechanical property data have been acquired, independently verified, and compiled. Static stress rupture tests have also been performed to confirm the stability of the material for use at high-stress and temperature conditions.

Component forming technologies were initiated. Casting and injection molding were selected as forming processes for the rotor and stator, respectively. Process development was conducted for a number of key operations including Powder Beneficiation, Slip/Pressure Casting, Injection Molding, Degas Heat-Treatments, HIP, and Post-HIP Heat-Treatments. Key process parameters and control ranges were identified for a number of these operations. Using this technology, rotor hubs and stators were formed, densified and characterized. Component properties, in both the green and dense state, conformed to program milestones and material specifications.

NTC has elected to utilize Taguchi-based experimental design techniques for all process engineering activities. A comprehensive Work Plan for individual experiments was prepared and submitted to GAPD. Taguchi designs are advocated because of their ability to simultaneously achieve process robustness and reduce cost.

NDE development has centered on the use of microfocus x-ray inspection. Component inspection protocols are being developed using seeded defect specimens. These specimens were prepared and characterized in compliance with program milestones. The microfocus unit was successfully implemented as an in-process inspection tool for the identification of high-density defects within green components.

The key elements and schedule of a comprehensive quality assurance program were identified and documented. Writing of specific QA documents has been initiated. Implementation of this program coincides with completion of the experimental work prior to final component deliverables.

Continued effort in process and component development is scheduled for the 1989 program year. Work will emphasize the elimination of impurity defects, address dimensional control issues, and the selection of additional process parameters. All activities are on schedule for achievement of overall ATTAP goals and milestones.

INTRODUCTION

Commercialization of advanced structural ceramics requires development of reliable component manufacturing processes. The Advanced Turbine Technology Applications Project (ATTAP) addresses this requirement. The ATTAP is a DOE-sponsored, 5-year ceramic component development program that utilizes the AGT101 gas-turbine engine as a functional test-bed. The goals of this program include: (1) The development and demonstration of reliable ceramic fabrication processes; (2) Production of the required ceramic components; (3) Evaluation of these components in actual engine tests; and (4) Preparation of a Ceramic Design Manual. The Design Manual will provide material specification and design methods for structural ceramics in a diversity of applications.

As a participant in ATTAP, and subcontractor to the Garrett Auxiliary Power Division (GAPD) of Allied-Signal Aerospace Co., Norton/TRW Ceramics (NTC) is developing ceramic fabrication processes for the AGT101 stator and rotor. NTC has performed this work in accordance with the overall program schedule of the Statement of Work (SOW) [1]* as shown in Figure 110. Identified within the SOW are seven tasks: (1) Design and Cost Analysis; (2) Forming Methods; (3) Process Engineering; (4) NDE; (5) Quality Assurance; (6) Deliverables; and (7) Project Management.

From the SOW, a comprehensive first-year Work Plan was developed. The schedule for the Work Plan is shown in Figure 111. The Work Plan further defines the technical approach of the program, extent of design and analysis, experiments, hardware, and activities directed at achievement of the program objectives and milestones. This report presents a summary of NTC's first year developmental endeavors. Work reported includes: (1) Assessment and qualification of a Si_3N_4 material for use in component fabrication; and (2) The initiation of process development and component fabrication operations including inspection and NDE techniques.

DESIGN AND COST ANALYSIS

As part of the ATTAP SOW, NTC and GAPD agreed to a set of material specifications and goals. These are presented in Table 26. The material selected for use within the program, NT154, is a 4% Y_2O_3-doped HIPed Si_3N_4. HIPing is accomplished using ASEA glass encapsulation techniques. Samples were supplied to GAPD for material assessment and qualification. Compiled physical and mechanical property data for this material are presented in Table 27. These results demonstrate that the material exceeds specifications and meets many of the program goals. Other researchers have independently obtained similar values.[2-3] The use of high purity raw materials coupled with HIP densification yields a Si_3N_4 with room-temperature and 1370°C strengths of ~1 GPa and ~0.6 GPa, respectively. Fracture origins on bend-test bars were predominantly machining flaws. However, inclusions associated with minor impurities have also been noted. Improvements in Weibull modulus are required; but are addressed within the ATTAP component development program.

*Numbers in parentheses designate references at end of report.

Figure 110
ATTAP Program Schedule For Norton/TRW Ceramics

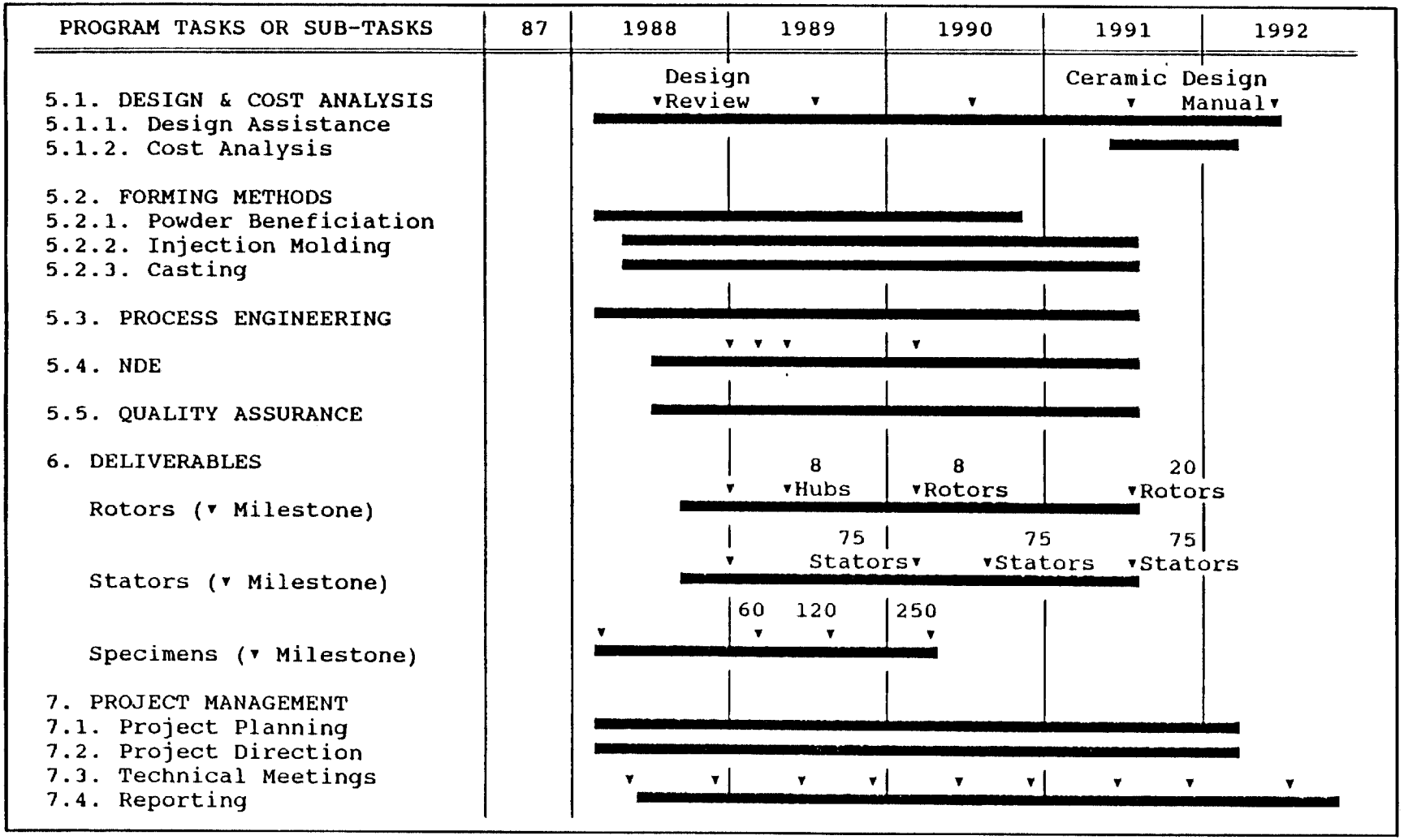

Figure 111
1988 ATTAP Work Plan Schedule For Norton/TRW Ceramics

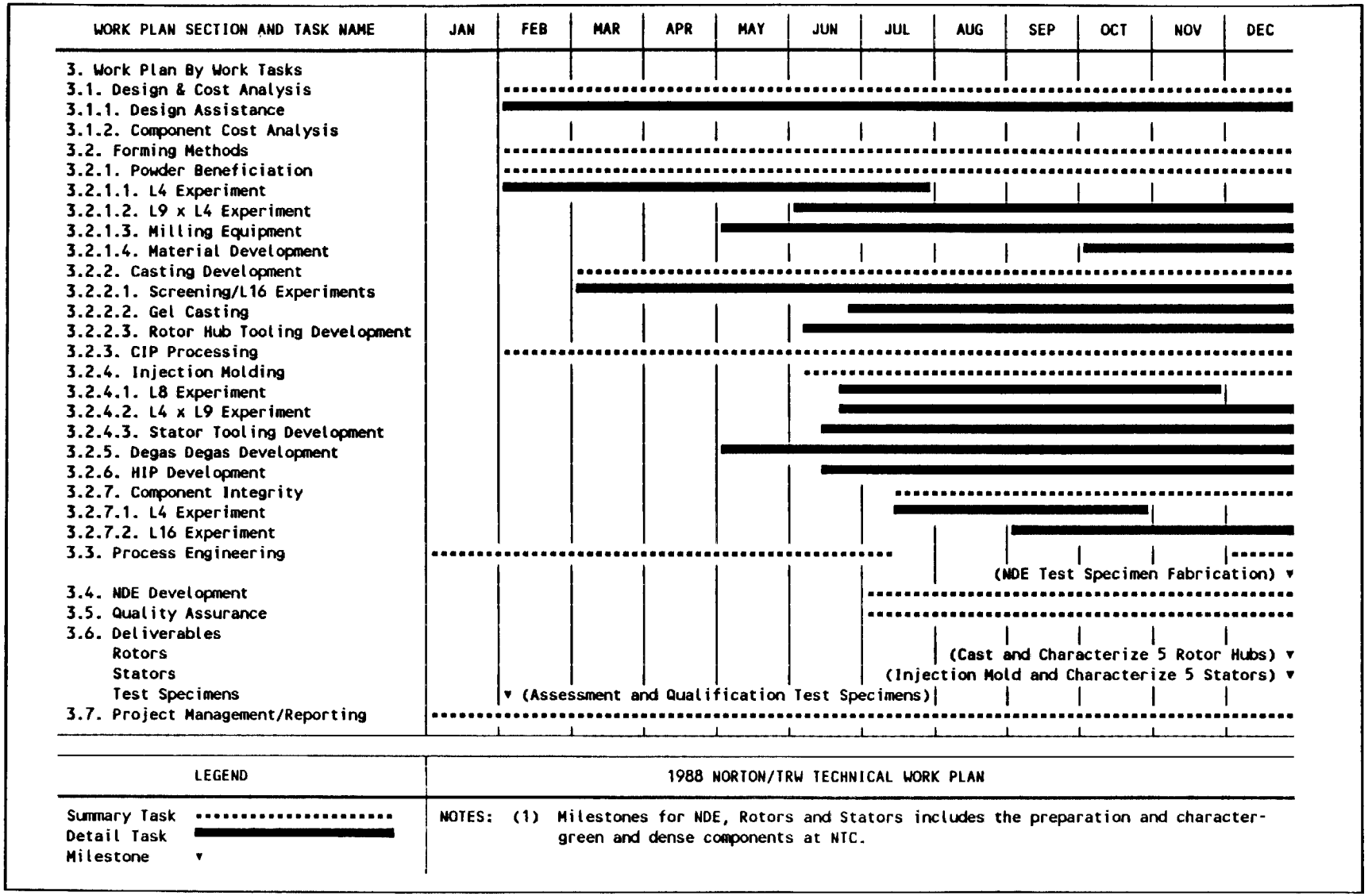

Table 26
ATTAP Si_3N_4 Material Specifications And Goals

Measured Property	Specification	Goal
1. Density (% of Theoretical)	99.5%	99.5%
2. 22°C Flexural Strength (MPa)	690	900
3. 1370°C Flexural Strength (MPa)	517	690
4. Weibull Modulus @ 22°C & 1370°C	8	18
5. Fracture Toughness ($MPa \cdot m^{1/2}$)	3.5	5
6. Flexural Stress Rupture Life (hrs)		
1260°C - 350 MPa	150	500
1370°C - 250 MPa	150	500

Table 27
NT154 Slip-Cast ATTAP Qualification Samples
Physical and Mechanical Properties

Physical and Mechanical Properties	Values
1. Density (g/cc)	3.232 ± 0.004
2. Elastic Modulus (GPa)	320
3. Shear Modulus (GPa)	126
4. Poisson's Ratio	0.273
5. Thermal Expansion Coefficient	3.93×10^{-6}/°C
7. Thermal Conductivity (W/m°K)	
(25°C)	37.6
(900°C)	20.7
(1400°C)	15.8
8. Room Temperature Mechanical Properties	
Flexural Strength (MPa)	920 ± 153
Characteristic MOR (MPa)	985
Weibull Modulus*	9.6 ± 0.6
Fracture Toughness ($MPa \cdot m^{1/2}$)**	3.6 ± 0.3
No. of Samples	66
9. 1370°C Mechanical Properties	
Flexural Strength (MPa)	531 ± 46
Characteristic MOR (MPa)	552
Weibull Modulus*	13.2 ± 1.3
No. of Samples	23

* Weibull Modulus at 95% confidence. Other error estimates are ± one standard deviation.
** Indentation Technique - Anstis equation for 110 measurements.
Note: Test bar size = 3.175 mm x 6.35 mm x 50.8 mm (.125" x .250" x 2"); Crosshead speed of 0.5 mm/min.; Outer span = 40 mm; Inner span = 20 mm.

Static stress rupture tests were conducted under severe conditions (300 MPa and 1370°C) to determine differences in material characteristics. Figure 112 depicts the stress rupture behavior of the material. Some variability in stress rupture life was observed. However, the material predominantly displays characteristics acceptable for the ATTAP. At temperatures less than ~1260°C and/or stresses below 300 MPa, test specimens exhibit lifetimes in excess of 200 hrs. Process induced impurities, and other microstructural inhomogeneities are believed to be the cause of some early specimen failures at higher temperature or stress conditions. Planned experiments in material and process development are directed at eliminating this type of failure.

FORMING METHODS

In accordance with the Work Plan, subtasks within the Forming Methods section include: (1) Powder Beneficiation; (2) Casting Development; (3) CIP Processing; (4) Injection Molding Development; (5) Degas Heat-Treatments; (6) HIP Development; and (7) Component Integrity Development. Experimental plans for these areas are shown in Figure 4.

Single or iterative Taguchi experiments were developed for each area. The labels L4, L8, L16 of Figure 113 refer to specific Taguchi designs. The "L" designates the experiment as a Taguchi array and the 4, 9 or 16 refer to the number of trials to be conducted within the array. Taguchi experiment design techniques were exclusively chosen for the program.[4] Taguchi methods are advocated because of their ability to simultaneously achieve process robustness and reduce cost.[5] In simple form, they are fractional factorial arrays which have advantages over traditional designs. Foremost among them is ease of use. Application and data analysis can be accomplished, in most instances, by relatively non-experts. A series of 22 base matrices are available including standard multilevel factor or mixed-level factor designs. These base matrices can be easily customized to handle almost any experimental condition. Experiments can be designed in a global (i.e., "one-shot") or iterative manner. Specific software has been developed to allow set-up, data tracking, and analysis. Because of these features, use of Taguchi methods leads to a high degree of experimental efficiency. Output includes significance and factor interaction testing, and experimental error. Response data can be plotted in the form of process maps. This is particularly effective in specifying process parameters and control limits. In many respects, Taguchi methods are similar to traditional designs; however, their ease of use, customization capability, efficiency, and data output make them distinctive from traditional techniques.[6]

From Figure 113 note that each of the five major process areas is linked to each other through the forming operation. Experiments in Powder Beneficiation, Pre-HIP (Degas), HIP and Component Integrity have been designed to allow interpretation of the results in light of the selected forming method. Cold isostatic pressing (CIP) is being used in the program as a control. Experimental efforts were initiated in each of the five areas.

POWDER BENEFICIATION - Three experiments were planned for this area. The first two involve Taguchi arrays designed to ascertain important powder preparation variables. The third is a matched-pair experimental design used for the selection of milling equipment. All powder beneficiation operations were

Figure 112
Stress Rupture Behavior of NT154 - Response Surface

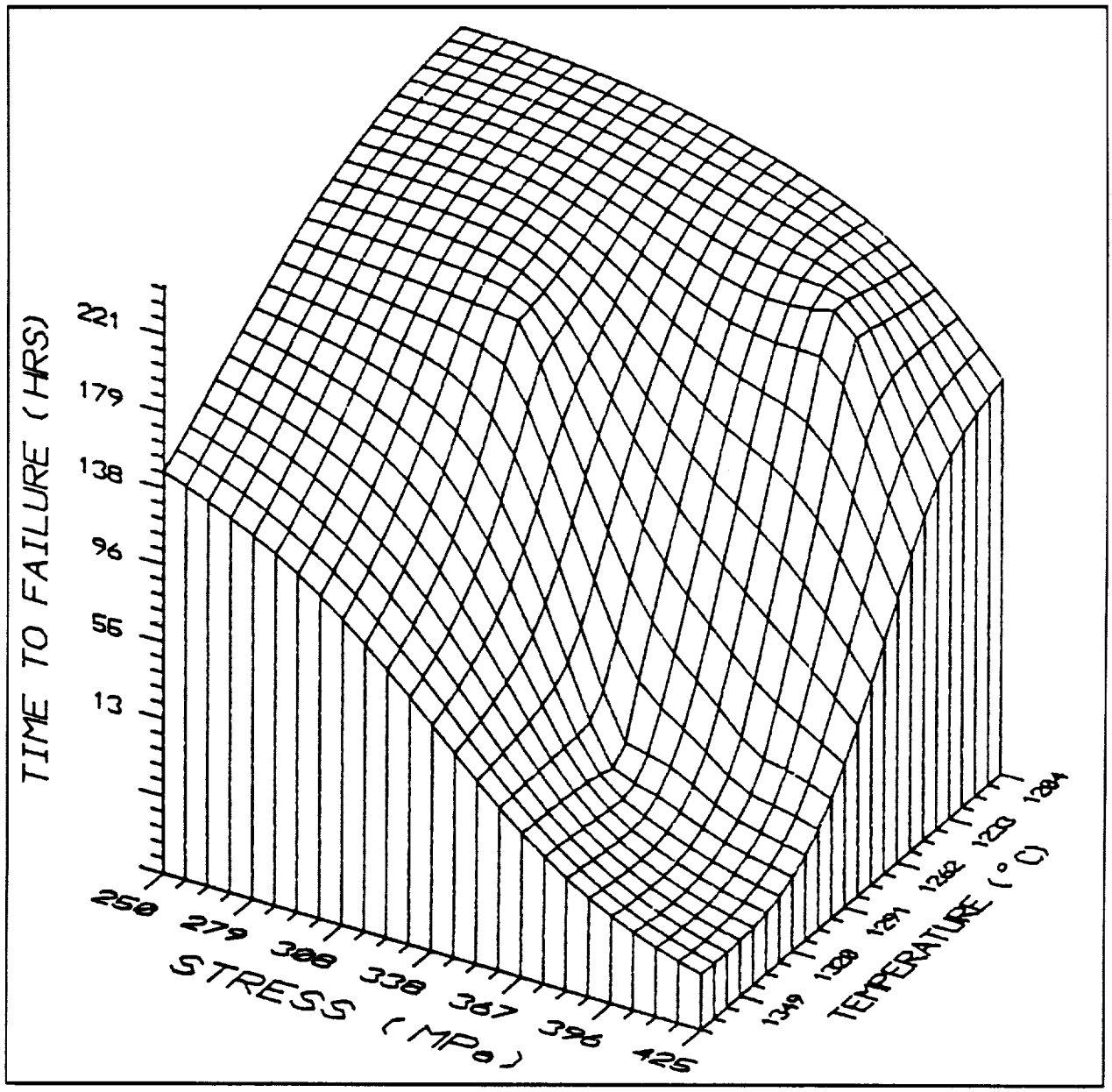

carried out under clean-room conditions.

The first Taguchi L4 was designed as a screening test to evaluate four factors: (1) Si_3N_4 Blend Source; (2) Y_2O_3 Blend Source; (3) Milling Time; and (4) Forming Method. Two forming methods, CIP and Slip-Casting,were selected as the control and outside factor, respectively. The experiment has been completed and analyzed using Taguchi ANOVA techniques. A summary of important results is presented in Table III. These data are presented in level average format. Conclusions from this experiment, along with selected processing parameters

Figure 113
ATTAP Component Development Using Taguchi Methods

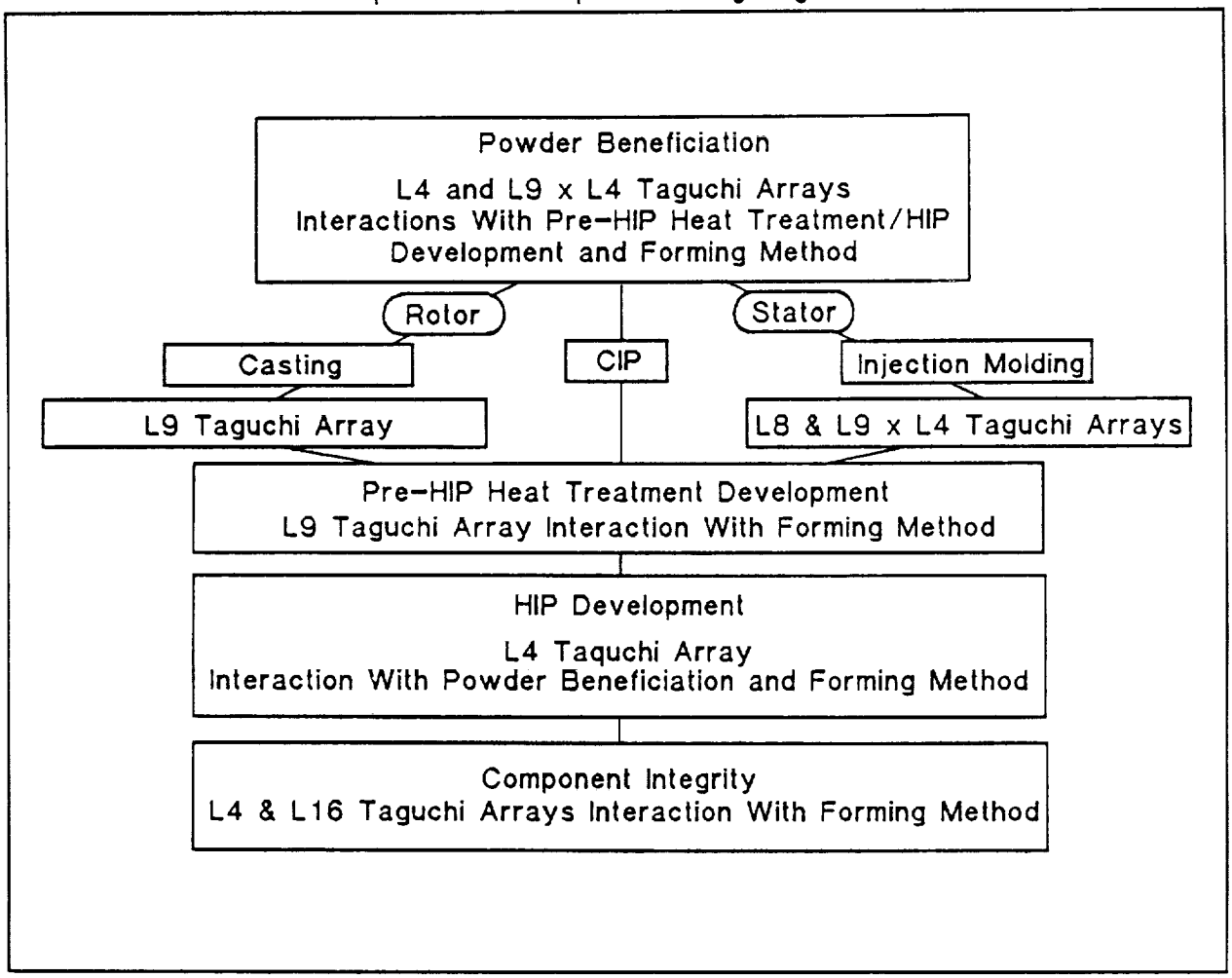

include:

- The Si_3N_4 blend was the significant contributing factor for green density, linear shrinkage, room and 1370°C flexural strength. Level 1 was selected because of its broader size distribution and superior high-temperature mechanical properties.
- Y_2O_3 was not a significant factor for any measured result. It was dropped as a factor in future designs. Level 1 was selected because of better overall mechanical properties.
- Milling time was significant in controlling stress rupture behavior. This may be related to particle-size or chemical composition changes which accompany the milling process. Level 1 was selected because of superior stress rupture life.
- The forming method was found to be an important controlling factor for

Table 28
Level Average Physical and Mechancial Properties For
L4 Powder Beneficiation Experiment

Factor & Level	Density (g/cc)	Fracture Toughness ($MPa \cdot m^{1/2}$)	22°C MOR (MPa)	1370°C MOR (MPa)	Stress Rupture Life (Hrs)
1. Si_3N_4 Blend Source					
- Level 1	3.22	3.7	940	563	134
- Level 2	3.22	3.7	1019	536	101
2. Y_2O_3 Blend Source					
- Level 1	3.22	3.7	1003	557	132
- Level 2	3.22	3.8	957	542	102
3. Milling Time					
- Level 1	3.22	3.8	992	550	168
- Level 2	3.22	3.6	968	549	66
4. Method of Forming					
- CIP	3.23	4.1	1005	583	149
- Cast	3.22	3.5	958	534	86

Stress Rupture Test Conducted at 1370°C - 300 MPa.

fracture toughness, room and 1370°C flexural strengths.

Output from this experiment was used as input to the second iterative Taguchi array--an L9 x L4 design. This experiment is presented in Figure 114. The experiment consists of an inside L9 powder beneficiation array coupled with an outside L4 HIP array. L9 factors included Si_3N_4 Blend Source, Milling Time, Solids Concentration, and the Interaction of Milling Time and Solids Concentration--each at three levels. The three level L9 design was selected so that process response maps could be generated. The L4 factors consisted of HIP Temperature, HIP Time and Cooling Rate--each at two levels. Again, CIP and Slip-Casting were used as factors for component forming comparisons. The experiment required 72 separate trials. It represents one-sixth of a full-factorial array. While the experiment has not been fully completed, components have been processed through the densification cycle, and are currently being ground into test-bar components. An analysis of powder and green-forming data has been completed. ANOVA data for selected response variables are presented in Figure 6. This graph shows results for two powder parameters and two forming methods. Percent contribution of individual factors for each response variable is given. Similarly, the error terms in the graphs depict contribution of experimental variability in relation to the treatment factors. These data suggests that the Si_3N_4 blend source and milling are important factors for surface area, particle size range, and green density. It is interesting to note that the ANOVA showed that CIP and cast green densities are controlled by different factors. The Si_3N_4 blend source controlled CIP density and milling time controlled cast density. For both forming processes, coarse powder blends

Figure 114
Taguchi L9 x L4 Powder Beneficiation Experiment Design

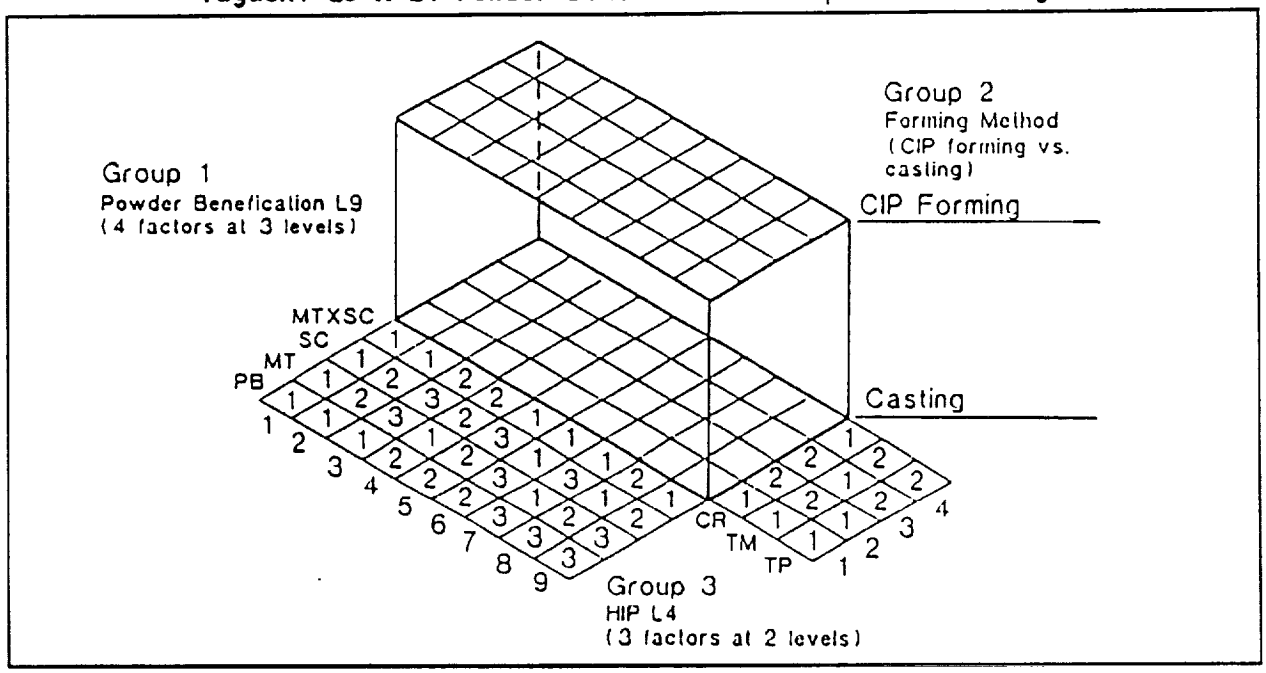

gave the highest values--averaging 1.80 g/cc and 1.93 g/cc for CIP and cast components, respectively. The large error term associated with the casting operation is believed to results from additional slip-batch preparation factors outside the control of this particular experiment. These factors were assessed under a separate L16 design dealing with casting operation itself described later in this report. Conclusions concerning the powder data are as follows:

- Milling time was a significant factor for all response variables. It was particularly important in controlling the particle size range and impurity content of the batches. Media wear was identified as the source of the impurity increase. Milling time was less important, but still significant for surface area and powder oxygen content. As expected, both of these response variables increased with longer mill times.

- The Si_3N_4 blend was significant in controlling surface area and oxygen levels within batches. Although milling time affected both surface area and oxygen, it was not as dominant as the Si_3N_4 blend source.

- Solids concentration was significant only for impurity contamination. Lower solids promoted greater media wear, and hence increased levels of impurities.

Conclusions from the forming data are as follows:

- Milling time was a significant factor for all response variables. It was particularly important for slip-cast density, and impurity contamination. Average cast densities were inversely proportional to milling time. Broad and coarse powder distributions provided the highest level of green density.

- The Si_3N_4 blend was a controlling factor in CIP density. Coarse blends, of

Figure 115
Significance Levels For Selected Factors From The
L9 x L4 Powder Beneficiation Experiment

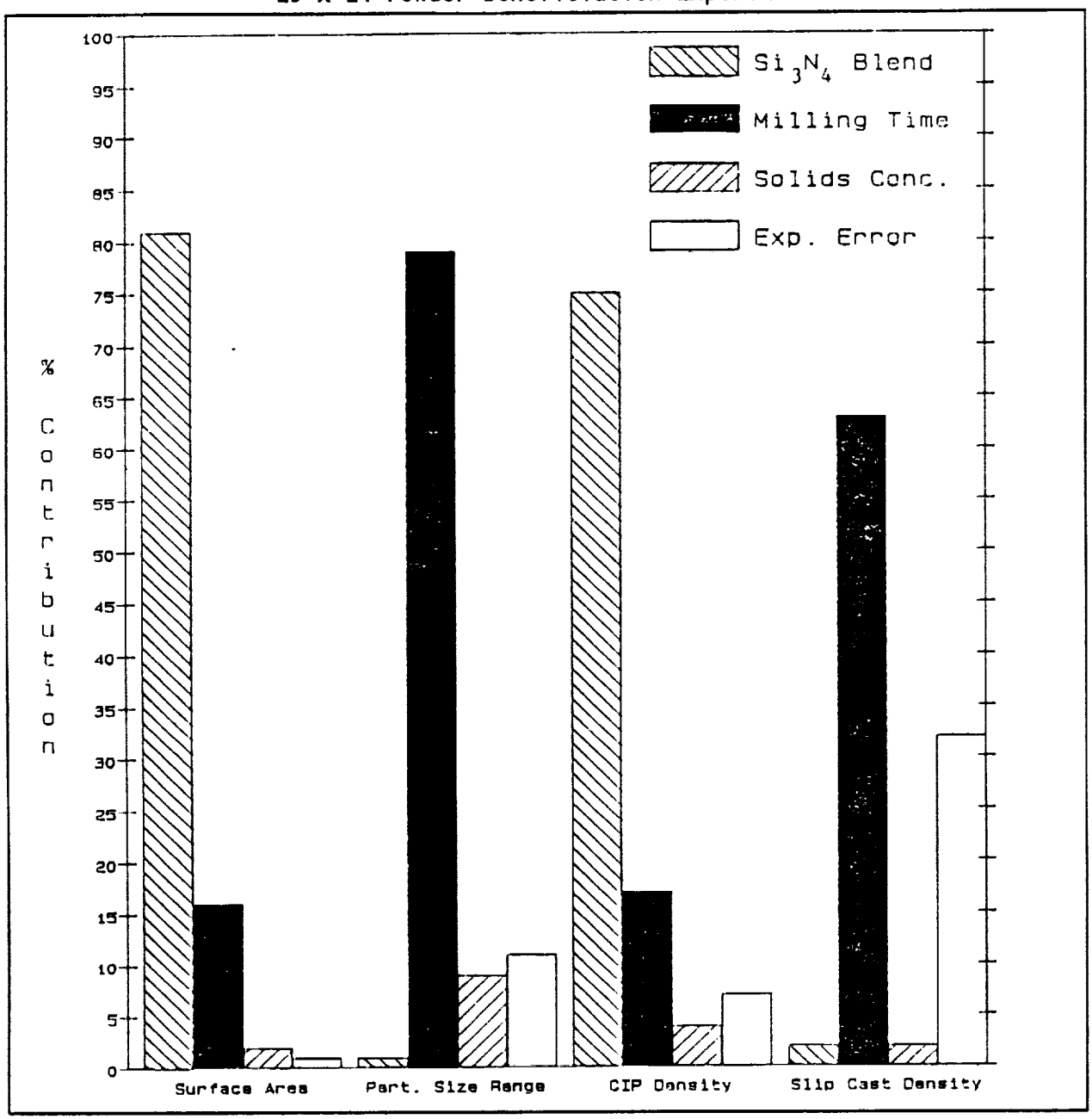

low surface area, resulted in high green densities.

- Solids content remained a significant factor for impurities in cast components.
- The interaction between Si_3N_4 blend and milling time was not significant for any response variable of the forming data.

From these analyses, additional processing parameters were tentatively selected for powder beneficiation conditions. They include the use of a coarse Si_3N_4 powder blend, short milling time, and high solids concentration. Advantages of these conditions are high green density and low impurity content. However, final recommendations on selected powder processing conditions will be conducted following correlation of these results with the L4 HIP portion of the experiment.

Another way of analyzing data from the L9 experiment is to prepare process response surface maps. A typical example is presented in Figure 116. This figure depicts a three-dimensional view of changes in slip-cast density as a function of milling-time and solids concentration. Such diagrams provide fundamental information for setting process control parameters. For instance, Taguchi methods teach that, where feasible, operational conditions are selected to minimize "noise". Noise is defined as observed product variability at selected process operational conditions. The response surface of Figure 116 suggests that noise can be minimized by selecting appropriate milling times and solids concentration. In this case, a high solids concentration and short milling time were preferred. At these conditions, cast density becomes relatively insensitive to changes in either process factor. Fortunately, in this instance, the minimum noise condition is also consistent with the highest green density. These data demonstrate that densities within the range of 1.96 to 2.02 g/cc can be obtained at minimum noise with a variety of solids concentrations and milling-times. Upon completion of the experiment, these process conditions will be further defined using input from other response variables such as shrinkage, sintered density, and mechanical strength. Overlays of several process contour maps representing all important response variables define critical operational ranges or engineering trade-offs. In this manner, Taguchi methods promote the selection of parameters which maximize properties and minimize the effects of noise.

The matched-pair milling equipment experiment involved a comparison of ball and vibratory comminution operations. The purpose of this experiment was to: (1) Examine alternative comminution equipment; (2) Scale the milling process from batches of $\leq$ 5 to 15+ Kgs; and (3) Evaluate and select one process for powder production. As of the close of 1988, this experiment was still being conducted. Powder was prepared from both processes at scaled-up batch quantities of between 15 and 25 Kgs. Tile components were formed using CIP, Injection Molding and Casting techniques. These components have been processed through HIP densification and are currently being ground into test-bars. While quantitative data from the experiment are incomplete, conducting these trials has been instructive. During operation of the vibratory grinding equipment, numerous problems were encountered associated with mixing and recirculation of the powder slurry. Slurry settling occurred and stable equipment operation was difficult to achieve. Furthermore, it is well known that vibratory grinding operations lead to narrow-size distribution powders. Conversely, the ball milling operation prevents settling, provides intensive mixing concurrent with comminution and yields a broad size distribution. Additionally, a ball mill is a simple device of high reliability. Based on these qualitative factors, a decision was made to exclusively utilize ball milling equipment for powder production. Quantitative data from this study will be correlated with the L9 x L4 experiment discussed earlier. Data from the milling equipment experiment

Figure 116
Effect of Milling Time And Solids Concentration
On Slip-Cast Density

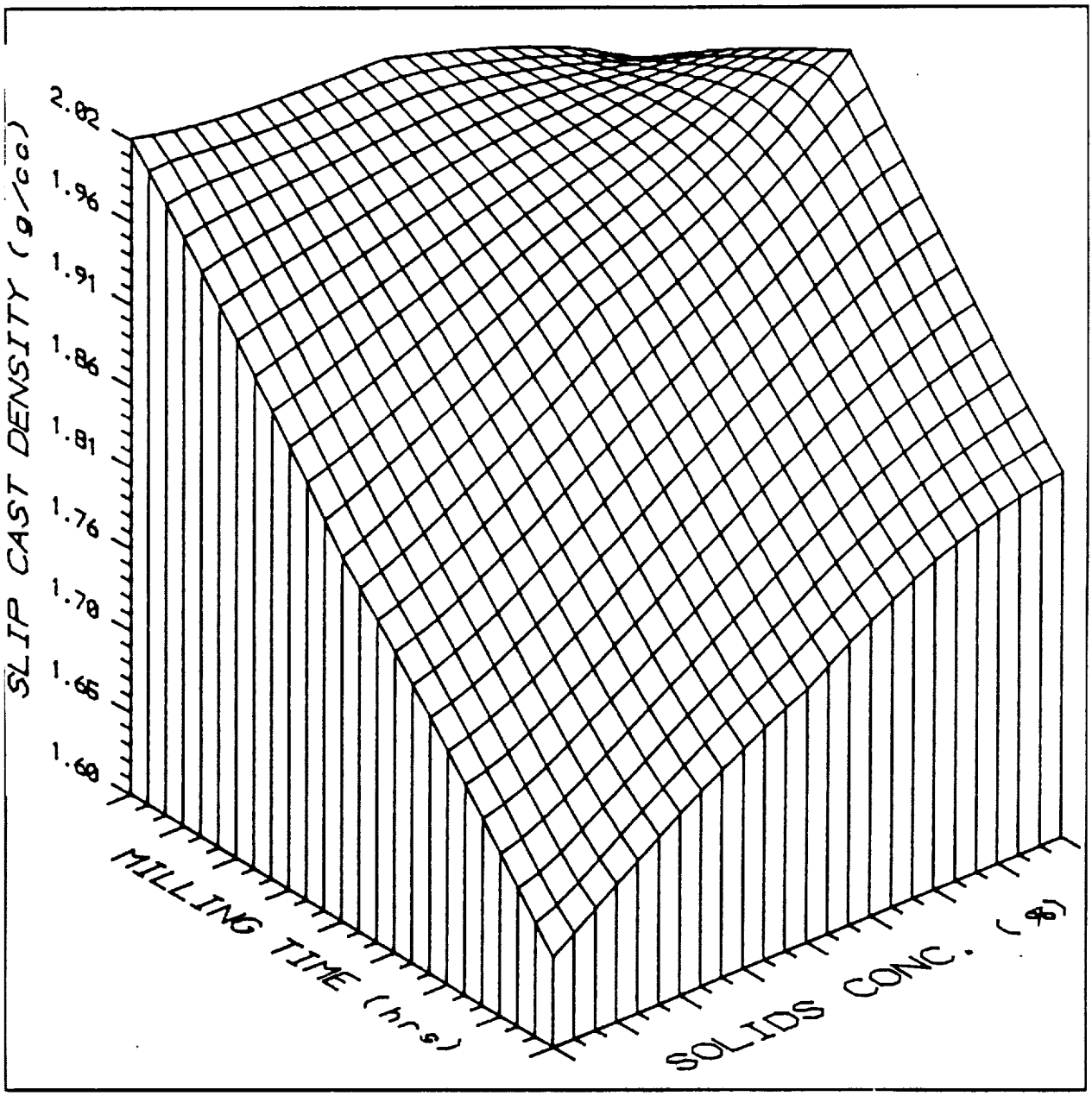

will therefore serve to confirm this decision and to further optimize the ball-milling parameters.

CASTING DEVELOPMENT - Casting was selected as the preferred method for forming the rotor. It is a proven process for complex shape fabrication. It requires minimal amounts of organic additives and therefore eliminates binder burn-out problems. Furthermore, the process is potentially automatable using

Table 29
L16 Casting Experiment - % Contribution of Experimental Factors On Each Response Variable

Response Variable	A	B	C	D	E	% Error
pH	5.74	42.56	-	22.32	11.62	17.75
Viscosity	8.06	19.03	2.26	51.29	-	19.35
Specific Gravity	4.21	6.04	-	75.00	6.04	8.33
Green Density	78.95	-	10.53	2.20	3.10	10.53
Cracking	0.89	-	5.84	5.84	37.86	49.58
Pour Lines	57.91	-	4.96	25.32	4.85	6.97
Surface Porosity	32.37	4.85	-	13.96	13.11	35.70
Surface Finish	3.07	-	13.41	14.75	19.69	49.07
Mold Release	-	-	-	-	7.95	92.05
Cast Time	55.15	3.97	-	24.49	8.37	8.02
Out-of-Mold Shrinkage	16.44	56.31	-	9.37	4.99	12.88

A = Mold Coating Technique or Additives.
B = NH_4OH Concentration.
C = Dispersant Concentration.
D = Solids Loading.
E = No. of Casts per Mold.

available pressure casting equipment.* Casting experiments within the ATTAP during the first year focused on slip-preparation methods and additives. An L9 experiment was originally proposed in the Work Plan. However, modifications of the experiment were implemented due to additional experimental factors which became apparent during exploratory studies. Eventually an L16 design was conducted. The experiment was set-up to correlate selected powder blends with additive levels, and mix preparation conditions. All work was performed using laboratory slip or pressure-casting equipment and plaster molds. For the L16 experiment, five factors were selected, each at four levels. They included Mold Coating, Dispersant Concentration, Ammonia Concentration, Solids Loading, and Mold Age (i.e., the number of casts per mold). Response variables included pH, viscosity, specific gravity, green density, out-of-mold shrinkage, casting time, pour lines, surface porosity, surface finish, mold release and cracking behavior. Table 29 presents the Taguchi ANOVA for the experiment. Level average results are given in Table 30.

The three response variables which describe slip properties are pH, viscosity, and specific gravity. As expected, the ANOVA demonstrates that viscosity and specific gravity are almost exclusively controlled by solids loading. pH was solely dependent on ammonia content. The ANOVA indicates that solids content plays a role in pH, but this is clearly discounted by the lack

* NTC is procurring pressure casting equipment from Dorst and Netzsch for potential use in the 1989 program year.

Table 30
L16 Casting Development Experiment - Level Average Results

Factors/Levels	pH	Viscosity (cps)	Specific Gravity (g/cc)	Green Density (g/cc)	Casting Time (min)	Out of Mold Shrinkage (%)
Mold Coatings						
Level 1	-	-	-	2.04	130	0.945
Level 2	-	-	-	2.04	113	0.922
Level 3	-	-	-	2.11	197	1.025
Level 4	-	-	-	2.09	142	0.912
Dispersant Concentration						
Level 1	10.11	21.75	1.92	2.08	145	0.938
Level 2	10.12	21.25	1.93	2.08	137	0.935
Level 3	10.20	21.00	1.93	2.06	151	0.958
Level 4	10.20	23.00	1.94	2.06	149	0.975
NH_4OH Concentration						
Level 1	9.92	20.50	1.92	2.07	157	1.080
Level 2	10.16	20.75	1.93	2.06	148	0.945
Level 3	10.28	24.25	1.95	2.08	148	0.885
Level 4	10.29	21.50	1.92	2.06	129	0.895
Solids Loading						
Level 1	10.01	20.25	1.91	2.06	123	1.003
Level 2	10.28	19.00	1.92	2.06	123	1.003
Level 3	10.10	22.75	1.93	2.08	173	0.930
Level 4	10.25	25.00	1.97	2.07	128	0.910
Mold Age						
1 Use	-	-	-	2.05	140	0.910
2 Uses	-	-	-	2.07	129	0.988
3 Uses	-	-	-	2.08	148	0.948
4 Uses	-	-	-	2.06	165	0.960

of any trend in the level average data of Table 30.

Green density and casting time were affected most by the mold coatings. In general, the highest green densities were achieved at longer casting times. Out-of-mold shrinkage was principally controlled by the ammonia content. This observation is considered important in decreasing drying stresses and eliminating cracking. Pour lines are minimized by the use of mold coatings along with lower solids content slips as the ANOVA indicates. Surface porosity, surface finish, cracking and mold release were all influenced by factors beyond the range of the experiment as shown by the high error terms of the ANOVA. Surface porosity is

usually caused by air bubbles in the slip that attach themselves to the mold surface during filling. The remaining response variables may be associated with handling and part removal procedures. Future designs will utilize other treatment factors that may affect these response variables.

Concurrent with the completion of this casting experiment, masters and plaster casting molds were developed for the preparation of AGT101 rotor hubs. Using casting parameters from the L16 design, approximately 15 rotor hubs were successfully cast. Six were used for characterization of the green state in fulfillment of the first rotor milestone. Hubs were degassed to give them added green strength, then each rotor hub was visually examined. Surface defects were observed and recorded. Each of the green hubs was subsequently sliced into nine sections--each of 12.7 mm thickness. Each section was characterized using microfocus x-ray radiography. Finally, all hubs sections were cored and measured for density using wax coatings and water immersion methods. A green density profile was determined for each hub.

Table 31
Green Density Values Obtained On Slip-Cast
AGT101 Rotor Hubs

Rotor Hub I.D.	Average Green Density (g/cc)	No. of Pieces Tested
154A	1.962 ± 0.016	49
154B	1.969 ± 0.012	51
155A	1.967 ± 0.016	49
155B	1.970 ± 0.017	46
156A	1.981 ± 0.016	52
156B	1.970 ± 0.006	51
Overall	1.970 ± 0.017	298
Six Individual Hubs	1.970 ± 0.006	6

Shown in Table 31 are average green density values for the six sectioned rotor hubs. These data are compiled from individual sectioned rotors as depicted in Figure 117. For individual ring segments cut from each of the rotor hubs, the average observed density variation within or between rotors was $\leq$ 0.085 g/cc. A slight density gradient was observed with increasing distance from the gate. These variations are well within the evaluation criterion for the ATTAP Rotor Milestone No. 1. Based on these data, linear shrinkage differences between components, or within a component should be less than 0.54 %.

The most common observed surface flaws on rotors were shallow surface pits along the mold seams caused by either a mold defect or flash removal. Minor surface porosity was also apparent resulting from bubble attachment to the mold during the filling operation. A summary of external defects by visual inspection for the six rotor hubs is presented in Table 32. For a corresponding view of

Figure 117
Average Green Density Distribution For Six AGT101 Rotor Hubs

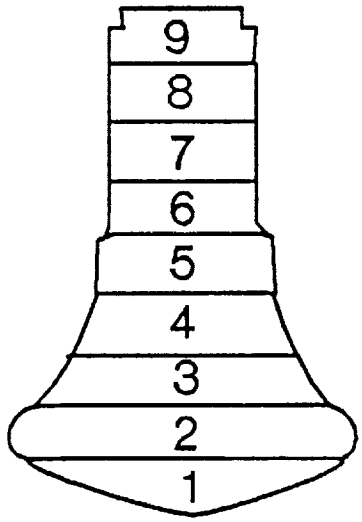

Ring No.	Average Green Density (g/cc)	No. of of Pieces Measured
9	1.954 ± 0.018	24
8	1.961 ± 0.015	24
7	1.965 ± 0.009	24
6	1.972 ± 0.013	24
5	1.970 ± 0.017	24
4	1.978 ± 0.017	25
3	1.973 ± 0.016	45
2	1.977 ± 0.014	66
1	1.964 ± 0.017	42

the location of these defects as well as a summary of observed defects for each rotor hub, refer to Figure 118. Few subsurface defects were detected by microfocus radiography. The most prominent feature was the presence of diffuse density gradients in the main hub body. These regions were observed to be typically ~3 mm to ~6 mm long by up to 1 mm wide. They extended along the axis of the hub parallel to the casting direction. This type of feature is thought to be caused by local slip inhomogeneities present during casting. While this feature may have a slight effect on shrinkage, it is not expected to affect strength.

Several additional hubs were HIPed, sectioned, and measured for physical and mechanical properties. In confirmation of the uniform green density, shrinkage for densified hubs was 14.59 ± 0.79%, (4 Hubs, 28 data points). The small standard deviation for shrinkage should aid in achieving dimensional control on bladed rotors. Flexural test-bars were cut from one rotor hub at two locations--the shaft and main body. Strengths were acquired for these components and compared to test-tile from the same casting batch and HIP run. These data are presented in Table 33.

Within statistical error, density and strength values for samples taken from various locations within the shaft and hub are equal. Density measurements obtained from the control tile show slight differences, but only at the third decimal place. These density and strength results conform to the program specifications. However, the strength values were lower than expected. Fracture analysis on the bars from either the hub or control tile showed iron as an impurity at many fracture origins. The source of the iron has been identified as an impurity in an additive used in the casting batch. Several sources for this additive were located and matched-pair tests conducted to assess improvements in properties. The results of these tests are shown in Table 34.

All rotor hubs were originally cast using the "A" concentration from "Vendor No. 2".

Table 32
Summary of External Defects Identified By Visual Inspection On Six Green AGT101 Rotor Hubs

Defect No.	Defect Description
1	Chips along top mold seam due to excessive flash sticking to the mold. This type of defect can be eliminated by removing the step and radiusing the top edge.
2	Small chips on second rim introduced during post cast handling.
3	Shallow surface defects along mold seam. Defects are estimated to be 0.051 - 0.239 mm deep. Defects can be eliminated by using tighter molds and more careful removal of the flash. The (a-c) denote locations for the defect--shaft, bevel step, or main hub body.
4	Handling defects consisting of shallow chips or pits. This type of defect can be eliminated with the use of better procedures. The (a-c) denote specific locations for the defect.
5	Region of general surface roughness. This appears to be a product of the mold. Estimated depth to be 0.051 - 0.229 mm.
6	Incomplete flash removal. Barely visible.
7	Shallow defects at the intersection of mold seams. Estimated depth of defects is 0.051 - 0.254 mm.
8	Incomplete removal of gate knob.
9	Small chip due to breaking off the gate knob. This type of defect can be eliminated by preventing casting into the gate.
10	Shallow defects along the mold seam. Estimated depth of defects is 0.051 - 0.229 mm.
11	Surface pore due to attached bubble during mold filling. This type of defect can be eliminated by more careful bleeding of slip lines and better control over the mold fill rate. The (a-c) denote specific locations of observed porosity.

Table 33
Physical and Mechanical Properties of An AGT101 Rotor Hub

Location of Test Bars	Density (g/cc)	Room Temperature MOR (MPa)	Room Temperature MOR (Ksi)
Hub Shaft	3.232 ± 0.001	747 ± 26	108 ± 4
Hub Body	3.231 ± 0.002	715 ± 76	104 ± 11
Control Tile	3.235 ± 0.001	727 ± 40	106 ± 6

Data is reported for 10 samples each from the Hub Shaft and Body; and 15 samples for the Control Tile.

Figure 118
External Defects Identified By Visual Inspection
For Six AGT101 Rotor Hubs

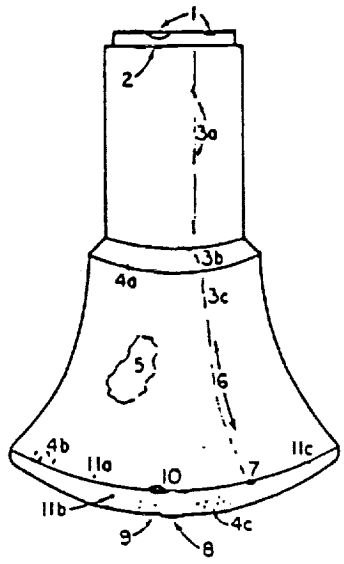

Rotor Hub No.	External Defects (Refer to Drawing & Table VII)
154A	1, 3c, 9, 10, 11b.
154B	1, 6, 7, 8.
155A	1, 3a, 5, 10, 11a.
155B	1, 3a, 3c, 4b, 4c, 6, 10.
156A	1, 2, 3a, 3b, 3c, 4c, 7, 10.
156B	1, 3a, 3b, 3c, 4a, 9, 10, 11c.

Table 34
Mechanical Properties of NT154 Cast Tile Using
Selected Casting Additives

Source and % of Additive	Room Temperature MOR (MPa)	Room Temperature MOR (Ksi)	1370°C MOR (MPa)	1370°C MOR (Ksi)
Vendor No. 1				
% A	903 ± 125	131 ± 18	524 ± 14	76 ± 2
Vendor No. 2				
% A	727 ± 40	106 ± 4	455 ± 8	66 ± 1
% B	680 ± 62	99 ± 9	578 ± 10	83 ± 1
% C (Cleaned)	828 ± 36	120 ± 5	581 ± 2	84 ± 0

RT strengths were compiled from between 7 and 15 samples for each condition.
HT strengths were compiled from between 2 and 5 samples for each condition.

The results of Table 34 suggest that substitution of a similar additive from "Vendor No. 1" should eliminate this problem. Alternatively, methods of removing the iron impurity from "Vendor No. 2" material were pursued. Preliminary data shown in Table 34 (for Vendor 2, Concentration "%C") show that cleaning of the additive improves strength. Part of the efforts within the second-year of the ATTAP is directed at further investigating solutions to this impurity-strength problem.

CIP PROCESSING - All activities in this area have been performed in conjunction with either Casting or Injection Molding. CIP processing is being used as a baseline comparison technique to the two component forming processes.

INJECTION MOLDING DEVELOPMENT - Injection molding was selected as the stator fabrication process. This forming method is applicable to intricately shaped components of thin cross-section. For parts similar to that of the stator (i.e., $\leq$ 8 mm thickness), binder removal is a less serious problem. As with the casting process, designed experiments were used to develop this forming technique. Two iterative Taguchi experiments were planned and conducted. An L8 experiment was initially designed as a screening experiment to broadly determine important variables in molding and binder removal. Injection molded tile (~50 x ~50 x ~6 mm) were used as the test component. This experiment was followed with an L4 x L9 design which correlated binder formulation, solids concentration and binder removal parameters with a range of molding conditions. The latter experiment was conducted using actual stator components. Collectively, these experiments were designed to address many of the critical features of the injection molding process. Of the two experiments, the first was completed during 1988. The second has been completed through HIP densification.

The original L8 injection molding experiment was simplified, by default, to an L4 array when one of the selected binder removal conditions produced predominantly bloated or cracked tile. Because of this, the balance of the

experiment was run comparing injection molding pressure and binder removal conditions as the factors--each at two levels. The interaction of these factors was also considered within the revised experiment. Due to limitations in existing tooling, work for this experiment was performed on the 150 ton injection molder. It was found that part weight varied with both the order of molding, and with machine settings. This is graphically presented in Figure 119. At constant machine settings, considerable "drift" was observed for both the low and high pressure conditions of the experiment. These results suggest that better machine controls are required.* Despite these observed weight changes, green density variation of the molded tile was minimal. Depicted in Figure 11 are part-to-part density values for both the low and high pressure molding conditions. Larger "noise" levels were observed at the higher molding pressure. At the low molding pressure condition, a larger number of void defects (low density inclusions) were observed by microfocus x-ray radiography. The density variability may therefore be attributed to the relative amounts of these types of defects present at the two pressures. The higher molding pressure reduced void defects by approximately 50%. Nevertheless, all variability was within the ATTAP evaluation criteria for this process.

Figure 119
Green Weight of Injection Molded Tile As A Function Of
Molding Pressure And Production Sequence

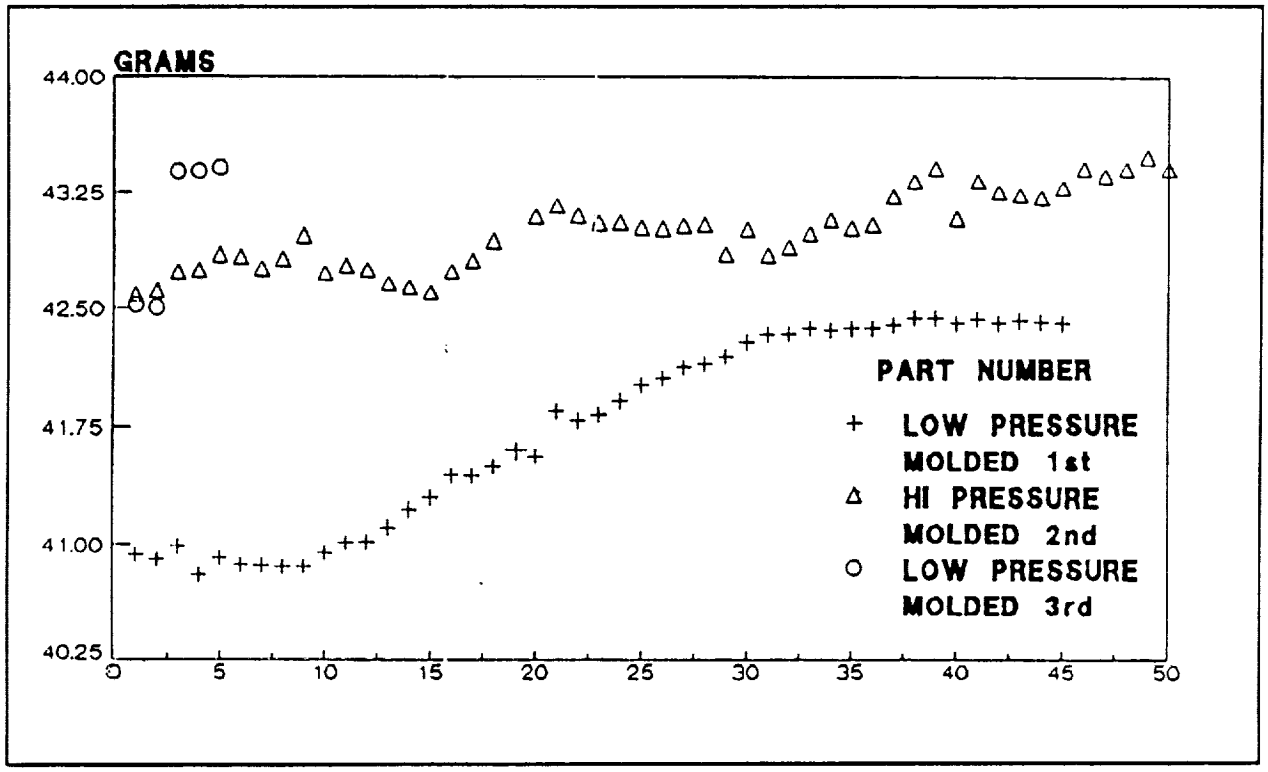

* To eliminate this problem, molding studies for the L4 x L9 array were performed on the smaller 30 ton machine.

Figure 120
Green Density of Injection Molded NT154 Tile As A Function Of Molding Cycle and Injection Pressure

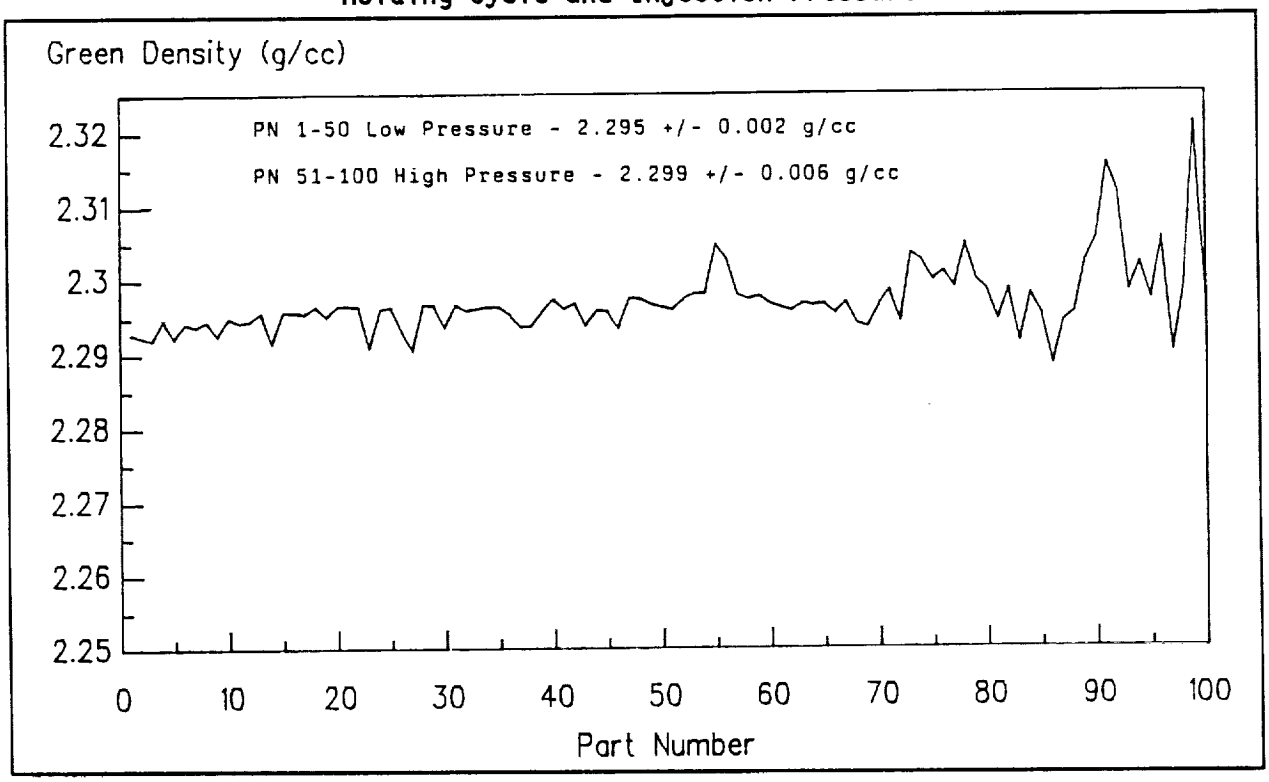

Mechanical property data were acquired for the L8 trials and are presented in Table 35. These results represent the first mechanical property values obtained using injection molded NT154 components. While these data meet program specifications, they are lower than CIP processed material. ANOVA of the simplified L4 array showed large error variances suggesting that factors outside

Table 35
L8 Injection Molding Experiment - Summary of Mechanical Property Results

Molding Pressure And Binder Removal Conditions	Room Temperature Flexural Strength (MPa)	(Ksi)	1370°C Flexural Strength (MPa)	(Ksi)
Low, Condition 1	877 ± 161	127 ± 23	575 ± 36	83 ± 5
Low, Condition 2	743 ± 223	108 ± 32	591*	86*
High, Condition 1	728 ± 123	106 ± 18	562 ± 122	82 ± 18
High, Condition 2	735 ± 168	107 ± 24	529 ± 49	77 ± 7

* Single data point. All remaining data compiled from between 3 and 15 samples for each condition.

of the experiment were controlling. The lower strength values, and large error variances were found to be attributed to impurity inclusions introduced by the binder raw material. These inclusions were observed by microfocus x-ray film radiography. Concurrently, filtration of the binder raw materials was initiated as a method for removing the contaminant. Presented in Figure 121 are histogram plots of these defects both before and after filtration.* These graphs are normalized to approximately 1000 cc of material. Before filtration, the incidence of defects was assessed at ~0.09 defects/cc. Subsequent to filtration, the level was cut to ~0.05 defects/cc. The coarse tail of the distribution was also eliminated by filtration. While filtration has aided in drastically reducing the number and size of defects, further improvements are necessary. Reduction of observable defects to levels equivalent to CIP or casting operations appears to be required. Planned activities for the 1989 program year address these issues. Cleaned or alternative additives will be used, along with an investigation of other potential contamination sources.

The L4 x L9 injection molding experiment has been completed through the densification step. Over 1620 stators were molded, from which 540 were HIPed. Test tile were also prepared at each of the experimental conditions. This "linked" experiment was set up to examine the following factors: (1) Binder

Figure 121
Inclusion Size Distribution In Injection Molded NT154 Tile

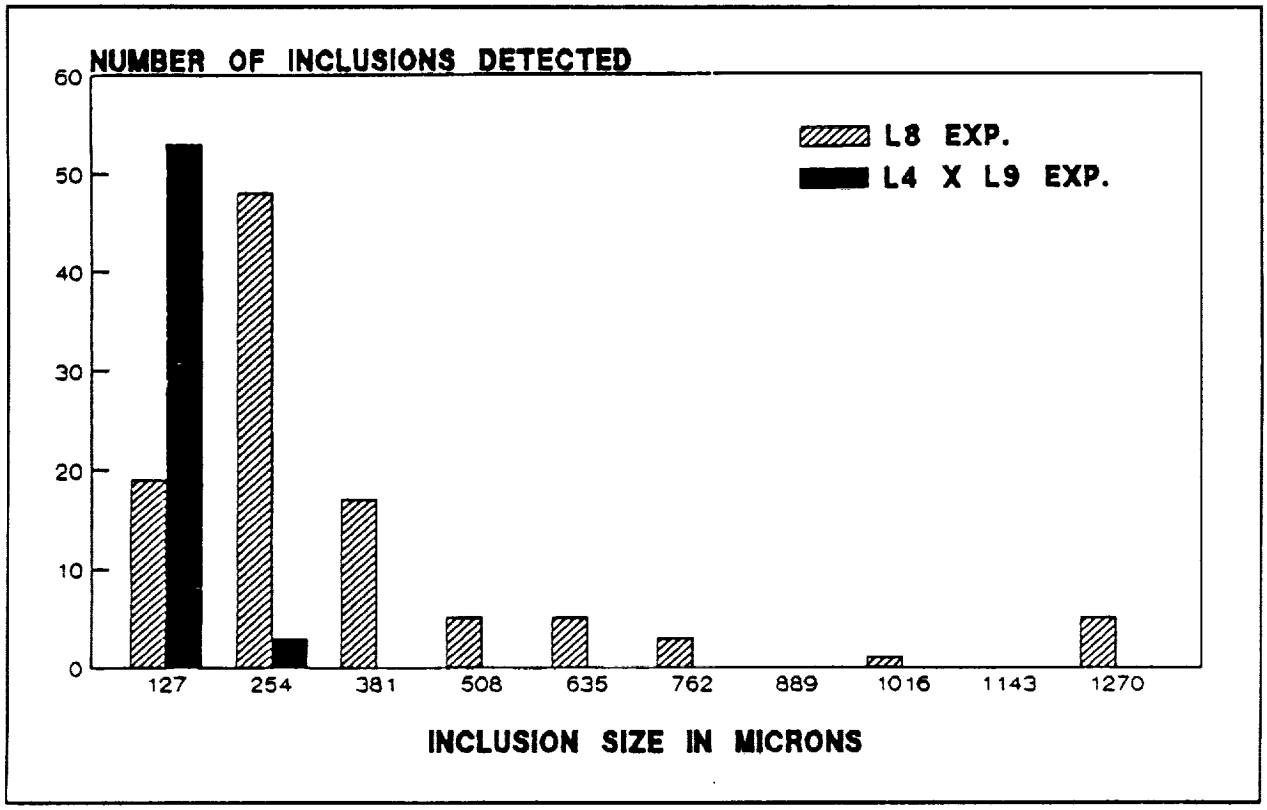

* Filtration was utilized in preparing mix batches for the L4 x L9 experiment.

Formulation; (2) Solids Concentration; (3) Injection Pressure; (4) Injection Rate; and (5) Injection Hold Pressure. Interactions between several of these independent variables were also designed into the experiment. Only a limited amount of data has been acquired to date. Preliminary results indicate that use of the 30 ton machine significantly improved part-weight control and green density. This control feature is shown in Figure 122. Presented in this graph are the four mixes of the L4 array at three different molding pressures. Unlike the L8 design discussed earlier, minimal changes in average weight are noted. However, higher variability was observed with Mix Nos. 3 and 4. Density variations for the entire 540 stators averaged less than 0.002 g/cc at all experimental conditions. Completion of this experiment and final data analysis is expected to occur in the first quarter of 1989.

Several small exploratory experiments were also conducted on a water-based injection molding formulation using improvements on existing technology.[7] Water-based processing has the potential advantage of reducing the amount of organic additives needed for good molding. Two AGT100 rotor hubs were formed using this technology. After forming, these components were allowed to air dry for up to 7 days. One of the components cracked during drying. The surviving part was successfully dried, degassed and HIPed without cracking. The part achieved a density of 3.21 g/cc. This screening test indicates that the process has potential as a simplified forming technique for complex-shaped, large cross-

Figure 122
Green Weight of Stator Components Versus Injection Pressure For The L4 Injection Molding Experiment

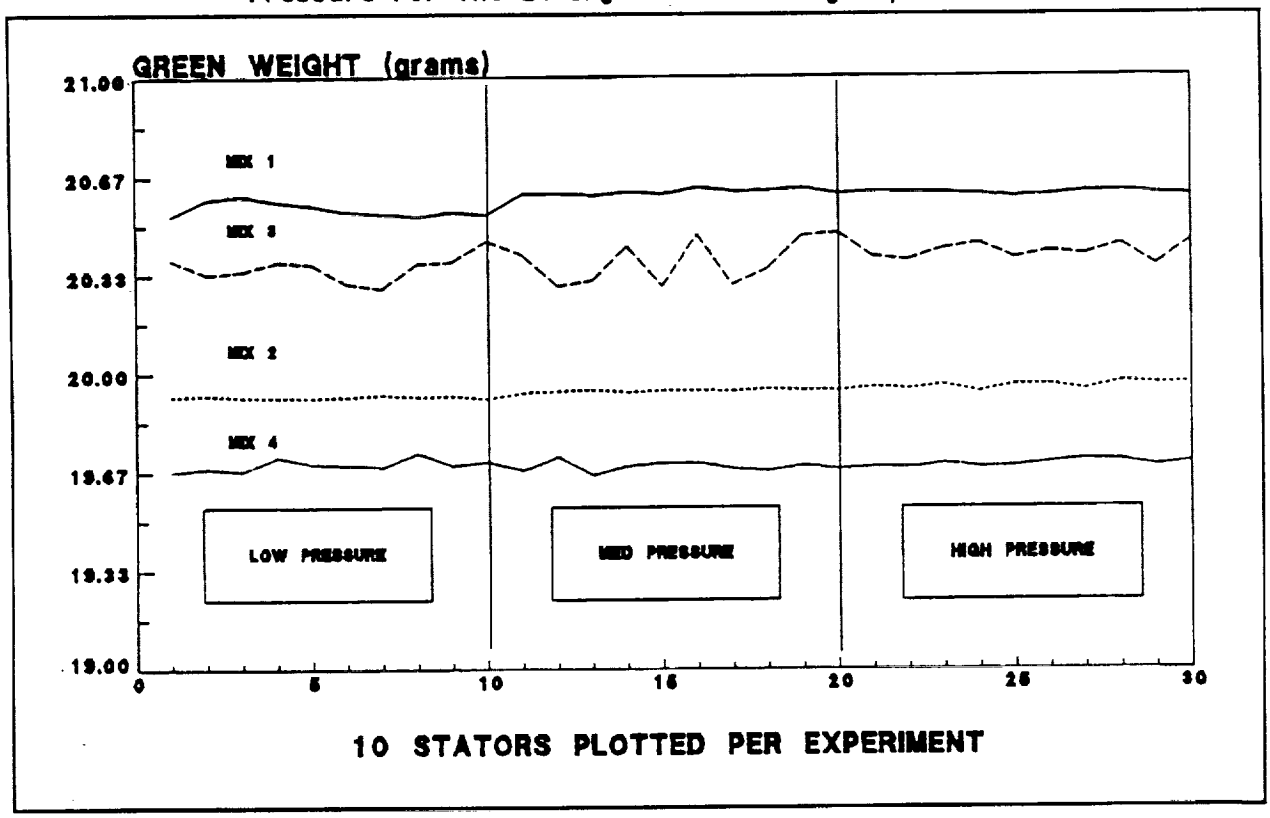

section components. Additional screening experiments, scheduled for the 1989 program year, will address batch formulation, mix rheology, and molding conditions. This effort is being pursued as a back-up process to the plastic-based injection-molding methods currently employed for the stator. However, it has potential applicability to the rotor as well.

DEGAS HEAT-TREATMENTS - This process step is being investigated to determine the effects of various degas schedules and/or atmosphere on final product properties. The degas operation is used to remove water and carbonaceous

Table 36
ANOVA For Degas Heat Treatment L9 Experiment
(% Contribution)

Forming Method And Treatment Factors	% Weight Loss	Tile Density	Test-Bar Density	22°C MOR	1370°C MOR
I. CIP PROCESS					
Temperature	46	50	9	29	74
Time	15	12	42	2	13
Temperature x Time	10	4	46	52	0
Atmosphere	0	0	0	13	0
Error	29	34	3	4	13
II. CASTING PROCESS					
Temperature	42	32	82	22	26
Time	11	20	6	60	42
Temperature x Time	16	11	0	9	15
Atmosphere	0	0	0	0	0
Error	31	37	2	9	17
III. INJECTION MOLDING					
Temperature	54	48	21	36	5
Time	29	12	26	5	35
Temperature x Time	0	5	44	8	24
Atmosphere	0	0	0	0	0
Error	17	35	9	51	36
IV. ALL FORMING METHODS					
Temperature	21	21	9	0	8
Time	9	6	3	1	7
Temperature x Time	4	3	3	1	0
Atmosphere	0	0	0	3	0
Forming Method	58	29	50	48	47
Temperature x Forming Method	0	9	3	16	11
Time x Forming Method	0	0	12	9	10
Atmosphere x Forming Method	0	0	0	0	0
Error	8	32	20	22	9

material from the body in preparation for HIP densification. In the Work Plan, an L9 experiment was designed. This experiment correlated time, temperature, atmosphere and forming method with physical and mechanical properties. The experiment has been completed and data analyzed using Taguchi ANOVA techniques. The ANOVA for this experiment is presented in Table 36. From this analysis, temperature or the interaction of time and temperature were found to be the critical controlling parameters. Atmosphere was of little or no significance. The analysis also suggests marked differences between the degassing behavior of components formed by the various processes.

Level average results for the experiment are presented in Table 37 and Table 38. Density and strength values are given. The differences between tile density and test-bar density is due to the presence of a reaction layer which forms on the components during HIP densification. Excellent high-temperature strengths were obtained for selected conditions. Individual values in excess of 700 MPa (102 Ksi) were observed for some slip-cast and CIP samples. A response surface plot of the interaction of temperature and time on 1370°C strength is presented in Figure 123.

No physical or mechanical property differences were observed for the cast and CIP material used in this experiment. However, injection molded material was significantly different. The difference is attributed to contaminants introduced with the binder raw materials as discussed earlier.

Table 37
ANOVA For Degas Heat Treatment L9 Experiment
Level Averages - Combined Data From All Forming Processes

Treatment Factors and Levels	Tile Density (g/cc)	Test-Bar Density (g/cc)	22°C MOR (MPa)	1370°C MOR (MPa)
I. ALL FORMING PROCESSES				
A. Temperature				
Level 1	3.226	3.233	840	561
Level 2	3.223	3.234	836	568
Level 3	3.211	3.236	826	597
B. Time				
Level 1	3.224	3.234	840	560
Level 2	3.222	3.235	840	573
Level 3	3.214	3.235	821	594
C. Atmosphere				
Level 1	3.219	3.235	825	578
Level 2	3.223	3.234	850	570
D. Forming Method				
CIP	3.225	3.236	857	609
Cast	3.226	3.237	876	592
Injection Molding	3.209	3.230	768	525

Table 38
ANOVA For Degas Heat-Treatment L9 Experiment
Level Averages

Treatment Factors & Levels	Tile Density (g/cc)	Test-Bar Density (g/cc)	22°C MOR (MPa)	1370°C MOR (MPa)
I. CIP PROCESS				
A. Temperature				
Level 1	3.229	3.235	861	567
Level 2	3.226	3.235	825	611
Level 3	3.220	3.237	886	651
B. Time				
Level 1	3.227	3.235	867	598
Level 2	3.226	3.234	856	598
Level 3	3.222	3.238	847	632
C. Atmosphere				
Level 1	3.224	3.236	845	607
Level 2	3.226	3.236	881	613
II. CASTING PROCESS				
A. Temperature				
Level 1	3.228	3.235	907	572
Level 2	3.227	3.238	863	582
Level 3	3.222	3.239	858	621
B. Time				
Level 1	3.227	3.237	863	585
Level 2	3.227	3.237	923	563
Level 3	3.223	3.238	842	626
C. Atmosphere				
Level 1	3.225	3.237	872	596
Level 2	3.227	3.237	885	583
III. INJECTION MOLDING				
A. Temperature				
Level 1	3.221	3.229	752	543
Level 2	3.213	3.229	819	512
Level 3	3.191	3.233	733	521
B. Time				
Level 1	3.217	3.229	790	496
Level 2	3.213	3.233	741	556
Level 3	3.198	3.229	773	523
C. Atmosphere				
Level 1	3.207	3.231	760	530
Level 2	3.214	3.230	784	515

Figure 123
1370°C Flexural Strength Response Surface Plot For The
L9 Degas Experiment

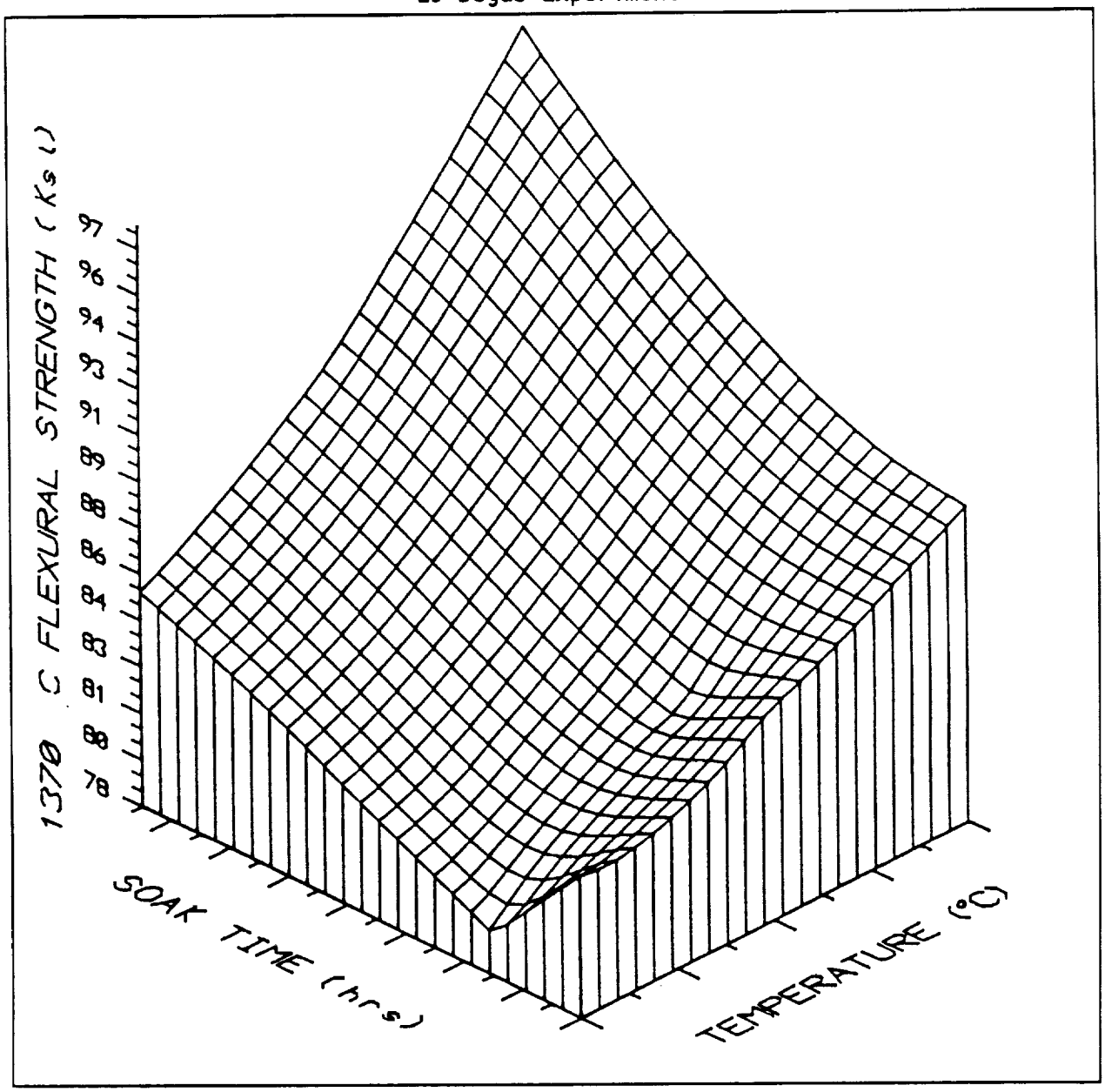

Additional evaluation of samples from this experiment will continue in 1989. The characterization of high-temperature stress-rupture and fatigue failure for the various treatment conditions of the experiment will be assessed. Future multilevel experiments are planned to fine-tune the appropriate process conditions for this operation.

HIP DEVELOPMENT - Optimization of this process step is being conducted as

part of a linked experiment with powder beneficiation. An L9 x L4 experiment was designed for this purpose as described earlier in this report. The experiment correlates powder beneficiation conditions with HIP densification. HIP factors include time, temperature and cooling rate. Tile components from this experiment have been formed, HIPed, and are being ground into test-bars for an assessment of physical and mechanical properties.

COMPONENT INTEGRITY DEVELOPMENT - Activities in this area are directed at investigating issues surrounding surface and bulk material properties. Two Taguchi experiments were planned. The goal of these experiments is to find appropriate processing conditions which ensure commonality of bulk and surface properties. The first experiment, an L4 array, was completed. The second, an L16 design, was initiated during 1988 and is planned to be completed in 1989.

The L4 Component Integrity experiment was designed as a screening test to examine the effects of a post-HIP high-pressure heat-treatment on the mechanical properties of "as-HIPed" and "bulk" ground test-bars. Factors included temperature, pressure and cooling schedule. The ANOVA for this experiment is presented in Table 39. Level average data are shown in Table 40.

The ANOVA suggests that temperature and surface condition were the dominant factors affecting mechanical strength. However, reductions in both room-temperature and 1370°C strengths were observed for all conditions studied. In general, strengths of less than ~724 MPa (105 Ksi) were obtained. An average value at room temperature of 841 MPa (122 Ksi) was observed for one of the L4 trials. However, no condition appeared to improve component properties above baseline data. The lower strength values obtained for the various heat-treatment conditions are believed to result from decomposition of the sample surface. Most samples showed a higher incidence of porosity following the applied treatments. While the general results of this experiment are negative, they provided insight into important factors and levels for the second Taguchi experiment in this series.

Table 39
ANOVA For The L4 Component Integrity Experiment
% Contribution of Individual Factors

Treatment Factor	Room Temperature Flexural Strength	1370°C Flexural Strength
1. HIP Temperature	58.73	12.23
2. HIP Pressure	14.32	7.30
3. Cooling Schedule	-	-
4. Surface Condition	-	33.87
5. Cooling Schedule x Surface Condition Interaction	-	27.75
6. Experimental Error	26.95	18.85

Table 40
Level Average Mechanical Property Results For the L4
Component Integrity Experiment

Treatment Factors And Levels	Room Temperature Flexural Strength (MPa)	(Ksi)	1370°C Flexural Strength (MPa)	(Ksi)
1. HIP Temperature				
- Level 1	790	115	440	64
- Level 2	604	88	-	-
2. HIP Pressure				
- Level 1	746	108	396	57
- Level 2	648	94	435	63
3. Cooling Schedule				
- Level 1	701	102	423	61
- Level 2	693	101	408	59
4. Surface Condition				
- Bulk Test Bars	751	109	529	77
- "As-HIPed" Test Bars	-	-	456	66

The L16 Component Integrity experiment of the Work Plan was initiated during 1988. This experiment was designed to examine various crystallization heat-treatment schedules at atmospheric pressure. Samples were processed through HIP densification, and are currently being ground into test-bars.

PROCESS ENGINEERING

This task was original comprised of two subtasks: (1) Experiment Design; and (2) Component Reliability Plan. Submission of the detailed Work Plan in July 1988 fulfilled the first-year requirements for these two subtasks. Annual updates to the Work Plan will be conducted to complete future requirements.

NDE

NTC is developing NDE techniques primarily using microfocus x-ray radiography. Work during 1988 involved activities in three areas: (1) Development of Standards; (2) Preparation and Characterization of Seeded Defect Tile; and (3) Component Inspection Development.

STANDARDS DEVELOPMENT - Utilization of microfocus x-ray radiography for both process development and on-line inspection has made it necessary to develop standards for periodic qualification of this inspection system. Standards for qualifying the microfocus x-ray radiography equipment are being developed to address: (1) Verification of spatial resolution; (2) Confirmation of x-ray exposure using film characteristic curves; and (3) Verification of defect detectability limits. These qualification standards will be used to quantify and verify the day-to-day reliability of the microfocus inspection system.

Verification of spatial resolution will be accomplished by performing a periodic measurement of the machine's focal spot size using a spot size measurement target.* Film characteristic curves and defect detectability limits will be addressed periodically using a series of seeded defect step wedges. Fabrication of these step wedges will occur in 1989 following completion of seeded defect studies.

SEEDED DEFECT TILE - All of the seeded defect tile identified under the ATTAP Work Plan have been fabricated. Three types of defects were chosen: (1) Iron inclusions; (2) Voids or porosity; and (3) Si_3N_4 agglomerates. Seed sizes ranged from 29 to 180 microns for the Iron inclusions; 98 to 464 microns for voids; and 66 to 315 microns for Si_3N_4 agglomerates. A volumetric seeding technique using pressure casting was developed for the fabrication of these specimens. Known seed quantities were added directly to flocced Si_3N_4 slips. Flocced slips were used to prevent seed settling during casting. Tile were formed by pressure casting at a nominal pressure of 60 psi. The work was subdivided into two test matrices. The first matrix involved screening tests to verify the volumetric seeding technique and confirm the selected range of seed sizes. The second matrix is being used to quantify detectability limits.

A total of 18 tile from the first test matrix were fabricated and characterized by film microfocus x-ray radiography in the green state. Qualitative results of these film exposures are summarized in Table 41. Seeds from the large seed size classification for all three seed types were readily detected. Visual examination of the x-ray films for these tile confirmed the presence of uniformly dispersed individual seed particles. Regardless of seed type, indications were not detected in any of the small seed size classifications. Conclusions to-date from Test Matrix One include: (1) Volumetric seeding by casting flocced slips is a viable technique; and (2) The range of seed size and tile designs successfully bracketed the detectability limits of the three defect types under study.

For the second test matrix, a total of thirty-six tile have been prepared. Twenty-four tile, (12 green and 12 dense) were prepared at seed concentrations of 100 seeds per tile. These tile will be used as x-ray characterization components to assess detectability limits. The remaining twelve tile were prepared at a concentration of 500 seeds per tile. They will be used for destructive analysis. Completion of the x-ray characterization studies is slated for 1989. However, preliminary visual examination of x-ray films for green tile seeded with intermediate size Fe-Al spheres indicates that the probability of detection starts to fall off at a thickness sensitivity of approximately 0.5 percent.

COMPONENT INSPECTION DEVELOPMENT - Film microfocus x-ray radiography has been successfully employed as a process development tool in identifying sources of high density inclusions in injection molding mixes. The iteration involving filtration of the injection molding binder described earlier in the report confirms the value of microfocus x-ray radiography in identifying coarse processing defects. As processing improves, with a concurrent reduction in

---

* Feinfocus U.S.A.

Table 41
Seeded Defect Tile Study - Summary of Microfocus X-Ray Shots On Green TM-1 Tile

Nominal Seed Type	Seed Size (Microns)	Number of Seeds/Tile	Green Thick. (mm)	Thick. Sens-itivity (%)	Magnifi-cation	Seeds Detected?
Pores	97.6	10	13.00	-0.81	2X	No
		100	12.75	-0.81	2X	No
		500	12.87	-0.81	2X	No
Pores	464	10	12.18	-3.90	2X	Yes
		100	12.09	-3.90	2X	Yes
		500	11.28	-3.90	2X	Yes
Fe-Al Spheres	28.9	10	12.39	-0.24	2X	No
		100	13.77	-0.24	2X	No
		500	11.98	-0.24	2X	No
Fe-Al Spheres	180.2	10	12.86	-1.50	2X	Yes
		100	13.36	-1.50	2X	Yes
		500	12.60	-1.50	2X	Yes
Si_3N_4 Agglomerates	66.1	10	14.14	-0.55	2X	No
		100	12.90	-0.55	2X	No
		500	9.10	-0.55	4X	No
Si_3N_4 Agglomerates	315.2	10	8.92	-2.60	2X	Yes
		100	11.79	-2.60	2X	Yes
		500	12.40	-2.60	2X	Yes

defect size, the value of the equipment will be directly related to its ability to detect smaller strength limiting flaws.

As a follow-up to the initial seeded defect tile study, seeded defect stators were fabricated for use in developing a microfocus x-ray inspection protocol for this component. Rotor hubs, possessing seeded defects, are also slated to be prepared during 1989. Inspection protocols for both components are to be developed as part of the ATTAP.

QUALITY ASSURANCE

Progress in developing a quality plan for the ATTAP rotor and stator has involved defining the scope of the ATTAP Quality Assurance Program, (QAP). An outline for the QAP is shown in Table 42, and identifies (1) Quality philosophy; (2) Quality directives; (3) Quality system elements; and (4) Component-specific inspection plans, as key components. This QAP format is wider in scope than a conventional quality manual in that it includes project-specific

Table 42
ATTAP Quality Assurance Program Plan (QAP)
Outline

I. Quality Philosophy
    A. Vision
    B. Policy

II. Quality Directives
    A. Quality Objectives
        1) Organizational
        2) Project-specific
    B. Guidelines
    C. Methodology

III. Quality System Elements
    A. Documentation
    B. Controls
        1) Procurement
        2) In-Process
        3) Completed-Item (Includes Inspection and Test)
    C. Equipment Calibration
    D. Customer Service/Contract Administration
    E. Field Performance Analysis/Corrective Action

IV. Component-Specific Inspection Plans
    A. ATTAP Rotor
    B. ATTAP Stator

quality objectives and component-specific inspection plans. Under quality philosophy, a clear, measurable vision of quality will be defined, as well as an overall quality policy. Quality directives will identify organizational and project-specific quality objectives, guidelines for meeting these objectives and methodologies for attaining quality goals. Quality system elements establish the scope of the formal quality assurance system, and define task-specific policies and directives. Manufacturing and Inspection plans for the ATTAP rotor and stator will specify fabrication operations and inspection techniques for each process step. Approximately 225 documents have been identified for written implementation. They cover a breadth of activities from the specification of raw material lots and powder processing conditions for batch qualification requirements, to in-process specifications for component production. Implementation of this program will be a continuing effort during the course of the ATTAP. Activities in this area will comprise a major effort during 1989.

DELIVERABLES

All scheduled milestones associated with deliverables were achieved during the contract period. These included: (1) The delivery of 60 test-bars to GAPD in February 1988 for Material Assessment and Qualification. Numerous additional

test specimens have been supplied to other material evaluation programs;* (2) The fabrication of NDE specimens in compliance with Milestone 1 of NDE Evaluation Criteria; (3) The fabrication and characterization of 6 rotor hubs in compliance with Milestone 1 of the Rotor Evaluation Criteria; and (4) The fabrication and characterization of > 5 stators in compliance with Milestone 1 of the Rotor Evaluation Criteria.

PROJECT MANAGEMENT

NTC submitted a detailed Work Plan and several submissions of cost-support information as requested by GAPD. Monthly reports and other technical information has been supplied per GAPD's schedule or upon specific request.

D. N. Heichel presented a paper entitled, "Slip Casting Development for Si_3N_4 Ceramics," at the 90th Annual Meeting of the American Ceramic Society held in Cincinnati, Ohio, May 1-5, 1988. B. J. McEntire and E. Bright attended the 26th DOE Contractor's Coordination Meeting in Dearborn, MI on October 24-27, 1988. B. J. McEntire presented a review of this program during the meeting, entitled "ATTAP Ceramic Component Development Using Taguchi Methods." A. P. Taglialavore presented a paper entitled, "Development of Si_3N_4 For Gas Turbine Applications" at the 3rd International Conference on Ceramics For Heat Engines held in Las Vegas, Nevada, Nov. 28-30, 1988.

SUMMARY AND CONCLUSIONS

Norton/TRW Ceramics has successfully completed the first-year's effort of the ATTAP program. Process and component development work was initiated for the AGT101 rotor and stator. Casting and injection molding were respectively selected as the preferred fabrication processes for these components. All first-year milestones and program goals were achieved. Significant accomplishments are summarized below.

- A Si_3N_4 material was developed and test-specimens were supplied to GAPD. The material was assessed and qualified for the ATTAP. Excellent strength characteristics at room and elevated temperatures were achieved along with adequate static stress rupture behavior. Further improvements in material properties are expected as a natural consequence of process development work within the program.

- Powder Benefication was initiated as a prerequisite to shape fabrication. Appropriate material and comminution conditions were investigated for their effects on forming and material properties. Ball-milling operations were preferred because of reliability, intensive mixing action, and broad particle size output. Powder blends, milling time, solids concentration, and other conditions were tentatively selected to provide a coarse material of a broad size distribution. Impurity pick-up was minimized through the use of high-

* Test specimens have been supplied to:
(1) Flexural and K_{IC} Bars to GAPD under the ETEC and NASA Durability Programs.
(2) Tensile Rods to Oak Ridge National Laboratories.
(3) Flexural Bars and Tensile Rods to The Univeristy of Dayton.

C-3

purity powders and media under clean-room conditions. Future experiments are directed at correlating preferred powder beneficiation conditions with HIP densification.

- Casting development was initiated for the rotor. Using a laboratory pressure casting apparatus and plaster molds, rotor hubs were successfully cast, densified and characterized. For green components, few internal and surface defects were observed. Excellent density and strength uniformity were achieved. An impurity contained within a casting additive was identified as the current strength limiting flaw. Green and dense component properties complied with ATTAP specifications. Future work is directed at eliminating impurities, developing enhanced manufacturing capabilities, and achieving dimensional stability for fully-bladed rotors.

- Injection molding is being developed for the stator. Experimental endeavors characterized binder formulation, molding parameters and binder removal conditions. Flexural strength was measured for test-bars and found to conform to ATTAP specifications. However, a particulate impurity from the binder was identified as the strength limiting defect. Filtration of the binder was therefore initiated, resulting in approximately a 50% reduction in the occurrence of this defect. Through a series of Taguchi experiments, over 1620 stators were formed. Of this number, 540 were carried through the densification step. Future work is directed at minimizing impurities, and achieving dimensional stability for this component.

- Various degas heat-treatments were investigated for their effect on physical and mechanical properties. Appropriate conditions were identified which maximize mechanical strength at both room and elevated temperatures. Trendline data suggests that 1370°C strengths in excess of 700 MPa (100 Ksi) are achievable through appropriate parameter selection. Additional work will be directed at identifying and/or setting other potentially important process factors in this operation.

- HIP development experiments were linked to the powder beneficiation process. Quantitative data for these experiments are still pending. Nevertheless, all components HIPed within the program have achieved density values $\geq$ 99.5% of theoretical. Future work is directed at solving problems associated with the formation of the reaction-layer that occurs during glass-encapsuated HIP densification.

- Two post-HIP Component Integrity experiments were planned. These experiments were designed to address the effects of surface condition and post-HIP heat-treatment parameters on the mechanical integrity of components. One of these experiments was completed. Unfortunately, all conditions selected within the design yielded unfavorable properties. Nevertheless, parameters from this experiment were utilized in finalizing the design of the second experiment of this series.

- Microfocus x-ray radiography is being developed as an NDE technique. A seeded defect component study was begun as a method for assessing detectability limits and developing inspection protocols. Microfocus x-ray film radiography was implemented for the inspection of green components. Using appropriate

film techniques, particulate impurities were identified as strength limiting defects for the injection molding process. Future work is directed at development of component specific inspection protocols.

- The basics of a quality assurance program were developed. A plan for implementation of this program was written. A comprehensive list of required documents was identified. Complete implementation is slated to coincide with the culmination of the process developmental work prior to delivery of the final components.

- All component milestones were achieved. Approximately 60 test-bars were supplied to GAPD for material assessment and qualification. Rotor hubs and stators were characterized for green density and defects. Material properties from dense components or test-tile were assessed and determined to meet the minimum ATTAP specifications. Seeded defect tile were fabricated and characterized in accordance with the milestone for this task.

Continued effort in each of the above areas is scheduled for the 1989 program year. Work will emphasize the elimination of impurity defects, address dimensional control issues, and selection of additional appropriate process parameters. Component development activities are on track for achieving all ATTAP goals and milestones.

ACKNOWLEDGEMENT

Work accomplished during the 1988 program year represents the combined efforts of a number of individuals. The following principal engineers are gratefully recognized for their key contributions: R. L. Yeckley--Materials Development, A. P. Taglialavore--Powder Beneficiation Degas and HIP Development, D. N. Heichel--Casting Development, J. W. Johnson--Injection Molding Development, and E. Bright--NDE and Quality Assurance. Additionally, G. P. Janulewicz, T. J. Sheridan, D. F. Moylan, J. M. Gulcius, G. C. Manoogian, B. J. McGeary, W. H. Hackett, and G. Watson are acknowledged and appreciated for detailed performance of the technical plan. Appreciation is expressed to G. A. Fryburg, P. K. Caneen, C. Brown, P. Oberhauser, L. F. Russell and K. Mitchell for their technical support and services in consultation, machining, experiment design and presentation graphics. The Characterization and Analysis Groups of Norton Company are acknowledged for their work in chemical analysis, x-ray diffraction, microfocus x-ray characterization, mechanical property testing, and electron microscopy. G. D. Roberts, R. T. Foy, C. K. Fekete, D. L. Sterner, and M. J. Sweeney are appreciated for accounting and secretarial services. Special thanks go to Drs. C. L. Quackenbush, S. D. Hartline and R. R. Wills who constructively reviewed program objectives, plans, and reports; and to C. M. Ford and F. P. Teta for government accounting and contract administration review and support. D. Kreiner, G. Boyd, L. Lindberg, J. Minter, and B. Morey of GAPD are acknowledged and thanked for technical guidance, analyses, program direction and support. Finally, appreciation is expressed to Norton Company, TRW, GAPD, NASA and DOE for financial support.

REFERENCES

1. Statement of Work, Norton/TRW Ceramics Subcontract, Advanced Turbine Technology Applications Project (ATTAP), Document No. 31-6866, (Phoenix, AZ: Allied Signal Aerospace Company), September 21, 1988.

2. N. L. Hecht, "The Experimental Evaluation of Environmental Effects In Toughened Ceramics For Advanced Heat Engines, "Semiannual Progress Report, ORNL Contract No. AC05-840R21400, (Dayton, OH: The University of Dayton, October, 1988).

3. L. J. Lindberg, Personal Communication, Garrett Auxiliary Power Division, Aug. 4, 1988.

4. G. Taguchi, Introduction To Quality Engineering, (Tokyo: Asian Productivity Organization, 1987).

5. D. M. Byrne and S. Taguchi, "The Taguchi Approach to Parameter Design," Quality Progress, 20, [12], (1987), 19-26.

6. B. Gunter, "A Perspective On The Taguchi Methods," Quality Progress, 20, [6], (1987), 44-52.

7. A. J. Fannelli and R. D. Silvers, "Process For Injection Molding Ceramic Composition Employing An Agaroid Gell-Forming Material To Add Green Strength To A Preform," U.S. Patent No. 4,734,237, (Mar. 29, 1988).

APPENDIX B

ANNUAL TECHNICAL PROGRESS REPORT
CARBORUNDUM COMPANY

(37 pages)

Contract No. DEN3-335

Advanced Turbine Technology Application Program (ATTAP)

Annual Technical Progress Report

No. 1

October 1, 1987 - December 31, 1988

Submitted by:

THE CARBORUNDUM COMPANY
Structural Ceramics Division
Niagara Falls, New York 14302

Prepared by: Harry Lawler Date: 3/7/89

Harry Lawler

Approved by: James W. MacBeth Date: 3/17/89

James W. MacBeth
Program Manager

Prepared for:

Garrett Auxiliary Power Division
Phoenix, Arizona 85010

Advanced Turbine Technology Applications Program (ATTAP)
Contract DEN3-335
Ceramic Component Development

First Annual Technical Progress Report

October 1, 1987 through December 31, 1988

Introduction

This report, prepared by The Carborundum Company (Standard Oil Engineered Materials Company), Structural Ceramics Division, represents the first annual technical progress report submitted under the ceramic component development subcontract. This subcontract is part of the U.S. Department of Energy sponsored and NASA administered 5 year contract DEN3-335, Garrett-Advanced Turbine Technology Applications Program (ATTAP) with Mr. D. M. Kreiner, Garrett Auxiliary Powder Division, Phoenix, Arizona, as Project Manager. Work reported in this report covers the period of October 1, 1987 through December 31, 1988.

As a major subcontractor Carborundum is to carry out the development of ceramic component fabrication processes through detailed analyses of materials and processes, controlled experimentation and destructive and nondestructive evaluation of green and finished components. The goal of this development program is to achieve increased reliability and reproducibility on near net shape turbine engine components.

1.0 Transition Duct (CBBA)
Drawing No. PA 3610213-2

Isopressing/Green Machining

Component fabrication started late in the AGT 101 program was continued during the initial phases of ATTAP. Green machining, sintering and grinding was carried out on two units. Although both failed on final inspection (one for surface flaws and one for dimensional distortion), no additional work was conducted since GAPD had sufficient engine quality hardware for test.

Injection Molding

Components from the last AGT 101 molding run (December 1986) continued to be processed under ATTAP. Several parts which passed as-fired NDE were processed through final grinding after minor rework.

One component was finished ground at an outside grinding facility. Other components submitted for finishing showed some warpage. A coordinate measuring machine was located locally and the finished transition duct was checked for compliance. Thorough dimensional evaluation showed only minor nonreworkable deviations. The part was supplied to GAPD as transition duct 8-135. It represented the first finished NDE acceptable injection molded transition duct.

A subsequent molding run was carried out in November of 1987. Two molding compounds, SX-05 and SX-09, containing identical plastics systems but varying in preparation of the starting powder were utilized to mold 72 transition ducts. Several of these parts were submitted for binder removal after minor green machining was carried out to completely remove the gate and flash from the tooling parting line on the large OD.

Five parts were processed through sintering. Three of these parts showed some distortion and reduced shrinkage on the large diameter. The remaining two parts exhibited good shrinkage behavior.

In order to characterize the density and compositional variations for later comparison with binder removed (baked) and sintered material, two SX-09 and two SX-05 as molded transition ducts were selected for a computed tomography (CT) study. CT scans using a dual energy dispersive system were conducted on as molded parts. Additionally, a 1/2" thick slice was cut from a green component and 1/2" wide sections were prepared for detailed immersion density measurements.

Injection molded calibration cylinders of 1/2" diameter and 4" length with varying wt.% plastics content were prepared and evaluated using the same dual energy tomography system. Initial evaluation of the CT scans showed expected progressive reduction in the CT numbers with increased plastics content (reduced green density). This indicates that the possibility of calibrating tomography results with component chemistry is very encouraging.

At this point, a more definitive activity flow diagram (Figure 124) was developed and major tasks were identified as follows:

Task I: Compound Preparation and Evaluation
Task II: SX-05/SX-09 Evaluation Matrix and Selection
Task III: Fabrication and Evaluation of Molded Rings
Task IV: Extended Transition Duct Molding Trials
Task V: Fabrication of Engine Quality Components

Task I: Compound Preparation and Evaluation

Since a single full scale transition duct weighs approximately 7 1/2 pounds, the batch size required for a reasonably extensive designed experiment approaches 600 pounds. Inhouse batch preparation equipment has a capacity of only 50 to 60 pounds.

A methodology was therefore developed whereby smaller sub-batches could be prepared, combined and qualified. In addition, rheology variations and sources of high density inclusions were investigated.

The rationale was to evaluate each sub-batch while minimizing material usage for analytical purposes.

Task II: SX-05/SX-09 Evaluation Matrix and Selection

During the course of the AGT program Carborundum used two injection molding compounds designated as SX-05 and SX-09. Both compositions have the same binder system but vary in the preparation of the starting SiC powder and the addition of some of the sintering additives.

Room temperature strengths of test bars fabricated from these compositions have not correlated very well with test bars sliced from injection molded components.

A program was initiated in which both test bars and transition ducts were molded from both compositions, processed under controlled conditions and tested for relative strength (Table 43).

Table 43
MOR Comparison for SX-05 and SX-09 Test Bars

	SX-05		SX-09	
	MOR, ksi	m	MOR, ksi	m
As-fired	54.6	5.8	58.2	15.1
Machined	55.2	6.2	52.7	2.9
Machined and Annealed	67.8	13.4	66.7	8.9

The low strength and Weibull Modulus for the machined SX-09 test bars are indicative of possible surface damage from machining. Samples have been submitted for fracture analysis to confirm this.

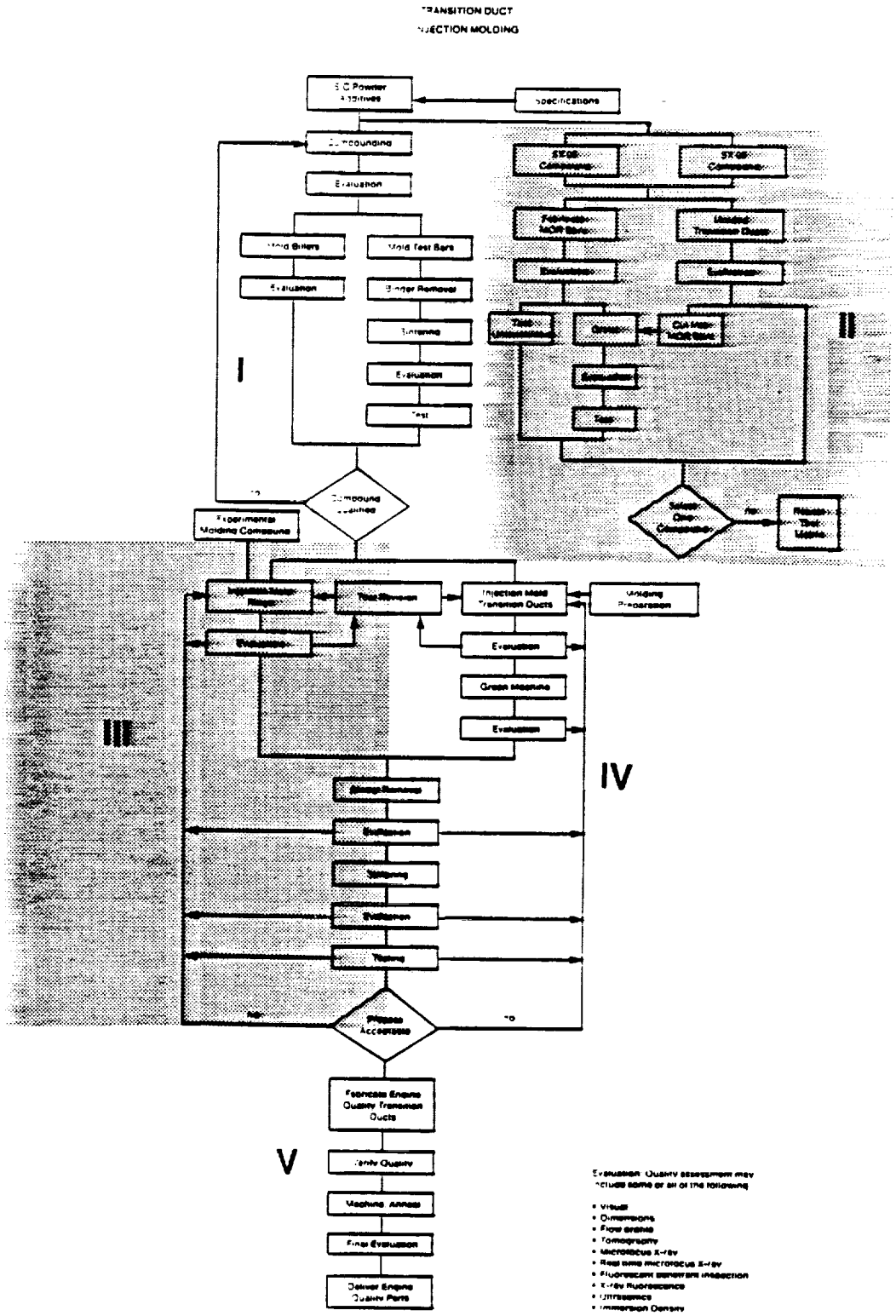

Figure 124: Activity Flow Diagram - Transition Duct

ORIGINAL PAGE
BLACK AND WHITE PHOTOGRAPH

Since test bar strength results were somewhat inconclusive and a review of the experiment disclosed that reground material was used for one batch molded into transition ducts and that different raw material lots were used for each composition, this program was suspended. A new and more rigorous comparative evaluation has been formulated as a designed experiment and is programmed for contract year 2.

Task III: Fabrication and Evaluation of Molded Rings

The objectives of this task were to conduct molding studies and gating studies on a small relatively simple and available ring mold compatible with an inhouse injection molding machine.

Initial moldings were done using both SX-05 and SX-09 compound in an existing tool. All showed some flow lines which could not be eliminated through further molding parameter adjustment. It is believed that the relatively narrow gating arrangement caused these molding deficiencies.

The tool was reworked to enlarge the sprue bushing, increase the gate thickness to that of the ring, provide a cold slug within the gate opposite the sprue, and provide a thermocouple port to better simulate the transition duct flow (**Figure 125**). The filling pattern approached that of a uniform front and the gate freezing off before the part was fully packed out was eliminated.

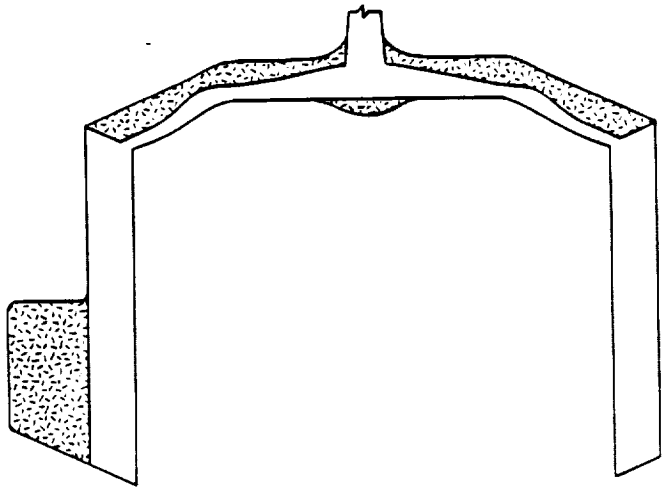

Figure 125: Ring Tool Modification

This tool was used to run a Taguchi L_{27} molding experiment. The seven factors under study - mold temperature, velocity, pack pressure, hold pressure, shot size, pack time, hold time - were ranked, the design was formulated, and three levels were systematically assigned to each.

The goal of this experiment was to determine molding conditions that minimized the number of flow lines.

The significant control parameters were found to be mold temperature and velocity.

Task IV: Extended Transition Duct Molding Trials

Component fabrication by injection molding started late under the AGT 101 program. Eight parts from the December 1986 molding run passed as-fired NDE, one of which was machined and supplied to GAPD. Another molding run was carried out in November 1987 using both SX-05 and SX-09. A molding was subsequently conducted in August 1988 using only SX-05 in a 3^2 Taguchi L9 experiment. Sintering distortion is a critical problem in injection molded components. The activities in this section focused on variations that could influence sintered properties. The resources used in this task included immersion density measurements, dual energy tomography, X-ray fluorescence, statistical experimental design, and flow modeling.

Immersion Density

One part from the 3^2 Taguchi L9 experiment molded under optimum conditions with respect to minimum number of flow lines was sliced green for immersion density of sections. Two axial slices were sectioned as shown in **Figures 126 and 127.** The density was found to be about the same both top to bottom as well as inside to outside. Both center and 60° slices had an average density of 2.030 g/cm^3 with a standard deviation of .033 g/cm^3.

Dual Energy Tomography

In this dual energy technique, described in Section 6.0, it is assumed that the specimen contains a spatially varying mixture of two basis materials, one with a higher atomic number (HI) and the other lower (LO). For medical use, HI is usually calcium and LO water. In the case of injection molded sinterable alpha SiC, HI will be silicon and LO polymer.

An axial slice (.31" thick) from a transition duct was evaluated using the dual energy method. **Figure 128** shows the HI image representing the higher atomic number density distribution - Si in this SiC/polymer composition. Some silicon asymmetry can be seen in the cross section. The inner surface, particularly near the axial center of the duct, appears to be lower in density than the surrounding portions which provide darker shades of grey.

ORIGINAL PAGE IS
OF POOR QUALITY

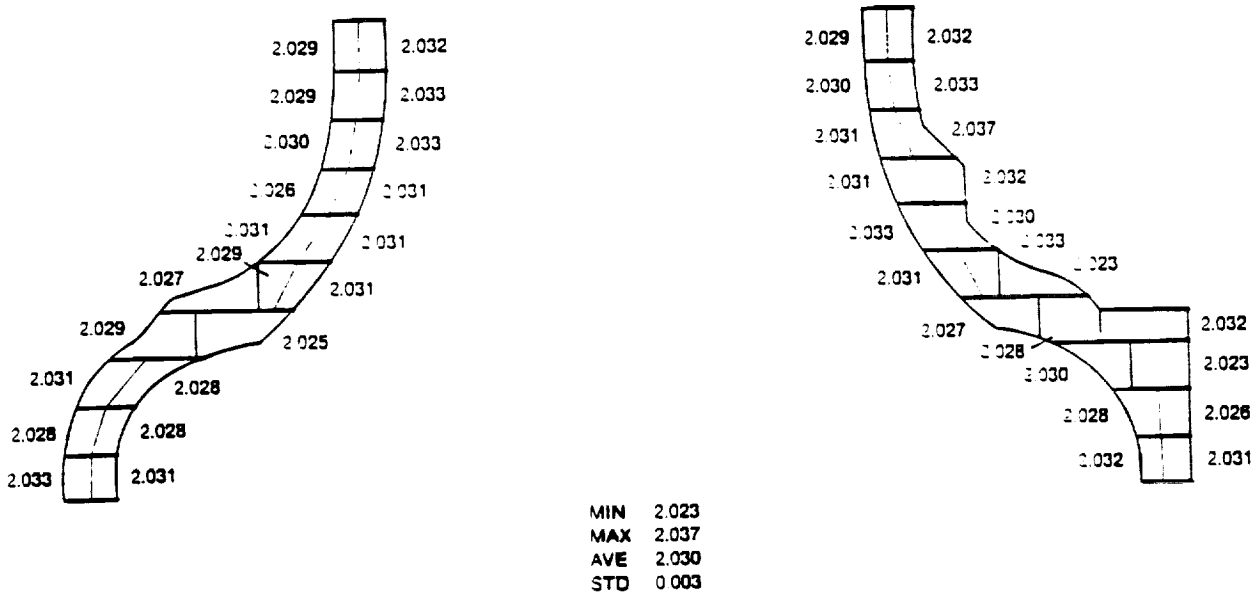

Figure 126: Immersion Density of Molded Transition Duct Sections Through Center Thermocouple Port

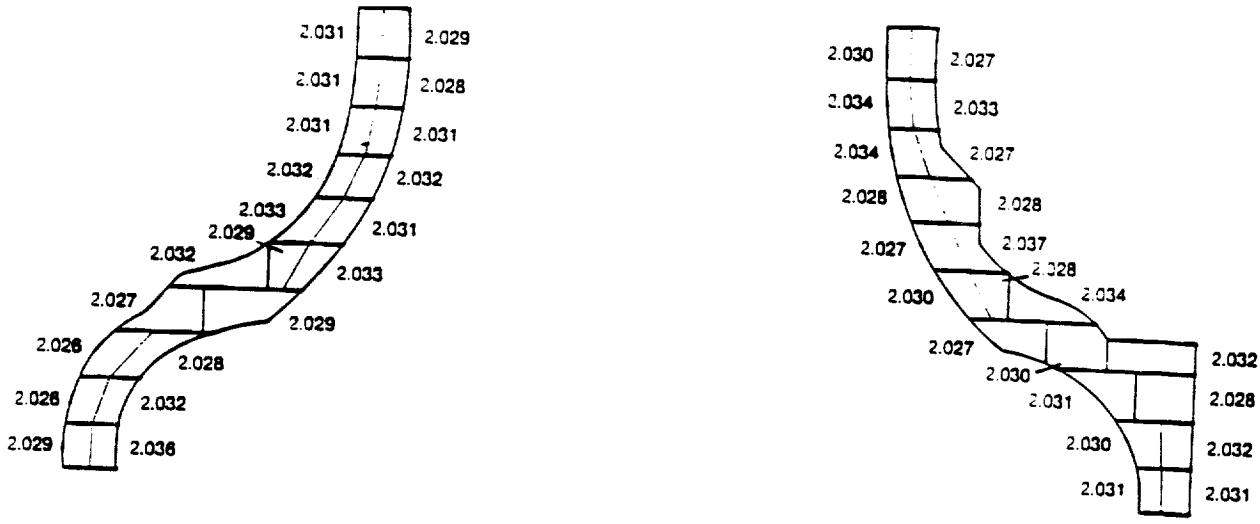

Figure 127: Immersion Density of Molded Transition Duct Through Right Side Thermocouple Port

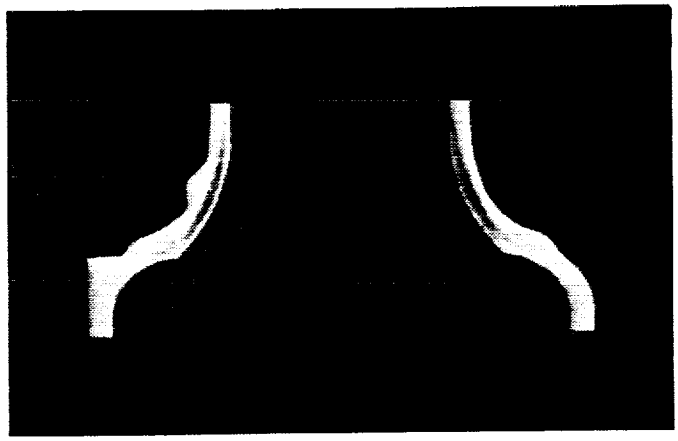

Figure 128: HI Image Axial Slice

While CT can detect density differences of less than 1%, the data must be examined carefully to ensure the variations are not due to imaging artifacts. The apparent reduction in silicon density along the inner convex region that is seen on a medical system is now thought to be a beam hardening artifact. Images taken on a higher energy (220 kv instead of 130 kv) industrial CT system do not show these variations. It is thus important to have independent methods for confirming CT results when techniques are being developed to evaluate different parts, particularly those having complex cross sections.

X-Ray Fluorescence (EDAX)

A standard analytical method for detecting compositional variations is to measure changes in the amplitude of the X-ray fluorescence (XRF) from different positions on the sample surface. Only a narrow range of the spectrum that is characteristic of the particular element is used. However, the test is destructive since the sample must be cut to expose the regions of interest. The test is made quantitative by calibrating with known standards, in this case injection molded rods with 35 to 20 wt% polymer content (65 to 80 wt% SiC).

The XRF spectrum analyzed with an energy dispersive spectrometer can be calibrated to measure the density of SiC within about 38 um of the surface. As shown in **Figure 129**, a linear relationship between net Si intensity and SiC concentration has been obtained having a correlation coefficient of 0.988. The same samples were scanned with dual energy tomography which correctly measured the average atomic number.

ORIGINAL PAGE
BLACK AND WHITE PHOTOGRAPH

ORIGINAL PAGE IS
OF POOR QUALITY

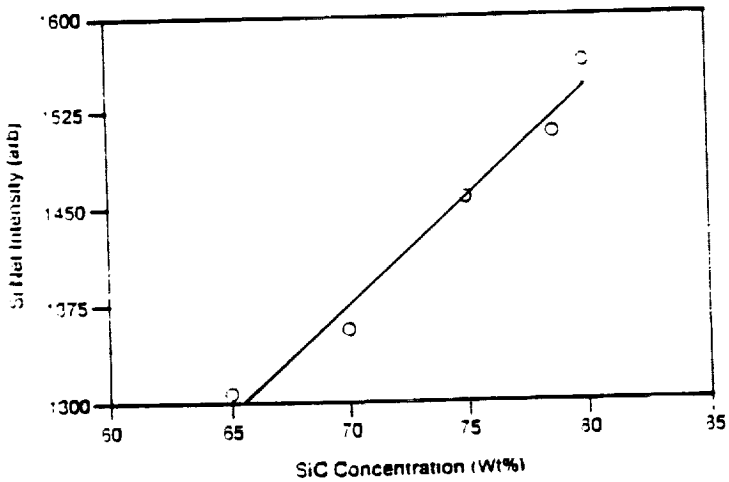

Figure 129: Si Intensity as a Function of SiC Concentration and Linear Least Square Fit

A molded transition duct was sliced in the axial direction approximately .5" thick and XRF measurements were done at several locations and compared with the HI tomography results. The areas that were expected to be a lower in SiC concentration from the CT are outlined with a dotted line in **Figure 130.** The crosses indicate the approximately analyzed areas.

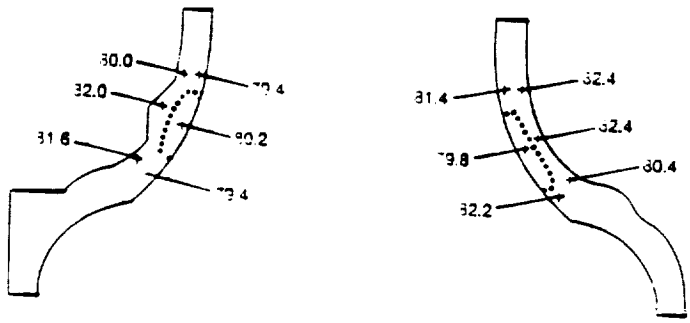

Figure 130: SiC Concentration Via X-Ray Fluorescence

While the fluorescence data was very repeatable, the measured differences do not unequivocally show consistent variations in the SiC concentration. This and the immersion density measurements of sectioned components suggest that there are some artifacts in the CT data for this particular part shape. Since the XRF data is so surface specific it is possible that smearing of the polymer or pullout of the SiC when the part was cut produced the observed variations. It is expected that improvements in the beam hardening corrections and the use of higher X-ray energies for dual energy measurements will make tomography a very reliable method for characterizing green ceramics.

Statistical Experimental Design

After the most significant molding variables were identified a 3^2 Taguchi L_9 experiment was designed for a transition duct molding trial.

The L_9 design for molding transition ducts is shown coded in Table 44. The goal of this experiment was to determine the mold temperature and pack time levels required to minimize the number of flow lines in a molded part.

Table 44. L_9 Molding Matrix

Exp.	Mold Temp.(1)	Pack Time	Mold Temp.(2)
1	100	50	100
2	100	100	100
3	100	150	100
4	106	50	106
5	106	100	106
6	106	150	106
7	112	50	94
8	112	100	94
9	112	150	94

(1) Initial Design
(2) Revised Design

Three parts were examined for each experiment. The midpoint mold temperature selected was the best value from the ring experiment. However, the experiment could not be run as originally planned because the part stuck to the fixed mold half at the midpoint temperature of 106 (coded). The last three experiments were therefore run at 94 instead of 112.

Based upon interaction plots, a number of conclusions can be drawn. The number of flow lines decreased with mold temperature and also with pack time at the higher temperatures. However, sticking (to the fixed mold half) increased with mold temperature but shows some improvement with increasing pack time. The molded weight increases with pack time and decreasing mold temperature.

This latter characteristic may be accounted for by material cooling, shrinking, and refilling under pressure. The cooler mold results in more rapid material cooling and shrinking. During pack time, new material is forced into the mold cavity compensating for cooling shrinkage. The effects of this phenomenon have yet to be determined.

Flow Modeling

Flow modeling was performed to verify field trial quality as well as to optimize specific molding variables which keep shear rates and shear stresses as low and uniform as possible. The sprue and gate were made approximately equal in thickness to the duct to permit filling as the component cools and shrinks during the packing cycle. In addition, the gate above the airflow diverter and thermocouple ports were made proportionally larger than the gate feeding the opposite mold half.

The mold temperature, melt temperature and fill time selected for modeling were those used in the "best" 3^2 base design for flow lines. Five response variables were compared: fill time, pressure distribution at instant of fill, flow front temperatures as material fills part, shear rate during filling, and shear stress during filling.

The duct short shots show the diverter side filling first due to the thicker gate permitting easier flow. The pressure distribution (**Figure 131**) asymmetry is magnified due to the duct filling imbalance and has shifted to the last place to fill on the right. The total pressure drop is still very low and over half is used in the sprue and gate.

The temperature gradient is negligible. The shear rate is a function of section thickness and flow front velocity. Most of the part has extremely low values below 150 sec^{-1}. The highest values are in the sprue and gate. Similarly, most of the shear stress during filling is confined to the sprue and gate while the stress in most of the part is between 30 kPa and approximately 50 kPa (**Figure 132**).

Flow modeling indicated that start-up conditions were well within standard injection molding guidelines. The only molding problem was the slight asymmetry due to gate configuration which was rectified by using a uniform gate thickness.

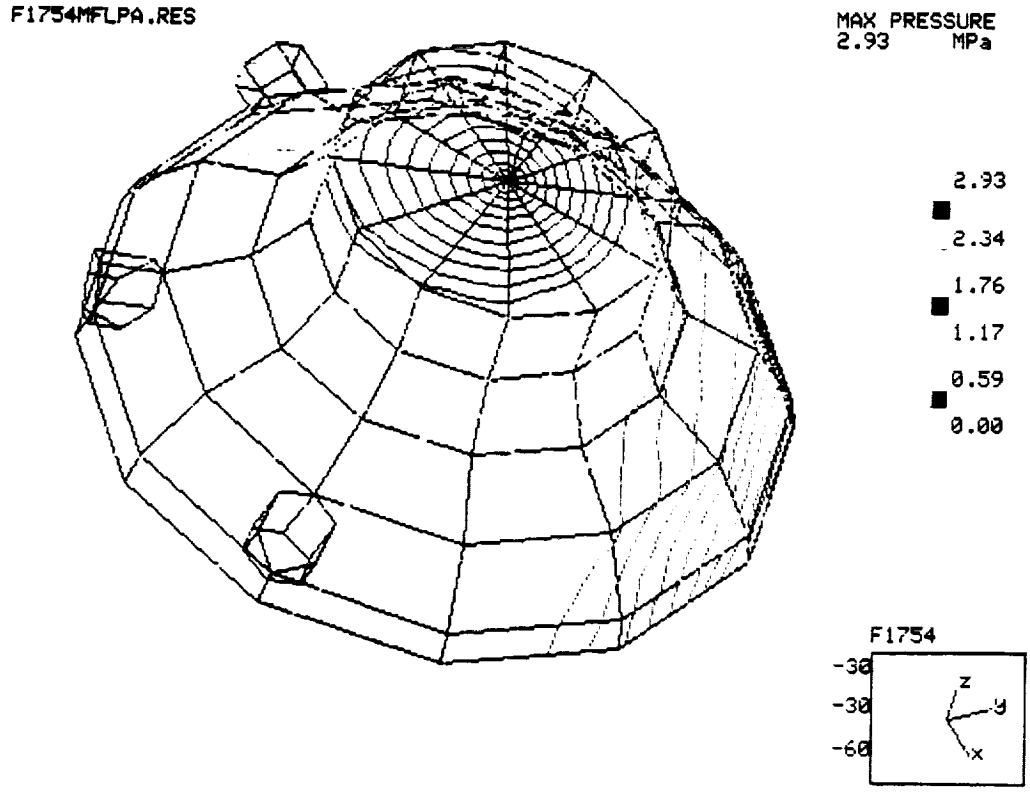

Figure 131. Pressure Plot

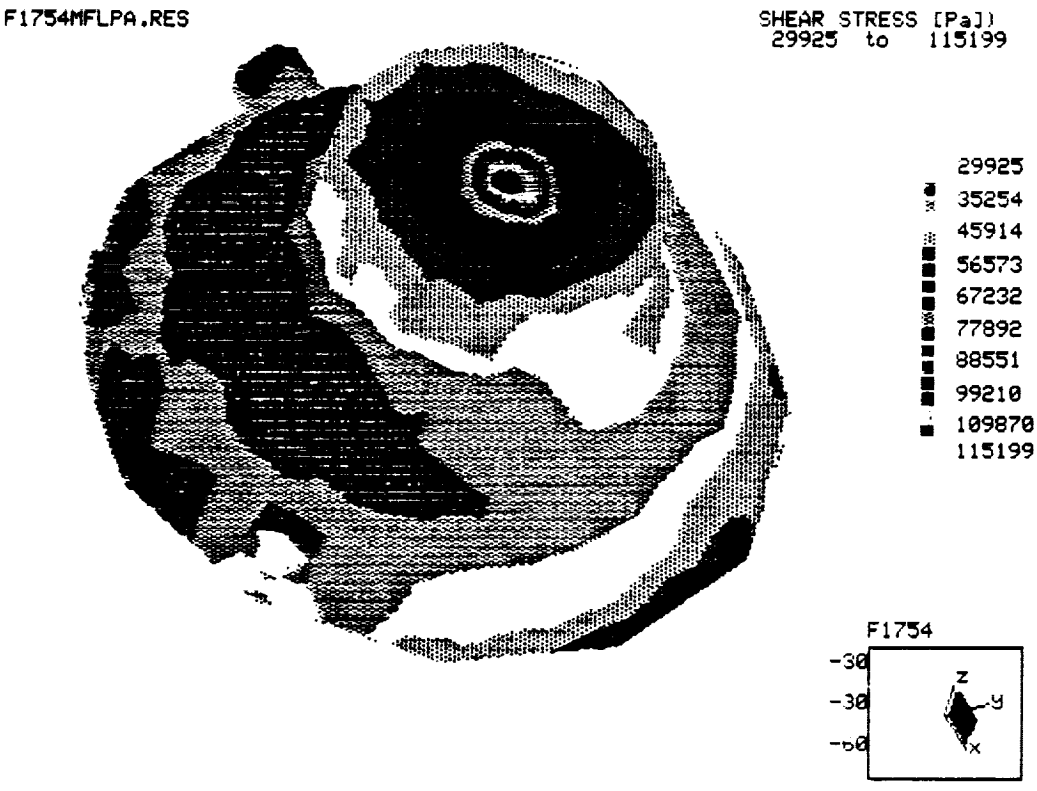

Figure 132: Shear Stress Plot

ORIGINAL PAGE
BLACK AND WHITE PHOTOGRAPH

ORIGINAL PAGE
BLACK AND WHITE PHOTOGRAPH

2.0 Turbine Backshroud (CBBB)

Hexoloy™ ST (a titanium diboride particulate reinforced pressureless sintered Alpha SiC) was chosen as an advanced material for this application over Hexoloy™ SA because of its increased fracture toughness and increased strength. The composition selected consists of 80 wt % SiC and 20 wt % TiB_2. A representative microstructure is given in Figure 133.

Three isopressed/green machined components finished to the specified dimensions were supplied in August of 1987 under the AGT 101 program. Because of configuration reasons it was decided to use 4" x 4" x 3/4" isopressed/green machined blocks for sectioning into MOR bars to obtain component characteristic MOR data. Four plates were prepared using the 80/20 composition. Two plates were supplied to GAPD and the remaining two were cut into standard MOR bars. Room temperature and elevated temperature strength and failure analyses are being carried out and compared with data from individually processed ST and SA MOR bars.

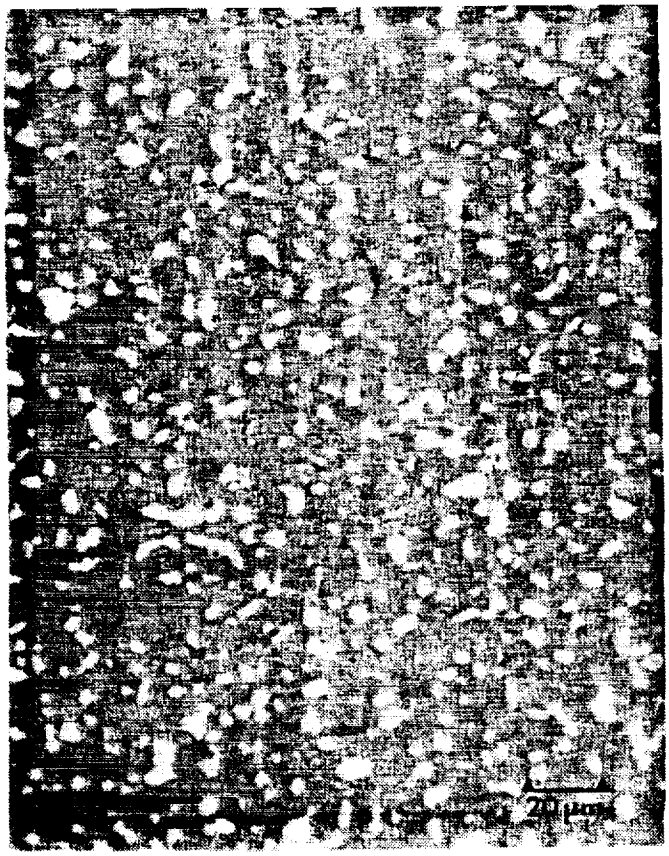

Figure 133: Hexoloy™ ST

Ram Pressing

Ram pressing was identified as a suitable near net shape forming process for this component. The process requires specialized equipment for material preparation and forming but is well established within the traditional ceramics industry.

Aqueous material processing of Alpha SiC as utilized for slip casting and extrusion, is being used to develop a suitable Ram press mix. Work started early in 1988 with the goal of developing a mix with the following essential properties: 1) high yield stress to prevent slumping after forming, 2) strongly shear thinning behavior (pseudoplasticity) to allow forming under high shear stress, 3) sufficiently high solids loading to obtain a system with reasonable shrinkage characteristics.

The ram pressing development was carried out in accordance with the activity flow diagram (**Figure 134**) as presented in the workplan. This diagram is divided into seven major development tasks:

Task I: Small Test Batches for Additive Screening
Task II: Fabrication of Rammed Test Plates
Task III: Scale-up to Prototype Equipment
Task IV: Evaluation of ST Ram Mix
Task V: Fabrication of Ram Pressed Turbine Backshrouds
Task VI: ST Turbine Backshroud Fabrication
Task VII: Fabrication of Engine Quality Components

During this period work focussed primarily on Task I and some exploratory work was carried out on Task II, III and IV. No work was scheduled on Tasks V through VII during this first year.

Because of the particle shape of the Alpha SiC powder used it is necessary to introduce surface modifying agents to improve plasticity, a material characteristic which is intrinsic to ceramics containing plate-like particles. Therefore, water soluble **polymeric** agents, such as cellulose based binders were investigated for initial composition screening. Viscosity at variable shear levels is the prime evaluation criteria for these experimental mixes. A Brabender Torque Rheometer reading and flow through a specified orifice using a Carver press are used to collect viscosity data.

Different mixing and compounding equipment for these relatively stiff mixes was also explored.

After reviewing company notebooks on Ram press mixes, appropriate aqueous additives were ordered. Laboratory mixing and evaluation equipment, such as an Eirich and a Hobart mixer and a small Carver press was obtained.

The Carver test utilizes a small press as shown in **Figure 135** which records the force necessary to press material through a

ORIGINAL PAGE IS
OF POOR QUALITY

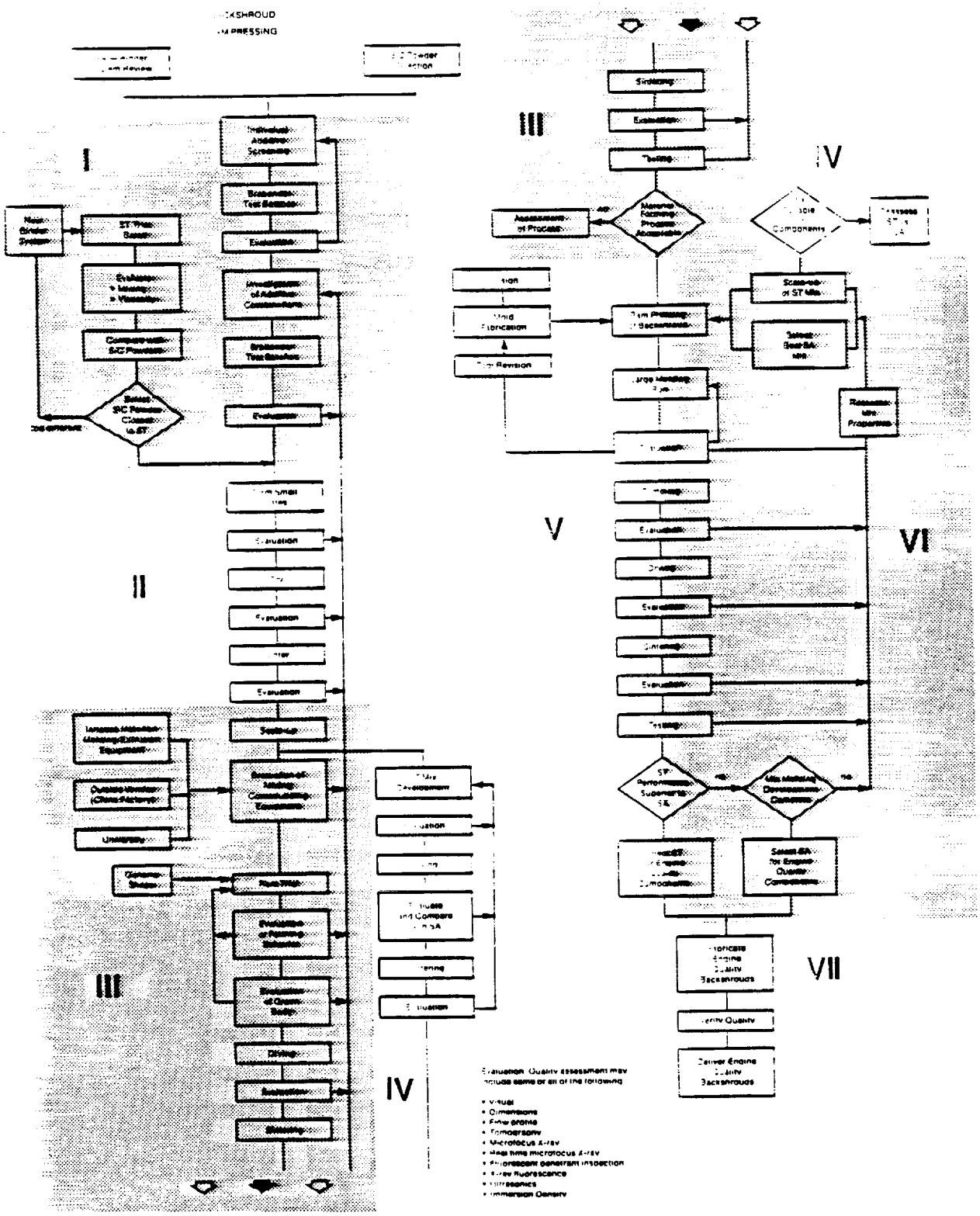

Figure 134: Activity Flow Diagram - Turbine Backshroud

stainless steel die with a 1/4" orifice (**Figure 136**). The reading is recorded in pounds and can be used as a relative measure to evaluate flow behavior of highly viscous materials.

An initial goal was to obtain a mix which exhibited a Carver reading of 700-800. In subsequent compounding by extrusion it appeared that the above mix was too stiff to flow adequately during pressing.

For further inhouse assessment a small Ram press mold for a 3.5" x 3.5" x 5/16" plate was constructed (**Figure 137**). This allowed more frequent feedback on small experimental batches prior to scale-up. A number of molded plates were processed to gain processing experience and to assess material characteristics.

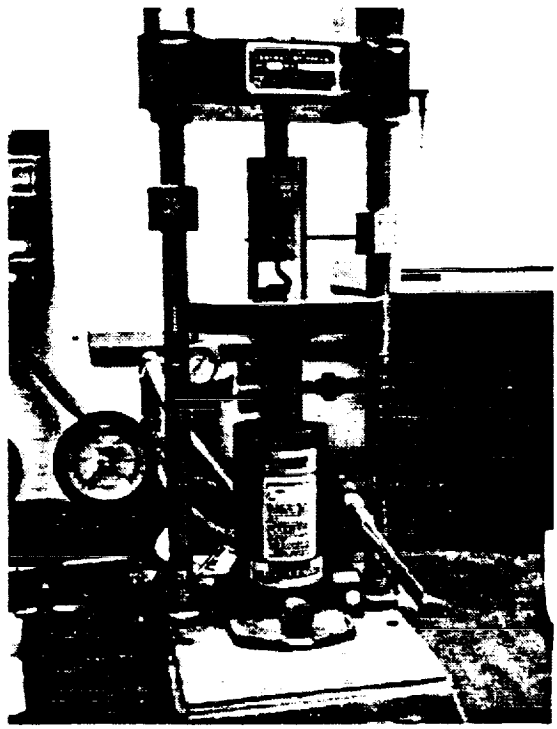

Figure 135: Carver Press With Die

ORIGINAL PAGE
BLACK AND WHITE PHOTOGRAPH

ORIGINAL PAGE
BLACK AND WHITE PHOTOGRAPH

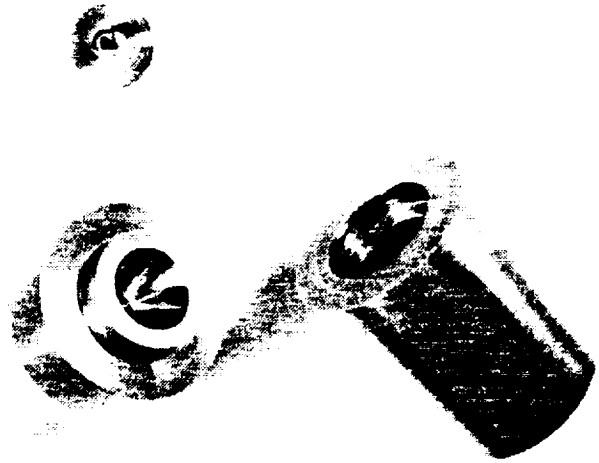

Figure 136: Die for Measuring Flow Behavior

Additive screening studies were performed using the small Hobart mixer to blend the individual mix components and a Brabender mixer to subsequently compound the material. SiC powder containing sintering aids was mixed with different binders and deionized water with and without surfactant.

In one set of experiments individual binders at the same concentration level were evaluated. Viscosity readings were taken incrementally at increased shear rates by increasing rpm. Binders showing the desired plastic behavior were selected for a follow on study where additive combinations were evaluated at two different pH levels. The goal was to achieve increased solids loading at acceptable viscosity levels. Brabender viscosity readings were recorded and mixes judged for sticking behavior.

Scaled up equipment commonly used for compounding of clay based materials did not give the desired mixing results. The SiC material showed distinctly different shear behavior than the plate like structure of the clays and severe sticking was observed in the similar Carver readings. An aqueous extruder was subsequently used for compounding larger batches.

Mixes containing a binder and one additive at varying pH and water additions were evaluated for reduced stickiness using the Carver method. Evaluation of mixes prepared in different equipment indicated a significant difference in apparent flow

behavior. Carver readings of the same composition showed a wide spread as shown in Table 45.

Table 45: Carver Readings

Equipment	Mix No. 39	Mix No. 51
Hobart		1200
Eirich		680
Extruder	310	
Brabender	185	170

These data clearly indicated the need for further studies on appropriate equipment, mixing procedure and evaluation criteria with different size test batches.

Two mixes which varied in water content by about 3% were used for scale-up work. Generic dish like shapes were formed and it was found that the mixes were too soft and stuck to the mold surfaces. These test pieces were sintered after drying first in air and then at elevated temperature (up to 200°F). Densities of up to 3.10 g/cc were obtained. Visual inspection of these parts showed that the drying procedure was adequate for this stage of development.

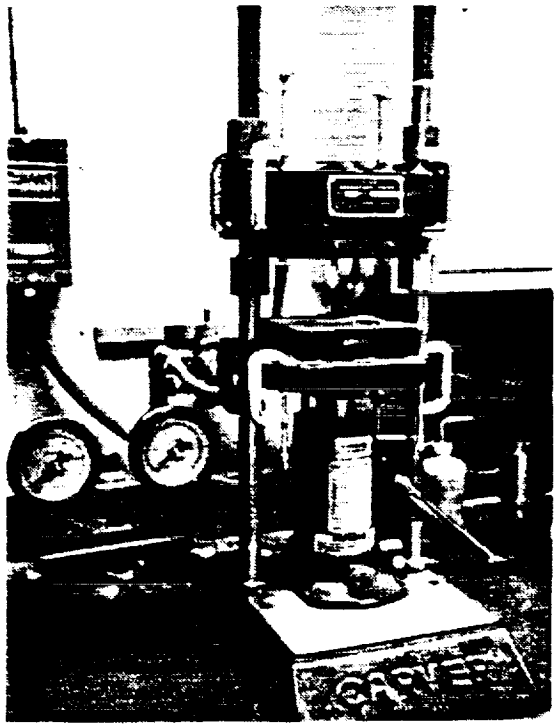

Figure 137: Carver Press With Ram Press Die

ORIGINAL PAGE
BLACK AND WHITE PHOTOGRAPH

The individual additive screening had shown that all binder systems investigated exhibited a shear thinning (pseudoplastic) behavior, that is lower viscosities were recorded with increasing rpm of the Brabender torque meter. Two binders selected for further studies because they allowed a high solids loading at a given viscosity range were further tested.

With one binder at a predetermined level, a preliminary test matrix was conducted varying the lubricant concentration (two levels) and the pH and amount of the water added as shown in **Figure 138.** The goal was to minimize viscosity and amount of water added while working with a system which shows relatively low viscosity sensitivity (robustness).

A semilogarithmic decrease in viscosity resulted. Increased pH (range 10-11) of the added water allowed significant water reduction. At the higher pH level an increased dependency on the amount of water added decreased the working range. An increase in lubricant level extended the working range at a given pH level.

In one experiment the mixing capability of the powder and the above binder was evaluated. Redissolving was found to give a better degree of dispersion in the mix during the initial mixing period **Figure 139.**

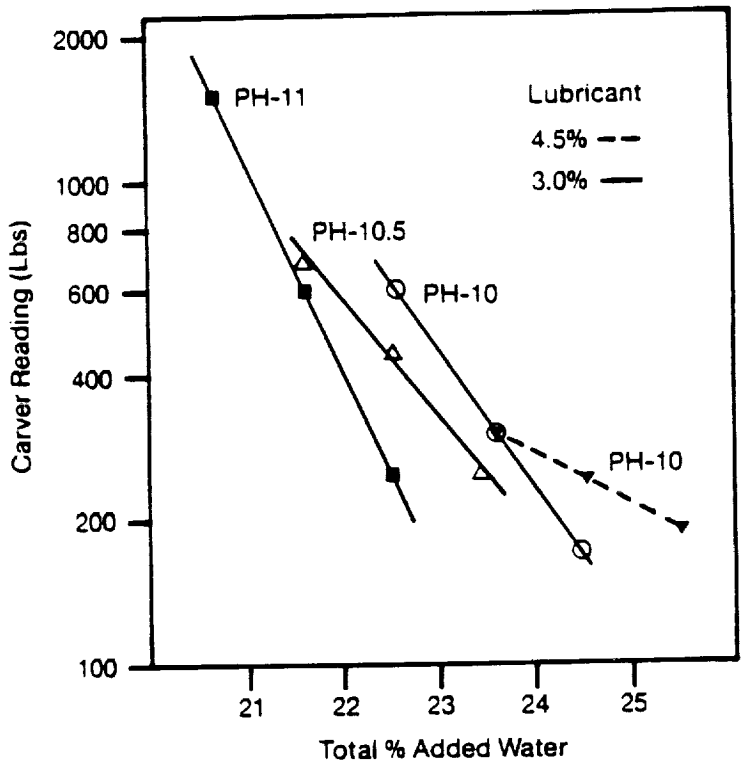

Figure 138: Viscosity Changes with pH and Amount of Water Added to Ram Press Mix

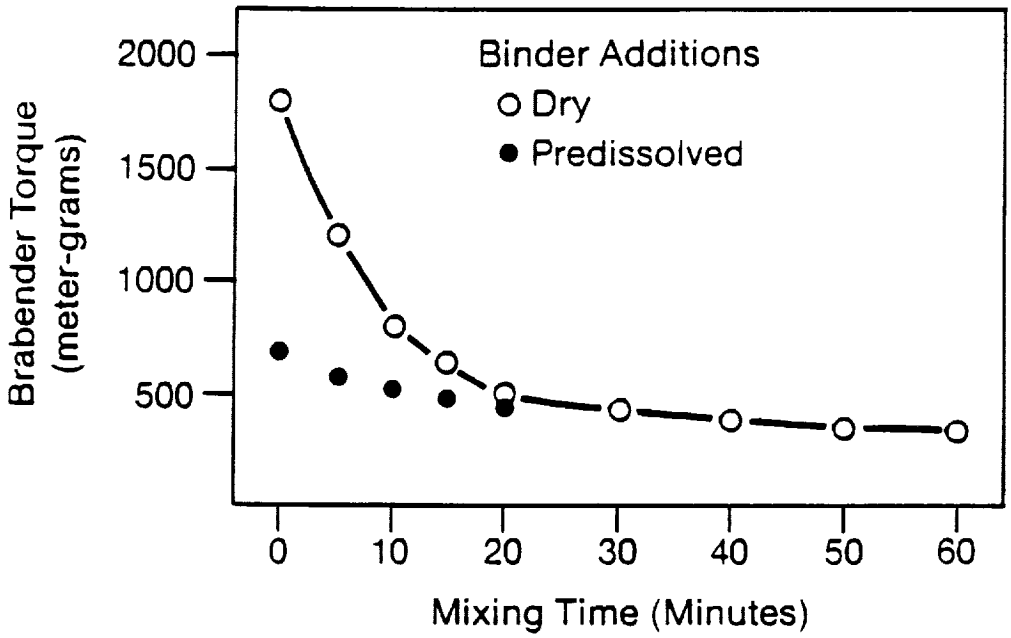

Figure 139: Viscosity Changes with Mixing Time

Two binders at three lubricant levels were investigated with submicron powder instead of the bimodal composition.

Each mix (approx. 100g) was formed in the small Ram die fabricated for the Carver press, dried and sintered under invariant conditions. Evaluation was based on qualitative attributes such as stickiness and cracking during drying but the achieved sintered density was used as the critical response.

It was found that increased water content led to increased fired density (**Figure 140**). This was related to increased flowability of these mixes under compression which resulted in increased green densities. Lower water additions gave dilatant behavior because of the interference of the particles with each other.

Six compositions (**Table 46**) were chosen for scale up during this period. Each composition consisted of two 6000 gram batches. They were mixed in the Eirich mixer with predissolved binders,

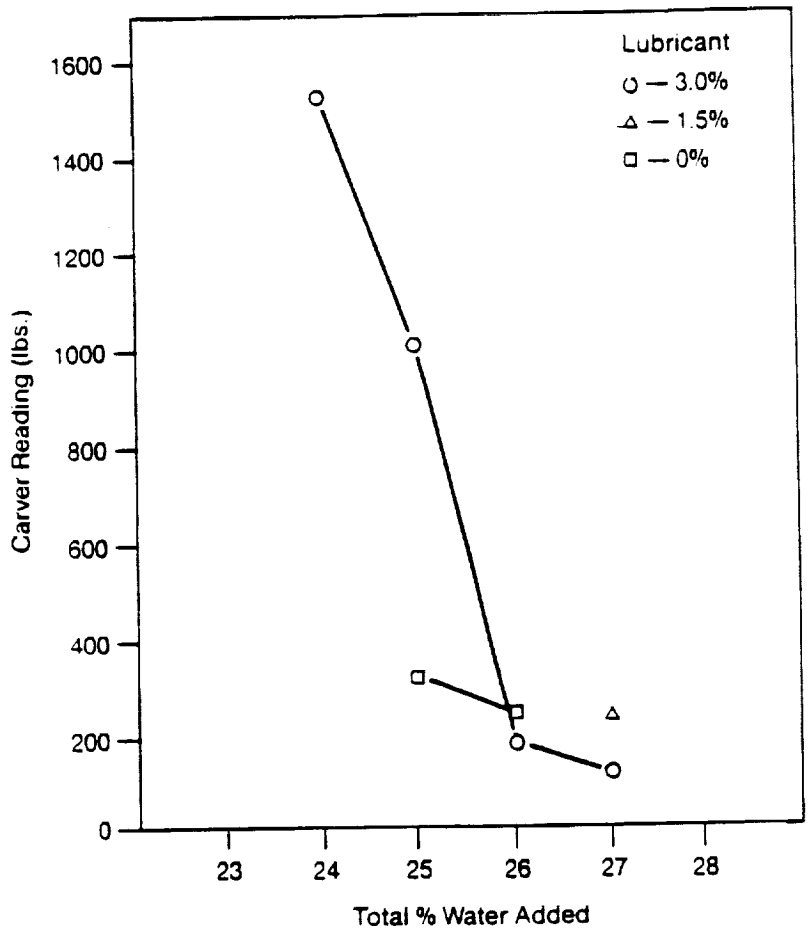

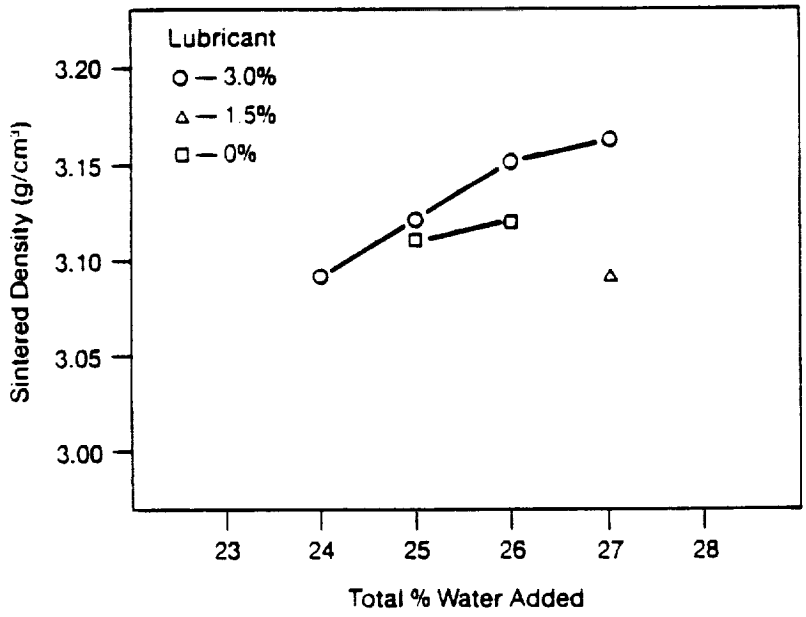

Figure 140: Viscosity and Sintered Density Dependency on Total Amount of Water Added

were transferred to the Readco for more intensified mixing and were then extruded under vacuum through the Loomis piston extruder. In the larger scale equipment the same intensity of mixing was not obtained as with the Brabender mixer. This fact is shown in Table 46 in the different Carver readings obtained for the same composition.

Table 46: Scale-Up Mix Experiment

Composition	Binders	Lubricant	Water Added	pH	Carver Readings		
					Eirich	Brabender	Readco/Extruder
1	2.5%	1%	25%	11	7500	175	
2	2.0%	1%	25%	10	5000	1000	
3	2.0%	1%	26%	10		400/295	1500. 1600 1800. 1700
4	2.0%	1%	27%	10		195	1000. 1010 1010. 1010
5	2.5%	1%	27%	10		205	2000. 1200 1600. 1400
6	2.5%	1%	28%	10		195	1200. 980 1000. 1000

Composition 1 had a very short working range and dried out most likely due to frictional heating during the Readco/Loomis processing step. Composition 2 was too stiff and adequate mixing could only be achieved in the Brabender. Compositions 3 through 6 were formed into slugs for pressing trials. Some variability, especially for the stiffer mixes, was experienced.

The four viable compositions (Nos. 3-6) were ram pressed at a local china company. The ram press speed was minimized to compensate for the stiffness of the mixes. The mixes containing higher water levels were more readily pressed but not significantly so. The ram mold would not close fully and pinch off the flash at the gutters as it was designed to do and as readily occurs with highly plastic clay bodies. The stiffness of the mix and its dilatant character reduced the flow as the shear gap decreased and the shear rate increased.

All of the rammed components exhibited surface delamination at any broken edges. It appeared as if only the surface layers compressed. Also, the bottom ram mold fractured under pressure indicating that the force was transferred directly through the material rather than forcing the material to flow horizontally in the mold.

The parts were not immediately trimmed. However, during subsequent air drying the weight of the flash caused cracks in many of the parts.

There was little or no sticking to the ram mold with any of the mixes. The higher water content mixes for each of the binder levels had Carver values of approximately 1000 lbs. This contrasts to a Carver value of about 300 lbs. for a mix which exhibited a serious mold sticking problem. This data indicates, that Carver values of 500 to 700 lbs. will provide adequate plasticity and satisfactory release characteristics.

Because of differences in the mixing processes, it is difficult to simulate large scale tests with the small Brabender experiments. It will be necessary to conduct subsequent designed experiments on the full scale ram press equipment.

An experiment was developed (Table 47) to determine the effect of increasing lubricant and water content on plasticity. The compositions were granulated, Readco-mixed and Loomis-extruded. Only one of the six Kg batches (115A) exhibited adequate plasticity even after Brabender testing at high shear rates. Moisture contents were determined to be less than the designed compositions, and, the proper make up water was added in the mixer to increase plasticities to the desired range. Results are shown in Table 48.

Table 47
Carver Values For Several Compositions
Encompassing Two Powder Lots

Comp.	Binders	Lubricant	Water Added (pH-10)	Total Water Added	Calc. % Water	Meas. % Water	Brabender/ Carver Value
114A	2.0%	1.0%	26%	28%	21.4	20.9	238
B						20.7	305
115A	2.5%	1.0%	27%	29%	21.9	20.6	20*
B						21.8	220
116A	2.5%	1.5%	25%	28%	21.2	19.5	80*
B						21.0	300

*Old Lot

This table shows that the two powder lots had distinctly different water requirements. In addition, inconsistencies were found in the Brabender values vs. total water added for earlier mixes.

Table 48
Carver Values with Variable Water Content for Two Compositions

Comp.	Binders	Lubricant	Total Added Water	Brabender Carver Value
114B	2.0%	1%	26%	440/295
			27%	195
			28%	305
115B	2.5%	1%	27%	205
			28%	195
			29%	220

Either errors in mix calculations or procedures or overheating in the mixer and/or Brabender dried out the material. This is an example of the difficulty of correlating small scale testing to larger scale processing.

The work accomplished and the information gained in the program described above provided insight for development of an experimental plan. The major problem was the difficulty in achieving identical properties on the large and small scales. The former will be chosen for all further work.

An experimental program which addresses more fundamental powder issues was designed and approved for the next program year. This design will focus on feedstock preparation and carbon source and will include binder, water content and mixing variables carried out on industrial scale equipment. The revised work plan consists of the following tasks:

Task I: Composition Development
Task II: Fabrication of Ram Pressed SASiC Backshrouds
Task III: Composition Development-ST
Task IV: Fabrication of Ram Pressed ST Backshrouds
Task V: Fabrication of Engine Quality Components

3.0 Wave Spring (CBBC)

The objective of this task is the development of a low cost fabrication process for high quality, reproducible wave springs with predictable properties.

Three configurations described below were under consideration:

Part No.	ID	Wall	Thickness	Wave Amplitude
3612423	6.235"	.200"	.200"	.200"
3612424	6.235"	.200"	.140"	.165"
3612425	6.120"	.402"	.100"	.170"

Although similar in configuration, these wave springs have thicknesses and wave form amplitudes which suggested two

potential fabrication methods. For the thinnest component a plastic extrusion and stamping process appeared viable. For the thickest component a dry pressing process was identified.

The fabrication process for the intermediate thickness wave spring was to be selected based upon the outcome of the above development efforts.

The major problems which preclude fabrication of this configuration include:

- Dimensional control of size and tolerance
- Elimination of distortion on sintering
- Formation of accurate wave form contour
- Low strength of "green" component due to very small cross sections
- Significant cost of diamond grinding if net shape components are not viable
- Reproducibility of optimum properties

In order to provide finished components for initial evaluation by GAPD, wave springs of all three designs were fabricated during 1987 and early 1988 using isopressing/green machining and final grinding. all parts were green machined into flat rings which were OD, ID and wave ground after sintering and NDE. Specific care was taken to minimize stresses within the parts through annealing prior to and after machining.

During contract Year I an extrusion/stamping process was investigated for the thinnest wave spring (P/N 3612423) and a dry pressing process was investigated for the thickest wave spring (P/N 3612424).

3.1 Extrusion/Stamping - Wave Spring P/N 3612423

Plastic extrusion and stamping were chosen because of the high green strength of this material which is of extreme significance for P/N 3612423 and its 0.040" thickness and 0.200" amplitude. Development was initiated in accordance with the activity flow diagram (**Figure 141**) essentially as presented in the workplan. This diagram can be divided into six tasks:

Task I: Fabrication of Sheet Stock
Task II: Processing of Flat Rings
Task III: Fabrication of MOR Bars
Task IV: Processing of Waved Rings
Task V: Evaluation of Process and Configuration
Task VI: Fabrication of Engine Quality Components

In order to establish a baseline composition with respect to maximum sintered density and strength and minimum distortion, three different plastic compound formulations were prepared and extruded and calandered into both thin and thick sheets. These differed with respect to particle size distribution of the

submicron silicon carbide but were identical in terms of composition and all processing parameters as established through prior work. The maximum sheet width was such that final sintered rings were approximately 1" undersize on both OD and ID.

Green sheet samples from each compounding lot were submitted to QC for X-ray examination to determine if internal flaws were present prior to sintering. No defects were found in green plates.

Flat rings approximately 6.500" OD x 6.000" ID were cut from the .050" thick sheet of each composition using a gasket cutter. These were sintered on a specially designed graphite sintering fixture along with plates cut from thick sheet stock (0.250") of each composition.

Several furnace runs with rings stacked three-high on the fixture were conducted to assess furnace conditions, shrinkage behavior and fixture requirements. Noticeable distortion and warpage were observed on parts sintered in stacks three high. Following a modification to the fixture the tests were repeated successfully.

Ten flat rings and thick sheet stock from each composition were sintered in a production furnace run and subsequently evaluated for density, X-ray defects and shrinkage. All rings densified to greater than 3.12 g/cc (97% + of theoretical) and were visually acceptable. The thick sheet stock was sliced into MOR test bars ground, annealed and re-inspected. Bars with gross grinding chips were removed from the group prior to testing. Based upon the NDE results, each group was separated into two subgroups; those that were defect free (without flaws) and those which contained defects (with flaws). This accounts for the variability in the number of bars tested for each group.

The strength and Weibull data are shown below. It is interesting to note that there is little difference in the results of groups containing flaws or flaw free.

Composition	A	B	C
Strength - Ave. w/o flaws	57 ksi	45 ksi	45 ksi
Strength - Ave. with flaws	55 ksi	45 ksi	45 ksi
Total No. Tested	37	61	43
No. Tested	20	50	30
Strength - High	68 ksi	55 ksi	65 ksi
Strength - Low	40 ksi	16 ksi	26 ksi
Std. Dev. w/o flaws	6	8	10
Std. Dev. with flaws	7	8	9
Weibull Modulus w/o flaws	11	4	5
Weibull Modulus with flaws	9	5	5

ORIGINAL PAGE IS
OF POOR QUALITY

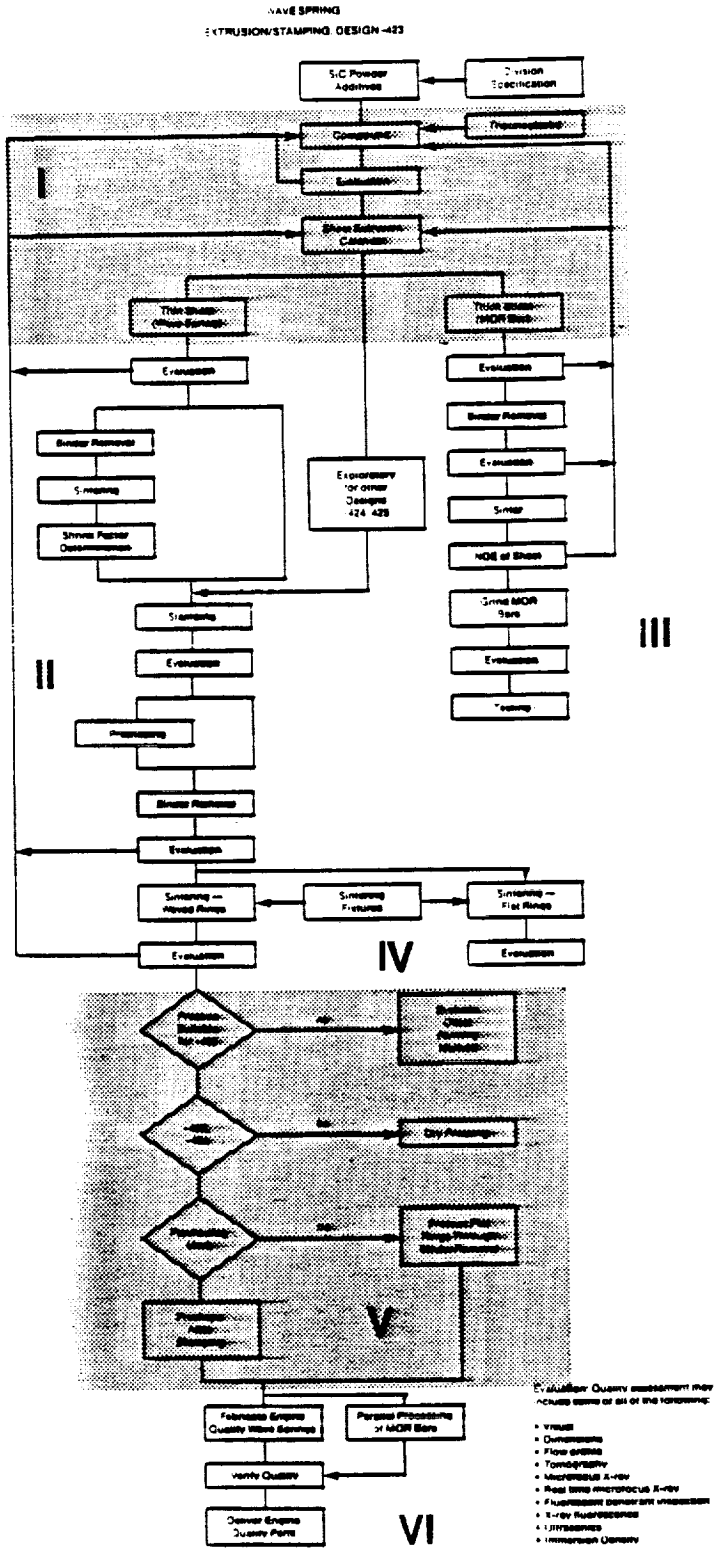

Figure 141: Activity Flow Diagram - Wave Spring (Extruded/Stamped)

The average shrinkage and density values of the three groups of rings are as follows:

Composition	Thickness (%)	Wall Width (%)	ID (%)	OD (%)	Density (g/cc)
A	19.34	20.63	17.43	17.44	3.14
Std. Dev.	1.55	0.67	0.20	0.21	0.009
B	20.82	20.17	16.85	17.15	3.12
Std. Dev.	2.31	0.67	0.08	0.10	0.009
C	19.04	20.79	17.12	17.18	3.14
Std. Dev.	0.65	0.66	0.20	0.12	0.004

The data generated to date indicates that Composition A has superior properties even though it appears to have a higher level of defects. It is also somewhat easier to process and as such should potentially be more readily fabricated defect-free.

An additional evaluation of green density variations as evidenced by sheet length and width shrinkage differences was initiated. Extruded wave springs and MOR sheet stock was cut into 2" square samples from the leading end, center and trailing end of the extrusion run. The samples were measured, checked for green density and subsequently processed through binder removal. The green density was again measured and recorded. This group of specimens will be sintered and characterized during the next reporting period.

Two fixtures for creating the wave form in flat rings were received. One is a mating two piece metal assembly with the "green" wave form configuration on both halves. This will be used to preform the flat rings during binder removal or to heat slump the plastic filled pre-cut flat rings.

The second is a mating two piece graphite fixture with the finished wave form configuration machined on both halves. This fixture will be used to sinter flat rings or rings that were pre-formed thermally or during binder removal.

In addition, a metal cutting die for punching out .050" thick rings from sheet stock was received. This should provide more uniform dimensions than a gasket cutter blade but may tend to damage the edges.

As directed by GAPD on December 14, 1988, wave spring Part Nos. PA3612423 and 3612424 were deleted from the workplan. Future efforts were to focus on Part No. 3612425.

Since extrusion/stamping appears viable for fabricating this 0.100" thick ring, Carborundum proposed to continue this effort as per the following revised tasks.

Task I: Process Optimization
Task II: Processing of Waved Rings
Task III: Process Verification
Task IV: Fabrication of Engine Quality Components.

The detailed activities proposed are described in the revised workplan.

3.2 Dry Pressing - Wave Spring P/N3612424

Part No. 3612424 was originally selected for dry press processing because of its more rugged thickness (0.140") and its minimum wave amplitude (.160). A standard batch of spray dried pressing powder was selected and sufficient material reserved to press approximately 2000 parts over the course of the development program described in the activity flow diagram (Figure 19).

Dry press tooling was designed and purchased for flat wave spring blanks and for MOR test bars. Tooling was designed for 17.2% shrinkage on sintering and 0.6% green springback. MOR test bar tooling was designed to press bars 2.00 ± .010 long x 0.250 ± .005 wide. Thickness may be varied from 1/16" to 5/16".

Pressing trials were conducted on a 125 ton Alpha automatic press. Fill and removal of the pressed rings were accomplished manually. Initially it was planned to press rings at three different green density levels. During initial pressing trials, however it was found that densities at 1.90 g/cc had inadequate green strength to sustain handling or additional processing. Two groups of rings were pressed at calculated densities of 1.92 g/cc and 1.96 g/cc. Densities were adjusted by varying the weight of premix used while maintaining a fixed die volume. Forming pressures were 16-18,000 psi.

Pressing of flat rings was conducted in April/May and subsequent processing continued thru the end of the first contract year. Two groups of 60-80 flat rings were pressed at densities of 1.92 g/cc and 1.96 g/cc. These parts were then used for all furnacing trials and sintering fixture evaluations. Graphite sintering fixtures were designed from a high expansion graphite routinely used in production sintering. During furnacing trials several unsuccessful runs were experienced in two different furnaces in the Technical Center. It was found that the larger heating zones of the production furnaces in the Manufacturing Center were required. Firing trials from these furnaces produced the following results (flat rings):

	O.D.	I.D.	Thickness	Wall Thickness
Green (Nominal)	8.020"	7.545"	0.170"	0.237"
Fired	6.638 ± .008	6.236 ± .004	0.136 ± .004	0.200 ± .004

These represent 10 flat rings from 3 different furnace runs. It is felt that these results are very satisfactory for as-fired dimensions on parts of this size.

Three groups of MOR test bars were also pressed at three different green densities. The bars were sintered in production furnace and subsequently evaluated for MOR. The low values shown in Table 49 were attributed to these bars being unchamfered and uncensored with respect to pressing and handling defects. They were examples of a strictly as-pressed, as-fired component.

Table 49
MOR of As-fired Dry Pressed Test Bars

Green Density (g/cm^3)	Test Temp. (°C)	MOR ksi	MOR MPa	Std. Deviation ksi	Std. Deviation MPa
1.90	1400	47.5	327	3.4	23.2
1.93	23	44.0	303	4.4	30.0
	1400	48.1	331	4.9	33.7
1.96	1400	45.7	315	5.3	36.3

Additional test bars were machined from isopressed billets from the same premix batch. These bars were also sintered in a production furnace, and then annealed at 1500°C in a separate furnace run. They will be examined and characterized for defects before MOR evaluation. This data will provide baseline strength of the specific material used.

ORIGINAL PAGE IS
OF POOR QUALITY

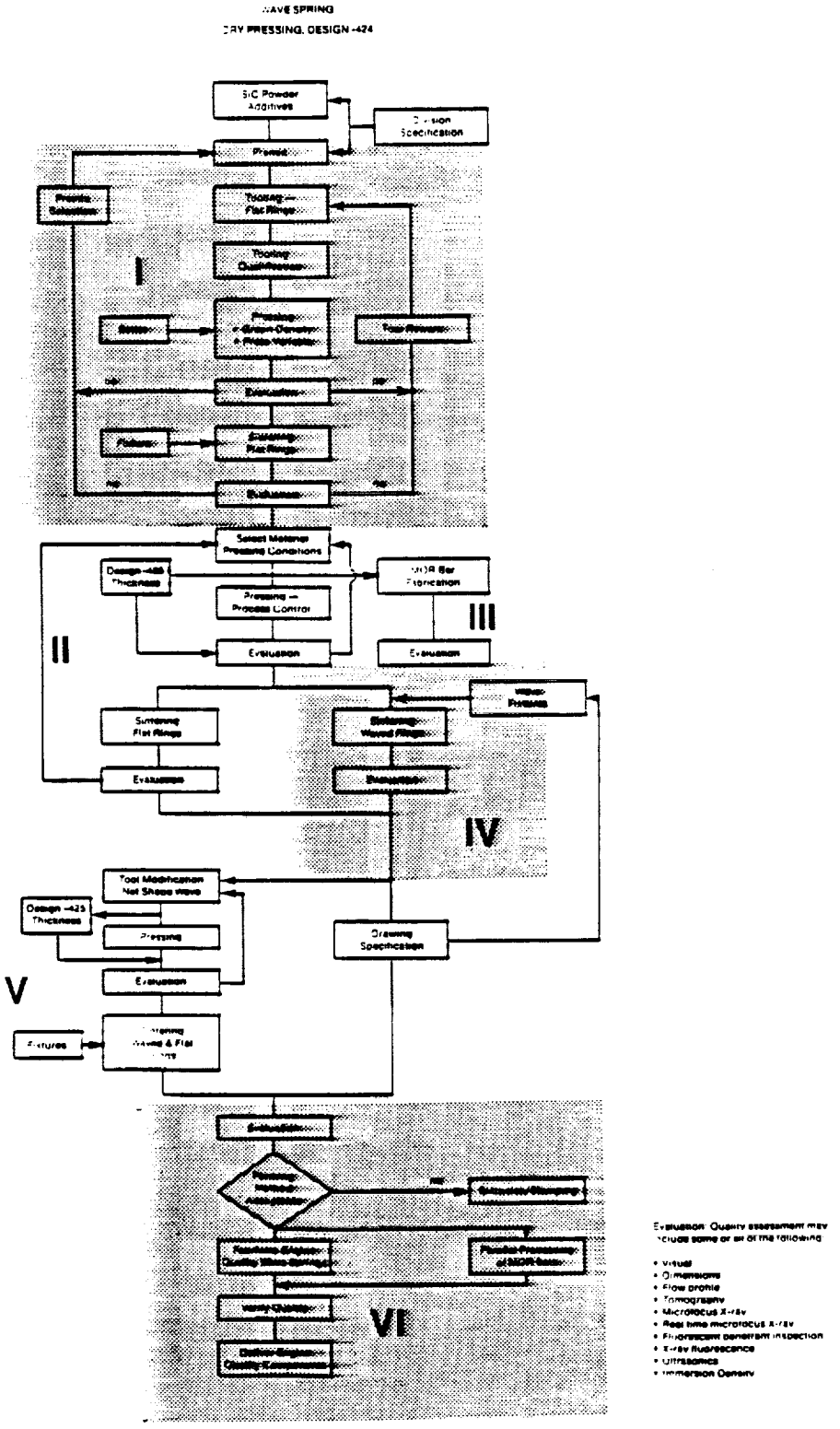

Figure 142: Activity Flow Diagram - Wave Springs (Dry Pressed)

The graphite furnacing fixtures were reworked to include the wave form specified for P/N 3612424 (Figure 143). Firing trials were begun in the latter part and continued thru the end of the first contract year. Initial work showed successful wave forming by firing green flat blanks on the net shape fixture.

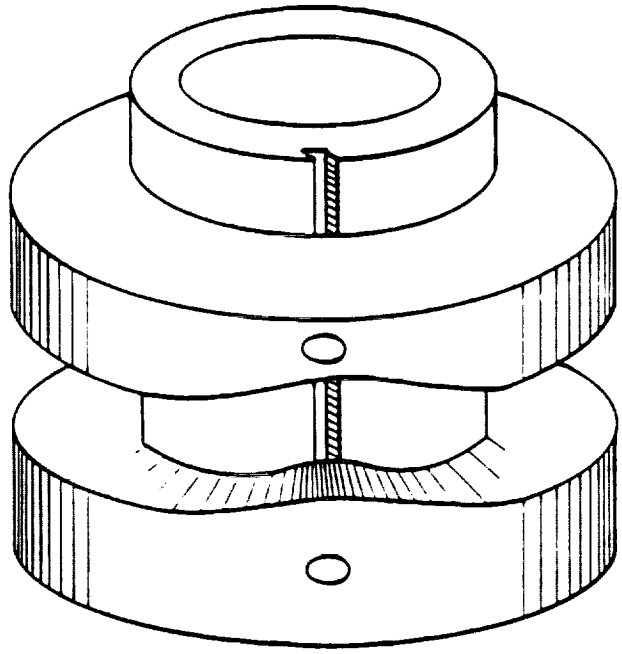

Figure 143: Sketch of Graphite Furnace Fixture with Wave Form

Wave amplitude, however, was undersize:

O.D.	I.D.	Thickness	Wall Thickness	Amplitude
6.634 ± .003	6.235 ± .003	.135 ± .002	.200 ± .002	.015

Trials continue in order to further evaluate this method.

At year end the decision was made to discontinue efforts on P/N 3612424 and concentrate on P/N 3612425. This part has a greater wall thickness but is thinner and has more wave amplitude. Initial work will be done with P/N 3612424 dry press tooling to assess the feasibility of pressing the thinner part. If pressing trials scheduled for early 1989 are successful, firing and wave forming will be evaluated on these parts before purchasing steel tooling for P/N 3612425. These activities are divided into the following tasks and described in the revised workplan.

Task I: Demonstration of .100" Pressed Thickness Capability
Task II: Procurement and Qualification of Tooling for Flat Rings (P/N 3612425)
Task III: Fabrication of MOR Test Bars
Task IV: Fabrication of Waved Rings
Task V: Fabrication of Engine Quality Components

4.0 Test Specimens

Non-Destructive Evaluation - Computed Tomography (CT)

X-ray tomography has been shown to be a useful tool for measuring internal density distributions in ceramic components. The result of the measurement is a determination of the linear X-ray absorption within each pixel of the two dimensional array of resolution elements that comprise a CT image. The absorption is a function of the materials composition, its density, and the distribution of X-ray energies used to make the measurement. One of the great advantages of CT over other forms of NDE is that the numerical representation of the absorption can be used to measure material properties such as density. Proper interpretation requires control over the measuring techniques and in some cases, assumptions about measurement conditions or material characteristics. For example if the material composition is independent of position and monoenergetic X-rays are used, then the absorption is directly proportional to the material density. Since ideal conditions such as monoenergetic X-rays are not commonly available, one goal of this work was to determine what conditions are necessary to make measurements of the density distribution within injection molded components to assess the effect of various molding parameters. The other goal was to develop methods for measuring compositional variations in green injection molded components using dual energy CT.

The major problem in making quantitative density measurements with CT is correcting for the change in the X-ray spectrum as the beam propagates through the part. The beam hardening is due to the preferential absorption of the lower energy components, the effective amount of spectral shift is a function of material. The most common correction technique uses measurements of the transmission through a uniform object to calibrate software corrections to the data. While water is used to calibrate medical systems, better corrections are obtained for ceramics when more similar materials such as glass or aluminum are used for the beam hardening calibration. While this was possible on our own machine, we chose to use machines located in medical facilities for the Garrett study because of their dual energy capability, thus re-calibration was not possible. A compromise is to surround the object with a material of similar X-ray absorption, thus most of the beam hardening occurs outside the region of interest. A water solution of potassium iodide can be adjusted to suit various materials. However, using a solution as absorbing as the part being tested reduces the X-ray flux to the detector and results in noisy images. A lower concentration was chosen based on its ability to suppress artifacts that extend from sharp corners or are tangent to long edges. These are also caused by incorrect beam hardening corrections. Experiments showed that 9% solutions by weight are suitable for sintered SiC and 3% solutions give uniform densities and reduced edge artifacts with green injection molded parts. Dual energy imaging had the advantage of producing acceptable images based on these

criteria using just plain water. Images with almost as few defects could also be obtained with green parts in air. Due to the absence of artifacts in immersed green transition ducts, it was taken as a working hypothesis that the small density variations seen in the dual energy images were real.

This hypothesis was tested using three techniques: X-ray fluorescence measurements of composition, immersion density of sectioned ducts, and measurements with more energetic X-rays on a high resolution industrial CT scanner.

After dual energy processing, the data can be presented in terms of the equivalent density of two materials, the high Z material is calcium (MAT HI), and water is the low Z component (MAT LO). Transverse MAT HI slices through the transition duct indicted circumferential density variations as large as 10%. Since these were the complement of the MAT LO images, it was interpreted as segregation between the SiC powder and plastic binder. A destructive test on a sliced-up duct measured the silicon distribution using X-ray fluorescence (EDAX). These initial results supported the tomography data. The EDAX system was calibrated in units of silicon density be measuring a series of injection molded samples with compositions ranging from 20 to 35% polymer by weight. Calibration is required because these low energy X-rays can only be emitted from within 20 um of the surface, and the intensity is dependent on the matrix which the silicon component is imbedded in. The calibration samples were cut and the surfaces smoothed with identical techniques, thus producing the expected linear response. However, it is possible to get erroneously low readings of silicon concentration because of the surface finishing. Two mechanisms are smearing the plastic so that it covers the SiC, or pulling out SiC particles from the surface during finishing. It is suspected that such a surface modification led to the EDAX results which appeared to confirm the CT results showing segregation of the SiC and plastic binder.

The actual density variation was determined by sectioning the duct into 42 small elements and measuring the immersion density of each one. The standard deviation was only 0.15% of the mean value with a maximum deviation of less than 1%. While the composition could vary without changing the average density, it is not likely that it could have changed by as much as that indicated by the CT or EDAX.

More insight was gained as part of a demonstration of a new CT system being purchased by BP America. These tomography measurements on a green duct in air using a 220 kV source on an industrial grade system at Scientific Measurement Systems in Austin, Texas did not show the previously noted density variations. There were also fewer artifacts in the image which is believed to be due to the higher resolution and having the beam hardening algorithm calibrated with aluminum, a material with similar absorption characteristics to silicon. It is

expected that dual energy measurements on this machine will also produce better results when that capability is available in the middle of 1989. A reason for this optimism is the successful use of a medical system to measure composition correctly in smaller samples, the previously mentioned one inch diameter calibration samples. Using the Siemens DR3 scanners basis material calibration, the MAT HI and MAT LO density of each calibration sample was first converted to average atomic number. The average atomic number can then be expressed in terms of the composition by calculating the concentration of the two known constituents of the calibration samples (SiC and plastic binder) that would produce the same X-ray absorption characteristics. The results agreed with the nominal composition to within better than 1%. The agreement was not as good when these same parts were scanned in water, thus indicating that there will be inaccuracies with larger parts such as ducts unless beam hardening corrects are handled more carefully. Since one has more control over the calibration and algorithms in an industrial tomography system, the new SMS system is expected to produce superior results when it becomes available.

APPENDIX C

ANNUAL TECHNICAL SUMMARY REPORT
GARRETT CERAMIC COMPONENTS DIVISION

(11 pages)

ADVANCED TURBINE TECHNOLOGY APPLICATIONS PROJECT

ANNUAL TECHNICAL SUMMARY REPORT
COVERING JULY THROUGH DECEMBER 1988

FOR GARRETT AUXILIARY POWER DIVISION

I. INTRODUCTION

The objective of this 37 month technical effort, begun in July 1988, is to develop a fabrication process with the potential for low-cost, mass production of AGT-101 turbine rotors using Garrett Ceramic Components GN-10 silicon nitride. Pressure slip casting will be the primary fabrication approach. Materials and components will be extensively characterized and NDE methods developed and evaluated for improved process control and material/component qualification. In Task A, fabrication of the AGT-101 rotor using GN-10 silicon nitride and pressure slipcasting will be developed. In Task C, GN-10 test specimens for material evaluation and NDE seeded defect standards will be fabricated by pressure slipcasting.

II. TECHNICAL PROGRESS SUMMARY

TASK A. FABRICATION OF ROTOR BY PRESSURE SLIP CASTING

SUBTASK A.A Fabricate Rotors and Billets Using Baseline Process - The goal of this task is to use the baseline GN-10 pressure slipcasting forming process to fabricate AGT-101 rotors and extensively evaluate raw materials. The results are then to be correlated and used to determine processes and properties in need of development and improvement, to be accomplished in subsequent tasks. Originally the task was planned as a four month effort from July through October 1988, but an earlier than anticipated program kick-off and some more detailed baseline experiments required extension of Subtask A.A through January 1989.

Raw material characterization is complete. Two lots each of silicon nitride powder and sintering aid A powder have been characterized along with one lot of sintering aid B powder. Raw material powders were characterized by particle size distribution, surface area, chemical purity, phase content, dry and aqueous surface chemistry, particle morphology and degree of agglomeration, and presence of high density inclusions.

The results are being correlated and will be reported in the January 1989 bimonthly report.

GN-10 baseline slip fabrication procedures were identified in July and August. Preliminary GN-10 slip properties and green and HIPed test billet properties generated in August and September indicated suitable rheological properties for baseline rotor casting development and mechanical properties meeting the Garrett Auxiliary Power Division ATTAP program minimum requirements. Pressure casting rigs for the AGT-101 rotor were designed and assembled from July through September. AGT-101 rotor molds and tooling left over from the previous AGT-101 program at Garrett Ceramic Components (then called AiResearch Casting Company) were used for the baseline rotor fabrication task.

Initially, a rotor was slipcast using the standard slipcasting process developed in the previous AGT program, where pressure is not used during casting, for comparative purposes. The resulting as-cast rotor is shown in Figure 144. No blades remained attached after mold removal and extensive porosity was observed throughout the hub and shaft regions.

A total of 15 AGT-101 rotors have been pressure slip cast from September through November. Compared to the previous slipcasting process, the baseline pressure slipcasting process reduces the time required to cast a rotor by two-thirds. A representative as-cast pressure cast rotor is shown in Figure 145. Three green rotors and three calcined rotors were cut up in December for destructive evaluation of microstructure, density, and porosity distributions. Three calcined rotors are currently being ASEA encapsulation-HIPed and will be evaluated by NDE as well as destructive techniques in January 1989.

Examination of the GN-10 slip and green rotors cast using the baseline pressure slip casting process revealed five aspects of the process which need development/improvement:

1) Voids were present in the shaft section directly above the tops of the blades, visually observable after casting. The voids were observed in all rotor shafts. In order to determine the origin of the voids, each powder (silicon nitride and GN-10 sintering aids A and B) were cast singly into quasi-rotor shapes. It was determined that one of the two sintering aids used in GN-10 (aid A)

ORIGINAL PAGE
BLACK AND WHITE PHOTOGRAPH

Figure 144. As-cast GN-10 rotor cast without pressure using previous generation fabrication process.

ORIGINAL PAGE
BLACK AND WHITE PHOTOGRAPH

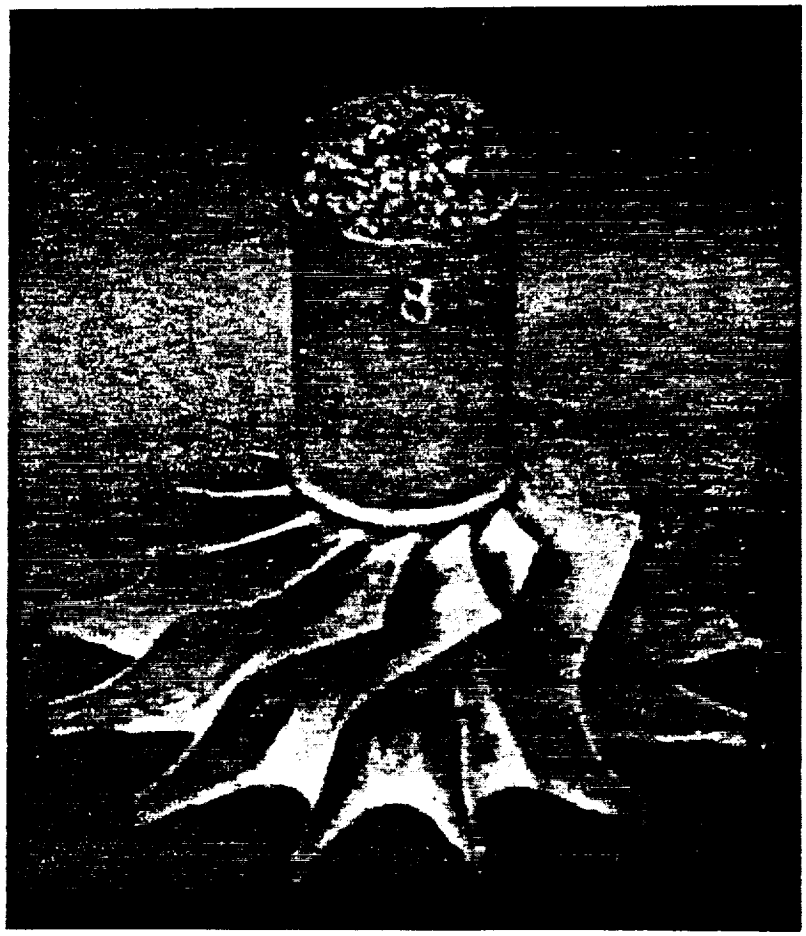

Figure 145. Baseline as-cast GN-10 rotor fabricated by pressure slipcasting.

was causing gas evolution after 8 to 10 hours and creating the voids in the cast rotor shaft areas.

2) The slip gels during casting before the last inch of top section of the shaft casts, generating an agglomerated microstructure with large visible porosity at the top of the shaft.

3) Blades exhibit cracking, sometimes extensive, both parallel to the shaft and radially where the base of the blade and hub intersect. Rotors with up to 12 of the 13 blade tips still attached after mold removal and green drying were achieved but some rotors exhibited extensive blade cracking and few blade tips attached after mold removal. Realtime microfocus x-ray examination of rotors after casting before mold removal indicates that much of the cracking has taken place during casting. In general, examination of the 15 rotors indicates that cracking of blades is not consistent from rotor to rotor.

4) Slip properties measured just before casting indicate that the slip properties (zeta potential, viscosity, and pH) varied more than desired, possibly resulting in irreproducible cast part results. It was determined that the baseline slip preparation procedure did not allow slip fabrication with reproducible results, as described further in Subtask A.B below.

5) The casting rig exhibited leaking and minor assembly/disassembly problems. Rotors exhibited extensive cracking of blades and on hub bases when the casting rig leaked. Modifications to the rig eliminated the leaking and cracking on rotor hub bases.

Overall, two rotors exhibited good surfaces and a majority of blades without cracks, but the baseline casting process results in as-cast rotors with variable amounts of cracked blades formed during the casting process.

Processing and characterization procedures for baseline fabrication of the AGT-101 rotor have been documented and standard procedures written and issued to assure rigorous adherence and reproducibility. The procedures include raw material characterization/ qualification, slip preparation, mold fabrication, rotor casting procedures, and property measurement and measurement device calibration procedures and standards. Initially, four slip property parameters are being monitored for statistical process control implementation: slip viscosity, pH, zeta potential, and

specific gravity. In addition, green, calcined, and HIPed densities and porosity are monitored on each part and as a function of location within parts.

Work remaining in Subtask A.A includes preparing a summary of the raw material, slip, and cast part results. The summary will be included in the January 1989 bimonthly report. The results of Subtask A.A are already being used to design experiments for Subtask A.B (Rotor Development).

SUBTASK A.B SLIP CAST ROTOR PROCESS DEVELOPMENT - The goal of this task is to investigate and implement improvements in rotor fabrication using statistically designed experiments, based on results obtained in Subtask A.A (baseline rotor fabrication). Subtask A.B was originally planned to run from September 1988 through August 1989 but was not begun until December 1988, due to delays in starting Subtask A.A.

Experiments to improve upon the results of the baseline rotor fabrication process have begun. In order to determine how and when blades are cracking during the casting process, a fixture is being designed and built to pressure cast rotors inside the realtime microfocus x-ray unit to examine the casting process in-situ.

Two preliminary experiments were initiated in December. GN-10 slip property reproducibility improvement was investigated by modifying the baseline slip preparation process. It was determined that the baseline process resulted in different amounts of electrolyte addition each time the slip was prepared, resulting in variable slip properties. The process was modified to add the same amount of electrolyte each time and initial results in December show large improvements in slip property reproducibility and large decreases in the standard deviation of specific slip properties. The final results of this experiment will be reported in the January 1989 bimonthly, when a statistically significant number of data points have been generated.

It was also determined in November and December that slip characterization technique procedures and instrument calibration procedures needed to be further defined and refined to generate accurate measurements. Well documented procedures and calibration techniques were implemented in December and

variation in characterization results has been decreased extensively.

The second experiment initiated in December was to examine the effect of shorter casting times during rotor fabrication to see if cracking during casting could be reduced. Shorter casting times result in short rotor shaft lengths but in 3 out of 4 casting runs, rotors were formed that retained all their blades and blade tips after casting, mold removal and drying. The rotors still exhibit some casting and drying cracks in the blades and hub regions compared to results of the baseline process, but blade cracking and detachment is greatly reduced by the shorter casting time. One of the three rotors which retained all of its blades is shown in the green state in **Figure 146.** The four rotors cast in December will be calcined and HIPed in January 1989 for delivery to Garrett Auxiliary Power Division in February as specified for Subtask A.B.

The results of Subtask A.A and results of Subtask A.B will be used in January 1989 to generate statistically designed experiments for Subtask A.B to address improvements that Garrett Ceramic Components has determined is required in four areas: GN-10 slip dispersion stability, rotor casting process, mold removal after casting, and rotor drying.

SUBTASK A.F SLIP CAST ROTOR COMPONENT QUALIFICATION/NDE DEVELOPMENT - The goals of this subtask are to evaluate new or improved non-destructive evaluation (NDE) techniques for their applicability to pressure slipcast rotor development, and to determine NDE equipment resolution capabilities and develop NDE examination and calibration techniques.

Garrett Ceramic Component's realtime microfocus X-ray unit became operational in September and has been used as an in-process control to characterize each rotor or test billet that has been fabricated after casting before mold removal, after mold removal before drying, after drying, after calcination, and after HIPing.

J. Gardner and D. Newson of Garrett Ceramic Components and J. Minter of Garrett Auxiliary Power Division received training in the use of the new realtime microfocus x-ray inspection system and its image processing capabilities in mid-November. Determination of resolution and detection limits of metal inclusions (iron wires) placed on green rotors and billets, and HIPed billets were investigated in November

ORIGINAL PAGE
BLACK AND WHITE PHOTOGRAPH

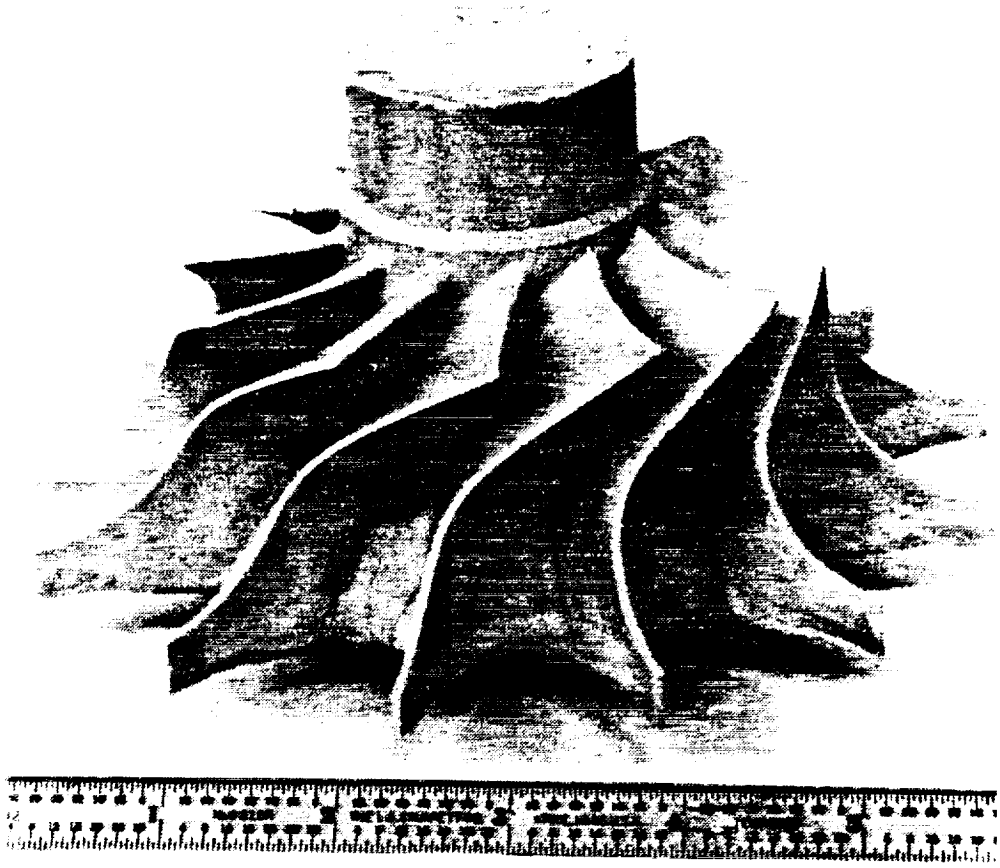

Figure 146. GN-10 Rotor (shown in green state) fabricated in Task AB which retained all blades and blade tips after drying.

and December. Preliminary results indicate that 25 um size iron inclusions can be detected through one inch green billets and 5/8" HIPed billets. Suitable radiography parameters were investigated and image processing techniques were under development to improve defect detection in rotors and billets.

Metal and GN-10 silicon nitride step gauges are being designed for microfocus x-ray calibration.

TASK C. FABRICATION OF TEST SPECIMENS AND NDE STANDARDS

SUBTASK C.A PRESSURE SLIP CAST TEST SPECIMEN FABRICATION-The goal of this subtask is to fabricate flexure and fracture toughness test bars of GN-10 silicon nitride by pressure slipcasting for delivery to Garrett Auxiliary Power Division in November 1988 for GN-10 material assessment. Due to processing concerns with slipcast billets, which will be subsequently described, the task has been extended and test bar delivery delayed to past this report period.

GN-10 billets from which test bars would be machined were pressure slipcast in September and October. Initial examination of green dried billets by microfocus radiography indicated defect-free parts. Visual inspection indicated no defects on the billet surfaces. The billets were subsequently examined in late October using recently developed image processing techniques. Fine cracks were detected in the interiors of a majority of the green dried billets. It was then decided to hold off on HIPing the billets until the origin of the cracks and their effect on HIPed part properties and microstructure was determined.

Further billet casting experiments revealed that the billets cracked one to two days after casting during the drying process, indicating that the baseline billet drying cycle is inadequate.

GN-10 billets previously slip cast using the same process in August under an internal research and development program were HIPed without radiographic inspection in the green state. The HIPed billets were received in early December and inspected by radiography using recently developed image processing techniques and no defects - cracks or inclusions, were detected. The slip cast GN-10 mechanical properties provided to GAPD in early 1988 for the preliminary GN-10 materials assessment were generated from test bars cut from

billets also dried by the same baseline technique. No cracks were detected in HIPed parts. The preliminary conclusion is that the ASEA HIP process eliminated the thin cracks detected in the green billets.

On the basis of this conclusion the billets fabricated in October were HIPed in December. The billets will be subsequently examined after HIPing, and if no defects are detected by NDE, will be machined into the required number of test bars and delivered to Garrett Auxiliary Power Division in early February 1989.

SUBTASK C.C FABRICATION OF SLIP CAST DEFECT SEEDED BILLETS FOR NDE DEVELOPMENT - The goal of this subtask is to fabricate pressure slipcast GN-10 seeded defect billets for use by Garrett Auxiliary Power Division and Garrett Ceramic Components for NDE technique calibration, examination technique development, and resolution determination. Subtask C.C was begun in July 1988 and is expected to finish as planned in February 1989, with the delivery of seeded defect specimens.

The configuration and number of pressure slipcast NDE seeded defect specimens was finalized by Garrett Auxiliary Power Division and Garrett Ceramic Components in September 1988. The seeded defect configuration is shown in Figure 147. Six NDE seeded defect billet blanks were pressure slipcast and dried in September 1988. Two of the blanks were calcined. The six blanks were provided to Garrett Auxiliary Power Division in September for ultrasonic imaging NDE technique development.

The pressure casting fixtures for fabrication of the seeded defect specimens were designed in November and December and are currently being fabricated. All required deliverable seeded defect specimens will be fabricated at the end of this reporting period.

NDE SEEDED DEFECT SPECIMEN CONFIGURATION

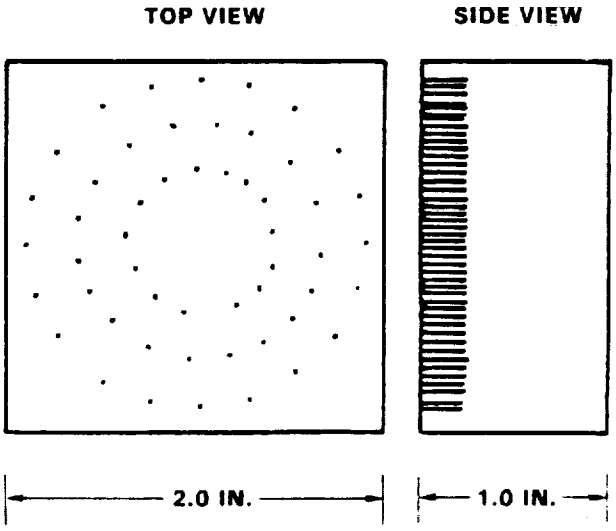

TYPES OF DEFECTS:

VOIDS

IRON INCLUSIONS

FABRICATION TECHNIQUE:

PRESSURE SLIP CAST GN-10 SILICON NITRIDE AROUND VARIOUS SIZE IRON WIRES

VOIDS – PULL WIRE OUT AFTER CASTING

IRON INCLUSIONS – LEAVE WIRE IN AFTER CASTING

SIZE OF DEFECTS:

0.001, 0.002, 0.005, 0.010, AND 0.020 IN. DIA

0.25 IN. DEEP

PROCESSING STATE OF SPECIMENS:

AS-CAST, BISQUE FIRED, HIPed

Figure 147. GN-10 Pressure Slipcast Seeded Defect Specimen Configuration.

1. Report No.	2. Government Accession No.	3. Recipient's Catalog No.
NASA-CR-185109		

4. Title and Subtitle	5. Report Date
Advanced Turbine Technology Applications Project (ATTAP) - 1988 Annual Report	April 1989
	6. Performing Organization Code

7. Author(s)	8. Performing Organization Report No.
Engineering Staff of Garrett Auxiliary Power Division A Unit of Allied-Signal Aerospace Company	31-8071(01)
	10. Work Unit No.

9. Performing Organization Name and Address	11. Contract or Grant No.
Garrett Auxiliary Power Division 2739 E. Washington Street Phoenix, Arizona 85034	DEN3-335
	13. Type of Report and Period Covered
12. Sponsoring Agency Name and Address U.S. Department of Energy Office of Transportation Systems, Heat Engine Propulsion Division, Washington, D.C., 20585	Annual Report 1988
	14. Sponsoring Agency Code DOE/NASA/0335-1

15. Supplementary Notes

Annual Report under Interagency Agreement
Project Manager T.N. Strom, Propulsion Systems Division
NASA - Lewis Research Center, Cleveland, Ohio 44135

16. Abstract

This report is the first in a series of Annual Technical Summary Reports for the Advanced Turbine Technology Applications Project (ATTAP), authorized under NASA Contract DEN3-335 and sponsored by the DOE. This report has been prepared by Garrett Auxiliary Power Division (hereinafter referred to as GAPD), a unit of Allied-Signal Aerospace Company. The report includes information provided by Garrett Ceramic Components Division (hereinafter referred to as GCCD), Norton/TRW Ceramics Co., and the Carborundum Co., all subcontractors to GAPD on the ATTAP. The project is administered by Mr. Thomas Strom, Project Manager, NASA-Lewis Research Center, Cleveland, Ohio. This report presents plans and progress from August 1987 through December 1988.

Project effort conducted under this contract is part of the DOE Gas Turbine Highway Vehicle System Program. This program is oriented to provide the United States automotive industry the high-risk, long-range technology necessary to produce gas turbine engines for automobiles with reduced fuel consumption and reduced environmental impact. The program is oriented toward developing the high-risk technology of ceramic structural component design and fabrication, such that industry can carry this technology forward to production in the 1990s. The ATTAP test bed engine, carried over from the previous AGT101 project, is used for verification testing of the durability of ceramic components, and their suitability for service at Reference Powertrain Design conditions.

This report reviews the effort conducted in the first 16 months of the project on development of ceramic technology, review and update of the Reference Powertrain Design, and improvements made to the test bed engine and test rigs. Appendices include reports of progress made by the major subcontractors to GAPD on the ATTAP: Carborundum, Norton/TRW Ceramics, and Garrett Ceramic Components Division.

17. Key Words (Suggested by Author(s))	18. Distribution Statement
Advanced Turbine Technology Applications Project	Unclassified - Unlimited Subject Category 85 DOE Category UC-96

19. Security Classif. (of this report)	20. Security Classif. (of this page)	21. No. of Pages	22. Price*
Unclassified	Unclassified	245	A11

* For sale by the National Technical Information Service, Springfield, Virginia 22161